University of Southampton

Faculty of Physical Sciences and Engineering

Electronics and Computer Science

Analysis of Thermo-Mechanical Stresses in Joints and Cables

by

Mohammad Anan Mohammad Hamdan

Thesis for the degree of Doctor of Philosophy

November 2019

University of Southampton

Abstract

Faculty of Physical Sciences and Engineering

Electronics and Computer Science

Thesis for the degree of Doctor of Philosophy

Analysis of Thermo-mechanical Stresses in Joints and Cables

by

Mohammad Anan Hamdan

The landscape of the power sector is undergoing a significant transformation. The growing demand for energy, the depletion of world's fossil energy resources and the greenhouse effect are well-recognized challenges for the power sector. Through the integration of renewable resources to the energy mix, the power sector is becoming cleaner and more affordable. A fundamental requirement to handle these new developments is to have an efficient transmission and distribution network. Effective transmission and distribution of electricity depends on the condition of underground power cables and joints. Any malfunction in these elements can affect the reliability of the entire grid and this could have an economic impact on the system. Undoubtedly, having an efficient and reliable transmission network implies the need to know and determine the electrical, thermal and mechanical limits of cable systems (cable + accessory). The stresses affecting the service performance of cable system may be classified as thermal, electrical, mechanical and chemical or a combination of the aforementioned. The contributory effects of thermo-mechanical stresses on the degradation of cable joints have gained great attention. Correct expectation of the thermo-mechanical behaviour of all the components in the cable system allows optimisation of both the performance and reliability of these components while maintaining the component life. This research explores some aspects of the thermo-mechanical stresses inside the cable system components in more depth. This work investigates thermomechanical stresses in silicone rubber pre-moulded cable joints and in three core submarine export cables.

It is known that the electrical breakdown strength of insulation interfaces in cable joints depends on the mechanical pressure. Based on the literature, it has been shown that

increasing the mechanical pressure in cable joints at the interface is important for ensuring high electrical breakdown strength. However, there is no clear benchmark for interface pressure, and little knowledge about how the thermal behaviour of the cable system will affect it. Furthermore, there is no correlation between interface pressure and different parameters such as material strain, temperature, thickness and elastic modulus. In this research, the mechanical design of solid-solid interface in cable joints is studied to evaluate the main effects of the relevant parameters. More specifically, a model is developed using the finite element method to calculate mechanical stresses based on a non-linear elastic model. In addition, an improved analytical approach is developed to determine the changes in interface pressure during operation. This proposed analytical approach takes proper account of material properties and their changes with temperature. The analytical algorithm is validated using finite element method. The use of a more realistic interface pressure model increases the integrity of the cable joint design and better enables industry professionals and system operators to determine the limits of their system during operation.

In three-core cables, the cores are subjected to higher internal thermo-mechanical stresses than single core cables since each core is expected to be more restricted. The effect of internal thermo-mechanical stresses on the electrical performance of the three-core cable should be examined properly, but is often neglected. During electrical testing of AC submarine cables, only one core of a three-core cable could be tested. In this thesis, the internal thermo-mechanical stresses generated inside a single core and a three core cable are examined. In particular, a 2D thermo-mechanical coupled model is developed using finite element modelling. The model is analysed through thermo-mechanical analysis, to investigate how the thermally induced deformations could affect the electrical performance of the cable. This study demonstrates the significance of testing the full three core submarine cable with armour rather than testing only one single core.

Table of Contents

Table of Tables

Table of Tables

Table of Figures

Table of Figures

Table of Figures

Table of Figures

Research Thesis: Declaration of Authorship

I, Mohammad Hamdan, declare that this thesis entitled *Analysis of Thermo-Mechanical Stresses in Joints and Cables* and the work presented in it are my own and has been generated by me as the result of my own original research.

I confirm that:

1. This work was done wholly or mainly while in candidature for a research degree at this University;
2. Where any part of this thesis has previously been submitted for a degree or any other qualification at this University or any other institution, this has been clearly stated;
3. Where I have consulted the published work of others, this is always clearly attributed;
4. Where I have quoted from the work of others, the source is always given. With the exception of such quotations, this thesis is entirely my own work;
5. I have acknowledged all main sources of help;
6. Where the thesis is based on work done by myself jointly with others, I have made clear exactly what was done by others and what I have contributed myself;
7. Parts of this work have been published as:-
    - M. A. Hamdan, J. A. Pilgrim and P. L. Lewin, "The Temperature Dependence of Insulation Mechanical Properties and its Effect on Interface Pressure in Cable Joints," IEEE 2nd International Conference on Dielectrics (ICD), 2018.
    - M. A. Hamdan, J. A. Pilgrim and P. L. Lewin, "Effect of Short Circuit Currents on Thermo-mechanical Properties of Insulated Cables," IEEE Conference on Electrical Insulation and Dielectric Phenomena (CEIDP), 2018.
    - M. A. Hamdan, J. A. Pilgrim and P. L. Lewin, "Effect of Sheath Plastic Deformation on Electric Field in Three Core Submarine Cables," IEEE Conference on Electrical Insulation and Dielectric Phenomena (CEIDP), 2018.
    - M. A. Hamdan, J. A. Pilgrim and P. L. Lewin, "Thermo-Mechanical Analysis of Solid Interfaces in HVAC Cable Joints," IEEE Transactions on Dielectrics and Electrical Insulation, 2019. (Accepted).

Signature: Date:

Acknowledgements

I wish to thank Dr. James Pilgrim and Prof Paul Lewin my supervisors for their guidance and support. I also appreciate my friends support and encouragement. I am most grateful to my parents and my sisters for support and love.

Chapter 1

Introduction

Power cables are an indispensable part of the transmission and distribution infrastructure. Since the introduction of polymeric insulated medium voltage cables in 1960, significant developments and improvements have been made in the cable design. Yet, the cable accessories are still considered as the most vulnerable point in the cable system "cable + accessory" [1].

Thermo-mechanical stresses generated in the cable system are one of the main concerns when designing cables and joints, as they contribute to the degradation process of insulation systems. Moreover, there are reports of failures in cable systems that are believed to be mechanically driven or mechanically initiated. Insulation materials which are subjected to thermal and mechanical stresses are prone to electrical failure. Thermal and mechanical stresses within high and medium voltage cable joints have remained a concern, particular in light of more dynamic load profiles seen due to the introduction of distributed generation in the medium voltage networks [1]. Export cables are one of main components of offshore wind farms. It contributes to the capital cost of the overall project by almost 5%. In 2018, wind energy accounted for 63% (€26.7 billion) of Europe's investments in renewable energy [2]. This huge investment stimulate the need to investigate stresses on cables in the presence of renewable generation. The intermittent nature of wind and solar radiation creates significant number of load current cycles during service. Cables connected to wind and solar farms could stay unloaded for a while then be rapidly loaded to maximum rated load in a short time. The variation of the output power from high power production to low or no power production means that cables will heat and expand, then cool and contract more frequently than those whose loads are demand driven. If the quality of the cable installation is low and depending on the soil condition, the expanding and contracting of cables may lead cables to move and rise from the ground [1, 3]. As a result, cables will be subjected to high temperature gradients producing severe mechanical stresses that will affect the cable system especially the weakest parts of the cable system; joints and terminations.

Chapter 1

In this chapter, the research motivation and novel contribution are presented. In addition thesis structure is outlined.

1.1 Research Motivation

In modern XLPE HV and EHV cable accessories, joint tubes made of pre-moulded elastomeric materials are widely used. Silicone rubber is an attractive material due to its electrical and mechanical properties. A Joint tube is installed on the connected cables with a certain expansion rate to establish the pressure required to assure enough electric breakdown strength at the interface. Pre-moulded joint tubes made of silicone rubber are manufactured in a certain number of sizes for each voltage level. To reduce cost, manufacturers prefer to offer joint tubes in as few different sizes as possible. To design reliable sizes of joint tubes, the acceptable maximum and minimum expansion rate has to be regulated. Minimum expansion rate depends on the minimum pressure needed at the interface and elasticity of the silicone rubber used. Maximum expansion rate depends on materials ability to handle elongation before it fails and breaks apart. For both limits, the working temperature of cables has to be considered. This connection between interface pressure and material properties is unclear in the standards. In IEEE standard 404 for extruded and laminated dielectric shielded cable joints rated 2.5 to 500 kV, no correlation is found between mechanical properties of the insulation and interfacial pressure. Using materials with suitable mechanical properties can contribute to the stability of the interface mechanically and electrically. Any defect in the design could produce unexpected mechanical stresses, and this will enhance the risk of partial discharge initiation. Then electrical trees at solid interfaces may be developed finally leading to insulation breakdown. It is necessary to evaluate the mechanical stresses generated at interfaces based on material properties and operating conditions to develop an optimal design of the interface.

Cables are also affected by thermo-mechanical stresses. The inherent non-uniform distribution of temperature inside three core cables will generate a non-uniform distribution of mechanical stress. The effect of the temperature distribution and materials mechanical properties dependency on temperature should be considered while testing. During cable testing the same level of stresses that the cable would experience under operating conditions must be considered. When cables are tested it is required to make sure that the cable will function as expected throughout its entire lifetime. Cables could be located in heavily and dynamically loaded circuits. Thermo-mechanical stresses developed inside three core cables are higher than single core cables since they are more constrained. Lead sheath is a ductile

material and during operation, the sheath could deform permanently increasing the chances of creating gaps at the interface between insulation and sheath. However, CIGRE WG B1.27 recommends that only one cable core from a three-core cable or a single-core cable without armour may be subjected to the electrical test. The advantage of electrically testing three core cables as a complete cable rather than a single core should be confirmed through a thermal mechanical electrical analysis.

1.2 Contribution

This thesis makes two significant contributions to the state of the art in the area of thermo-mechanical analysis of cables and joints. Firstly, an assessment of mechanical stresses in a joint tube made of silicone rubber is conducted. The mechanical pressure is determined based on silicone rubber elasticity and expansion rate. The mechanical pressure in joint tubes have been calculated based on a nonlinear elastic model using the finite element method. To include the effect of temperature and material properties namely elastic modulus and thermal expansion, an improved analytical algorithm for estimating the change in interface pressure due to thermal cycling is presented. This work shows the significance of linking material mechanical properties and temperature with mechanical stresses at the interface in the design process. Therefore, a demonstration of how to calculate mechanical stresses before and during operation taking into account material properties (elastic modulus and thermal expansion) is provided. The method described in this thesis helps to show that the correlation between material mechanical properties (elastic modulus and thermal expansion) and mechanical pressure will lead to a more stable design.

The second key contribution of this thesis is that it demonstrated the benefit of testing three core cables as a whole cable with armour, rather than testing a single core. Through a 2D thermo-mechanical coupled model, it has been possible to highlight the importance of electrically testing three core cables. The variation of cable insulation elastic modulus and thermal expansion with temperature and metallic sheath plastic behaviour were taken into account in the model. Moreover, the main factors that affect metallic sheath deformation are discussed. The effect of metallic sheath deformation on the electrical performance of the cable is investigated by a finite element model (FEM). An electrical model is built to study the effect of thermo-mechanical deformations on the electrical performance of the cable. In addition, the effect of evaluated temperature on the thermo-mechanical properties of

insulated single core cables is presented. The work presented in this thesis will enrich the insight of designers and operators regarding the thermo-mechanical stresses faced by cables and joints. Taken together, these two main contributions offer a step forward in the state of the art for cable system design and testing by making it possible to determine and understand the thermo-mechanical stresses generated in the cable system.

1.3 Thesis Structure

Chapter 2 provides the background for the research presented in this thesis. It also presents a comprehensive literature review of mechanical pressure at solid interfaces in cable joints. A brief description of the main components of single core cable, three core cables and cable joints is presented. In addition, the different types of cable joints are described. Moreover, some of the main thermo-mechanical degradation mechanisms are outlined. Furthermore, an introduction to material mechanical properties namely elastic modulus and coefficient of thermal expansion and their change with temperature is provided. Linear and non-linear elastic behaviour are also defined. Elastic and plastic deformation are discussed. Hyper-elastic models are presented and compared. Heat sources inside cables and joints are outlined. The mechanical equations used throughout the thesis and some of the mechanical assumptions in the models used and how to implement those using FEM are demonstrated. Then the factors that affect the interface breakdown strength are listed. The relation between interface pressure and electric breakdown strength is described. Types of interfaces and insulation materials are outlined. Furthermore, the parameters that influence interface pressure and its changes are discussed. A critique of the existing models to calculate interface pressure is included.

Chapter 3 introduces a model that is proposed to calculate mechanical pressure in a joint tube. The calculation of radial and circumferential stresses in a joint tube made of silicone rubber based on hyper-elastic model is described. The values of the circumferential stresses for different materials elasticity are determined. Moreover, the influence of silicone rubber elasticity, expansion rate and thickness on mechanical pressure is assessed. The model proposed allows the designer to determine the mechanical pressure based on silicone rubber mechanical behaviour.

Chapter 4 commences by presenting how elastic modulus and thermal expansion vary with temperature. To include these variations, an enhanced analytical model is developed to estimate the change in interface pressure. This analytical approach is compared to a finite

element model to verify the accuracy. Moreover, factors that affect the thermal stresses are explored through a sensitivity analysis. The analytical approach is used to obtain the change in interface pressure for a cable joint at high and low temperature. The results obtained demonstrate that including the effect of material properties is useful to explain some of the failures.

Chapter 5 shifts the focus to deal with thermo-mechanical stress in single core and three core submarine cables. It commences by explaining the difference between full transient analysis and quasi-static analysis. This elucidation is necessary especially when dealing with thermal stress problems. In addition, the effect of huge thermal input on thermo-mechanical properties of a single core cable is examined assuming that the elastic modulus and thermal expansion changes with temperature. This provides a profound understanding of thermo-mechanical stresses faced by a single core cable at high temperatures. Furthermore, thermo-mechanical stresses inside a three core submarine cable and their effect on sheath deformation are investigated. The factors that affect sheath deformation is evaluated. The electrical performance of the cable is linked to the mechanical condition of the cable. The link between the electrical performance of a cable and the thermo-mechanical stresses generated is recognised and acknowledged.

Chapter 6 presents a summary of the main findings and the conclusions of the work. Furthermore it presents the future projects that could be developed from this research.

Chapter 2

Literature Review

This chapter commences by providing the essential background knowledge to support all the work in this thesis. More specifically, this chapter presents a brief description of the main components of single core and three core cables. It introduces the different types of cable joints. Then, the aging mechanisms including the thermo-mechanical degradation mechanisms are explained. This chapter also provides an overview to material mechanical properties namely elastic modulus and thermal expansion and their change with temperature. Furthermore, elastic and plastic deformation are discussed. This chapter demonstrates the behaviour of linear and non-linear elastic materials. The mechanical equations used throughout the thesis and some of the mechanical assumptions in the models are demonstrated. This chapter presents the parameters that affect insulation interfaces in cable accessories. In addition, the relationship between electrical breakdown strength and interface pressure is highlighted. Types of insulation interfaces and the main properties of insulating materials are also presented. Furthermore, the factors that influence the interface pressure are discussed through a thorough literature review. The different methods used to calculate interface pressure are presented and compared.

2.1 Power Cables

Power cables are constructed by covering one or more core(s)/conductor(s) with suitable insulation and they are surrounded by protective covers. The structure of power cables may seem simple. However, every component has its own purpose and it should be carefully selected to assure high performance and reliability. Schematic diagrams of a single core and a three core power cables are shown in Figure 2.1a and Figure 2.1b, respectively. The basic cable components are summarized in the following [4-8]:

1. Conductor: The role of the conductor is to carry load currents of the cable. Conductors can be solid or stranded. Stranded conductors are used to provide flexibility and to reduce both skin effect and proximity effect [9]. The most common

conductor used in a cable system is aluminium (Al) or copper (Cu). Aluminum is cheaper, lighter and preferred at medium voltage level even though more volume of material is needed. On the other hand, at high voltage and at extra high voltage, copper is used because of its smaller size since it has higher conductivity, meaning less material is needed to carry a given current.

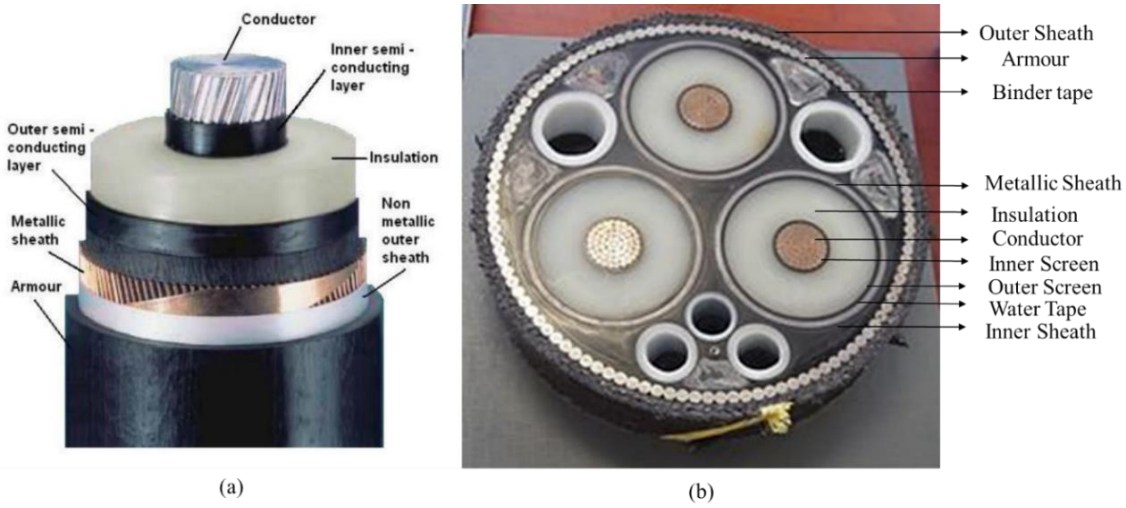

Figure 2.1: (a) Single core high voltage power cable design structure [10]. (b) Three core high voltage power cable design structure [11].

2. Insulation: One of the most crucial components of a power cable is the insulation. It ensures no electrical connection between the energized conductor and any other surfaces with considerably lower voltage (ground). Cross-linked polyethylene (XLPE) is one of the most commonly utilized insulation material in HV extruded cables. XLPE is made by crosslinking polyethylene (PE) to enhance the thermal and mechanical properties of the polymer. When using XLPE it is possible for cables to operate at a rated maximum conductor temperature of 90 ℃ and a 250 ℃ short circuit rating [7].

3. Semi-conducting layers (Inner and outer screens): These two layers are included to obtain a uniform electric field distribution within the dielectric insulation. Moreover, it provides a good contact and smooth interface between conductor and insulation to avoid electric field strength enhancements, which lead to partial discharge. Furthermore, it guarantees close contact between the insulation and the metallic screen to avoid partial discharge on top of insulation. These layers are made of polyethylene based co-polymers filled with 40% carbon black [12]. The high carbon

content in the semi conductive screens makes the electrical parameters vary over a wide range. The maximum volume resistivity is regulated by international cable specifications. According to IEC 60840 the inner layer resistivity must be smaller than 1000 Ω·m and the outer layer resistivity should be lower than 500 Ω·m [12].

4. Metallic Sheath/ Wire Screen: A metallic sheath is included over the insulation to maintain the integrity of the insulation. The sheath will provide a path for earth fault current to ground in case of a fault event. Usually metallic sheaths are made of lead, aluminium or copper [7]. Lead is utilized due to its high corrosion resistance especially when a cable is installed in a moist environment. Aluminium sheaths are also adopted since they are light and flexible. In some cable designs, the sheath is constructed with concentric neutral wires instead of a solid sheath. The wires can be made of copper or aluminium. If water sealing in a longitudinal direction is required, a water swelling tape is used under the metallic sheath [8].

5. Armour: To protect the cable mechanically and to assure stability under tension, metal armour strands are wound around the cable core in a helical configuration. Galvanised steel is the most common material used for armouring, however other metals can be utilized such as aluminium, copper, brass, bronze and stainless steel [7].

6. Outer Sheath (External Covering): an outer cover is applied over the armour to add extra protection to the cable from environmental conditions. It also protects the corrosion protection of the cable armour. The serving is made of PE, polyvinyl chloride (PVC) or wound yarn layers [8].

2.2 What is a Cable Joint?

The insulated and fully protected connection between two or more cables is known as a cable joint. Cable joints are essential elements in the cable system. Cable sections are usually linked every 1000 m. The reliability of the cable system is dependent on the quality of these accessories. A good cable joint must fulfil certain electrical, thermal and mechanical requirements. Some of these requirements are listed below [13, 14]:

1. Good electrical connection between conductors to pass the required current.

2. Contain a connection to ground through cable sheath or wire screen to provide a path for short circuit current.

3. The electric field inside the cable joint should be graded and controlled to assure an even distribution of voltage (electric stress) between the conductor and ground.

4. The interfaces between the cable and joint body should not be contaminated or have any voids.

5. The cable joint must be protected from environmental stresses.

6. Having the ability to handle thermal contraction and expansion due to heating and cooling of the conductor.

7. To withstand the thermomechanical forces generated from the connected cables.

2.2.1 Types of Cable Joints

High voltage cable joints can be classified into several categories based on different criteria [14]. According to the cables connected, cable joints are classified into straight, transition and Y-branch joints. Straight joints connect two cables of the same insulation type. If the two cables connected have a different type of insulation, then it is called a transition joint. Joints are considered as transition joint if they connect cables of the same type but with different conductor size. A Y-branch joint connects three cables together regardless of the insulation type of the cables. Cable joints are also categorised based on the way the joint insulation is employed [14]. As illustrated in Figure 2.2, straight joints are sub divided into three types; taped, prefabricated and field moulded joints. In taped joints an elastomeric semi-conducting and insulating tapes are taped around the connected cables to create the insulation screen, the insulation and stress control profile. During the installation, the tape is stretched to make the layers connected to form a solid mass. In other types, the insulation is melted, moulded and integrated to the connected cables in the field. These types are known as field moulded type joints.

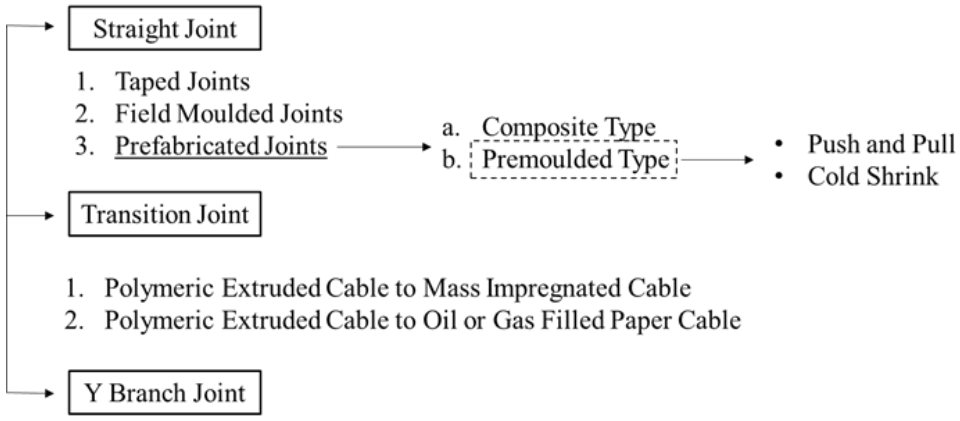

Figure 2.2: Schematic overview of HV cable joint types [14].

To reduce the skill and time needed to assemble the joint, premoulded type has been adopted. Premoulded joints utilize an insulation that has been manufactured and tested in the factory and to be installed on site [15, 16]. An elastomeric insulation is moulded into one single rubber block which contains insulation layer, semiconducting connector screen, stress control profile screens and insulation screens. There are two typical installation techniques for high voltage elastomeric cable joints; cold shrink and push-pull designs [1]. In the cold shrink, the pre-moulded joint body will be pre-expanded on a support tube with larger expansion ratio so it can be placed around the cable in the right position then by removing the support tube the joint body will shrink by its own elasticity memory [15, 16]. The second technique is called the push-and pull where the pre-moulded joint body is expanded with just the size of the cable and by using grease and special push on tools it is set onto the right position. The pre-expanded cold shrink technology is popular since it does not need any push on tools. However in high voltage applications the joint body is of high thickness. This will require high forces to pre-expand the joint body and will impose high pressure on the support tube which is a matter that must be considered during the design.

2.2.2 Joint Construction

The structure of cable joints is not that different from the cable structure and usually it consists of connector, stress control, joint insulation, joint shield and outer sheath as illustrated in Figure 2.3.

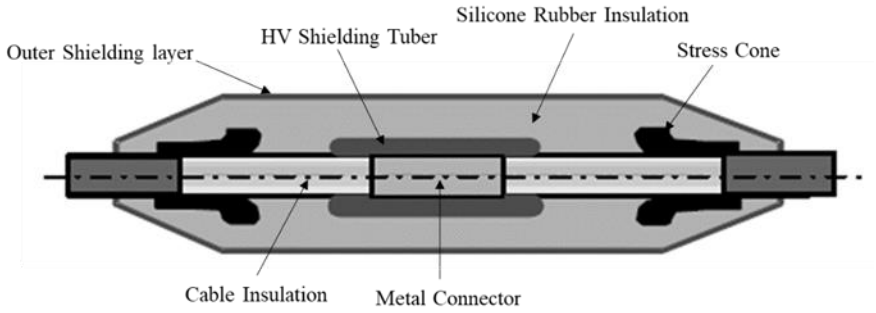

Figure 2.3: Diagram of a prefabricated cable joint [17].

Copper is an easy metal to handle in a joint and different ways of connecting two copper conductors could be done: compression, welding, heat fusion and soldering. In contrast, when performing aluminum connections, a great deal of attention should be paid to matching the compression tool, die, and connector, especially for larger sizes [5]. Connecting the conductors is accomplished by a connector that can be pressed, welded or mounted by screws. A stable operation of the connector during load cycling and its ability to handle maximum amount of current without initiating thermal degradation of the joint are of high importance. The metal of the connectors is chosen to be the same as the cable but in some cases this is not possible such as when connecting copper conductor with aluminum conductor. Using an aluminum connector over a copper conductor is acceptable, whereas using a copper connector over an aluminum conductor is not recommended since through load cycles the relative rates of expansion of the two metals will lead the aluminum to cast out and eventually will result in a poor connection. The surface of the connector should be cylindrical and smooth to avoid the electric field peaks. A semiconducting tape over the connector is added to smooth the surface [5].

The removal of the insulation screen from the end of the cable is required during the installation of cable joint. However, the electric field will increase considerably at the cut edge of the insulation screen. This electrical stress can reach values high enough to ionize the air leading to discharges. Making the interface between joint insulation, cable insulation and insulation screen is not an easy task, methods of stress control is needed. Moreover, even the critical breakdown strength of the insulating material can be reached with higher potential or voltage spikes [18].

Refractive stress control and geometrical stress control are two common types of stress control applied. In refractive stress control, two layers of insulation with high permittivity

are added. The first layer is a high permittivity tape that covers the areas with high electrical stress and its role is to assure that no voids are created. The second layer is a stress control tube with much higher permittivity than the permittivity of the insulation to distribute the electric field concentration at the cut edge of the insulation screen in a more uniform manner. On the other hand, in geometrical stress control, a cone shaped conductive electrode is added on the top of the cable at the cut edge of the screen to minimize the electric field strength and to distribute the electric field more uniformly [18].

Depending on the cable type used, different materials could be applied as an insulating material of the joint such as plastics, tapes, paper ribbons, cable mass and cable oil. The role of the joint insulation is to add more dielectric strength and to transfer heat out from the joint effectively. To assure a smooth transition from the joint insulation to the grounded joint shield, an insulation screen for the joint with semiconducting materials is applied. As a final layer, the joint is covered with an outer sheath made of plastic or metal to protect it from mechanical stress [5, 18].

There are different types of dielectric interfaces in cable joints. The interface between the cable insulation and joint insulation is the most basic kind. These interfaces could be formed between cross linked polyethylene cable (XLPE) insulation and rubber stress cones in joints and terminations or between rubber stress cones and epoxy parts in joints. Part of these interfaces will function parallel to the electric field. It is accepted that the dielectric strength of interfaces is weaker than bulk insulation [17]. The dielectric strength of interfaces is proportional to the interface pressure. In the design stage of any cable joint, it should be assured that mechanical pressure at the interface will be sufficient to avoid any electrical breakdown at the interface. The drop in the mechanical pressure could lead to a poor long-term performance or even failures [17]. In chapters three and four of this thesis more details about interfaces can be found.

2.3 Aging and Deterioration of Cables and Joints

Aging is defined as the permanent changes in the electrical insulation system because of stresses imposed by operating and environmental conditions [19]. There are number of external and internal factors that impact the lifetime of the cable. External factors are those unintentionally introduced in the electric insulation system such as voids and contaminants due to the production process, errors in manufacturing and poor workmanship faults. On the other hand, internal factors are formed from mechanical, thermal, electrical and

environmental factors combined all together during the operation lifetime of the cable [19, 20].

- Insulation in accessories is faced by electrical stress which could lead to partial discharge and electrical treeing under normal voltage and over-voltage conditions. Insulating materials are affected by high temperature and heat cycles.
- High temperature gradients produce mechanical stresses that will affect the cable joints. Bending, tension, compression are all forms of mechanical stress that would affect the insulation. In the long term, creep and fatigue will also contribute to the deterioration of the insulation [21].
- The speed of chemical decomposition of materials increases as the temperature increases. Oxidation of the polymer materials in the joint and the connected cables might occur under high temperatures, leading to auto-oxidation and embrittlement [22]. This can finally initiate partial discharges in micro-cracks and eventually will cause the cable to fail.
- During thermal heating the characteristics of the stress release tube may be changed since in oxidation, the formation of carbonyl groups in the materials could increase the electric conductivity significantly and this increase could change the electric field distribution leading to more stress in the joints [22].
- Environmental stresses that could accelerate the deterioration of the performance are solar radiation, soil thermal conditions, salt, dust, acid rainfall and humidity. In this section the main focus will be on mechanical and thermo- mechanical stresses [16].

In cable accessories, the aging and degradation of the insulation units themselves is not the only aspect that should be considered. The compatibility between different insulating materials and changes in the state of interface are of equal importance. Failures of interfaces in accessories can have a significant impact to cause a blackout as the one happened in the Netherlands in 1993 [23]. Multiple of breakdowns in a series of 150kV terminations took place during service. Signs of electrical treeing at the interface were found. In order to prevent such problems, the stresses that interfaces face during operation should be studied and analysed. In cable accessories, different materials and components are in mechanical contact, this would case deterioration by the mechanical stresses generated during operation. Examples of mechanical aging and deterioration are outlined below:

- Relief of elasticity: In premolded cable joints, the elasticity of rubber molded unit is one of the main factors responsible for maintaining the required interface pressure between cable insulation and joint tube. Interface pressure should be high enough to assure good dielectric strength. During the long-term there is a possibility that the interface pressure is reduced due to elasticity relaxation of rubber. Elasticity relaxation of rubber unit should be considered during the design stage and in life expectancy calculations. However, a survey in [16] reported no failures because of elasticity relaxation of the rubber unit.

- Creep: It is defined as the tendency of a material to slowly deform under the influence of a constant stress. Creep deformation depends on stress, time and temperature. This deformation is irreversible and is more noticeable as temperature increases. In general, creep can happen in all materials but it was first noted in metals. Creep usually happen at stresses below the yield stress of the material. During the operation of power cable system, insulating materials are heated and cooled many times which could increase the chances of material creep [16].

- Thermo-mechanical forces: The definition of the thermo-mechanical rating of an accessory is “The capability of the accessory to handle mechanical forces, which are generated because of the operation of the accessory and related cable at the maximum temperature permitted in normal operation” [24]. The mechanical forces are classified into internal and external forces. The scale of the external forces is the only type identified as symmetrical and asymmetrical conductor forces emerging from the linked cables. Thermo-mechanical forces in accessories can emerge from two sources; first elements inside the accessories known as internal forces and second from cable conductor known as external forces [24]. Different internal thermo-mechanical forces such as expansion, contraction and pressure are simulated in real thermal IEC tests by supplying conductors with maximum rated temperature cycles [24]. External components (cable conductor) and their installation create external thermo-mechanical forces on accessories. The thermo-mechanical forces in cables are significantly affected by the cable type, cable construction, current loading, operating temperature and installation method. The rate of expansion of the individual materials of the cable joint system is influenced by the friction between these materials and by the cable joint and surrounding soil [25]. As a result, the expansion coefficient of each material should be considered, adding more complexity

to the matter because of the fact that the temperature profile within a cable system is inhomogeneous and it is controlled by the load current and ambient conditions.

2.3.1 Forces in Rigid Installations

There are different installation methods for power cables such as direct buried in the ground, trenches, ducts and shafts. However, in general the installation techniques can be classified into the following approaches [25]:

1. Rigidly constrained cable systems (buried cables or close cleated).
2. Flexible (unconstrained) cable systems (snaked, waved and sagged).
3. Transition sections between rigid and flexible installations (semi-flexible: the cable is permitted to demonstrate a controlled deflection but constrained).
4. Duct installations.

The cable installation is considered as rigid installation if the heating and cooling do not lead to significant movements. Such cases are when the cable is laid directly in well compacted ground or if the cable is installed in air and cleated at short intervals due to confined space. On the other hand, if the cable leaves the ground, the consideration as rigid installation is no longer valid and special attention should be taken to the design. The longitudinal forces of the cables affect mostly the cable joints. In case the cable is blocked and prevented of expanding in the longitudinal nor sideward direction, then the force is given by the below equation [26, 27]:

$$F_{tot} = EA\alpha_{th}\Delta T, \tag{2.1}$$

where α_{th}: Thermal expansion coefficient [K^{-1}]. E: Modulus of elasticity of the cable in compression (Young's modulus) [$N.m^{-2}$]. A: Effective cross sectional area of the cable [m^2]. ΔT: The difference of the temperatures of unloaded cable and the conductor temperature at a certain current load [K]. It is noticeable that the theoretical force depends on the cross-section of the conductor whilst the length of the cable involved has no effect on this force.

It was found that the magnitudes of the forces obtained in an experiment were significantly lower than the case of a rigid bar having the same cross section as illustrated in Figure 2.4 [27]. Moreover, it was found that there is a difference in the

forces generated from a virgin cable and with a cable with thermal history. The thermo-mechanical forces of a 400 kV XLPE cable with a cross section of 2500 mm^2 was tested by [28]. It was found in [28] that the virgin sample produced a maximum force of 80 kN. On the other hand, for a cable with thermal history the peak force reduced to 55 kN due to the relaxation of conductor strands when initially heated [28]. In the thermal cycling response test, it was concluded that the maximum force happens in the first load cycle and it lowers as the number of cycles increases as illustrated in Figure 2.4. A series of compressive and tensile forces will be generated inside the cable after some load cycles as shown in Figure 2.4. System design engineers should consider external thermo-mechanical as well as other mechanical forces on the accessories. Moreover, designers must take into account the allowable value of mechanical forces affecting the accessory, which is provided by accessory's supplier, the cable's thermo-mechanical properties (e.g. bending moments, permissible thrust) that is provided by the cable's supplier and the real installation conditions [24].

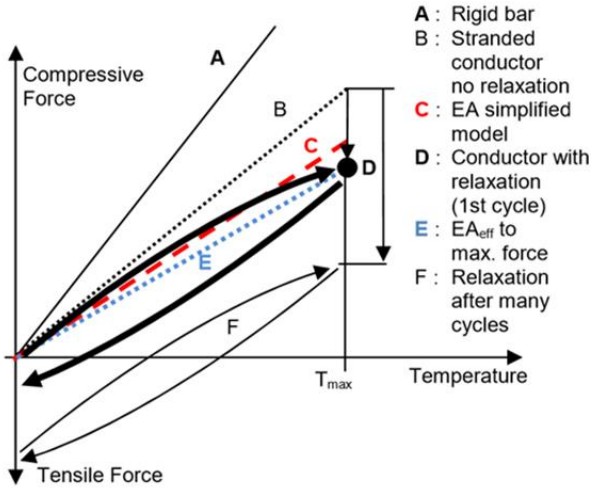

Figure 2.4: Forces in cable systems during load cycles [25].

In addition, the variation of length due to thermal expansion and the generated mechanical forces of different materials could cause some restrictions on the accessories, especially if the cable laying method is not appropriate and the applied connection technology is poor. As changing the thermo-mechanical behaviour of the utilized materials in cables is not possible, much attention should be paid to the cable and accessory installation methods.

2.3.2 Joint Failures Due to Thermal and Mechanical Stresses

Dynamic load cycles generate temperature fluctuations. Extension and contraction forces are generated by high cycling current. Figure 2.5 shows the mechanical forces that could affect a prefabricated cable joint and potential cause of failures. The impacts of thermo-mechanical forces could be deformation of the cable, dislocation of the conductor, bending because of longitudinal expansion and loss of grip or contact owing to differences in the thermal expansion coefficients of the different materials utilized. If there is a mismatch between the connector and the cable conductor, the connector will come disassembled from the conductor [26, 30]. A lot of heat will be generated at these high currents and high interface resistances. Thus, voids will start forming in the surrounding insulation leading to high electrical fields in the gas filled voids which eventually causes the joint breakdown [26]. In some cases, connectors are covered with an additional insulating material for more protection. Although this behaviour will not cause an instant failure, at cyclic load it will start moving continuously and various number of bending events will cause mechanical breakdown of the insulation [26]. Test outcomes indicated that screen wires could penetrate in particular, thermoplastic semiconducting shields, which might cause an increase in the electrical stress [29]. Conversely, the penetration for thermoset shields is not considered enough to shorten the expected lifetime even when cycling the cable up to 145 ℃ and because the maximum penetration is recorded to happen rather quickly, it is not deemed a limiting factor [30].

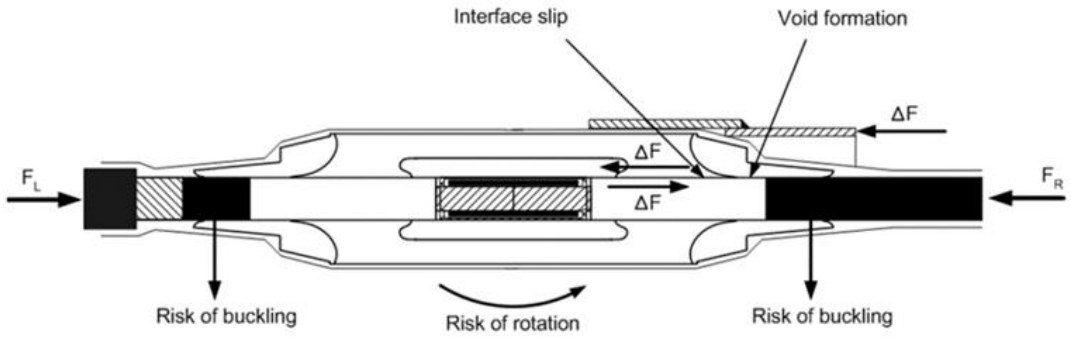

Figure 2.5: A differential force and slip interface in a 138kV one-piece straight joint [29]

Moreover, mechanical forces could cause loss of interfacial pressure between insulating materials of the cable joint leading to a weaker insulation and the possibility of insulation breakdown is increased. Movement in cable interfaces may happen due to expansion and contraction. Movement can lead to incorrect positioning of joint elements, leading to higher electric fields and eventually to insulation breakdown. Moreover, the speed of chemical

decomposition of materials increases as the temperature increases. High temperatures with mechanical stresses are sufficient to damage the insulation layer, to create a fault location or holes in the insulation that can finally initiate PD in micro-cracks.

The mechanical properties are essential to determine the mechanical limits of the cable system. Correct expectation of the thermo-mechanical behaviour of all the components in the cable system allows optimisation of both the performance and reliability of these components while maintaining the component life. The main goal of the next section is to present the basic concepts associated with mechanical properties and material mechanical behaviour.

2.4 Material Mechanical Properties

When a material is subjected to mechanical stress, its behaviour is defined by its mechanical properties. The mechanical properties include elastic modulus, coefficient of thermal expansion, tensile strength, hardness and other properties. Undoubtedly, having an efficient and reliable transmission network implies the need to accurately know or determine mechanical limits of the cable system.

2.4.1 Basic Definitions

Stress is defined as the force acting on a unit area. The SI unit for stress is load per unit area $N.m^{-2}$, also called Pascal (Pa). When the applied force acts normal to the area of interest, it is said it is under normal stress. Normal stresses can be tensile or compressive. Tensile stress causes elongation in the same direction of the applied force. On the other hand, compressive stress tends to squeeze the material and causes shortening. To distinguish between the two types, tensile stress has a positive sign and compression has a negative sign. If the applied force acts in a direction parallel to the area of interest and causes adjacent portions of the material to slide against each other, then it is called shear stress. Strain is a dimensionless quantity that represents the change in dimension (deformation) per unit length [33, 34].

A material is said to be elastic if it totally recovers its original dimension once the load is removed. In addition, if the relationship between stress and strain is linear then the material is a Hookean material (linear and elastic). The behaviour of linear elastic material is governed by Hooke's law, which is defined by [33, 34]:

$$\sigma = E\epsilon, \tag{2.2}$$

where σ is the applied stress in ($N.m^{-2}$), ϵ is the strain and E is a constant known as Young's modulus or elastic modulus. The SI unit of Young's modulus is Pascal. The elastic modulus is linked to the stiffness of a material. The stiffer the material, the higher its elastic modulus. A material with high elastic modulus will experience less elastic deformation when compared to a material with a lower elastic modulus. This indicates that a more elastic material has a lower elastic modulus [33, 34]. Some materials exhibit nonlinear elastic behaviour, where they experience large deformations and still return to their original geometry. However, the stress strain relationship is no longer linear and cannot be described by a simple constant elastic modulus. A typical example is rubber, which is a nonlinear elastic material. A typical behaviour of a non-linear elastic material is shown in Figure 2.6. There is a limit for materials' ability to revert to its original shape after the removal of the stress. This limit known as the elastic limit (yield point) of the material. Increasing the applied stress beyond the elastic limit will cause the material to yield and exhibits plastic deformation. The value of the stress at which the deformation enters the plastic region is known as yield stress. Once the material have undergone plastic deformation, the material does not go back to its original shape even after the removal of the stress. The maximum value of the applied stress can reach before the material fails and break apart is referred to as the tensile strength. Tensile strength and yield stress are important strength properties during the design calculations [33, 34]. Figure 2.7 shows a typical stress strain curve for a ductile material where, it illustrates the transition from elastic to plastic region after passing the yield point.

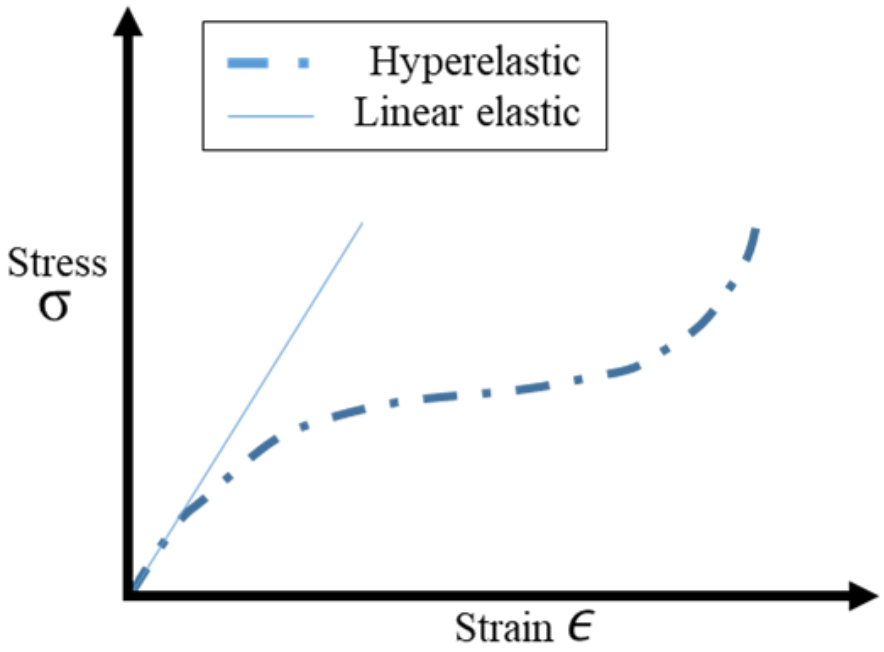

Figure 2.6: Hyper-elastic material vs. linear elastic material [35].

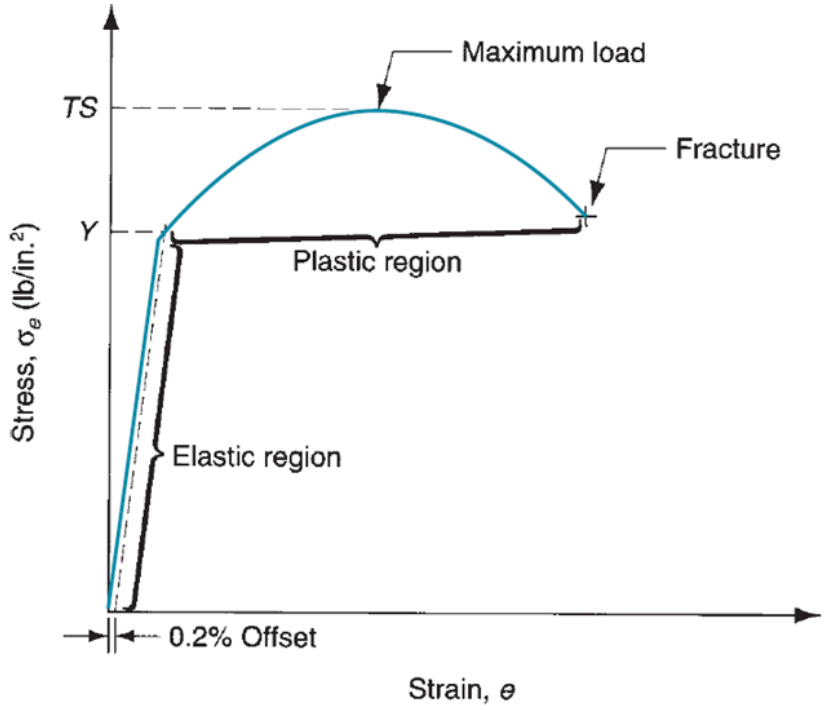

Figure 2.7: Typical stress strain curve in a tensile test of a metal [34].

Elastic and plastic deformations can be a function of time (often the case with viscoelastic materials) or independent of time. In general polymers have a viscoelastic behaviour, where the material exhibit both viscous and elastic characteristics. However, the degree of viscoelasticity is highly dependent on temperature, rate of deformation, degree of crystallinity, crosslinking and molecular mass of the polymer. In viscoelastic material, the

strain gradually increases over a period of time and when the stress is removed, only the elastic strain is recoverable over a period of time. Part of the strain developed is permanent and cannot be recovered. If a viscoelastic material is exposed to a constant strain, the initial stress will be proportional to the applied strain and will gradually decrease with time at a rate specified by the relaxation time. This behaviour is known as stress relaxation [33, 34].

2.4.2 Hyper-Elastic Materials (Non-Linear Elastic Materials)

At small strains, stress strain relationship of elastomeric materials could be described by a simple linear relation [36]. However when analysing their behaviour for large strains, hyper-elastic models should be used. Hyper elastic models are used to describe non-linear elastic materials [36]. Hyper-elastic materials are characterized by a strain energy function, which describes the potential energy stored due to a given deformation. Strain energy functions are represented in terms of stretch ratios λ, or indirectly in terms of strain invariants I. The stretch ratio is defined as the ratio of the deformed length divided by the original length and is presented as [37]:

$$\lambda = \frac{l_1}{l_0}, \tag{2.6}$$

where l_1 is the length after deformation and l_0 is the original length. Strain invariants are the measures of strain which are independent of the coordinate system. The three strain invariants in terms of the three principal stretch ratios can be expressed as [37-39]:

$$I_1 = \lambda_1^2 + \lambda_2^2 + \lambda_3^2 \tag{2.7}$$

$$I_2 = \lambda_1^2\lambda_2^2 + \lambda_2^2\lambda_3^2 + \lambda_3^2\lambda_1^2 \tag{2.8}$$

$$I_3 = \lambda_1^2\lambda_2^2\lambda_3^2 = \left(\frac{\Delta V}{V}\right)^2 = J_{el}^2. \tag{2.9}$$

J_{el} is known as volume ratio and it represents an indication of how the volume of a material element has changed after deformation. If the material is assumed to be incompressible (i.e. no volume change) then J_{el}=1. The strain energy density is decomposed into distortional elastic response function W_d and volumetric elastic response function W_V as defined below [37-39]:

$$W = W_d(\lambda_1, \lambda_2, \lambda_3) + W_V(J_{el}). \tag{2.10}$$

The first term represents the strain energy needed to change the shape and the second to present the strain energy required to change the volume. The second term is added to account for compressibility. If the material is considered as nearly incompressible then the Poisson's ratio is between 0.49-0.5. The simplest form of the volumetric strain energy is given by [37-39]:

$$W_V = \frac{1}{2}K(J_{el} - 1)^2, \tag{2.11}$$

where K is the bulk modulus GPa, also known as modulus of compressibility, is defined as the ratio of the pressure required for a unit relative decrease in volume. The strain energy satisfies the condition $W_d = 0$ for $J_{el}=1$. Neo-Hookean, Mooney Rivlin, Yeoh and Ogden are examples of hyper-elastic material models that can be used to represent the stress-strain relationship. Each model covers a certain strain range. Here the main features of each model are presented.

- Neo-Hookean model:

This model is known as the simplest model used to represent hyper-elastic behaviour. The form of strain energy function for this model can be written as [37, 38]:

$$W = \frac{\mu}{2}(I_1 - 3) + \frac{K}{2}(J_{el} - 1)^2, \tag{2.12}$$

where μ is the initial shear modulus (Pa) and K is the bulk modulus (Pa). This form can be used to describe both compressible and incompressible deformations. For incompressible version of the model $K=\infty$. The incompressible form is easier to handle in the theoretical derivations [37]. For finite element modelling and experimental studies, the compressible (nearly incompressible) form is usually more beneficial. Moreover, increasing the order of the volumetric part of the strain energy function will rarely improve the accuracy of the model. This model fails to capture the large strains and the non-linear response which results from them.

- Mooney Rivlin model:

In an attempt to improve the accuracy of modelling hyper-elastic behaviour, the Mooney Rivlin model was proposed. The model included a term to add a linear dependence on I_2. The model is considered as a better fit than pure elastic models. The general strain energy form of this model is given by:

$$W = \sum_{i,j=0}^{N} C_{ij}(I_1 - 3)^i (I_2 - 3)^j + \frac{K}{2}(J_{el} - 1)^2, \quad (2.13)$$

where C_{ij} are material constants and C_{00}=0. Different orders of this model can be employed. All of the different orders need number of constants that are used to define the strain energy function of the model. To obtain a better approximation to the stress strain curve high orders are used [35, 39].

- Yeoh model:

This model is known as the third order reduced polynomial form. The model is based on the first invariant I_1 only. Unlike the Neo-Hookean and Mooney Rivlin models, the Yeoh model can capture the upturn of the stress-strain curve. In addition, this model can be applied to a wider range of strains. The strain energy density function for this model is presented as [37, 40]:

$$W = C_{10}(I_1 - 3) + C_{20}(I_1 - 3)^2 + C_{30}(I_1 - 3)^3 + \frac{K}{2}(J_{el} - 1)^2, \quad (2.14)$$

where C_{10}, C_{20} and C_{30} are all material constants. Setting C_{20} and C_{30} to zero, Yeoh model can be reduced to the Neo-Hookean model. The Yeoh model is suggested to improve the precision of the Neo-Hookean model. Adding higher order I_1 terms gives the model the accuracy needed to describe the stress-strain curve better than the Neo-Hookean model. Moreover, excluding the dependence on I_2 helped to avoid some of the stability problems of the Mooney-Rivlin model particularly for uniaxial compressive strains less than 0.5 for example. The Yeoh model is proposed with no dependence on I_2 since it is noticed that elastomers have a weak dependency on the invariant I_2 and it is difficult to determine the dependency constants of I_2. The Yeoh model is known to be accurate for strains more than 200% and can describe carbon –black filled rubber deformations with good precision [38].

- Ogden model:

The Neo-Hookean fails to model hyper-elastic deformations at high strains. To fill this gap, Ogden proposed a strain energy function that is based on the principal stretches λ_1, λ_2 and λ_3 as given below [37, 41]:

$$W = \sum_{p=1}^{N} \frac{\mu_p}{\alpha_p}\left(\lambda_1^{\alpha_p} + \lambda_2^{\alpha_p} + \lambda_3^{\alpha_p} - 3\right) + \frac{K}{2}(J_{el} - 1)^2 . \quad (2.15)$$

The advantage of using the principal stretches is that they are directly measurable unlike the strain invariants. The constants (μ *and* α) are related to the shear behaviour of the material. The initial shear modulus in this model is defined as [37]:

$$2\mu_0 = \sum_{p=1}^{N} \mu_p \alpha_p . \quad (2.16)$$

It is worth noting that setting N=1 and α_2=1, then the Ogden model becomes equal to the Neo-Hookean model. A summary of the applicable strain ranges of each model is provided in Table 2.1.

Table 2.1. Applicability of Hyper-elastic Models and their Functions [35, 37-40].

Model	Strain limit	Function Form
Neo-Hookean	≤ 30%	$W = \frac{\mu}{2}(I_1 - 3) + \frac{K}{2}(J_{el} - 1)^2$
Mooney Rivlin	30-200%	$W = \sum_{i,j=0}^{N} C_{ij}(I_1 - 3)^i (I_2 - 3)^j + \frac{K}{2}(J_{el} - 1)^2$
Yeoh	≥ 200%	$W = C_{10}(I_1 - 3) + C_{20}(I_1 - 3)^2 + C_{30}(I_1 - 3)^3 + \frac{K}{2}(J_{el} - 1)^2$
Ogden	≥ 700%	$W = \sum_{p=1}^{N} \frac{\mu_p}{\alpha_p}\left(\lambda_1^{\alpha_p} + \lambda_2^{\alpha_p} + \lambda_3^{\alpha_p} - 3\right) + \frac{K}{2}(J_{el} - 1)^2$

2.4.3 Plastic Deformation

During linear Elastic deformation, strains are linearly proportional to the stress, so the relationship is described by Hooke's law. However, after the elastic limit (yield point) is exceeded, the material will demonstrate permanent non-recoverable deformation known as plastic deformation [33, 34]. Once the plastic deformation starts, the total strain can be considered as the sum of the elastic and plastic strain. Usually the elastic component is neglected since there could be a large amount of plastic deformation and plastic strain is larger than the elastic strain (i.e. $\epsilon_{\text{elastic}} << \epsilon_{\text{plastic}}$). To determine the elastic limit, a tensile test is done where the material is stretched by applying a tensile force until it finally fractures

[34]. During the tensile test, the tensile force and the change in length of the specimen are recorded. A stress strain curve is obtained by converting the force elongation data.

The transition from elastic to plastic state is gradual and does not occur as a sudden change in slope. Therefore, to easily identify the yield point, a straight line is drawn parallel to the initial part curve offset by 0.2% as shown in Figure 2.6 earlier. The point where this line intersects with the stress strain curve is considered as yield point. Other offset strains could be used. Beyond the yield point as the material enters the plastic region, it is noticed that the stress must be increased to drive the plastic flow. This phenomenon is known as work hardening or strain hardening. Strain hardening is a property that most metals exhibit to different degrees depending on the nature of the metal [33, 34]. There are different mathematical expressions used to describe the stress strain relationship. Here the basic models are presented [42-44]:

- Perfectly plastic

If no strain hardening is considered, the plastic curve is horizontal and the model is said to be perfectly plastic as shown in Figure 2.8. After exceeding the yield strength, the material will deform plastically at constant stress. Such models are particularly suitable for studying metals when heated to high temperatures where strain hardening is small. After passing the yield point, the total strain is expressed as [42-44]:

$$\epsilon = \epsilon_e + \epsilon_p = \frac{\sigma}{E} + \epsilon_p. \tag{2.17}$$

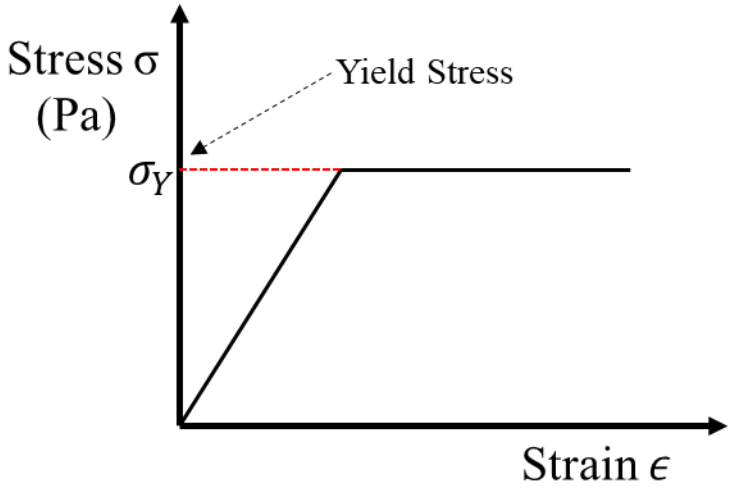

Figure 2.8: Perfectly plastic model [45].

- Linear Hardening Relationship

In this model, the stress strain curve is approximated using a linear hardening relationship where the curve has two slopes E_1 and E_2 as illustrated in Figure 2.9. The first elastic modulus is to represent the material's elastic behaviour and the second to describe the relation in the plastic region of the curve. The total strain representing this model is expressed as:

$$\epsilon = \frac{\sigma}{E_1} + \frac{(\sigma - \sigma_Y)}{E_2}, \tag{2.18}$$

where σ_Y is the yield stress, E_1 is the elastic modulus for the stress-strain relation in the elastic region and E_2 is the elastic modulus of the linear hardening relation.

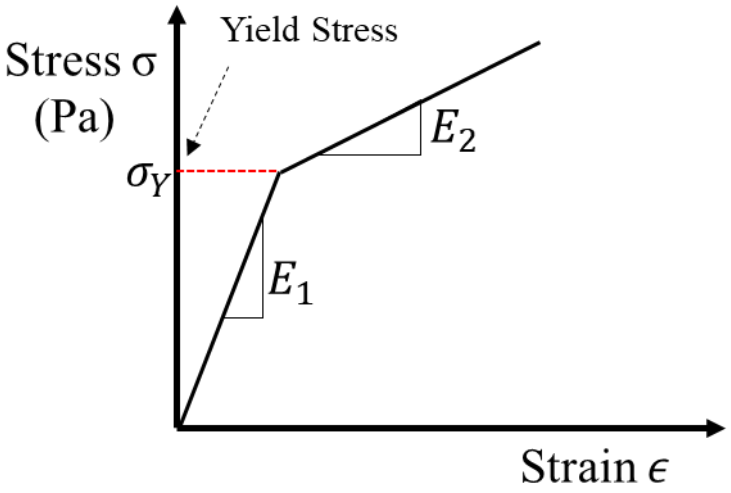

Figure 2.9: Linear hardening model [45].

- Power law Hardening

The power law approximation is the most commonly used representation of plastic response. It represents the work hardening behaviour by assuming a gradual decrease in the slope of the curve as plastic strain increases. The equation that describes this model is given as [42-44]:

$$\epsilon = \epsilon_e + \epsilon_p \tag{2.19}$$

$$\sigma(\epsilon_p) = \sigma_Y + k\epsilon_p^n. \tag{2.20}$$

The constant *k* is known as the strength coefficient in MPa and parameter *n* is known as the strain hardening exponent (dimensionless). The exponent n is an indication of the persistence of hardening. The constants *k* and *n* depend on the nature of the material, temperature and

strain. Usually n is between 0.2 and 0.5, whereas the values of *k* varies between G/100 and G/1000, G being the shear modulus [42, 43]. A higher n value indicates that the material could be strained more before it starts necking under the effect of a tensile force. If the stress is in the elastic region namely (ϵ_p=0, $\sigma \leq \sigma_Y$) then it has a linear relation with the strain. On the other hand, when the strain develops after exceeding the elastic limit it is prescribed by nonlinear relationship as in equation.

2.4.4 Effect of Temperature Properties

Mechanical properties of materials are temperature sensitive. In the design process, it is important to determine the operating temperatures of the cable joint during service to know how temperature affects the mechanical properties. In general, yield strength, tensile strength and elastic modulus decrease as temperature increases, but ductility increases. Unlike metals and ceramics, the elastic modulus of polymers shows high dependence on temperature. In Figure 2.10, the variation of the elastic modulus of common cable system polymers with temperature is shown. The rate of decrease is not uniform; the significant and sharp drops in elastic modulus are clear at temperatures linked to molecular transitions. At low temperatures, below the glass transition temperature T_g, the polymer is glassy and stiff with high elastic modulus. As temperature increases above the glass temperature, the elastic modulus drops dramatically and the polymer becomes soft and rubbery [45, 46]. It is worth noting that the glass transition temperature for XPLE is from -130 to -80 ℃ and for EPR is -60 ℃ [47].

The change in the dimension and shape of solids due to temperature change is measured by coefficient of thermal expansion α ℃$^{-1}$. The thermal expansion is defined as the change in length with temperature for a material is presented as [34]:

$$\alpha_L = \frac{\Delta L}{L_0 \Delta T}, \tag{2.3}$$

where ΔL is the change in length in mm, L_0 is the initial length in mm and ΔT is the temperature change in ℃. The temperature change does not affect the length only, rather it affects all the dimensions of a material, which results in change in the volume. The change in volume of an isotropic material when temperature changes can be calculated using:

$$\alpha_v = 3\alpha_L. \tag{2.4}$$

Coefficient of thermal expansion is a function of temperature. Usually it is presented as a constant but this is only valid for a particular temperature range. In general, polymers and elastomers have a coefficient of thermal expansion higher than metals by a factor of ten. The high thermal expansion coefficient of polymers indicates that high thermal stress could be developed especially when they are restricted and subsequently heated [48].

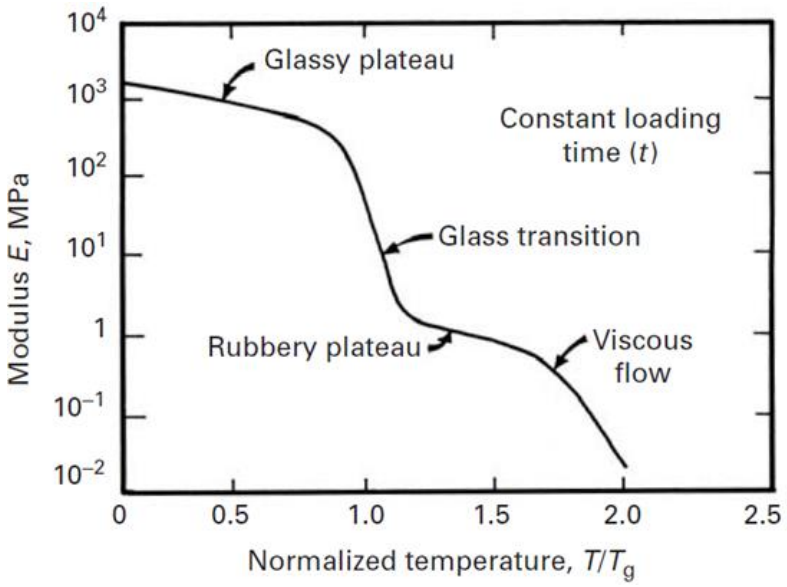

Figure 2.10: variation in the elastic modulus of a polymer with temperature [45].

Thermal stresses are linked to the coefficient of thermal expansion, elastic modulus of the material and temperature change by [48]:

$$\sigma = \alpha E \Delta T. \tag{2.5}$$

Cables should be designed to handle thermal stresses developed from insulating materials during heating otherwise it will cause radial stress on the sheath [48].

2.5 Thermal Modelling of Cables and Joints

In order to determine the temperature distribution in cable and joints, the heat transfer equation of thermal conduction should be solved [49].

$$\rho C_p \frac{\partial T}{\partial t} = \nabla.(k \nabla T) + Q, \tag{2.21}$$

where ρ is the mass density (kg. m^{-3}), C_p the specific heat capacity (J. kg^{-1}. K^{-1}), T the absolute temperature (K), k the thermal conductivity (W. m^{-1}. K^{-1}), and Q is the heat source (W.m^{-3}). It should be noted that under steady state, the term on the left side of equation 2.21

equals zero. Based on the structure and installation conditions of the cable or joint, the sources of heat inside the cable system can be identified. Losses generated within a power cable can be divided into current dependent losses and voltage dependent losses [8, 50]. The current dependent losses include the heat developed in the metallic components of the cable. The conductor, sheath and armour losses are all current dependent losses. The contribution of conductor losses to the total losses within the cable is the largest. To calculate the heat source presented by the conductor, sheath and armour losses per unit length the following equations are used [8, 50]:

$$W_c = I_c^2 R_{ac} \tag{2.22}$$

$$W_s = \lambda_s W_c \tag{2.23}$$

$$W_a = \lambda_a W_c, \tag{2.24}$$

where I_c is the current and λ_s, λ_a are the sheath loss factor and armour loss factor respectively. R_{ac} is the AC resistance of the conductor per unit length at its maximum operating temperature and it is calculated using the following equation [8, 50]:

$$R_{ac} = R_{dc}\left(1 + y_s + y_p\right), \tag{2.25}$$

where R_{dc} is the DC resistance at maximum temperature ($\Omega.m^{-1}$), y_s is the skin effect factor and y_p is the proximity effect factor. The dc resistance of the conductor is given by [8, 50]:

$$R_{dc} = R_0\left(1 + \alpha_{20}(\theta - 20)\right), \tag{2.26}$$

where R_0 is DC resistance of the conductor at 20˚C, α_{20} is the constant mass temperature coefficient for the conductor at 20˚C (°C^{-1}) and θ is the cable conductor operating temperature in ˚C. It should be noted that, the DC resistance depends on conductor size, material resistivity and temperature. However, AC resistance considers more factors such as proximity and skin effects. Both effects rely on the current passing through the conductor, operating frequency and magnetic fields of any multiple conductors installed alongside. To elaborate more, the skin effect is a phenomena that occurs due to self-inductance which causes an enhancement to the current density at the outer surface of the conductor. While proximity effect results from mutual inductance between conductors of adjacent phases and it causes the current densities on the sides facing each other to decrease and those on the remote sides to increase, due to the difference in the magnetic flux densities.

The voltage dependent losses are represented by the dielectric losses. Due to the energy storage ability of the insulating material in the cable when it is subjected to alternating voltage, the dielectric losses are developed. The cable will behave like a capacitor and the work needed to charge this capacitor is known as the dielectric losses. The dielectric losses are calculated using the following equation [8, 50]:

$$W_{dielec} = 2\pi f C_{el} U_0^2 tan\delta = \frac{U_0^2}{R_i} , \tag{2.30}$$

with f being the system frequency, C_{el} is the electrical capacitance of the cable, U_0 is the phase to ground voltage and $tan\delta$ is the dielectric loss factor.

Once the sources of heat inside the cable are calculated, the temperature rise of cable conductor above the ambient temperature can be easily determined using [8, 50]:

$$\begin{aligned}\Delta\theta = {} & (W_c + 0.5W_{dielec})T_1 + [W_c(1+\lambda_1) + W_{dielec}]nT_2 \\ & + [W_c(1+\lambda_1+\lambda_2) + W_{dielec}]n(T_3 + T_4),\end{aligned} \tag{2.31}$$

where T_1,T_2,T_3 and T_4 are the thermal resistances. T_1 represents the thermal per unit length between one conductor and the sheath ($K \cdot m \cdot W^{-1}$), T_2 is the thermal resistance per unit length of the bedding between sheath and armour ($K \cdot m \cdot W^{-1}$), T_3 is the thermal resistance per unit length of the outer cover of the cable ($K \cdot m \cdot W^{-1}$) and T_4 is the thermal resistance per unit length between the cable surface and surrounding environment [8, 50]. Different papers have discussed modified approaches to calculate T_2 more accurately than the one adopted in IEC 60287 for three core SL-type (Separate Lead) [51-53]. In addition, the calculation of T_4 for cables installed in free air is discussed in [54], where a new model to determine this thermal resistance in free air is presented. In this work, the equations and methods used are based on IEC 60287. Using IEC standard approach is satisfactory since studying the loss generation in depth is out of the scope of this research. Generally the interest here is in the overall response of the system.

2.6 Mechanical modelling

In this section, the governing equations and the assumptions that determine how the model is simplified from a three dimensional object to a two dimensional model are presented. In addition, the principal stresses developed in a thick cylinder subjected to internal pressure are defined.

2.6.1 Governing Equations

When objects are deformed, the distribution of stress and strain can be obtained by finding a solution to the basic equations of the theory of elasticity. The equations that govern a solid object's deformation are the equations of equilibrium, strain-displacement relations and strain-stress relations. The equation of equilibrium is based on the principle of conservation of linear momentum which states that the rate of change of the total momentum of a closed system equals to the combination of all the external forces acting on the body. More specifically, in case the object is deformed, internal forces will be generated in the material. These forces per area are defined as stresses. The internal forces which are expressed as stresses should together with external and inertial forces be in balance based on Newton's second law. Now the momentum balance equation based on Newton's second law can be expressed as [55-57]:

$$\nabla \cdot \boldsymbol{\sigma} + \boldsymbol{F_v} = \rho \frac{\partial^2 \boldsymbol{u}}{\partial t^2}, \tag{2.32}$$

where $\boldsymbol{F_v}$ is body force per unit volume, $\boldsymbol{\sigma}$ is the stress tensor, ρ is the mass density and $\boldsymbol{u}$ is the displacement field. The first term ($\nabla \cdot \boldsymbol{\sigma}$) in equation (2.32) represents the internal forces generated due to deformation. While $\boldsymbol{F}$ is the external applied force. The strain displacement equation is expressed as [55-57]:

$$\boldsymbol{\epsilon} = \boldsymbol{\nabla_S u}, \tag{2.33}$$

where $\boldsymbol{\epsilon}$ is strain and $\boldsymbol{\nabla_S}$ is a gradient matrix operator. According to Hooke's law, the stress-strain relation is expressed by [55-57]:

$$\boldsymbol{\sigma} = \boldsymbol{E}\epsilon, \tag{2.34}$$

where $\boldsymbol{E}$ is the stiffness matrix which depends on the material properties and whether plane stress or plane strain assumption is adopted.

2.6.2 Plane Stress versus Plane Strain Assumptions

When dealing with deformation problems there are certain assumptions that could be used to reduce the complexity of the problem. Plane stress is a state of stress in which the normal stress and the shear stress directed perpendicular to the plane are assumed to be zero namely

(σ_z,τ_{xz} and τ_{yz}=0). In general plane stress is considered when objects have one dimension that is extremely small compared to the other two dimensions (e.g. rings or extremely long cables without end constraints). However, if objects have one dimension extremely large compared with the other (e.g. extremely long cables with constrained ends) or structures that are constrained at its ends, then plane strain can be assumed. Plane strain is that state of strain where the strain normal to the xy plane ϵ_z and shear strains γ_{xz} and γ_{yz} are considered to be zero. The stress-strain relationship in both cases are listed below and table summarizes the way to convert from plane stress to plane strain and vice versa [56, 57].

Plane stress:

The stress relations are expressed in polar coordinates form as:

$$\sigma_r = \frac{E}{1-v^2}[\epsilon_r + v\epsilon_\theta] \tag{2.35}$$

$$\sigma_\theta = \frac{E}{1-v^2}[\epsilon_\theta + v\epsilon_r] \tag{2.36}$$

$$\sigma_z = 0. \tag{2.37}$$

$$\epsilon_z = \frac{-1}{1-v}[v(\epsilon_r + \epsilon_\theta)] \tag{2.38}$$

Plane strain:

The stress and strain relation in polar coordinates form are given as:

$$\sigma_r = \frac{E}{(1+v)(1-2v)}[(1-v)\epsilon_r + v\epsilon_\theta] \tag{2.39}$$

$$\sigma_\theta = \frac{E}{(1+v)(1-2v)}[(1-v)\epsilon_\theta + v\epsilon_r] \tag{2.40}$$

$$\sigma_z = \frac{vE}{(1+v)(1-2v)}[\epsilon_r + \epsilon_\theta] \tag{2.41}$$

$$\epsilon_z = 0 \tag{2.42}$$

When comparing the equations of plane stress and plane strain, it can be noticed that each of the plane strain equations can be converted into its corresponding plane stress equation and vice versa by changing the material parameters as listed in Table 2.2.

Table.2.2. Transformation between Plane Stress and Plane Strain Solutions [56, 57].

Solution	To transform to	*E* is Replaced by:	*v* is Replaced by:
Plane stress	Plane strain	$\frac{E}{1-v^2}$	$\frac{v}{1-v}$
Plane strain	Plane Stress	$\frac{1+2v}{(1+v)^2}E$	$\frac{v}{1+v}$

2.6.3 Principal Stresses in a Thick Wall Cylinder

In case a joint tube is considered as a thick circular cylinder subjected to an internal pressure, then three types of principal stresses are generated: radial stress σ_r, hoop or circumferential σ_θ and axial or longitudinal stress σ_z as illustrated in Figure 2.11.

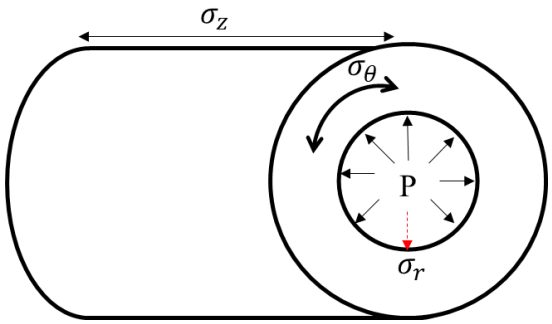

Figure 2.11: Stresses Developed in a Thick Cylinder [58].

Principal stress is defined to be the maximum value of the normal stress at the point, which act on plane on which the shear stress is zero [58]. Radial stress is the stress developed from the pressure difference across the wall of the cylinder. In general radial stress is negative indicating that it is compressive stress. Hoop stress or tangential stress is the stress developed due to the pressure difference between the inner and outer surface of the cylinder, which tend to separate or press the structure along the axial planes or (diameter planes), creating two cylindrical half shells [58]. It is worth noting that the circumferential direction and tangential direction have the same meaning. Therefore, hoop stress can be termed as circumferential or tangential stress. Axial or longitudinal stress is developed from the pressure employed on the closures. Furthermore, axial or longitudinal strain ϵ_z can be either

zero or constant based on the constraint and load conditions at the end of the body (clamped ends or free ends) [58].

2.7 Interface Parameters

When studying interfaces, there are parameters that influence the initial or short-term breakdown strength of the interface and long-term aging properties. The short-term and long parameters are summarized in the Table 2.3.

Table 2.3: Short and long term parameters affecting the performance of interface [17].

Initial/Short-term Breakdown Strength	Long-term Performance of Interfaces in Cable Accessories
1. Smoothness of the surface 2. Contact Pressure 3. Lubricant 4. Electrical field distribution 5. Temperature and Temperature change 6. Quality of accessory installation	1. Migration of the lubricant 2. Movements in the interface 3. Reduction of the interface pressure due to relaxation of materials 4. Electrical aging of interfaces

The electrical breakdown at the interface is influenced by a combination of different parameters. Smoothness of the surface, contact pressure, type of lubricant in the interface, electric field distribution, quality of installation and temperature changes are all factors should be taken into account during the design of interfaces [17, 59]. In this work, the interest will be more on the short term effects. More particularly, the effect of interface pressure, temperature changes and insulation temperature properties on the mechanical stability of the interface. From an electrical point of view, at the interface the electric field has two components, normal and parallel to the interface as shown in Figure 2.12. The parallel or tangential component is the most critical component [17, 59].

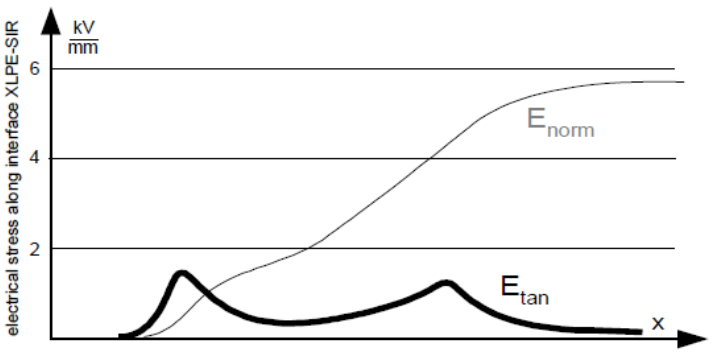

Figure 2.12: Electric field patterns along the interface of a cable joint [17].

Although, the tangential component is much lower than the dielectric strength of the bulk insulation, defects at the interface (such as micro-cracks, cavities and contaminations) enhance the local electrical field. This enhancement can lead to electrical treeing and partial discharge initiation. Moreover, if the electrical stress is employed parallel to the interface, the longitudinal breakdown strength is low. Loss of interface pressure between insulating materials should be avoided in practice to make sure that the electric field does not cause any breakdown in the insulation. When interface pressure is low, micro air gaps at the interface get larger and the chances of triggering partial discharge is higher. In the literature there is an agreement that there is a strong connection between the interface pressure and electrical breakdown strength at interfaces.

2.8 Interface Pressure and Electrical Breakdown Strength

As illustrated in Figure 2.13 the electrical breakdown strength is improved along with the increase of interface pressure.

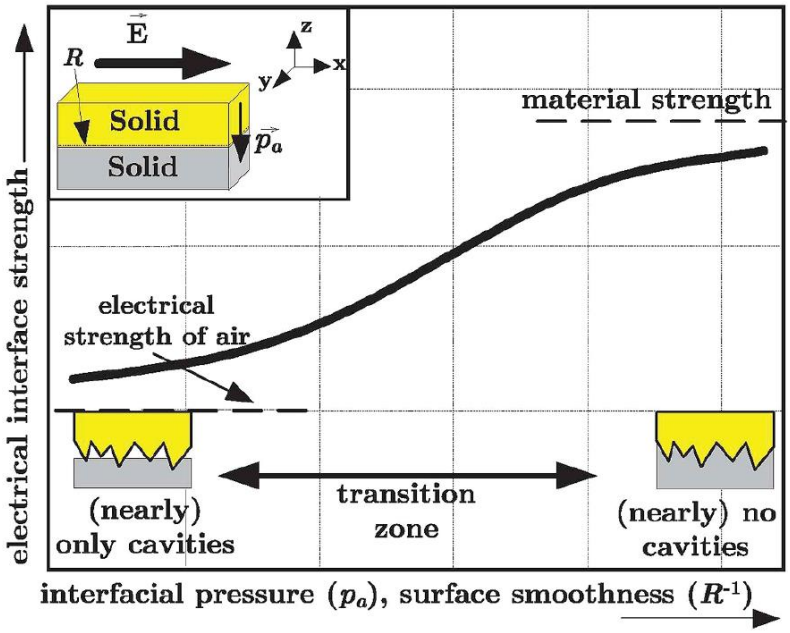

Figure 2.13: Electrical interface strength vs. interface pressure and surface smoothness [17].

However further increase of interface pressure tends to saturate the breakdown strength [60]. The graph also shows that the breakdown strength of the interface is higher than air and lower than the bulk of solid insulating material. This relation was confirmed and validated experimentally and theoretically. Different types of solid-solid interfaces were studied under

AC and DC excitation. It was found that electrical breakdown strength at the interface is improved with increasing the applied pressure [62-64]. Measurements of breakdown voltage and pressure at interfaces of a field aged cable joints were conducted. It was concluded in [64] that aging could lead to a drop in interface pressure causing a reduction in dielectric strength. In another study, it was found that that increasing the interface pressure from 20 kPa to 300 kPa for XLPE-SiR samples will increase the initial discharge voltage by a factor of 1.7 [65]. Using image processing, the effect of interface pressure on interface discharge and tracking failure at the interface was investigated [66]. It was noticed in [66] that the propagation of discharges were limited and the tracking failure were delayed at interfaces of XLPE-SIR samples with increasing interface pressure.

It was found in [67-69] experimentally and theoretically that the breakdown strength of insulating materials is affected significantly by the elastic modulus. This suggests that there is a close relationship between breakdown strength and mechanical properties. In [67], an analytical relationship to approximate the interfacial tracking resistance of polymers was developed. The model shows that breakdown strength is linearly proportional to the fourth root of Young's modulus. Based on contact theory, a model was established to study the effect of surface roughness, applied pressure and elastic modulus on the breakdown strength of interfaces made of silicone rubber and XLPE [68, 69]. Breakdown tests were performed to confirm the model results. It was shown that breakdown strength is improved significantly in the presence of a softer material (lower Young's modulus) while increasing the applied pressure. This enhancement in the breakdown strength was explained by the smaller voids that will result in the case of increasing the applied pressure when a softer material is used. Although the electrical tracking resistance is improved with a stiffer material, the local field enhancements because of discharge cavities is also increased considerably. As a result, it is noticed that the breakdown strength is reduced with enhancing the elastic modulus. This is attributed to the increase in cavity dimension and thus a smaller contact area [69].

The mechanical stresses at the interface influence electrical degradation mechanisms. Electrical treeing is a pre-breakdown phenomena that is one of the main causes of failure and degradation in insulation [70, 71]. Treeing can happen and progress by partial discharge activity when the branches are being developed [70, 71]. It is known that electrical tree propagation is affected by mechanical stresses. In a study to explore the effect of mechanical stresses on electrical treeing, different types of insulation samples were subjected to bending as illustrated in the Figure 2.14. It was noticed that, the tree growth is accelerated in the tensile region and is decelerated in the compressive part [72]. The effect of mechanical stress

on electrical tree initiation and growth in silicone rubber and EPDM samples was studied [73, 74]. It is observed that increasing the tensile stresses will make the electrical tree structure more dense and packed. The damaged area was larger as the tensile stress is increased. Under compressive stresses, the damaged area was smaller and the electrical tree structure was sparse. It is believed that the compressive stress increases the cohesion strength and therefore restrains the propagation of electrical trees [73, 74]. In [75], it is observed that fast propagation rates of electrical trees were noticed in elastomers that suffered from accumulated strain. Moreover, a material's ability to withstand crack propagation is linked to tree propagation and growth.

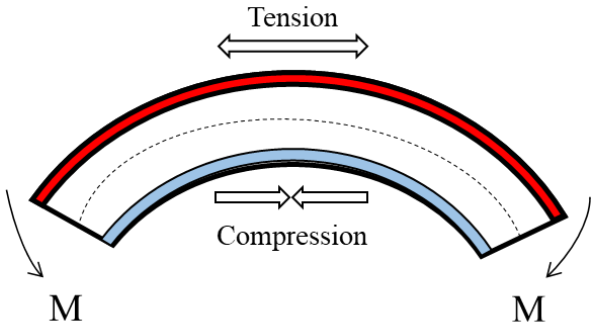

Figure 2.14: Samples subjected to bending stress [72].

In addition, if the mechanical properties of the insulating material are degraded, the resistance of the material to electrical tree growth is decreased. It was demonstrated that the tree inception time was less in a material with a lower tensile strength [76]. Moreover, it is suggested that the effect of temperature on the initiation and progress of the electrical tree is mechanically related [76]. There is a pronounced decrease in the tensile strength, elastic modulus and fracture toughness as the temperature is increased. At evaluated temperatures, the material's resistance to crack propagation becomes weaker. As a result, the initiation and growth of electrical trees become easier. The behaviour of electrical trees in XLPE samples at high temperatures was examined in [77]. The time needed to initiate the tree was reduced as the temperature increased. However, the effect of increasing temperature on tree growth time was minimal. It was concluded in [77] that the reduction in tree initiation time at higher temperatures is associated with the decrease in the threshold energy required to cause damage.

2.9 Types of Interfaces & Insulating Materials

When cable joints are installed, interfaces between different insulating materials are established. In cable accessories, interfaces are formed between two different insulating materials. Interfaces could be between rubber insulating body and cable insulation or between stress cone and epoxy body or between adaptor sleeve and joint body. Some of insulating materials that are part of these interfaces are Cross linked polyethylene (XLPE), Silicone rubber (SiR), Ethylene Propylene Rubber (EPR) and Ethylene Propylene Diene Terpolymer (EPDM) [15]. The fact that interfaces consist of different insulating materials make it less resistant to electrical stress than uniform insulation. Moreover, some accessories are assembled on site which increases the risk of having low electrical strength at the interface compared to fully factory made products [58]. Interfaces are the weakest region in a cable accessory but at the same time cannot be avoided. There are different types of interfaces inside a cable joint as shown in Figure 2.15. Electric field simulation of a cable joint is presented in the appendix.

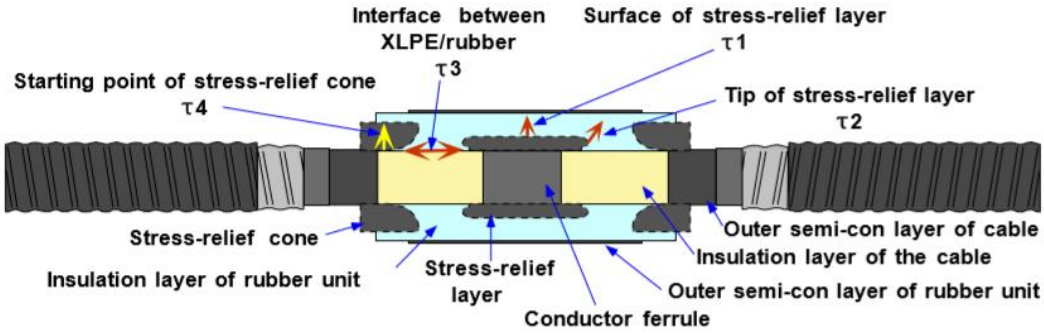

Figure 2.15: Interfaces inside Cold shrinkable joint for 110 kV XLPE Cable [78].

The four main critical interfaces inside a cold shrinkable joint are [78, 79]:

1. Interface between Cable insulation (XLPE) and Joint insulation (SiR).
2. Tip of the central (electrode) stress relief layer (semiconducting SiR).
3. Starting point of the stress relief cone.
4. Interface between the central (electrode) stress relief layer (semiconducting SiR) and joint insulation (SiR).

The structure of a joint tube consists of three layers as shown in Figure 2.16. The outer shield and the inner deflector are made of semiconducting rubber [80]. The main insulation is made of insulation rubber. The two most common materials used are SiR and EPDM.

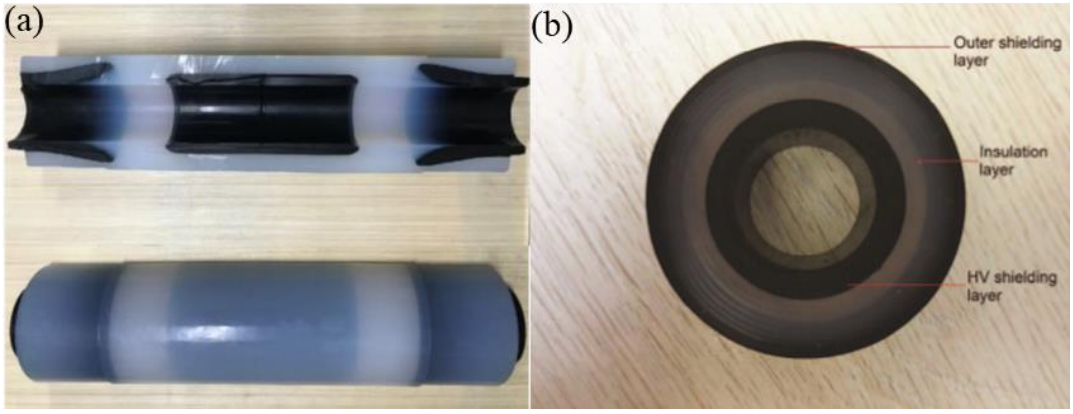

Figure 2.16: a) Joint tube [81]. b) Cross section of a joint tube [80].

Silicone rubber is a rubber that has an inorganic main backbone chain of Si-O bond called silicone-Oxygen (polysiloxane) [82, 83]. The Si-O connection has a higher bonding energy than C-O and C-C bonding energies by almost 30% [82, 83]. This will result in an insulating material that has a better mechanical properties when compared to EPR and EPDM [83]. Table 2.4 and Table 2.5 list various properties of silicone rubber, EPR and EPDM. Silicone rubber is composed of a base polymer, reinforcing and non-reinforcing fillers, special additives (such as processing acids, heat aging additives and colour pigments) and curing agents.

Table 2.4: Comparison between Silicone rubber and EPR properties [83-85].

Property	**Silicone Rubber (SiR)**	**EPR**
Ultimate elongation	790%	750%
Hardness (A)	30-40	60
Tear strength (A) (N/mm)	21.5	11.8
Permanent elongation set at 100%	2.6%	32.4%

Table 2.5: EPDM and Silicone rubber properties [13].

Property	**Silicone Rubber (SiR)**	**EPDM**
Chemical Structure	O-Si chains as basic	C-chain as basic
Elasticity (MPa)	1-2	2-4
Dielectric strength (kV/mm)	25	20
Service Temperature (°C)	-50 to +180	-40 to +100

The outer shield and inner deflectors are made of carbon black filled silicone rubber. The mechanical and electrical properties of the rubber can be reinforced by adding carbon black. Semi-conductive silicone rubber can be made by adding conductive filler such as carbon

black. Adding carbon black will increase hardness, elastic modulus, tensile and tear strength and fatigue of unfilled silicone rubber. The improved properties will depend on the loading level of carbon black. Normally the concentration of these fillers is selected such that it will result in a dielectric loss factor tanδ of 0.1 and a relative permittivity of 20 (higher than XLPE by 10 times) [84]. Mechanically the inner deflectors used would be stiffer than the main insulation by 30% [29]. Common values for tensile strength of silicon rubber are in range of 5MPa to 12 MPa. A higher interface pressure should be maintained at the points where it is expected to be under high electric stress.

2.10 Interface Pressure Parameters

The interface pressure can be divided into initial interface pressure and changes in interface pressure. Initial interface pressure is defined as the pressure developed as soon as the pre-molded rubber unit is installed on the cable. The change in interface pressure is the variation in interface pressure during operation. The four main parameters that affect the initial interface pressure as illustrated in Figure 2.17 are rubber elastic modulus, expansion ratio, rubber thickness and the condition of the cable (e.g. Residual stress). Several factors could influence the changes in interface pressure, including relief of elasticity of rubber, temperature, thermal cycling, thermo-mechanical forces and mechanical properties of materials [17].

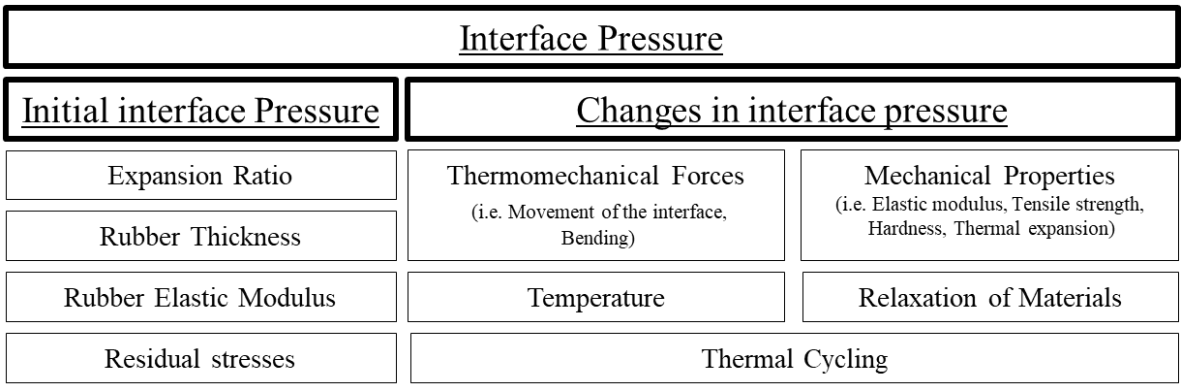

Figure 2.17: Parameters having an influence on initial interface pressure and its change [17].

In the following sub sections, the factors that affect the initial interface pressure are discussed. In addition, the main parameters that affect the changes in interface pressure are presented.

2.10.1 Initial Interface Pressure

Usually, to accomplish the necessary interface pressure two different approaches have proven to be appropriate [17]:

1. A pressure device composed of springs and pressing elements is used to apply an external mechanical force. This approach is utilized in the inner cone model of composite joints or dry type termination.
2. The elasticity of the rubber body is used when expanded on the cable insulation. This approach is utilized in slip on joints and stress cones. It is recommended that the expansion ratio should be in range of 5 to 50% [17]. Three main factors controls the interface pressure achieved by this method: elastic modulus of the applied rubbers, strain of the rubbers and wall thickness of the rubber.

As mentioned previously in section 2.2.1, there are two methods to install a pre-moulded cable joint namely cold shrink and push-pull [83, 86]. Cold shrinkable technique is attractive since its fast and easy. In cold shrinkable tubes, to ensure that the required interface pressure is achieved, manufacturers try to increase either the expansion ratio or using rubber with higher elastic modulus [86]. Two expansion rates should be clear; pre-expanding expansion rate and operation expansion rate. The pre-expanding expansion rate is the difference between the diameter of expanded joint body on the support tube and the original (initial) diameter of the joint body. On the other hand, the operation expansion rate is the difference between the outer diameter of cable insulation and the inner diameter of the pre-moulded joint body which is normally smaller than the outer diameter of cable as seen in Figure 2.18.

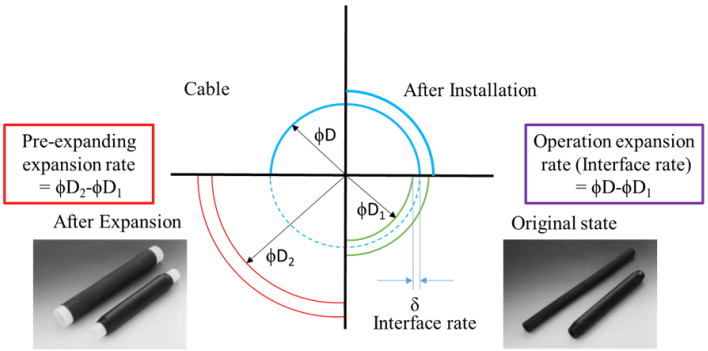

ϕD: Outside diameter of cable insulation
ϕD_1:Inner diameter of original cold-shrinkable tube to guarantee needed interference pressure with respect to cable insulation
ϕD_2:Inner diameter of expanded cold-shrinkable tube

Figure 2.18: Diameter changes pre and post installation using cold shrinking [84, 85].

Using a stiffer rubber (i.e. higher elastic modulus) does increase the pressure [81]. However, it was indicated in [78, 79] that the lower elasticity of silicone rubber shows a better performance at the interfaces even at low interface pressure. This conclusion matches the result found by [68, 69] where soft materials presented a higher interfacial breakdown strength. Moreover, increasing the elastic modulus could increase the tensile forces and if there is any defect at the interface, the insulation could be at risk especially at pre-expanding expansion rate [86].

Joint tubes for pre-moulded cable joint are made from silicon elastomers. They are manufactured in a specific number of sizes depending on the voltage level [87]. Each joint size covers a limited range of cable sizes. For example one joint tube can accommodate cables from 95 to 300 mm^2 [88]. Reducing the number of sizes needed for each voltage would be cost effective for manufacturers. In order to develop a standard product of stress cones and joint tubes the maximum and minimum expansion should be clear and well correlated with the minimum interface pressure [87]. The minimum interface pressure depends on the expansion ratio and elasticity of the material. Materials with high elastic modulus need low expansion ratio and vice versa. The maximum expansion ratio is limited by the materials elongation at break. It would be necessary to explore the operation temperature effect on the minimum and maximum expansion ratios [87]. Accordingly, more investigation is required to define an expansion ratio taking into account the elastic modulus, operating temperature and materials mechanical limit to assure electrical integrity of interfaces in cable accessories.

Residual stresses develop during manufacturing as the cable insulation cools and influence both mechanical and electrical properties of the cable. During cable installation or maintenance, they pose a challenge for cable joints because the insulation tends to shrink back in the axial direction on the conductor. Shrink back behaviour depends on the degassing stage which is one of the most common methods to reduce this effect. Moreover, it was found that there is no significant influence of residual mechanical stresses on insulation breakdown strength, tree inception voltage and tree propagation rate [89, 90]. In addition, the residual stress in the radial direction is compressive and has no impact on the strength of the cable because it is aligned in the electrical field direction. Residual stresses in the angular direction were measured for cables between 132 and 400 kV and it was concluded their values were low to cause any impact on cable performance [90].

2.10.2 Changes in Interface Pressure

During operation, there are parameters that change the initial interface pressure. In this sub section, the main factors affecting the initial interface pressure are discussed.

2.10.2.1 Stress Relaxation due to Material Relaxation

To maintain the necessary interface pressure between joint tube and cable insulation, a joint tube with high elastic modulus is used. During long–term use, relief of elasticity of rubber can occur. Therefore, critical low interface pressure should be prevented by making sure that the rubber will stabilize at a safe value. However, there are no reports in [16] about failures due to relief of elasticity of rubber. For pre operation, stress relaxation of rubber depends mainly on storage conditions (time and temperature) [88]. Stress decay in rubber is very slow and it may take several days to relax and stabilize. Furthermore, the relaxation time increases with temperature [88]. A test was performed to ensure the stability of interface pressure during operation [91]. The interface pressure was measured in a transition joint using sensors for 10 heat cycles to a maximum conductor temperature of 105℃. The results showed stable changes during the heat cycles [91]. The interface pressure was monitored in a 275kV prefabricated cable joint [92]. No extreme drop in pressure was found over 10 heat cycles. These results confirm with the findings in [93] where interface pressure was recorded for 10 heat cycles from -10℃ to 80℃. It is revealed that adequate pressure is kept with no excessive variation. In [94] the changes in interface pressure were measured in a sample device similar to a 275kV prefabricated straight cable joint for 10 heat cycles. It was noticed that at high/low temperature the interface pressure reached a set value at 10 cycles. Moreover, it was observed that the changes in interface pressure become smaller after the tenth cycle. However, the minimum interface pressure at low temperature did not reach the minimum threshold that was set by design. In addition, the device sample was disassembled after 100 days of heat cycling and there were no signs of deformation in the cable insulation [94]. The amount of reduction in the change of interface pressure was not mentioned. Moreover, the changes in interface pressure were measured using an experimental device not an actual joint which will make it difficult to reach a solid conclusion about these observations. In [78, 79] it was shown that drop will be very small. It was estimated that the interface pressure will drop by 20% from the initial interface pressure in a time scale of 30 years.

2.10.2.2 Thermomechanical Forces

Interface pressure can be affected by mechanical and thermomechanical forces. Thermomechanical forces are generated due to different thermal expansion of materials which can lead to movements at the interface or cable bending. Thermomechanical forces can contribute to the formation of cavities or gaps at the interface in a cable joint. Partial discharge can be initiated in these voids or gaps which can affect insulation. In a report for Electric Power Research Institute (EPRI) [29], the effect of bending and cable pull-through forces on interface pressure in a 138kV 760 mm^2 cable joint was investigated. It was found in [29] that bending the joint to 2 m bending radius has a minimum effect (6% reduction) on interface pressure. Furthermore, it was shown that the expansion ratio has the largest effect on interface pressure. Elastic modulus and thickness of joint insulation came in the second and third place respectively [29]. However, the pressure drop due to bending could be higher with smaller cross sections where the bending forces could have a higher impact. Moreover, in [29] all materials were modelled as being elastic. Metals could deform plastically under bending and insulating materials have nonlinear elastic behaviours that could influence the outcome. The joint simulated showed a withstand capability of 2000 N under longitudinal axial load before it starts to slip above this force. It was shown that a void will be formed at the tail of the stress cone at a load of 8000 N [29]. These calculated forces could be less with higher friction coefficients. Furthermore, the thermo-mechanical forces in cables are significantly affected by the cable type, cable construction, current loading, operating temperature and installation method. The rate of expansion of the individual materials of the cable joint system is influenced by the friction between these materials and by the cable joint and surrounding soil. In a thermal cycling response test, the cable was heated from ambient up to 90 ℃ for 20 cycles [25]. It was concluded that the maximum force happens in the first load cycle and it lowers as the number of cycles increases [25, 28].

In an attempt to determine the effect of bending on the interface pressure. A model based on hyper-elastic material was developed using FEM simulation to determine the change in interface pressure [96]. A formula to calculate radial deformation before and after bending was proposed. It was found that interface pressure in the middle part of the upper surface of the joint will increase and at both ends will decrease. However, in the formula proposed the elastic modulus of silicone rubber and semiconducting rubber were considered as the same. The difference between the two materials elasticity can reach up 30% [29]. Moreover, friction was not considered.

In a report of CIGRE working group dealing with mechanical forces in large conductor cross section XLPE cable, it is recommended that before installation of the joint, the connected cables are snaked in an ‘S’ pattern [97]. This approach will mitigate the effect of mechanical forces on cable joints.

Clearly, thermo-mechanical forces have a significant impact on the changes of interface pressure although it is complicated to predict. There are different parameters that influence these generated forces such as cable design, way of installation, load and environmental conditions. These parameters should be taken into account during the design stage.

2.10.2.3 Temperature and Temperature Change

The resistance of insulating materials to deformation decreases with temperature [17]. At high temperature interfaces could be deformed due to thermomechanical stresses. The fact that many of the insulation properties (i.e. thermal expansion, elastic modulus, tensile strength) are temperature dependent makes the temperature a significant parameter. In addition, cable failures due to mechanical damage could occur at low temperatures. During cooling down materials shrink which might affect the interface pressure. Cable joints could be located in cold environments. As temperature decreases insulating materials become brittle and less flexible which represents a more critical condition for interfaces [98]. During operation, thermal expansion and contraction of cable and joint insulation happen due to thermal cycling caused by load current and ambient temperature changes, therefore the interface pressure changes accordingly. Temperature and temperature changes should be taken into account during the design process.

2.10.2.4 Mechanical Properties

Breakdown strength is affected by the mechanical properties of the materials such as elastic modulus, thermal expansion, tensile strength limits, and hardness [17]. The reliability of the interface is dependent on the right combination of insulating materials and their properties. Temperature has a strong pronounced impact on mechanical properties of insulating materials. The mechanical properties of XLPE and EPR were compared in [48, 99]. It was found that XLPE is very sensitive to temperature when compared with other insulating materials (i.e. EPR and silicon rubber). In a temperature range of 20°C to 150°C, the elastic modulus of XLPE changes by an order of magnitude higher than corresponding changes in EPR and SiR. The mechanical properties of XLPE changes with time and temperature at a

higher rate than EPR. This indicates that if XLPE is subjected to mechanical stress it will lose its mechanical strength faster than EPR only at high temperatures (above 80 °C). As temperature increases XLPE thermal expansion is 10 times higher than that of copper and aluminium [100, 101]. Moreover, rubber and rubber like materials (elastomers) have a coefficient of thermal expansion in a range of 2.5×10^{-4}-4.8×10^{-4} K^{-1}, which is a tenfold difference when compared to copper thermal expansion as an example 1.9×10^{-5} K^{-1} [36]. The high thermal expansion coefficient of rubber indicates that thermally induced stress in the rubber could be high, especially when rubber is restricted and subsequently heated. Measuring the modulus of elasticity of elastomers is not an easy task. It is common to describe the deformation behaviour of elastomers by means of defining the shore A hardness of the material. Joint insulation is often made of silicone rubber of shore hardness in the range of 30 shore A to 40 shore A [83]. This is equivalent to an elasticity in range of 1 to 2 MPa [36]. Semi-conductive materials are made of rubber loaded with carbon black filler, and this makes it stiffer than unfilled material. Mechanical properties of insulating materials and their effect on the stresses at the interface need more attention.

2.11 Are we calculating The Interface Pressure correctly?

Since the mechanical design of the interface affects its electrical strength in the cable joint, determining the minimum or maximum value of the interface pressure is useful in the design process. The design process will start by finding the minimum interface pressure needed. The relationship between electrical breakdown stress and the interface pressure at interfaces should be established. To do so, sample units of insulating materials used in the cable joint are placed in a way to form an interface similar to the ones found in a joint. Depending on the materials used in the cable joint, interfaces between XLPE and SiR or XLPE and EPR are developed. By applying a certain amount of mechanical pressure on the samples, different interface pressures is created. Then AC and impulse breakdown strength tests are performed on these model samples. A relationship between electrical breakdown stress and the interface pressure similar to the one shown in Figure 2.19 is created [92, 93, 94, 102].

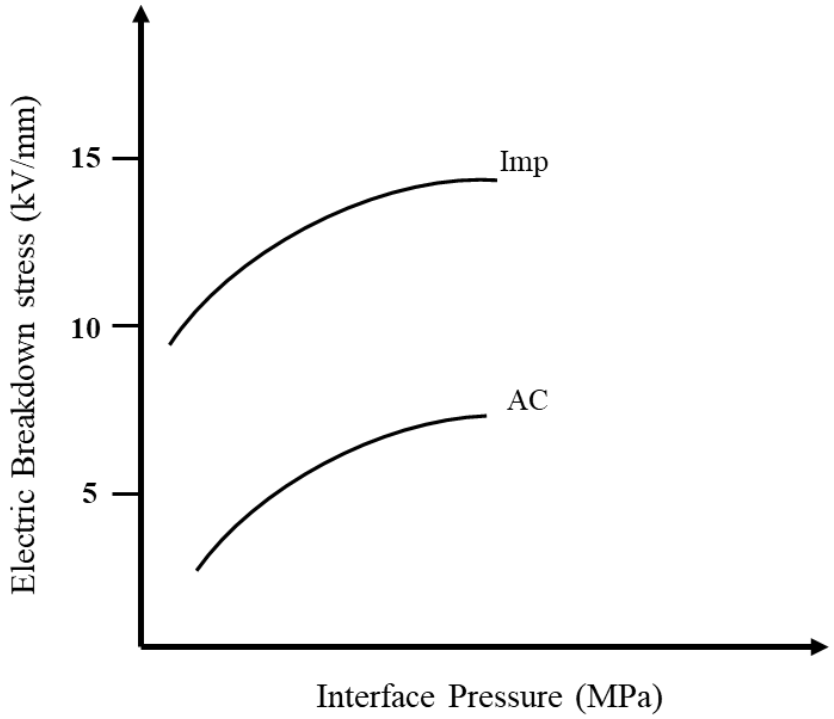

Figure 2.19: Relation between interface pressure and dielectric breakdown stress [102].

The minimum value of interface pressure should be at the point where the electric characteristics begin to saturate [102]. More specifically, it is the point, where further increasing the interface pressure will no longer improve the breakdown strength of the interface. After identifying the minimum value, the maximum value is set at either the allowable pressure of cable core during the heat cycle or at the pressure that could cause any deformation in the cable insulation at high temperature also known as pressure that cause the bamboo effect [81]. Then thermal cycling test is conducted to make sure that interface pressure does not exceed any of the chosen limits during expansion and contraction as illustrated in Figure 2.20.

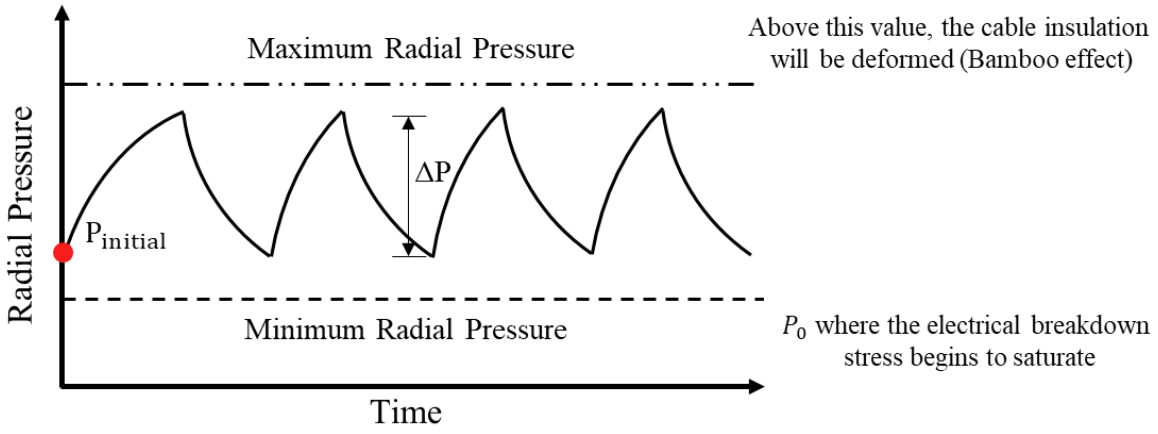

Figure 2.20: Interface pressure during thermal cycling showing the change interface pressure and maximum and minimum values.

Recently it was found that even at low interface pressure, interfaces between silicone rubber and XLPE show good interfacial breakdown strength [78, 79]. The electrical breakdown strength at the interface does not depend only on interface pressure. Surface roughness, elastic modulus, type of lubricant and temperature change are all factors that affect the breakdown strength at the interface. It is hard to set a minimum interface pressure from a simple test because different parameters are involved. There is no solid agreement on the interface pressure even in the same range of voltage. Designers have different minimum interfacial pressure depending on voltage level, materials used and joint type, leading to variation in the minimum radial interfacial pressure from 0.04 up to 1 MPa [29, 78, 79]. These limits are dealing only with radial interface pressure only. The circumferential (also known as hoop) stress limits are not mentioned, despite being critical in the long term performance of the joint. The internal stresses inside the joint tube are radial and hoop as shown in Figure 2.21. Assuring enough radial interfacial pressure is vital. However, if the hoop stresses exceed the tensile strength of material, cracks at the interface may be developed. During the design process of the interface, calculating the hoop stress is important as much as determining the radial stress.

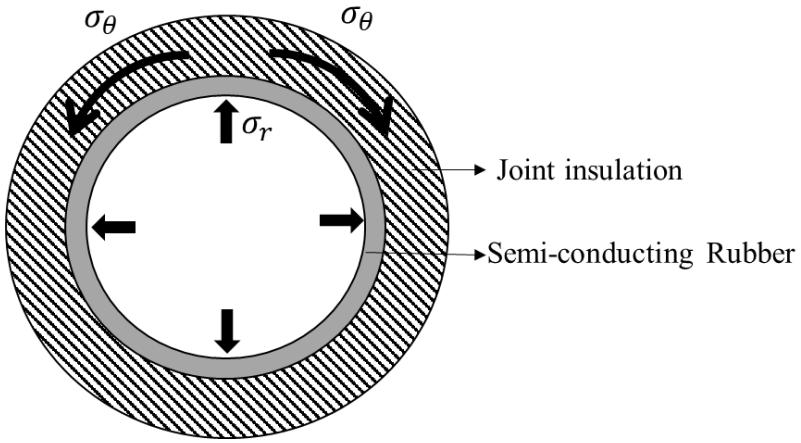

Figure 2.21: Decomposition of stress inside a joint tube [86].

In the literature, three main approaches have been used to determine interface pressure and its changes either by measurement or/and finite element method (FEM) or/and analytical solutions. In this section, a review of the main approaches is provided.

A. Measuring Interface Pressure: There are different methods used to measure the interface pressure and its changes. A number of studies have made measurements of the interface pressure experimentally using pressure sensors [78, 91-95]. In Table 2.6 a summary of thermal cycling tests performed to measure interface pressure and its change by pressure sensors. It is noticed that EPR interfaces have higher interface pressure compared to SIR interfaces. This can be explained due to the higher elastic modulus of EPR. However, installing a pressure sensor at the interface could damage the interface which may affect the reliability of the readings. Another approach for measuring pressure is to substitute the cable by an aluminium tube with a strain gauge, but this test model does not reflect the actual structure of the cable joint [103]. In [104] the authors proposed that air could be injected at different pressures into the installed cable joint. The pressure of air that is capable of lifting up the joint insulation is equal to the interface pressure. Nevertheless in these attempts, pressure is determined in sample units that are built to do the measurement. The sample units are similar to a cable joint but not an actual cable joint which could deviate from the real case.

Table 2.6. Measured Interface Pressure and its Change by Pressure sensor.

Reference	Number of thermal cycles	Temperature range (℃)	Voltage (kV)	Initial interface pressure (MPa)	Change in interface pressure (MPa)	Interface type
[78]	1	15-90 ℃	66	0.22	0.05	XLPE-SIR
[91]	10	20-105℃	154	0.5	0.6	XLPE- EPR
[92]	10	20-90 ℃	275	0.4	0.3	XLPE- EPR Epoxy- EPR
[93]	10	-10-80℃	154	0.15	0.2	XLPE- EPR Epoxy- EPR
[94]	10	20-90 ℃	275	0.4	0.3	XLPE- EPR
[95]	10	25-90 ℃	25	0.1	0.015	XLPE-SIR

B. Finite Element Method & analytical models: Models used to calculate initial interface pressure can be divided into two groups. Models based on linear elastic models (Hooke's law) [29, 85, 86, 104, 105, 106] and models based on nonlinear elastic models (hyper-elastic models) [96, 107, 108] as illustrated in Figure 2.22. Usually the nonlinear elastic models are solved using finite element method. A summary of the models based on linear elastic relations are listed below.

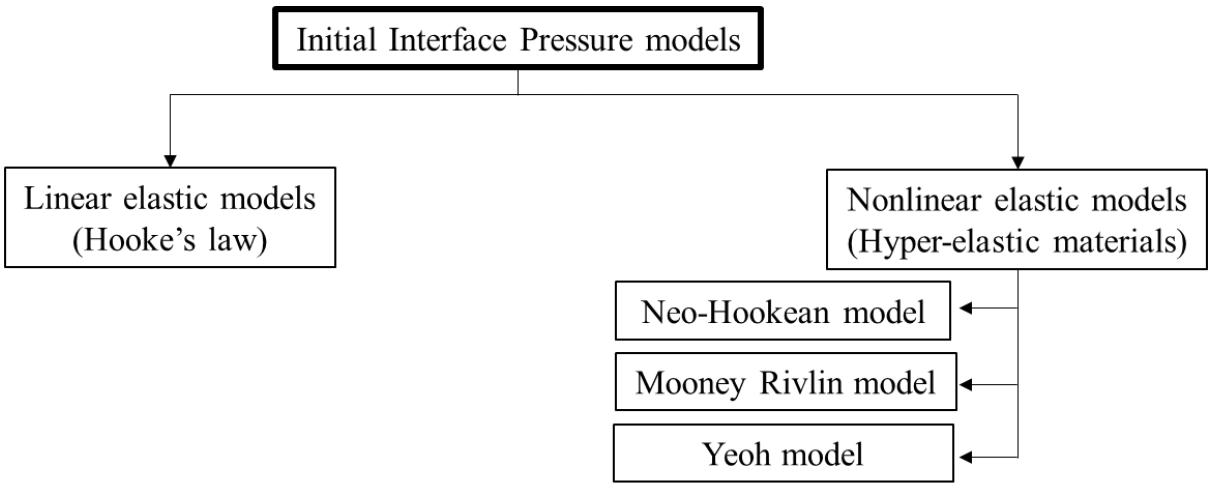

Figure 2.22: Models used to calculate initial interface pressure.

1. Linear Elastic Model 1 [83, 105]:

The interface pressure is calculated using the following equation:

$$P = \frac{(b^2 - a^2)}{(1-v)a^2 + (1+v)b^2}\frac{\delta}{a} \cdot E, \qquad (2.43)$$

where a is the inner radius of joint tube, b is the outer radius of joint tube, δ is the expansion ratio and E is the elastic modulus of joint insulation. This model is based on the assumption that the joint tube is a thick cylinder under an internal pressure as illustrated in Figure 2.23 [85, 105].

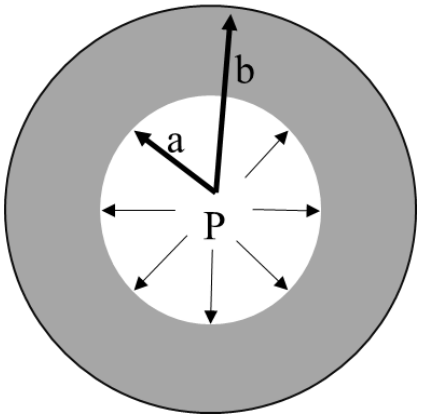

Figure 2.23: Model 1 Assumption to Calculate Interface Pressure.

It considers the cable conductor and its insulation as a one rigid object that causes the internal pressure. Based on this model the equation takes into account the properties of joint tube and it assumes that it is composed of one material.

2. Linear Elastic Model 2 [104]:

   Using this model, the cable structure is included as shown in Figure 2.24 and interface pressure is determined by:

$$P\left[\frac{1}{E_b}\left(\frac{R_1^2(1-v_1)+R_2^2(1+v_2)}{R_2^2-R_1^2}\right)+\frac{1}{E_a}\left(\frac{R_1^2(1-v_2)+R_0^2(1+v_2)}{R_1^2-R_0^2}\right)\right]=\frac{\delta}{2R_2}, \quad (2.44)$$

where R_0 is the conductor radius, R_1 is the cable insulation radius, R_2 is the Joint insulation radius, δ is the expansion ratio, E_a is the elastic modulus of power cable, E_b is the elastic modulus of joint insulation, v_1 is Poisson's ratio of power cable, v_2 is Poisson's ratio of the joint insulation.

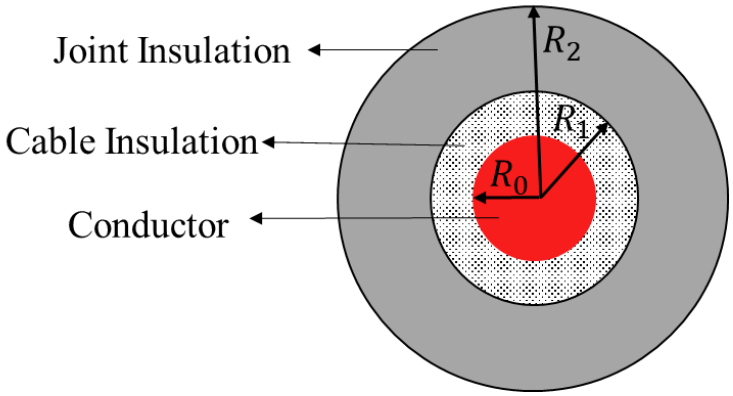

Figure 2.24: Cable Joint Based on Model 2.

The second model uses the equation used to calculate interface pressure in multilayer iron tubes [104]. In this model the elasticity of the cable is considered. A comparison between the two models shows that both models indicate that interface pressure is linearly proportional to expansion ratio. It is noticed that interface pressure values obtained from model 2 is higher than values of model 1. At 50.7% expansion ratio the difference is almost 1.3%. However, the first two models did account for the deformation in the joint tube. The joint tube will expand when it is subjected to an internal pressure as shown in Figure 2.25 where the inner radius and outer radius change. The wall thickness of the joint tube will be reduced and the length will be shorter. In an attempt to find a link between the pressure and the deformation, a third model was proposed [106].

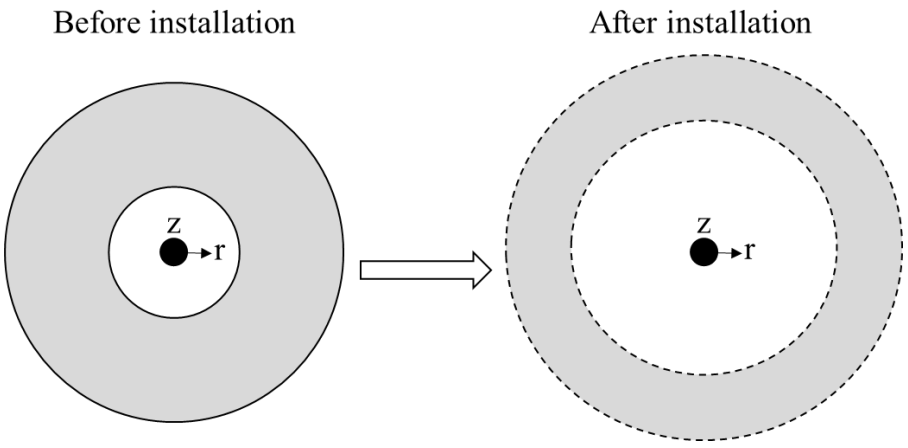

Figure 2.25: Deformation of joint tube cross section before and after installation [107].

3. Linear Elastic Model 3 [106]:

   This model calculates the interface pressure using the equation below which is based on the fact that the radius of the joint will change as shown in Figure 2.26:

$$P = \frac{E}{R_i}\left(\left(R_i - \frac{d}{d_0}R_{i0}\right)\ln\frac{R_{o0}}{R_{i0}} + \left(\frac{d}{d_0} - 1\right)d\right), \tag{2.45}$$

where R_{i0} is the initial inner radius of cold shrink tube, R_{o0} is the initial outer radius of cold shrink tube, d_0: initial thickness of cold shrink tube, R_i: working inner radius of cold shrink tube, R_o: working outer radius of cold shrink tube, d: working thickness of cold shrink tube, E: Elastic modulus of joint insulation.

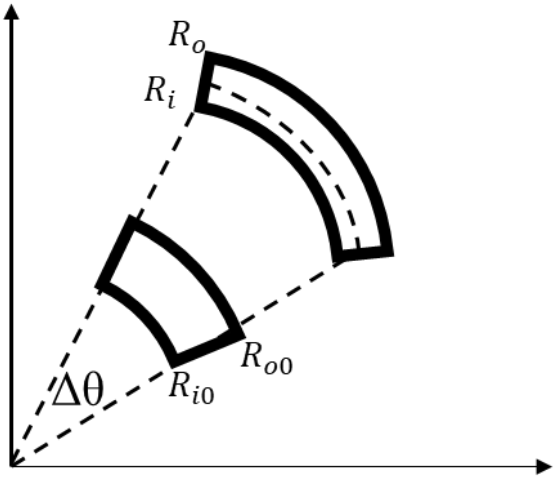

Figure 2.26: Model of Cold Shrinkable Joint [106].

The change in length was ignored. The method relied on measuring the deformations after installation then calculating the pressure. However, the calculation of deformations would be more useful before installation to know the expected pressure. To calculate the radial deformations, it was proposed that change in volume is zero and change in length is less than 1.5% so it can be ignored [87]. The cross section area of the joint tube is considered constant. The inner radius is given (i.e. the outer radius of cable insulation). Then, the new outer radius after deformation can be calculated [87]. In another study, the axial and radial deformations were calculated [109]. But, again all these calculations were based on the assumption that silicone rubber has a linear elastic behaviour.

Rubber have high values of bulk modulus *K* (1.5-2 GPa) and low shear modulus G in range of (0.5 to 2 MPa) which means that G<<*K*. As a result, the Poisson's ratio v is almost 0.499 ≈ 0.5 [36]. If the rubber is assumed to be totally incompressible then *v*=0.5 and for small strains the elastic behaviour can be described by a single elastic constant G. It is worth noting that when rubber is compressed almost no volume change is expected. Volume will change

only if the pressure were extremely high [87]. It is claimed that rubber has no constant elastic modulus because the stress strain relation is nonlinear. However, for small strains the stress-strain relation could be approximated by a linear relation. No clear benchmark exists for strains where the stress-strain relation can be estimated by a linear relation [36]. It has been indicated that for a material following the statistical theory for rubber elasticity, an experimental stress-strain data can be fitted by the best straight line yielding an elastic modulus that deviates from the exact elastic modulus at infinitesimal strain by an amount of the ε% where ε is the maximum strain in the experiment. In other words, for strain of 5% or 10% the error in approximating the elastic modulus would be in range of 5% or 10% depending the strain value [36]. Moreover, the outcomes of another experiment showed 5% deformation of silicon elastomer gaskets at a pressure of 10^9 Pa [87]. In high voltage cable accessories the mechanical stresses expected during normal operation is in range of MPa which is three orders of magnitude smaller than pressure in the later experiment. In case of large deformations (e.g. pre-expanding expansion ratio) the elastic behaviour of rubber can no longer be explained by a simple constant elastic modulus. Large elastic deformations can only be described by nonlinear elastic relationship. Material laws for hyper-elastic materials are commonly used to describe the nonlinear behaviour of rubber material. The difference between the linear based models and nonlinear based models are shown in Figure 2.27. The interface pressure values using the three linear based models and one of the nonlinear based models are compared [85, 96, 104, 105, 106]. It is noticed that the third linear based model is the closest to the non-linear based. This indicates that linear models fails to provide a good estimation for interface pressure, although it is mathematically simple.

Material laws for hyper-elastic materials are commonly used to describe the nonlinear behaviour of rubber material. Hyper-elastic material models that can be used to represent the stress-strain relationship. The authors in [108] modelled the stress-strain relation for silicon rubber and semi-conductive layers by Neo-Hookean model. Also, in [107] Mooney Rivlin model is used to improve the accuracy of the calculations. Neo-Hookean material model is only reliable and sufficient for material strain up to 30%. Miscalculation of the initial pressure could be the reason behind increasing joint insulation thickness or using materials with higher elastic modulus to reach the desired interface pressure. The calculation of the stresses inside the joint tube must take into account the non-linear behaviour of silicone rubber and semiconducting rubber. In addition, the calculation of initial radial and circumferential stresses are of equal importance. It was proposed that if the semi-conductive material is too stiff and it was expanded, high circumferential stress can be established at the

interface between the semi-conductive and joint insulation. In the next chapter, circumferential stress is calculated to check if it exceeds the strength of the insulation materials.

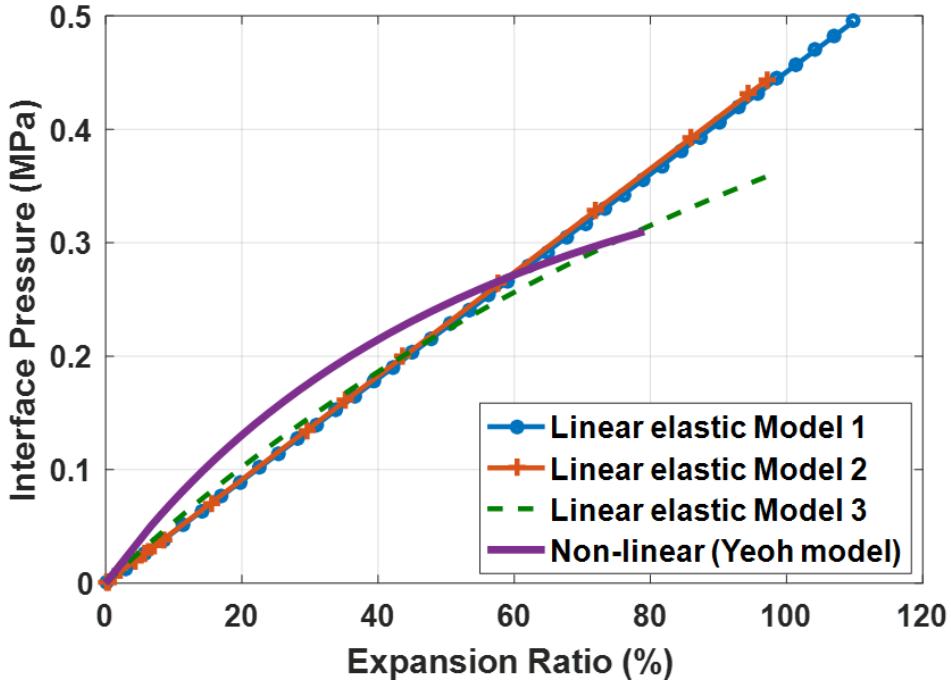

Figure 2.27: Comparison between the three linear models and Non-linear model (Yeoh model).

2.12 Reported Failures

Failures among 110kV and 220kV silicon rubber pre-moulded cable joints have been reported [86]. It was proposed that, high mechanical forces could trigger the initiation and propagation of electrical trees as shown in Figure 2.28. Microscopic cavities at the interface may be developed by mechanical forces where partial discharge could initiate and finally lead to insulation breakdown. High radial pressure at the interface is desirable. But, if the circumferential (hoop) stress is close to the tensile strength (50% of the tensile strength) of the insulation, micro-cracks can be developed [86]. If one of the insulating materials at the interface is too stiff (i.e. high elastic modulus) and it is expanded above a certain limit, this will pose high tensile stresses on the interface.

Moreover, joint and termination failures have led to multiple interruptions in a 380kV transmission circuit [110]. It is believed in [110] that the presence of impurities at the interface between the joint body and cable insulation have affected the interfacial pressure

between the two insulations initiating electrical trails on the insulation surface. The failures in the terminations were caused by a flashover between the stress cone and the epoxy-resin insulation. It is suggested that inadequate interface pressure between the stress cone and the insulator is the main cause of this failure. In the following section, the relation between interface pressure and electrical failures is explained [110].

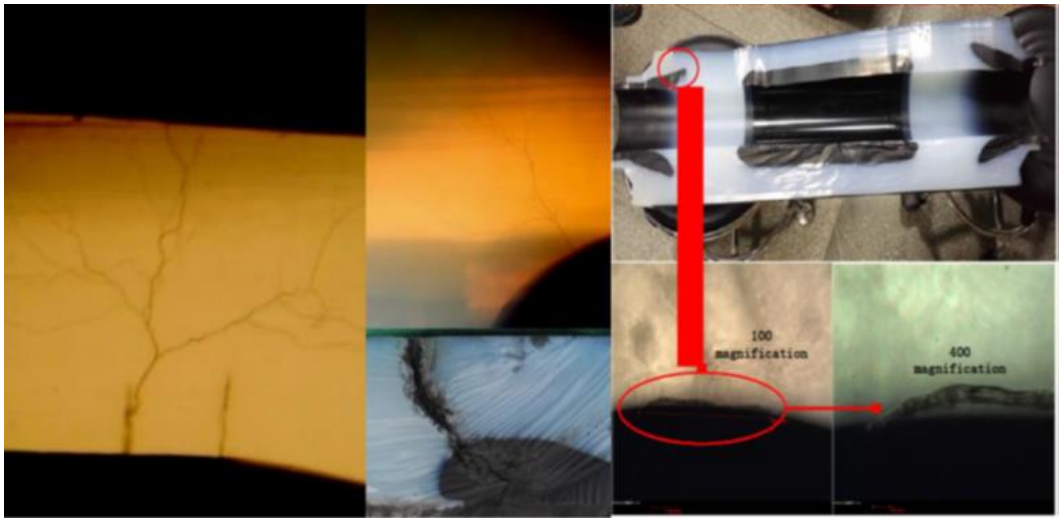

Figure 2.28: Breakdown paths for 220kV Silicon rubber pre-molded joints with microscopic defects [86].

There is a high possibility that these failures are mechanically driven [86]. The unclear connection between interface pressure and the insulation mechanical properties during the design stage, could lead to this type of defects. This belief is the motivation for this research. In IEEE standard 404 for Extruded and Laminated Dielectric shielded cable joints rated 2.5 to 500 kV, there is no clear link between interface pressure and insulation mechanical properties. Therefore, there is a need to fill this gap. The importance of considering insulation mechanical properties in the calculations is highlighted in chapters three and four.

2.13 Thermo-mechanical Stress in single and three core cables

Submarine power cables have been employed in offshore wind farms, offshore oil platforms, interconnection of islands and interconnection of power systems. The increased number of these projects has placed a high demand on submarine cables. Therefore, researchers have been motivated to try to ensure cable's reliability in future projects. One of the basic approaches to do so is to perform tests on these cable. All new cables undergo different types of tests to guarantee that the cable will operate as anticipated throughout its lifetime. Different tests are accomplished from the design phase up to the installation phase such as

prequalification tests, type and routine tests and tests after installation. Specifications for different tests are described in national and international standards. In the tests, cables are subjected to electrical, thermal and mechanical stresses similar to the stresses the cable encounters during service. The main aim of these tests is to identify any defect in the cable and to assure its ability to handle different stresses. Understanding thermo-mechanical stresses within the cable are fundamental to be able to test the cable's capability to manage these stresses.

Thermo-mechanical stresses within the cable are generated due to the interaction between the components of the cable of different materials. The difference in thermal expansion coefficients between the materials will establish mechanical stresses. Moreover, temperature distribution in the cable plays a key role in these stresses. The non-uniform distribution of temperature in a three core could develop a non-uniform distribution of mechanical stress. This non-uniform distribution of mechanical stress must be studied to assure that it is tolerated by the cable sheath and do not cause any malfunction in the cable. It is known that lead (Pb) sheath is a ductile material and during high cable loading, the sheath could yield, increasing the possibility of creating gaps or voids at the interface. Moreover, the dependency of insulation's mechanical properties on temperature is an important factor in determining these stresses. As temperature increases XLPE becomes soft and it has a high thermal expansion compared to other materials in the cable. All of these factors should be examined in cable testing. In this section, a literature review about thermo-mechanical stresses in single core and three core cables and its effect on cable sheath are presented.

2.13.1 Thermo-Mechanical Stresses in Single Core Cables

XLPE is a semi-crystalline polymer that undergoes significant change especially during in the temperature range between 90 to 130 ℃. In this temperature range, XLPE goes through a transition point where its elastic modulus drops by one order of magnitude. Moreover, this turning point is accompanied by a huge increase in XLPE's volume due to its high thermal expansion. A 15% increase in volume is expected when the cable is heated from 25 to 115 ℃, which will be translated into a mechanical pressure on the sheath [111].

In a study performed to investigate the thermomechanical performance of three concentric neutral distribution cable designs, it was found that neutral conductors could penetrate the semiconducting shields if it is exposed to sufficient mechanical stress [117]. It was

concluded that the penetration level will largely depend on the cable design and temperature. The level of penetration will be almost 100% in case of round neutral wires while very little damage was noticed in case of flat strap neutrals and no damage to the semicon in case of tape neutrals. In an experiment to investigate of effect temperature rise of XLPE cables subjected to emergency loading [118], it was concluded that the high thermal expansion of the insulation will create thermo-mechanical forces that will lead the copper strips to penetrate the insulation semiconductor layer at high temperature. This occurs after losing the mechanical strength of the insulation and semiconducting layer at 105 to 115℃. It is also noticed that flat-strap neutrals could buckle or twist at 130℃ emergency temperature. In other types of failure, the loosening of the semiconducting extruded shield away from the insulation was noted. It was concluded that this failure is related to the thermal expansion of the insulation and it does only happen during the cooling cycle [118]. The high thermal expansion of cable insulation in the radial direction while the cable is hot can fill or cover any separation that could occur. However, when the insulation cools down and goes back to initial position, these type of defects start to be visible.

In [119], cables with copper concentric wires and tapes were subjected to 202 cycles at conductor temperature of 130℃ and 145℃. No failures happened. Copper tapes did not cut into the insulation screen. Copper wire screen deformed the insulation shield by causing a small helical indentation. However, a very minor deformation was transmitted to the insulation and it did not affect the electrical behaviour of the cables tested. This is a different behaviour from the behaviour found by [118], this was explained due to the long lay of the wires in the shield.

In [100], it is believed that the penetration of the copper wire screen into the insulation semiconducting layer could be beneficial as it reduces the severity of the thermo-mechanical forces generated due high temperatures and different thermal expansions of cable components. In [120], EPR cable system was heated up to a range of 105℃ continuous service and 140℃ emergency operation, the outcome of the thermal tests was that the insulation was neither badly affected or distorted while exposed to the 140℃ test. Such stable behaviour is expected for an insulation such as EPR. Comparing EPR with XLPE, EPR undergoes no significant change in its elasticity and stays coherent. Furthermore, its thermal expansion is lower than XLPE's thermal expansion especially at high temperatures [121]. EPR has a volume thermal expansion that could reach 8% while XLPE 16% at the same temperature. In a recent study on medium voltage jacketed cables, it was observed that the encapsulated jacket reduces the pressure on the neutral (round wire and flat strap) and

limit its movement [121]. Therefore, the resulted deformations did not have any significant impact on the insulation. However, it was found that the deformations could be worse for unjacketed cables [122].

In some cable designs where non-metallic sheath is used, an additional metal shield is added to protect the cable from moisture. This metal shield is made of either copper, aluminium or lead (Pb) with an overlap seam. This type of design should be sealed in the overlap region with a hot melt adhesive, otherwise water can penetrate through the unsealed overlap. During load cycles, this overlap is expected to move due to temperature changes. The adhesive should be able to accommodate the expansion of the insulation and tolerate wide range of temperatures without losing their adhesive properties. The properties of the hot melt adhesive was investigated [123]. It was found that the adhesive should show a highly viscous liquid like behaviour at high temperatures to absorb mechanical forces. These cable designs managed to pass thermal loading tests, however there is a chance that the sheath does not fully return to its original dimensions after expanding during heating cycle because of losing the strength of the overlap seal [124]. If the adhesion force of the bond is decreased or fails due to delamination then rapid degradation of the insulation could occur if moisture managed to find its way to the insulation. Moreover, load cycling at higher temperature limits could cause a fracture or a split in the metal shield especially when it's used on large diameter power cables [124].

2.13.2 Thermo-mechanical Stress in Three-Core Cables

All of the above cases dealt with single core cable cases, but in three-core submarine cable, the core is subjected to higher internal thermo-mechanical stresses than single core cables since it is more restricted before heating. Cables connected to wind farms could stay unloaded for a while then be rapidly loaded to maximum rated load in a short time. The variation of the output power from high power production to low or no power production means that cables will heat and expand then cool and contract, more frequently. If the cables are severely load cycled this will increase the internal thermo-mechanical stresses. The ability of cable sheath to handle thermo-mechanical stress during operation should be tested.

During the electrical test of three core submarine cables, the test should represent the same kind of voltage stress that the cable would experience under service conditions. In the electrical test, the cable is exposed to 20 thermal cycles of 24 hours duration. The cycle

consists of an eight-hour period of full load current followed by 16-hours period of natural cooling [125]. However, based on CIGRE TB 490 only one cable core from a three-core cable or a single-core cable without armour may be exposed to the electrical test [126]. This does not represent accurately what happens during operational conditions since the tested core is highly concentric whereas cores in laid up cables may be more eccentric. Testing the complete cable with armour will expose the sheath in each core if not to the highest but at least to the closest value of thermomechanical stress that the sheath will face in service. As a result, the sheath will deform and the chances to notice possible defects in sheath integrity will increase. If one core is thermally cycled, stresses and deformations will be lower therefore; the chances to spot any problem will be lower.

Sheath must be able to withstand thermal stresses from other components in a three-core design, pressure from water depth and the stress from cyclic heating. Once the cable is loaded, the insulation will expand radially because of thermal expansion of the insulation and conductor. The sheath surrounding the insulation will be subjected to thermal stress and it will expand radially. This expansion will generate a circumferential strain in the sheath. By contrast, when the load current is reduced, the insulation and conductor will cool and shrink. The external pressure must be enough to force the lead sheath back to its initial condition and if it is too high, this pressure may lead to sheath collapse and buckling [125]. It is recommended that the cable should be able to withstand an external pressure not lower than 3.5 MPa [127]. The internal pressure should be kept above the external pressure at the deepest part of route. The contribution of cable insulation to sheath thermal stresses cannot be neglected.

Lead (Pb) is a common metal used for metallic sheaths due to its corrosion resistance and ease of manufacturing. The elastic modulus of lead is 20 GPa which is lower than that of other common metals (cast iron is 7 times stiffer; copper is 5.5 times stiffer; aluminium is 3.5 times stiffer). Alloy elements such as tin, calcium and tellurium are used with lead to improve long-term stability, creep and extrusion properties of lead sheaths. Lead and lead alloy are ductile materials and must be protected against mechanical stresses during manufacturing, cable transport, installation, operation and maintenance. The lead sheath is vulnerable to fatigue processes, vibration, repeated bends and mechanical loading. In addition, thermal cycling can cause recrystallization of the lead alloy (recrystallization temperature of pure lead happens in range of -50 to 50°C) leading to crystal boundary growth, which helps in developing micro-cracks and reduces its water tightness strength [8, 126].

Pure lead has yield stress of 5.5 MPa and lead alloy can have a yield stress of maximum of 66 MPa [132]. If the sheath used has a low yield stress, there is a possibility that the thermal stresses exceed the yield stress of the sheath. Then, the sheath will start to deform in the plastic region (irreversible deformation) increasing the chances of forming voids at the interface between the sheath and insulation. Moreover, radial compression during heating could cause damage to the semi-conducting screen when compressed on the conductor and metallic sheath. This failure type must be considered when determining the possible threats during heat cycles [136].

In the following section, the difference between dynamic and quasi-static analysis is discussed, which is useful especially when dealing with thermo-mechanical analysis.

2.14 Dynamic Analysis & Quasi-Static Analysis

The calculation of strain and stress distribution throughout the structure due to thermomechanical forces is done by stress analysis. Different types of analyses are performed on solids and structures depending on load magnitude and frequency. Static analysis is conducted when, all quantities associated with the problem such as applied load and material properties are assumed to be constant (loads applied with zero frequency) and time invariant. Inertia is also ignored. In Quasi-static analysis all variables loads and material properties can vary with time, but with a sufficiently slow rate that inertial and damping effects can be neglected. On the other hand, in dynamic analysis all variables in the problem changes with time so rapidly that inertial effects cannot be ignored [128].

The governing equation of the displacement distribution can be written in the matrix form as [129]:

$$\begin{bmatrix} \mathbf{M} & \mathbf{0} \\ \mathbf{0} & \mathbf{I} \end{bmatrix} \begin{bmatrix} \ddot{\mathbf{U}} \\ \dot{\mathbf{U}} \end{bmatrix} + \begin{bmatrix} \mathbf{C} & \mathbf{K} \\ -\mathbf{I} & \mathbf{0} \end{bmatrix} \begin{bmatrix} \dot{\mathbf{U}} \\ \mathbf{U} \end{bmatrix} = \begin{bmatrix} \mathbf{R} \\ \mathbf{0} \end{bmatrix} \tag{2.46}$$

$$\mathbf{M}\ddot{\mathbf{U}} + \mathbf{C}\dot{\mathbf{U}} + \mathbf{K}\mathbf{U} = \mathbf{R}, \tag{2.47}$$

where **M**, **C,** and **K** are the mass, damping and stiffness matrices. **R** is the vector of externally applied load and **I** is the identity matrix. **U**, $\dot{\mathbf{U}}$ and $\ddot{\mathbf{U}}$ are displacement, velocity and acceleration vectors of the finite element assemblage. It should be noted that these terms may be rewritten so all of them are time dependent as [129]:

$$\mathbf{F_I}(t) + \mathbf{F_D}(t) + \mathbf{F_E}(t) = \mathbf{R}(t), \tag{2.48}$$

where $\mathbf{F}_I$ (t) is the inertia force, $\mathbf{F}_I$ (t) = $\mathbf{M\ddot{U}}$, $\mathbf{F_D}(t)$ is the damping force,$\mathbf{F_D}(t) = \mathbf{C\dot{U}}$ and $\mathbf{F_E}(t) = \mathbf{KU}$ is the elastic forces. In a similar manner, the heat conduction equation in matrix form can be represented as:

$$\mathbf{C\dot{T}}(t) + \mathbf{KT}(t) = \mathbf{F}(t), \tag{2.49}$$

where **C** is the heat capacity matrix (thermal mass), **K** is the conductivity matrix and **F** is the thermal load. When the load is considered to be static, this means that the load is applied slowly so that the generated deformation also happens slowly and velocity and acceleration of any point of the structure during deformation are very small, so they can be ignored. The dynamic effects are generated from the existence of the inertia and the damping in a system and the related motion of the structure is known as vibration. Generally it is accepted to neglect the dynamics effects if the load is applied gradually in a sense that it takes an order longer to finish one cycle than the natural vibration period of the structure [130]. If a structure were subjected to sudden load input, it could be solved as a quasi-static problem. The transient heat conduction equation is solved to find the transient temperature distribution. The temperature solution is injected into the thermo-elastic equations to generate the resulting thermal stresses. Ignoring the inertia effect under such loading is not applicable in all cases. It was shown that for a sufficiently thin beam exposed to a thermal shock vibration behaviour is observed [131]. Therefore, in the analysis presented in this work quasi-static analysis is adopted for thermomechanical stress since vibration effects are minimal. In case of short circuit applied to the cable, the heat conduction equation must be solved in transient state to capture the effects of thermal capacitance.

2.15 Summary

Throughout this chapter, the structure of XLPE cables and joints are described. The main types of cable joints are presented. Moreover, premoulded cable joints common installation approaches are listed. It has been presented that the cold shrinkable joint is a common technique used, where the rubber elastic memory is responsible for establishing the needed pressure. In addition, the key effects of thermomechanical stress on the performance of the cable joint is highlighted. A broad introduction about materials mechanical behaviour is provided. In particular, linear and non-linear elastic deformation are discussed. It is presented that non-linear elastic materials such as rubber cannot represented by a constant elastic modulus. More specifically, at non-linear elastic materials should be represented by hyper-elastic materials. Furthermore, hyper-elastic models are described and it has been shown that Ogden and Yeoh models present strains accurately up to 700% and 200%

respectively. Additionally, different models of metal plastic deformation are discussed. Power law model is one of the common models used. Additionally, the main partial differential equation to mechanical deformations in finite element method are outlined. Plane stress and Plane strain are common assumptions used to simplify models. The conversion from plane stress to plane strain can be done easily using the method provided. This chapter has presented the factors that affect the breakdown strength of the interface. It is shown that interface pressure and breakdown strength are closely related. It is presented that some of the failures at the interface might be mechanically driven. There are four main critical interfaces inside a cable joint. They are located at the interface between XLPE and SiR, tip of the central electrode, starting point of the stress cone and interface between the central electrode and joint insulation. The parameters that affect the initial interface pressure and interface pressure changes are discussed. A review of the methods to calculate interface pressure is presented.

This chapter presented some of the reported failures in cable joints. These reported failures are the motive for studying the stresses inside in a joint tube. In IEEE standard 404 for extruded and laminated dielectric shielded cable joints rated 2.5 to 500 kV no correlation is found between insulation mechanical properties and interface pressure. In the next chapter, the calculation of radial and hoop pressure inside a joint tube is presented based on a non-linear model. The main factors that affect these mechanical stresses are discussed and it is shown that materials properties play an important role in these stresses. Then in chapter four the change in interface pressure due to thermal cycling is determined. The change in interface pressure is calculated considering temperature profile in a cable joint and material properties function of temperature.

Thermo-mechanical stresses in single core and three-core cables are discussed. According to CIGRE TB 490 recommendations, electrical testing of only one core of the whole cable is permitted, although this could be considered a deviation from the operational conditions. In three-core cable, the core is exposed to higher internal thermo-mechanical stresses than single core cables since it is more constrained and subsequently heated. In chapter five, a 2D simulation of a single core and a three core cable to investigate thermo-mechanical stresses is presented. The importance of testing a complete three core cable with armour in highlighted.

Chapter 3

Analysis of Mechanical Pressure in a Silicon Rubber Joint Tube

In this chapter, an evaluation of mechanical stress in a silicone rubber joint tube based on its elasticity and expansion rate is presented. More specifically, the calculation of mechanical stresses in the joint tube based on elasticity of the rubber is demonstrated. Interface pressure calculations using finite element method based on hyper-elastic models are established. Considering the mechanical behaviour of rubber helps in the design process of a stable interface.

3.1 Radial and Circumferential Stresses in Silicone Rubber Joint Tube

In this section, stresses inside three joint tubes made of silicone rubber each having different elastic modulus are explored. Then one of the silicone rubber materials is simulated with three semi-conductive materials each having different elasticity. The joint tube is modelled as a cylinder under internal pressure. Two cross sections are of interest, first a cross section of a joint tube without the semiconducting rubber layer is studied. Second, a cross section of a joint tube including a semiconducting rubber layer is explored. Figure 3.1 shows the cross sections investigated in this section. The joint tube and semiconducting materials are considered as silicone rubber and rubber reinforced by carbon black filler, respectively. Furthermore, rubber has a non-linear elastic behaviour to capture this effect, hyper-elastic models are used.

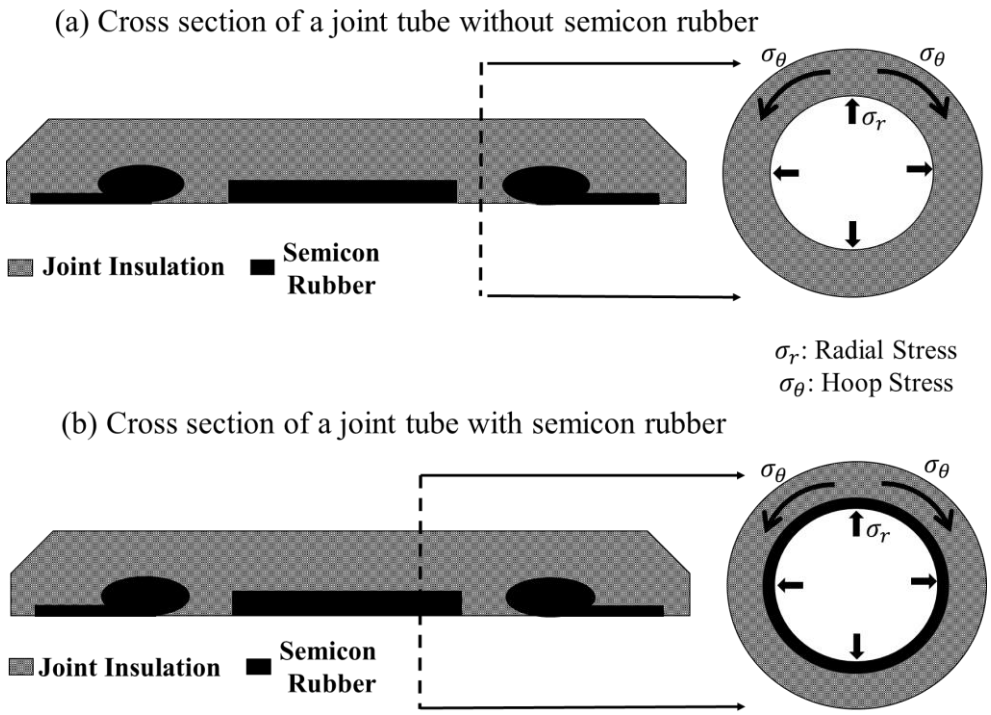

Figure 3.1: Cross sections of a pre-molded joint tube.

3.1.1 Hyper-Elastic Models Used in this Chapter

Hyper-elastic materials are characterized by a strain energy function, which describes the potential energy stored due to a given deformation. Strain energy functions are represented in terms of stretch ratios λ or indirectly in terms of strain invariants *I*. Stretch ratio is defined as the ratio of the deformed length divided by the original length. Strain invariants are the measures of strain which are independent of the coordinate system. For hyper-elastic materials, a second term is added to account for compressibility. In this simulation, the material is considered as nearly incompressible with a Poisson's ratio between 0.49-0.5. The bulk modulus *K* GPa, also known as modulus of compressibility, is defined as the ratio of the pressure required for a unit relative decrease in volume.

Using finite element method, Yeoh and Ogden functions are adopted for semi-con and joint insulation respectively. The hyper-elastic models used for this purpose were chosen to be sufficient for a strain more than 100%. To describe stress-strain relation of carbon-black filled rubber, Yeoh model is suitable. The general form of Ogden and Yeoh model are described respectively as:

$$W = \sum_{p=1}^{N} \frac{\mu_p}{\alpha_p}\left(\lambda_1^{\alpha_p} + \lambda_2^{\alpha_p} + \lambda_3^{\alpha_p} - 3\right) + \frac{1}{2}K(J_{el} - 1)^2 \qquad (3.1)$$

$$W = \sum_{i=1}^{N} C_{i0}(\bar{I}_1 - 3)^i + \frac{1}{2}K(J_{el} - 1)^2, \tag{3.2}$$

where W is the strain energy potential J.m^{-3}, N is the number of terms, μ_n is a constant MPa, α_n is a dimensionless constant, λ_i (i=1, 2, and 3) is known as the principle stretch in the principal directions of the deformation, C_{i0} are material constants MPa, I_1 is the first invariant of the deviatoic strain and J_{el} is the elastic volume ratio.

3.2 Finite Element Model of a Joint Tube without Semiconducting Rubber

Taking advantage of symmetry, a 90° sector is analyzed. It is worth noting that analyzing a full sector generates similar results. In Figure 3.2, the mechanical boundary conditions are shown. Under the mechanical physics, two lines are set as symmetry (**n**·**u**=0) where; **n** is the unit vector normal to the surface and **u** is displacement in mm. The circumference of joint insulation is defined as free. A boundary pressure **P** MPa is applied at the inner radius to represent the pressure from either the cable or the support tube. The parameters for the Ogden relation are those given in Table 3.1. These constants are taken from [133] and [134] to represent silicone rubber in the model with three different elastic modulus. It should be noted that the equation (2.32) mentioned earlier in chapter two is the equation used in this simulation to evaluate the stresses.

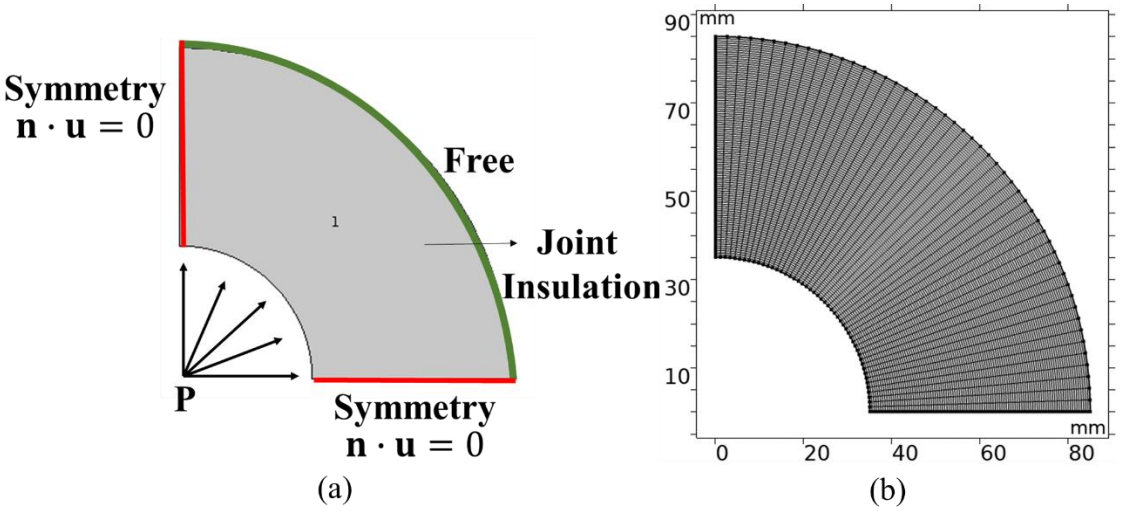

Figure 3.2: Quarter section of joint insulation tube without semi-conductive material.

Table 3.1: Values of the hyper-elastic function parameters for joint insulation.

Material	N	Coefficients (Ogden model) Bulk modulus (*K*)= 2 GPa	
Silicone Rubber (SR1) [133]	4	μ_1= 0.291 μ_2= 0.0034 μ_3 =2.01e-11 μ_4= -1.15e-2	α_1=2.17 α_2=9.06 α_3=34.3 α_4=-5.4
Silicone Rubber (SR2) [134]	3	μ_1=0.46, μ_2= 0.00027 μ_3 = -0.0074	α_1=1.4 α_2=10 α_3=-3.3
Silicone Rubber (SR3) [134]*	3	μ_1=0.3764 μ_2=0.00022 μ_3 =-0.0061	α_1=1.14 α_2=8.18 α_3=-2.7
***SR3 constants are the same as SR2 constants multiplied by a factor.**			

3.2.1 Simulation Results of Joint Insulation without Semi conductive layer

The distribution of radial and hoop stresses inside a joint tube made of SR2 are shown in Figure 3.3. The negative sign in the radial stresses is to indicate that these stresses are compressive. The positive sign in the hoop stresses indicates that they are tensile stresses. It is noticed that both stresses are maximum at the inner radius and it decreases as the outer radius is reached.

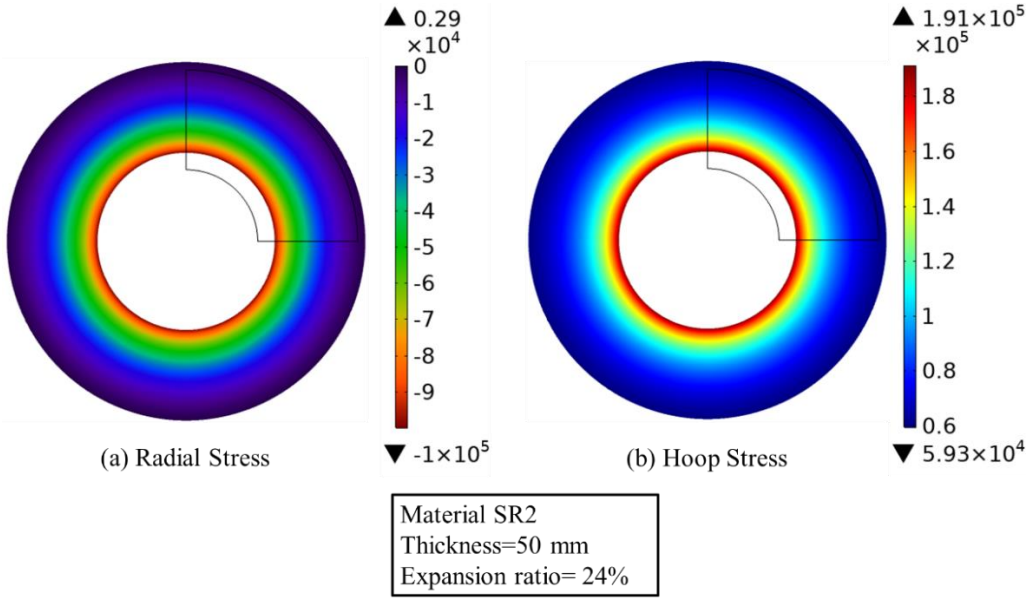

Figure 3.3: Radial and hoop stresses distribution in a cross section of a joint tube made of SR2 at 24% expansion ratio.

The hoop stresses for different expansion ratios are presented in Figure 3.4. The hoop stress increases as the expansion ratio increases. The hoop stress reaches 1.74 MPa at 119% expansion ratio. This expansion ratio is a pre-expanding expansion ratio since it is higher than 50%. It should be noted that there are no clear limit for pre-expanding expansion ratio.

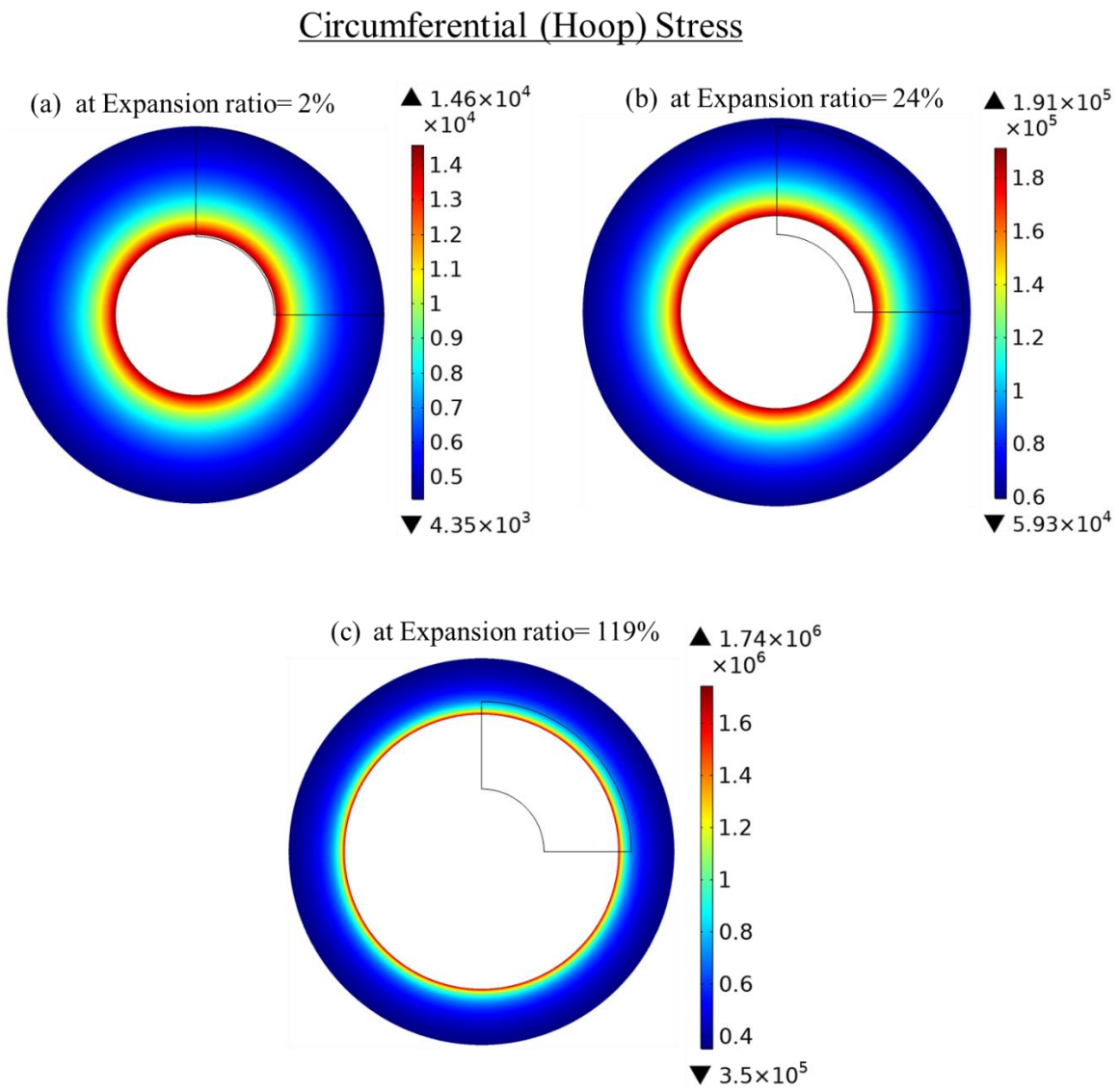

Figure 3.4: Circumferential stress of a joint tube without semiconducting rubber made of SR2 of thickness 50 mm at different expansion ratios.

This hoop stress could reach higher values in case a stiffer material is used. Figure 3.5 shows the relation between the interfacial pressure (radial stress) and hoop stress versus expansion ratio for three different elastic relations of silicone rubber. The quarter sector of joint insulation modeled is presented next to Figure 3.5 and the red marker shows the measuring point. At 50% expansion ratio, a radial pressure of 0.200, 0.165 and 0.110 MPa are achieved for SR1, SR2 and SR3 respectively. This implies that SR3 has the lowest elastic modulus.

To obtain higher radial pressure when utilizing SR3, a higher expansion ratio is needed. The materials can be arranged from the highest to lowest elastic modulus as SR1>SR2>SR3. It is noticed that the radial pressure can be increased by either increasing the elastic modulus or expansion ratio. From Figure 3.5b, the hoop stress at 100% expansion ratio is 3.69, 1.17 and 0.70 MPa for SR1, SR2 and SR3, respectively. The tensile strength of silicone rubber is between 7-9 MPa [108]. Although the tensile strength is not exceeded by any of the simulated materials, the risk of approaching 50% of the tensile strength is present for SR1.

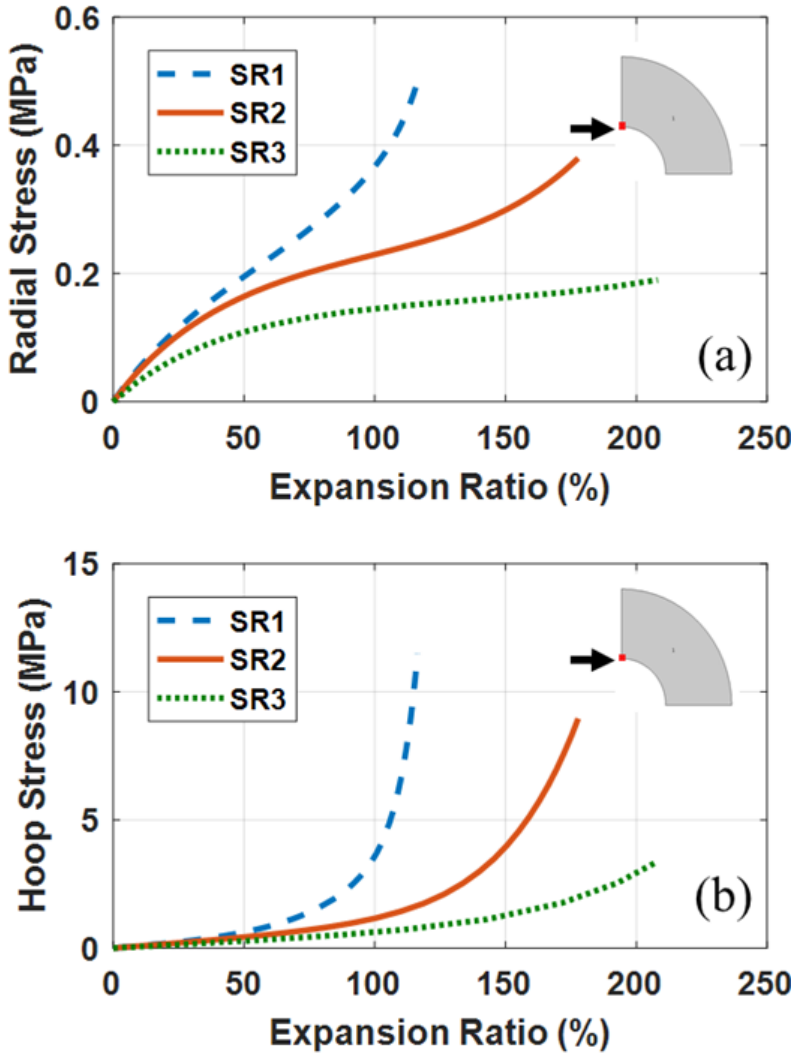

Figure 3.5: (a) Radial and (b) hoop stresses verses expansion ratio for three different parameters of silicone rubber of thickness 50mm.

3.2.2 Sensitivity Analysis

A sensitivity analysis is performed to investigate the effect of expansion ratio, elastic modulus and thickness of a silicone rubber joint on the stresses. Table 3.2 lists the factors investigated with their high and low values. Since there are three factors each having two

levels, a full factorial design would require 2^3 runs [138]. In Table 3.3, the results of each run are presented. The levels are termed as 1 and 0 to represent high and low values respectively. The columns that are defined as (1&2), represent the interaction of the two factors. Interactions are to study the combined effect of the two factors.

Table 3.2: Factors with two levels.

Factor	**High Value (1)**	**Low value (0)**
Expansion ratio	80%	22%
Elastic modulus	SR1	SR2
Thickness	60 mm	40 mm

Table 3.3: Results from different runs using main and interaction effect.

Run	1 Expansion Ratio	2 Elastic Modulus	1&2	4 Thickness	1&4	2&4	Radial Stress (MPa)	Hoop Stress (MPa)
1	0	0	1	0	1	1	0.09	0.188
2	1	0	0	0	0	1	0.19	0.827
3	0	1	0	0	1	0	0.1	0.220
4	1	1	1	0	0	0	0.27	1.78
5	0	0	1	1	0	0	0.1	0.171
6	1	0	0	1	1	0	0.23	0.758
7	0	1	0	1	0	1	0.11	0.198
8	1	1	1	1	1	1	0.31	1.7

Figure 3.6 shows the effects of expansion ratio, elastic modulus and thickness of a joint tube on the radial stresses. The red line is added to represent significance of these factors. A numerical significance of 10% of the largest effect is chosen [139]. This results in considering any effect that exceeds 10% of the largest effect to be significant. Based on this, the expansion ratio has the highest effect on radial stress then elastic modulus and thickness come in the second and third place, respectively. It is noted that all the factors have a positive effect on radial stress.

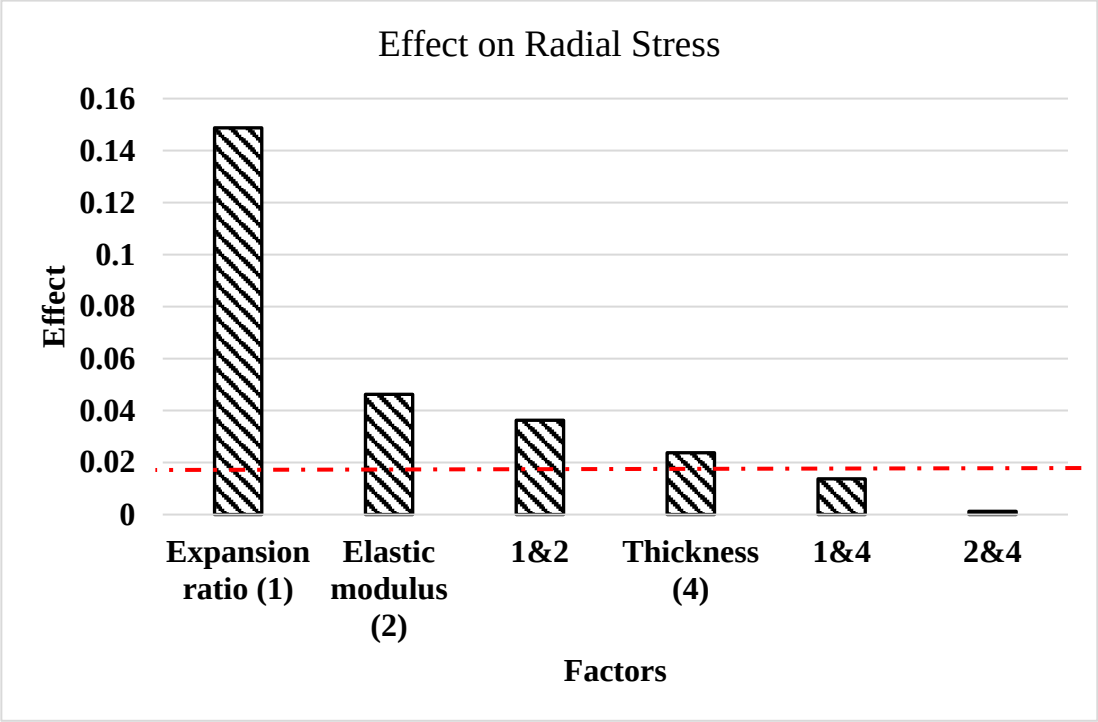

Figure 3.6: Plot of effects on Radial Stress.

The effect on the hoop stresses is presented in Figure 3.7. It is noticed that the effect of the factors on hoop stress have the same sequence as the radial stress. Expansion ratio has the largest effect and thickness has the smallest. Unlike the radial stress, the thickness has a negative effect on hoop stress implying that when thickness changes from low level to high, the hoop stress decreases.

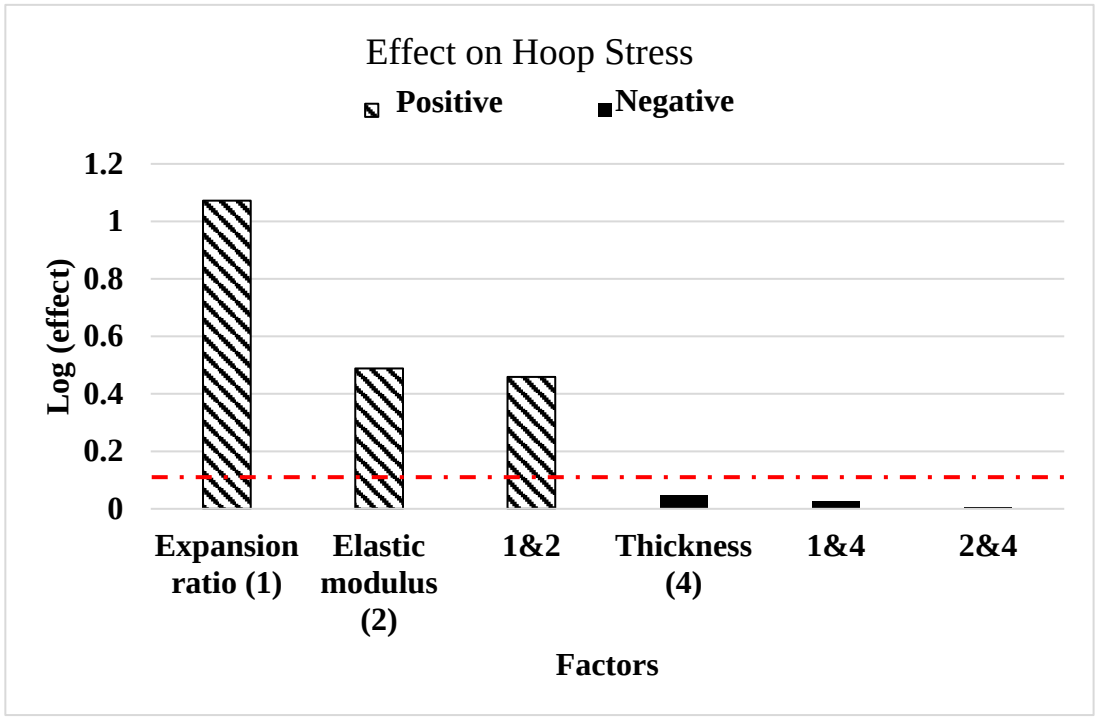

Figure 3.7: Plot of effects on Hoop Stress.

Based on the results presented for a cross section of a joint tube that does include a semiconducting layer, the following can noticed:

- The maximum radial and hoop stresses are at the inner radius and they decrease until they reach their minimum value at the outer radius.
- Using silicone rubber with higher elastic modulus increases both radial and hoop stresses developed in the joint tube modelled.
- Radial stress can be increased by increasing either expansion ratio or elastic modulus or thickness although expansion ratio has the largest effect.
- Hoop stress is also increased by using materials with higher elastic modulus or with larger expansion ratio, but it decreases as thickness increases.

In the next section, a cross section of the joint tube with a semiconducting layer is analysed. The high elastic modulus of the semiconducting layer could generate high hoop stresses at interface between the semiconducting layer and joint insulation.

3.3 Finite Element Model of a Joint Tube with a Layer of Semiconducting Rubber

In this sub section, a ¼ sector of a joint tube with a semicon rubber layer is studied. In Figure 3.8, the mechanical boundary conditions are presented. The stresses at semi-con screen interfaces is also of interest. In Table 3.4, the coefficients of Yeoh model for three semi-con materials are listed.

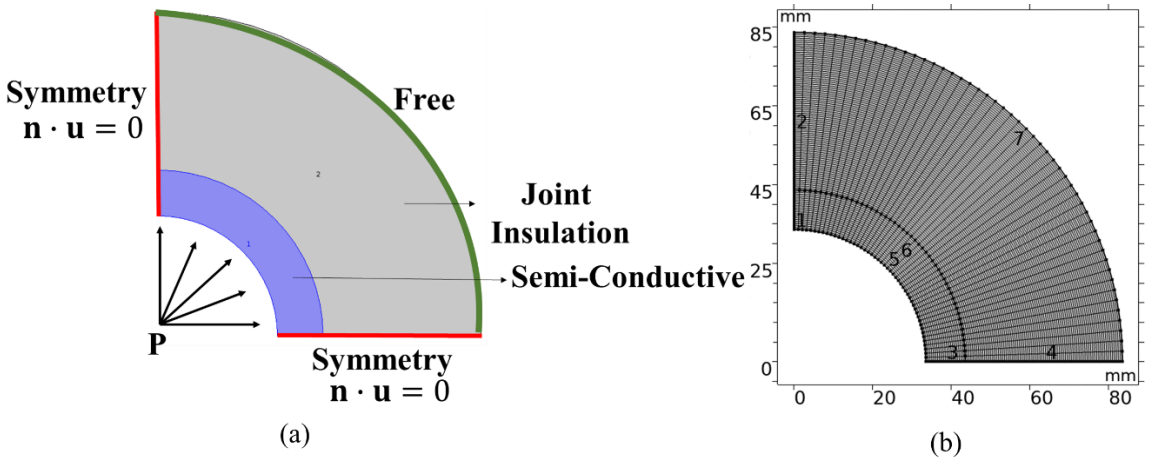

Figure 3.8: Quarter section of a joint tube with semi-conductive layer.

Table 3.4: Parameters of Yeoh Model for Semi-con.

Material	N	Material constants (Yeoh model) Bulk modulus (K)=2 GPa
Semi-Con1 [135]	3	C_{10}=0.8216 C_{20}=0.1115 C_{30}=-0.0036
Semi-Con2 [135]	3	C_{10}=0.6278 C_{20}=0.0900 C_{30}=-0.0023
Semi-Con3 [136]	3	C_{10}=0.4989 C_{20}=0.0347 C_{30}=-2.28e-4

3.3.1 Simulation Results of Joint Insulation with Semiconducting layer

Figure 3.9 shows the radial and hoop stress distribution in a joint tube including a semicon layer. The maximum stresses are located at the inner radius of the tube and it decreases until it reaches its minimum value at the outer radius.

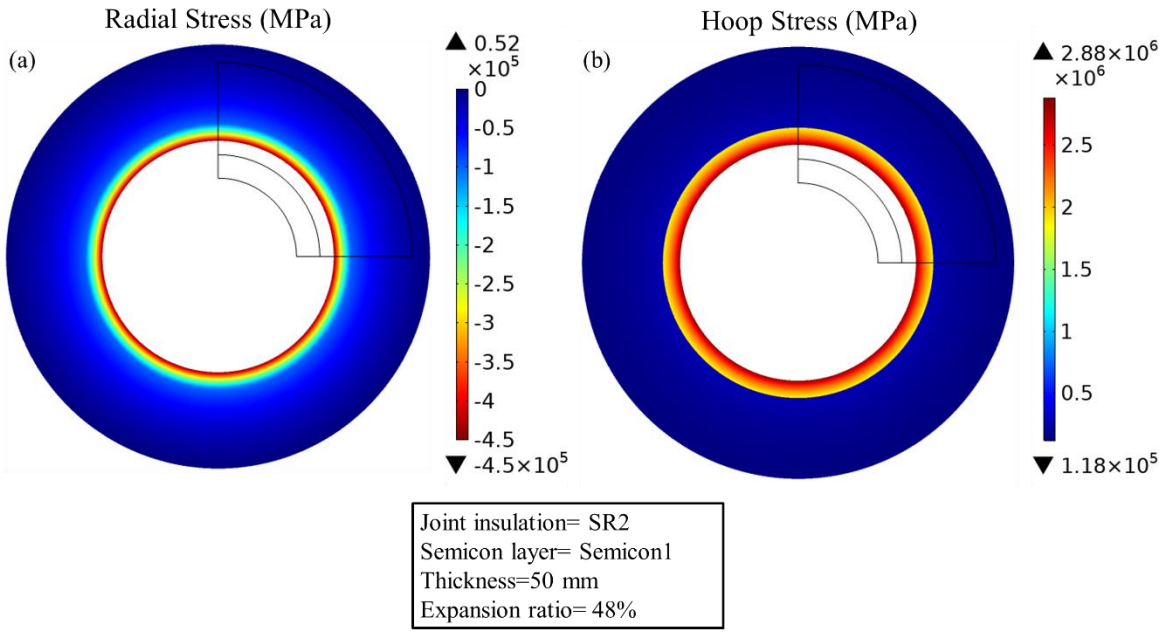

Figure 3.9: (a) Radial stress distribution (b) Hoop stress distribution.

In Figures 3.10a and 3.10b the radial and hoop stresses are plotted, respectively, along the cutline defined. Due to change of material, there is a clear discontinuity at the boundary between the joint insulation and semiconducting layer. It should be noticed that the hoop stress at the interface between the semiconducting layer and the joint insulation is higher at the inner boundary of the joint insulation.

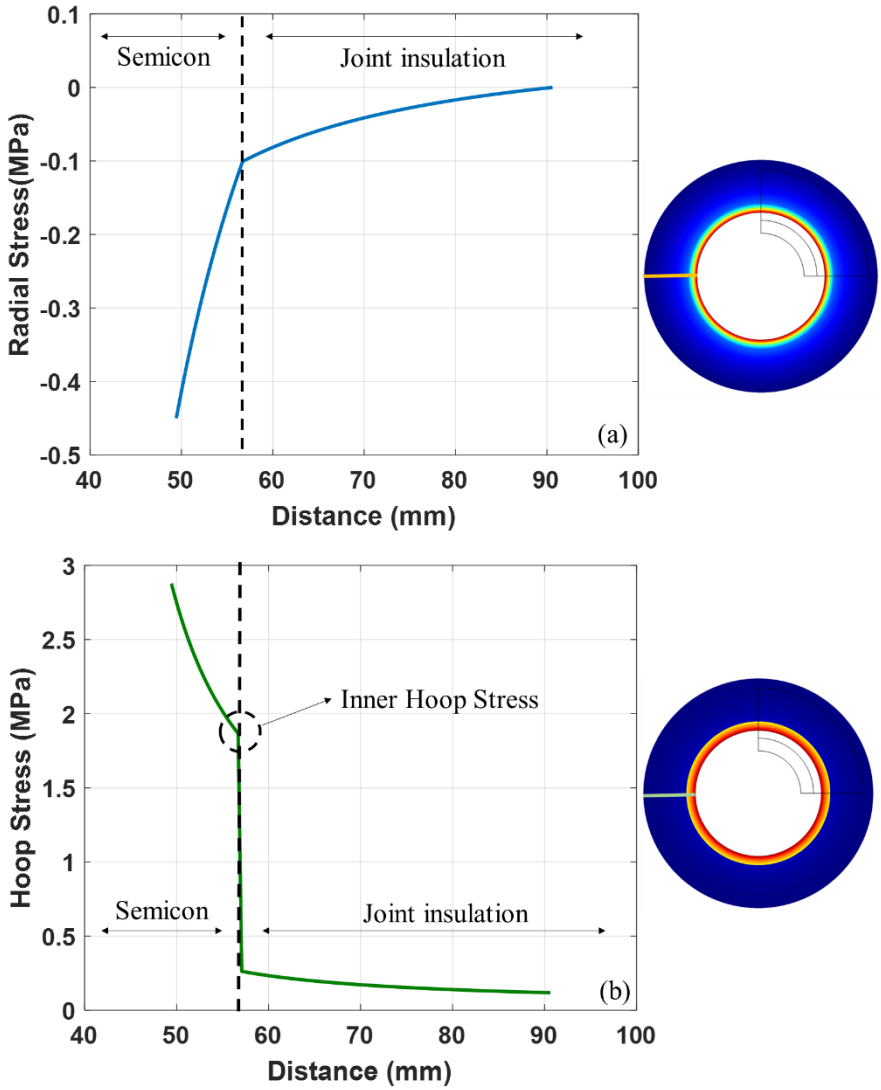

Figure 3.10: (a) Radial Stress along the radial cutline (b) Hoop stress along the radial cutline

To explore the effect of different elasticity of semiconducting materials on the stresses, one of the silicone rubber materials namely SR2 is simulated with three semi-conductive materials each having different elasticity. Figure 3.11 shows the radial and inner hoop stresses versus expansion ratio three different semi-con materials. As shown in Figure 3.11a the radial stresses obtained at 50% expansion ratio are 0.45, 0.37 and 0.3 MPa. Generally, the radial stresses are higher than the stress obtained for SR2 alone in Figure 3.5a. This is expected since the semi-con is stiffer than the joint insulation.

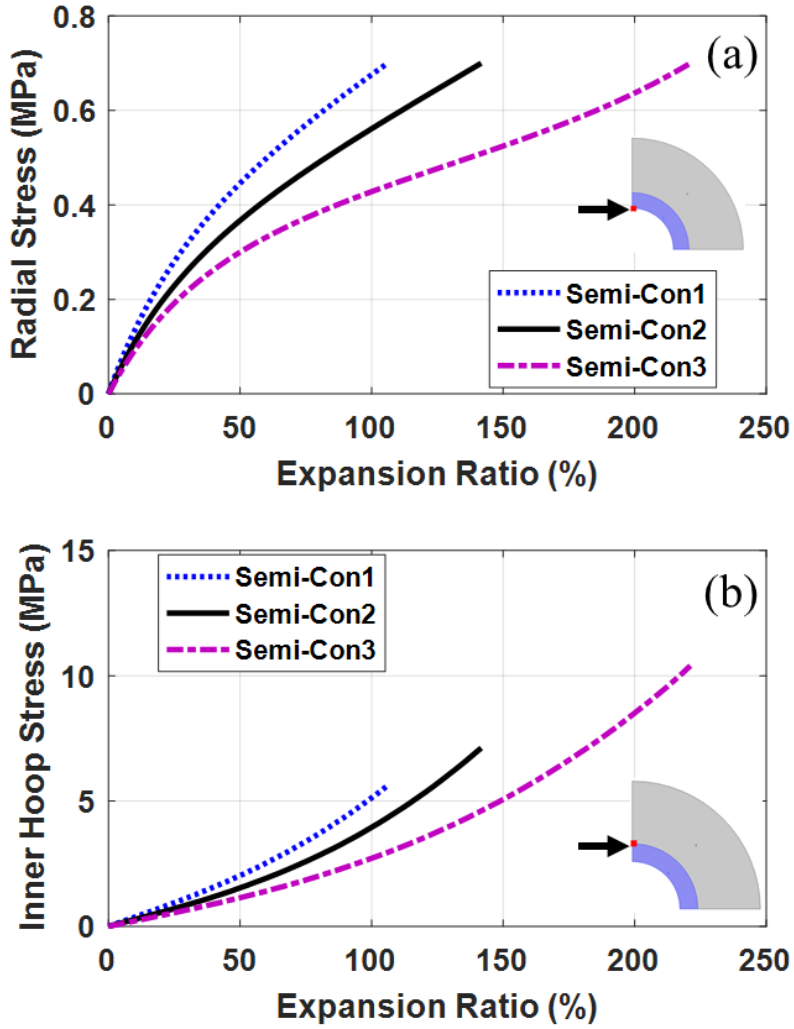

Figure 3.11: (a) Radial and (b) inner hoop verses expansion ratio for three semi-con materials.

The inner hoop stresses at the interface between the joint insulation and the three semi-con materials are 2.06, 1.56 and 1.14 MPa at 50% expansion ratio. Also at 100% expansion ratio, the stresses are 5.2, 3.94 and 2.75 MPa for the three semi-con materials respectively. It can be inferred that even at low expansion ratios, a semi-con with high elastic modulus could introduce high hoop stresses. When a softer (lower elastic modulus) joint insulation than SR2 is used, the inner hoop stresses increase by 50%. On the other hand, increasing the elastic modulus of semi-con material increased the inner hoop stress by 80%. As the expansion ratio increases the risk of having stresses near the tensile strength limit increases. Achieving the highest permissible interfacial pressure by controlling the expansion ratio only without linking it to the elastic modulus is not enough to design a mechanically robust interface. Controlling the expansion ratio only may lead hoop stress to reach 50% of the tensile strength of joint insulation if the elastic modulus of material is high. Furthermore, expansion ratio above 60% and up to 150% in the pre-installation stage needs to be correlated

with the elastic modulus of both materials to make sure that the hoop stresses do not exceed the critical values. When defining the value for the tensile strength of a material, a group of tests is performed and statistical analysis is done. The outcome of this analysis produces an average value, which is used to represent the material property [137]. This implies that some samples could have a lower tensile strength, which increases the probability of reaching the lower limit of material tensile strength.

The results obtained represent the worst case. It is known that rubbers have a viscoelastic behaviour, where the material exhibit both viscous and elastic characteristics. However, the degree of viscoelasticity is highly dependent on temperature, degree of crosslinking and type of fillers incorporated. These stresses will decrease by time depending on the storage conditions (time and temperature). However, the designer should avoid reaching the material limit since this could create a faulty interface before it relaxes and stabilizes at a certain value.

3.3.2 Sensitivity Analysis

To explore the effect of different parameters on the radial and hoop stresses inside a joint tube slice with a semiconducting layer, a sensitivity analysis is presented. Table 3.5 lists five factors with their high and low values.

Table 3.5: Factors and levels for sensitivity analysis

Factor	High Value (1)	Low Value (0)
1. Joint Insulation Thickness	60 mm	40 mm
2. Semicon Thickness	10 mm	20 mm
3. Elasticity of joint insulation	SR1	SR2
4. Expansion Ratio	80%	50%
5. Elasticity of Semicon	Semicon1	Semicon3

In this case a full factorial design would require to run 2^5=32 runs [138]. However, the interest here is in the effect of main factors. Thus, running a half factorial design (2^{5-1}=16 runs) will not cause any significant loss of information. In table 3.6, the outcome of each run is presented. For each run, the radial stress and the inner hoop stress are recorded.

Table 3.6: Results from different runs using main effect.

Run	Joint Insulation Thickness	Semicon Thickness	Elasticity of joint insulation	Expansion Ratio	Elasticity of semicon	Radial Stress (MPa)	Hoop Stress (MPa)
1	0	0	0	0	1	0.46	1.974
2	0	0	0	1	0	0.395	1.953
3	0	0	1	0	0	0.32	1.0856
4	0	0	1	1	1	0.65	3.66
5	0	1	0	0	0	0.41	0.7714
6	0	1	0	1	1	0.88	2.371
7	0	1	1	0	1	0.66	1.333
8	0	1	1	1	0	0.55	1.314
9	1	0	0	0	0	0.33	1.109
10	1	0	0	1	1	0.64	3.558
11	1	0	1	0	1	0.5	1.98
12	1	0	1	1	0	0.46	1.904
13	1	1	0	0	1	0.66	1.304
14	1	1	0	1	0	0.56	1.324
15	1	1	1	0	0	0.44	0.767
16	1	1	1	1	1	0.915	2.3

Figure 3.12 shows the main effect of each factor on the radial stress. To elaborate a little further, all factors seem to have a positive effect on the radial stress. This means that an increase in any of these factors will be translated in an increase in the radial pressure. Moreover, it can be observed that the properties of the semiconducting layer have a higher impact on the radial stress than the properties of the joint insulation. This result explains the benefit of increasing these factors for radial pressure. However, for inner hoop stress increasing these factors could be a concern. As illustrated in Figure 3.13, where the effect on inner hoop is presented, increasing the elasticity of the semiconducting layer increases the inner hoop stress. Furthermore, the thickness of the semiconducting layer has a negative effect. Also increasing the elasticity and thickness of joint insulation can mitigate the inner hoop values although their effect is minimal. The red line represents a numerical significance of 10% of the largest effect is chosen. Based on this line, the elasticity, thickness of the semiconducting layer and expansion ratio are significant [139].

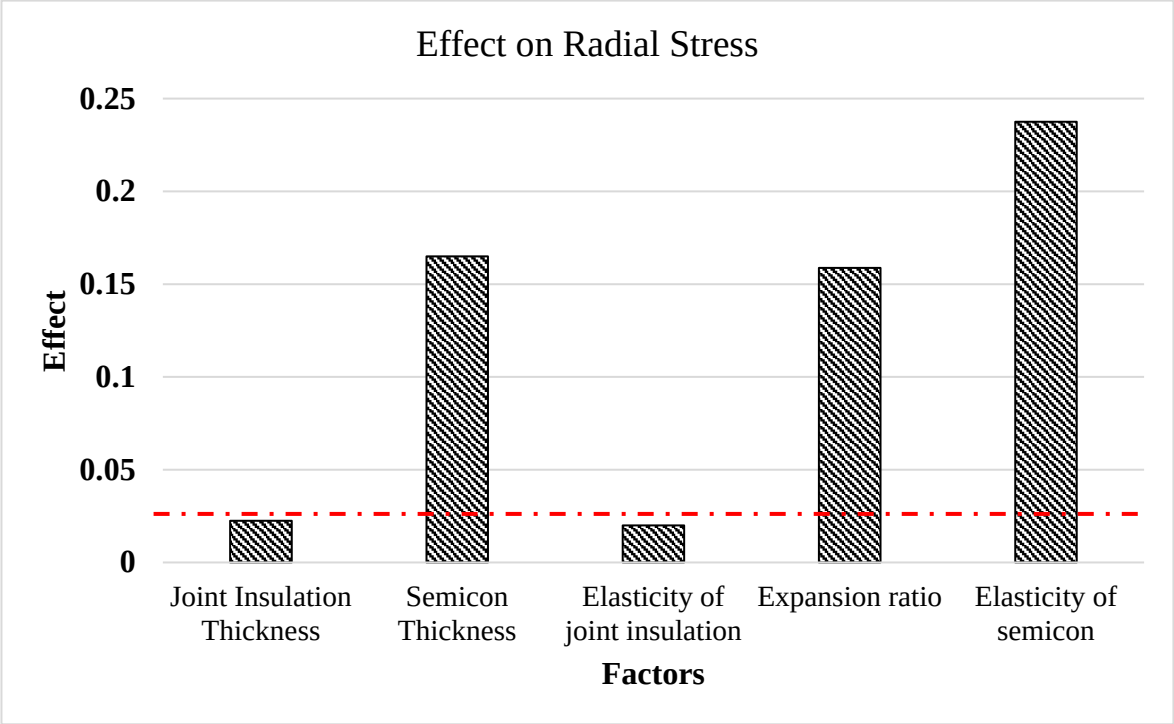

Figure 3.12: Plot of effects on Radial Stress.

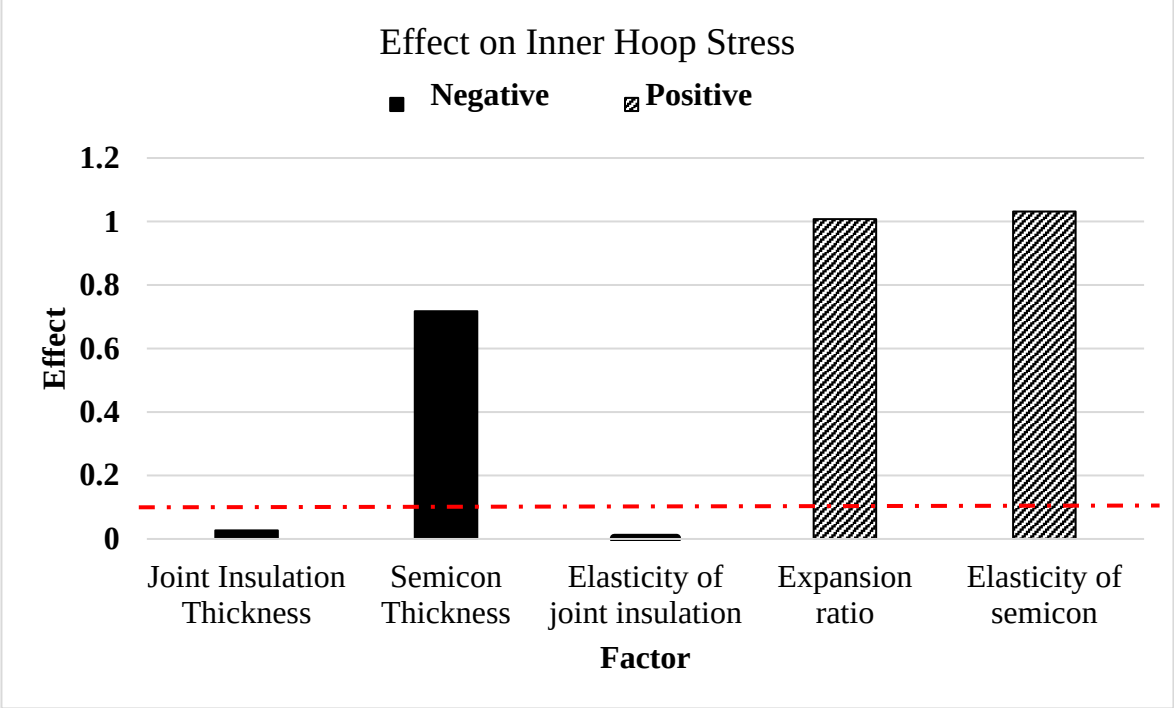

Figure 3.13: Plot of effects on Inner Hoop Stress.

According to presented results in this section, it can be noticed the strong influence of the semiconducting on the radial pressure or on inner hoop. Taking into account the properties

of the semiconducting rubber during the design is important to avoid any possible increase in the internal stresses in the tube that could affect its performance during operation.

3.4 Summary

It is shown that the motivation for this study is failures in 110 kV and 220 kV silicone rubber pre-moulded joints. In this chapter, the stresses inside an expandable joint tube made of silicone rubber are analysed. Calculation of radial and hoop stresses inside a joint tube at operation and pre-expanding expansion ratios is demonstrated. The maximum stresses are located at the inner radius of the joint tube. The expansion ratio has the largest effect on the internal stresses, then comes elastic modulus and thickness in the second and third place, respectively. Hoop stresses could reach critical values at the interface depending on the material elastic modulus and expansion ratio. Limiting the expansion ratio only is not sufficient to assure a mechanically stable interface. High initial circumferential (hoop) stress could result due to utilizing materials with high Young's modulus even within the permissible limit of expansion ratio, especially at the interface of the semiconducting layer and the joint insulation. Stiffer semiconducting layer was found to increase the inner hoop stresses by 80%.

After determining the initial mechanical pressure, it would be important to evaluate the change in the pressure due to temperature. Temperature has a pronounced effect on the elasticity and thermal expansion of insulating materials. In the following chapter, the variation of interface pressure during operation is calculated. An improved analytical model is proposed that takes into account the variation of elasticity and thermal expansion with temperature. This approach is useful to explain some of the failures since it incorporates the effect of temperature and material properties.

Chapter 4

Change in Interface Pressure

Temperature changes and temperature cycling are an important factor that affects the interface pressure. In this chapter, the change in interfacial pressure due to temperature changes and temperature cycling are presented. The change in contact pressure depends on the temperature profile in the bulk material, the thermal characteristics and mechanical properties of the insulating materials. In this chapter, a mathematical model using the thermo-elastic equations is developed to estimate the change in contact pressure taking into account how the mechanical properties (elastic modulus and thermal expansion) change with temperature along with a more realistic temperature profile. The methodology is demonstrated based on the theory of elasticity under steady state implantation. In the previous chapter, the initial radial and hoop stresses were calculated. Figure 4.1 shows the parameters that affects mechanical and thermal stresses. Temperature dependency and material properties effects on the change of interface pressure are investigated in this chapter.

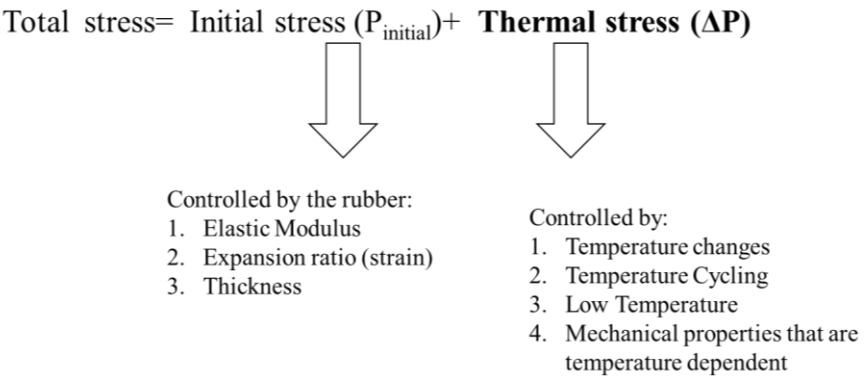

Figure 4.1: Mechanical stress and thermal stress and their main factors.

4.1 Calculating Change in Interface Pressure

Few approaches had been presented on how to calculate the change of interface pressure. In [105], the change in interface pressure is assumed to be affected by elasticity of silicone rubber only. The thermal stresses generated from cable insulation were ignored. However, the effect of material's thermal expansion must be taken into account. XLPE has a high

thermal expansion. XLPE will expand by 15% when heated from 25 to 105℃, while copper will expand by 3% in the same temperature range [111]. XLPE's thermal expansion as function of temperature is shown in Figure 4.2. This implies that XLPE can develop high stress when heated and restricted. Elastic modulus of insulating material is temperature dependent. The decrease in elastic modulus of (XLPE) insulation at high temperature in Figure 4.3 could also affect the interface [114, 115].

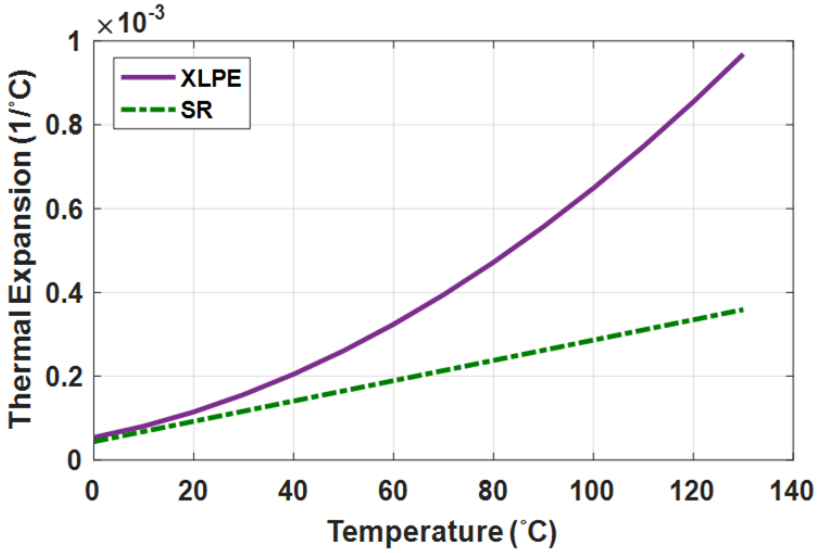

Figure 4.2: Thermal expansion of cable and joint insulation [112, 36].

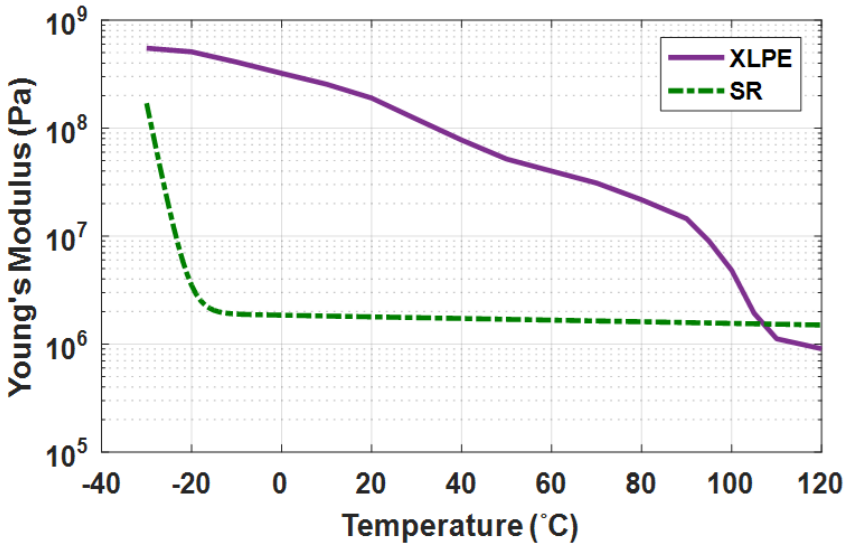

Figure 4.3: Elastic modulus of the cable and joint insulation [29, 113].

In order to evaluate the change in interface pressure due to thermal cycling and temperature change, a model was proposed by [95]. It was found that the effect of thermal cycling on the interfacial pressure depends on the insulating material [95]. However, the model did not consider the variations of the materials moduli of elasticity and thermal expansion

coefficients with temperature. In addition, the temperature in each material was supposed to decrease linearly with radius leading to deviation from the real situation.

In IEEE standard 404 for extruded and laminated dielectric shielded cable joints, no correlation is found between mechanical properties of the insulation and interfacial pressure [116]. The correlation between material properties and interface pressure is a necessity to assure mutual compatibility and long term performance after installation. Furthermore, the existing algorithms that estimate the interface pressure and its changes, rarely correlate the mechanical properties of insulating materials and the mechanical stress they experience. In this chapter, a link between material properties, temperature changes and interface pressure changes is established. The main focus will be the interface pressure in radial direction rather than axial direction. It was found that the pressure in the axial direction is almost uniform. The expansion and contraction of the cable has a minor effect on the change in interface pressure in the axial direction. This can be explained by the fact that the change in temperature in the axial direction would be not significant in this case.

Temperature distribution in cable joints is found by determining the sources of heat which similar to method used for cables. Figure 4.4 illustrates the steady state temperature distribution inside this joint where, the maximum temperature is at the center of the joint. The axial conductor temperature inside a 132 kV cable joint is shown in Figure 4.5. It can be seen that the temperature in the axial direction of the cable joint does not change significantly. The temperature change along the axial direction of the conductor inside the joint is almost 2.5℃. Unlike temperature in the axial direction, temperature in the radial direction of the cable joint changes considerably, as illustrated in Figure 4.6. The difference in temperature between the conductor and the outer insulation of the joint in almost 51℃. This implies the importance of calculating the thermal effects in the radial direction rather than the axial direction in this case presented. Different slices of the cable joint showing the temperature distribution in the radial direction are shown in Figure 4.7.

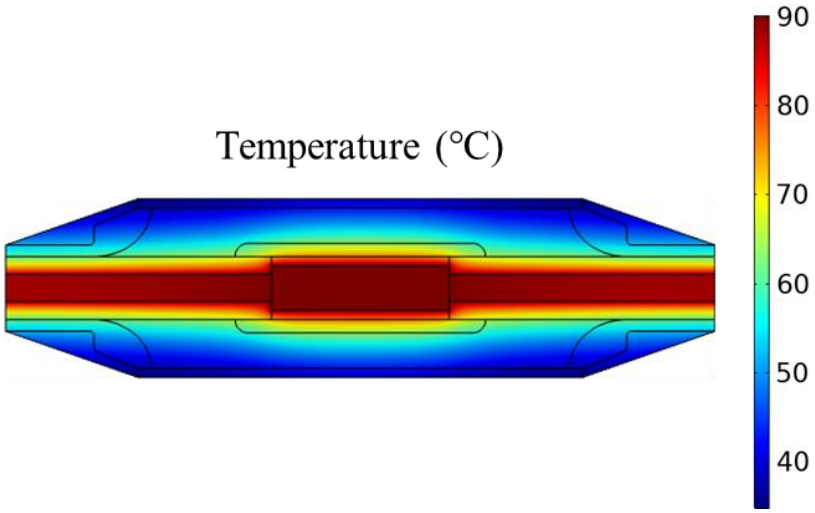

Figure 4.4: Temperature distribution inside a 132 kV cable joint installed in air.

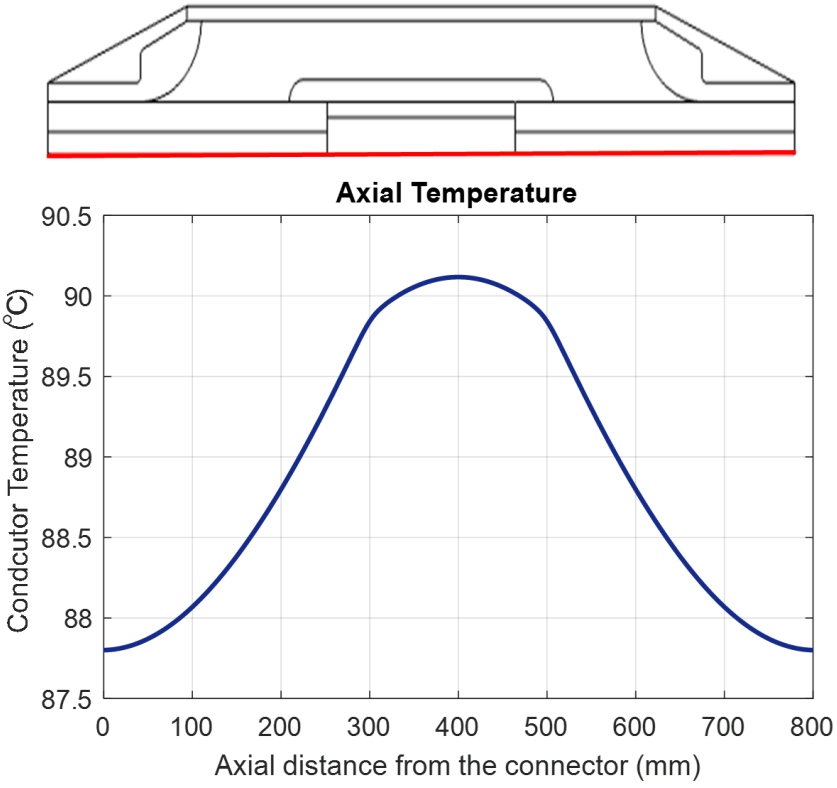

Figure 4.5: Temperature profile in a 132 kV cable joint in axial direction.

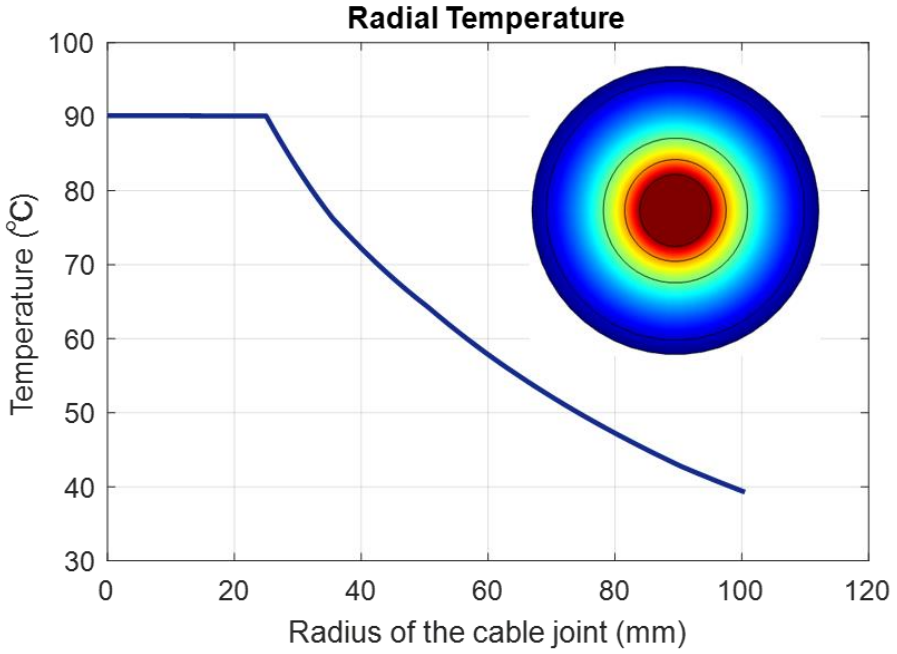

Figure 4.6: Temperature profile in a 132 kV cable joint in radial direction.

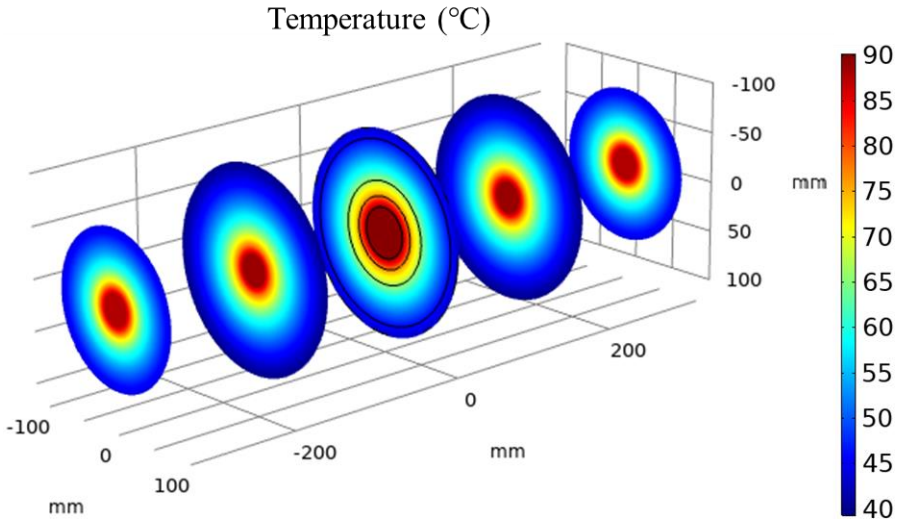

Figure 4.7: Different slices of temperature distribution inside a 132 kV cable joint installed in air.

4.2 Analytical Model

The cable joint is modelled as a thick wall cylinder where the ratio of wall thickness *s* and the inside diameter *di* is higher than 0.05 [58]. Plane strain state equations are considered where the cylinder is either constrained at the ends or infinitely extended along the axis. If

the thick wall cylinder is in the elastic state, the deformation can be determined using the displacement approach and in that case the solution will satisfy the equations of the boundary value problem of elasticity with the corresponding boundary conditions. When analyzing thick wall cylinders, stress, strain and displacement are considered as functions of the radial coordinate *r*, irrespective to the tangential coordinate θ. The shear stress is equal to zero because of the axial symmetry of the model. By ignoring the tangential coordinate θ, the tangential stress σ_θ and radial stress σ_r are functions of the radial coordinate *r*. The deformation and the expansion in cable accessories can be studied by the thick wall cylinder model since it belongs to the elastic category. The stress to strain relations including the effect of a temperature change is expressed as [58]:

$$\sigma_r = \hat{E}(1-v)\epsilon_r + \hat{E}v\epsilon_\theta - \frac{E\alpha\Delta T}{1-2v} \tag{4.1}$$

$$\sigma_\theta = \hat{E}v\epsilon_r + \hat{E}(1-v)\epsilon_\theta - \frac{E\alpha\Delta T}{1-2v}, \tag{4.2}$$

where $\hat{E}$ is the effective modulus in terms of the Poisson's ratio and it is expressed as:

$$\hat{E} = \frac{E}{(1-2v)(1+v)} \tag{4.3}$$

where *e* and *σ* are the strain and the stress (N.m^{-2}), respectively along r and θ. *α, E and v* are the thermal expansion coefficient (˚C^{-1}), Young modulus (MPa) and Poisson's ratio respectively and ΔT (˚C) is the temperature increase above ambient. Assuming *u* and *w* are the displacement components along the radial and θ directions. Then the strain-displacement relations are:

$$\epsilon_r = \frac{du}{dr} \tag{4.4}$$

$$\epsilon_\theta = \frac{u}{r} + \frac{1}{r}\frac{\partial w}{\partial \theta} \tag{4.5}$$

Radial symmetry is assumed as illustrated in Figure 4.8 and the variation along the θ axis is neglected ($\frac{\partial}{\partial\theta} = 0$) all the four shear stresses are intrinsically balanced due to annular symmetry. The governing equation is derived by equating the stress in both radial (r) and circumferential (θ) directions

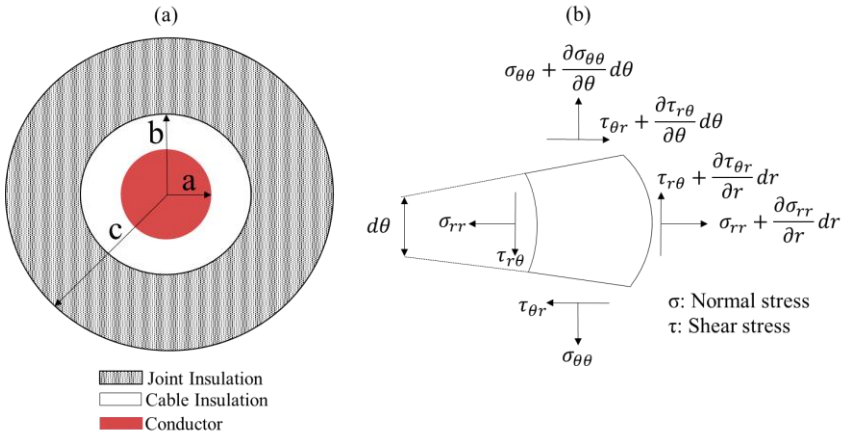

Figure 4.8: (a) Joint Model [95] (b) local stress on an infinitesimal element [58]

The equilibrium equation in radial direction can be written as:

$$\frac{d\sigma_r}{dr} + \frac{\sigma_r - \sigma_\theta}{r} = 0 \tag{4.6}$$

The elastic modulus E_a and E_b at the inner and outer radius a, b in Figure 4.8a are determined based on equation 4.7 where T is temperature °C and A, B, A_1, B_1, and C_1 are fitting constants. Using curve fitting, the elastic modulus and thermal expansion of each material were expressed as functions of temperature. The variation of the elastic modulus within the material is calculated based on these values and the constants m_1 and m_2, which are determined by Equation 4.9, the thermal expansion, is presented by a similar approach.

$$E(T) = Ae^{BT} \tag{4.7}$$

$$\alpha(T) = A_1 T^2 + B_1 T + C_1 \tag{4.8}$$

$$E(r) = E_a \left(\frac{r}{a}\right)^{m_1} \; where \; m_1 = \frac{ln\left(\frac{E_a}{E_b}\right)}{ln\left(\frac{a}{b}\right)} \tag{4.9}$$

$$\alpha(r) = \alpha_a \left(\frac{r}{a}\right)^{m_2} \; where \; m_2 = \frac{ln\left(\frac{\alpha_a}{\alpha_b}\right)}{ln\left(\frac{a}{b}\right)} \tag{4.10}$$

Using the relations (4.1)-(4.6) the Navier equation in terms of the displacement is

$$\frac{d^2u}{dr^2} + \frac{1}{r}\frac{du}{dr} - \frac{u}{r^2} + \frac{1}{E(r)}\frac{dE(r)}{dr}\left(\frac{du}{dr} + \frac{v}{1-v}\frac{u}{r}\right) = \frac{1+v}{1-v}\left[\alpha(r)\frac{dT(r,t)}{dr} + T(r,t)\frac{d\alpha(r)}{dr} + \alpha(r)T(r,t)\frac{1}{E(r)}\frac{dE(r)}{dr}\right] \tag{4.11}$$

Within a power cable, resistive losses are the main source of heat, combined with the external heat sources (e.g. solar radiation). For this cable joint, the causes of heat generation are considered to be heat generation due to AC resistance (Conductor losses) and heat generation due to dielectric losses. To calculate the heat source in the cable joint presented by the joule losses and dielectric losses W_{dielec} per unit length, respectively the following equations are used:

$$W_c = I_c^2 R_{ac} \tag{4.12}$$

$$W_{dielec} = 2\pi f C_{el} U_0^2 tan\delta, \tag{4.13}$$

where R_{ac} is the AC resistance of the conductor per unit length at its maximum operating temperature, I is the current, f is the system frequency, C_{el} is the electrical capacitance of the cable, U_0 is the phase to ground voltage and $tan\delta$ is the dielectric loss factor.

This cable joint is assumed as a cylinder that consists of several layers. Each layer has a thermal resistance that depends on a number of parameters. For a single core cable with a cylindrical conductor, the thermal resistance T_1 of the cable insulation (Km. W^{-1}) is calculated using the below equation:

$$T_1 = \frac{\rho_{th1}}{2\pi} \ln\left(1 + \frac{2t_1}{D_c}\right), \tag{4.15}$$

where ρ_{th1} is the thermal resistivity of cable insulation (Km. W^{-1}), t_1 is the thickness of insulation (mm) and D_c is the diameter of conductor (mm). T_2 represents the thermal resistance of the joint insulation and it is computed by:

$$T_2 = \frac{\rho_{th2}}{2\pi} \ln\left(1 + \frac{2t_2}{D_i}\right), \tag{4.16}$$

where ρ_{th2} is the thermal resistivity of joint insulation (Km. W^{-1}), t_2 is the thickness of the joint insulation (mm) and D_i is the diameter of the cable insulation (mm). Cables laid in free air (protected from solar radiation) its thermal resistance T_4 is given by:

$$T_4 = \frac{1}{\pi D_e h (\Delta\theta_s)^{.25}} \tag{4.17}$$

$$h = \frac{Z}{{D_e}^g} + Y, \tag{4.18}$$

where h is the heat dissipation coefficient (W. m^{-2}. $K^{-5/4}$), $\Delta\theta_s$ is the excess of cable surface temperature above ambient temperature in (K) and Z, g and Y are constants used to

calculate the heat dissipation coefficient. The temperature distribution inside each layer of the cable joint can be computed using the following equation, assuming the internal and external radii of the layer to be r_1 and r_2 respectively:

$$T(r) = \frac{\theta_1 - \theta_2}{\ln \frac{r_1}{r_2}} \ln \frac{r}{r_2} + \theta_2. \tag{4.19}$$

Once the temperature distribution is known, the governing equation eq. (4.11) which is in the form of a second order non-homogeneous differential equation with variable coefficients can be solved to find the radial displacement. This kind of problems is also known as boundary value problem. The full solution is obtained by finding the general and the particular solutions for the differential equation. If the material properties are introduced as a power law functions the second order differential equation takes the form of Euler-Cauchy differential equation with constant coefficients and the complete solution for *u* can be written as:

$$u(r) = u_g(r) + u_p(r), \tag{4.20}$$

where $u_g(r)$ is the general solution and $u_p(r)$ is the particular solution. As a result, the general solution is assumed to be in the form of

$$u_g(r) = A_1 r^{\beta_1} + A_2 r^{\beta_2}, \tag{4.21}$$

β_1 and β_2 are the roots of the characteristic equation and A_1 and A_2 are constants that can be found by applying the boundary conditions. The boundary conditions for this problem are given by [95]:

$$u_{cable}(a) = a\alpha_{cond}\Delta T \quad , \quad u_{cable}(b) = u_{joint}(b) \tag{4.22}$$

$$\sigma_{cable}(b) = \sigma_{joint}(b) \quad , \quad \sigma_{joint}(c) = 0, \tag{4.23}$$

where *a*, *b* and *c* are radius of the conductor, cable insulation and joint insulation respectively. α_{cond} is the linear thermal expansion of the conductor and ΔT (˚C) is the temperature increase above ambient. u_{cable} and σ_{cable} are, the displacement and stress function is the cable insulating material respectively. On the other hand, u_{joint} and σ_{joint} are displacement and stress function is the joint insulation material respectively. Once the displacement u is determined, the radial and hoop stresses can be presented by:

$$\sigma_r = \frac{E(1-v)u'}{(1-2v)(1+v)} + \frac{Ev(1-v)u}{(1-2v)(1+v)r} - \frac{E\alpha\Delta T}{1-2v} \tag{4.24}$$

$$\sigma_\theta = \frac{Evu'}{(1-2v)(1+v)} + \frac{E(1-v)u}{(1-2v)(1+v)r} - \frac{E\alpha\Delta T}{1-2v}. \tag{4.25}$$

4.3 Finite Element Model

Using Finite element method, the analytical model was verified. Thermal and mechanical physical interfaces are linked to analyse this mechanical stress problem. Assuming symmetry only a quarter of the cable joint is modelled. The boundary conditions for the thermal and mechanical physics are shown in Figure 4.9. The thermal losses are for a 132 kV cable joint with 630 mm^2 conductor cross section area; joule and voltage dependent dielectric losses are calculated based on IEC 60287-1-1 and are set as heat sources. For this joint, dielectric losses were almost 3% of the joule losses. The external thermal resistance is obtained assuming the cable joint in free air. Thermal and mechanical symmetry is set at boundary 1 and 2. Free boundary condition is considered at boundary 3 under the mechanical physics. The mathematical equation for the thermal physics is stated where *k* is the thermal conductivity W.m^{-1}.K^{-1}, and *Q* is the heat source W.m^{-3}. For the mechanical physics, the equation for a deformable body is used to find the internal forces where σ is the stress Pa and Fv is the body force per unit volume. Insulation properties and model parameters are listed in Table 4.1 and Table 4.2 respectively. The elastic modulus values of the cable and joint insulation as function of temperature were taken from [29] and [113] respectively. Thermal expansion of cable and joint insulation were taken from [36] and [112] respectively. The material functions used in this model are listed in Table 4.3.

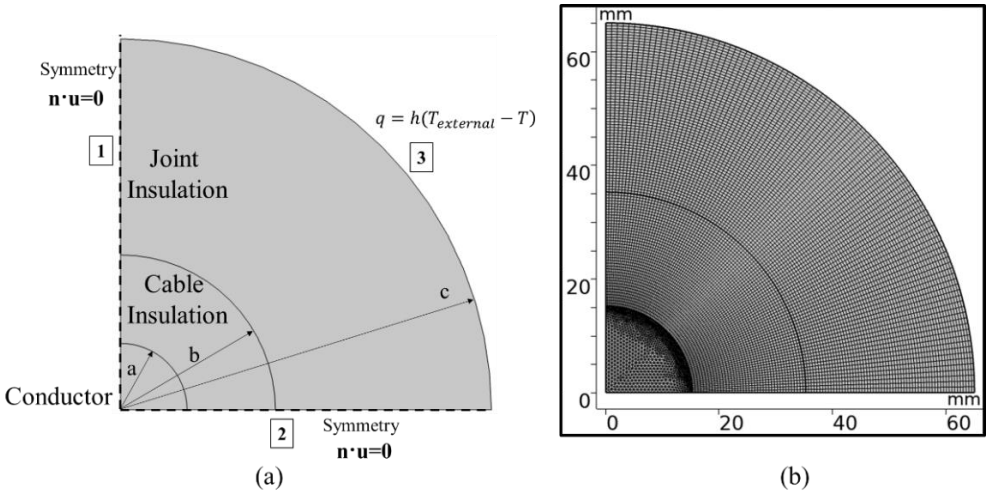

Figure 4.9: (a) Illustration of model geometry and boundary setting (b) Mesh of the Model.

Table 4.1: Insulation Properties

Parameter	Cable Insulation	Joint Insulation
Thickness	20.25 (mm)	49.5 (mm)
Thermal Resistivity	3.5(m.K.W^{-1})	5 (m.K.W^{-1})
Poisson's Ratio	0.46 [95]	0.49 [95]
Tanδ	0.005	0.013

Table 4.2: Model Parameters.

Parameter	Value
Conductor Material	Copper
Thermal Expansion (Cu)	1.9×10^{-5} (˚C^{-1})
Ambient Temperature	25 (˚C)
Heat Transfer Coefficient (h)	4.54 (W.m^{-2}.K^{-1})

Table 4.3: Fitting constants used in the model

Property	Function
Elastic modulus of cable insulation (Pa)	$E_{Cable}(T) = 3.8 \times 10^{8} e^{-0.038T}$
Elastic modulus of joint insulation (Pa)	$E_{Joint}(T) = 3.6 \times 10^{6} e^{-0.01713T}$
Elastic modulus of semiconducting rubber (Pa)	$E_{Semi}(T) = 5.4 \times 10^{6} e^{-0.01713T}$
Thermal expansion of cable insulation (˚C^{-1})	$\alpha_{Cable}(T) = 3.6 \times 10^{-8}T^{2} + 2.3 \times 10^{-6}T + 9.4 \times 10^{-5}$
Thermal expansion of joint insulation (˚C^{-1})	$\alpha_{Joint}(T) = 2.4 \times 10^{-6}T + 8.9 \times 10^{-5}$
Thermal expansion of semiconducting rubber (˚C^{-1})	$\alpha_{Joint}(T) = 2.4 \times 10^{-6}T + 5.4 \times 10^{-5}$

4.4 Results

In this section, the accuracy of the analytical method is confirmed. The outcome of the analytical is compared with finite element method. One radial cross section of a cable joint is presented. Then a sensitivity analysis is undertaken to examine the effect of material properties on the change in interface pressure. Finally, the effect of changing input current and ambient temperature on interface pressure changes is discussed.

4.4.1 Interface between cable and Joint Insulation

Figure 4.10a shows the cross section of the cable joint analyzed. The interface studied in this section is between the cable and joint insulation. The change in radial and hoop stresses within the cable joint assembly in air, when the conductor temperature is at 90˚C are shown in Figure 4.10b and Figure 4.10c respectively.

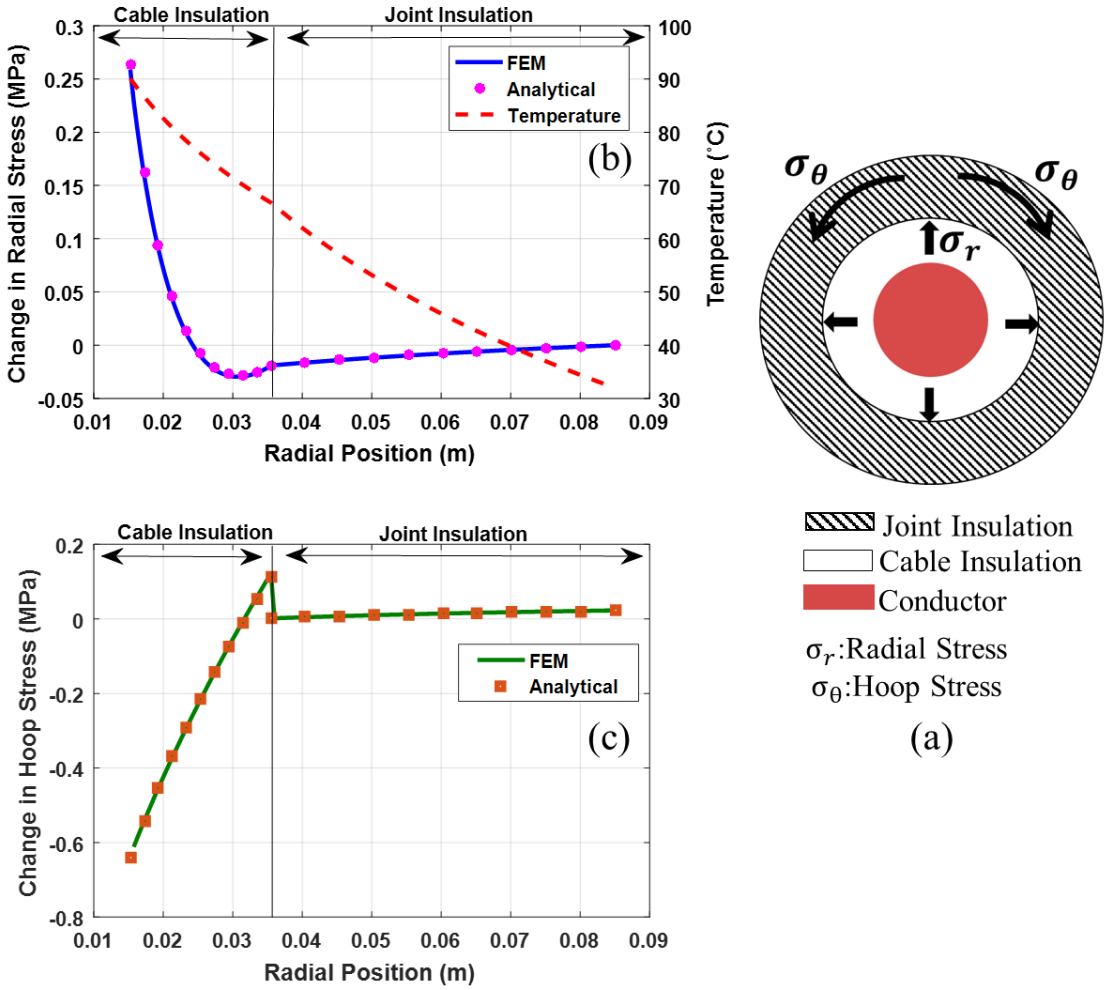

Figure 4.10: (a) Cross section of a cable joint. (b) Change in radial stress within the cable joint at 90˚C (c) Change in inner hoop stress within the cable joint at 90 ˚C

The negative value of the radial stress at the interface means that it is an increase in the initial compressive radial stress, which it is established by the joint tube at installation. If the initial compressive stress is 0.1 MPa an increase of 19% in radial compressive stress is expected at 90˚C. The change in hoop stress versus radius within the cable joint assembly in air, at 90˚C is illustrated in Figure 4.10c. The hoop stress at the interface is tensile stress. As can be seen from Figure 4.10c, the absolute maximum stress value is reached by hoop is at the side of cable insulation.

Figure 4.11 shows the change in radial stress at different conductor temperatures due to different current inputs. The change in hoop stress at different conductor temperatures is shown Figure 4.12. It observed that the analytical model has the ability to respond to the changes in the elastic modulus and thermal expansion properties because of temperature change. The conductor temperature for each case is listed. The difference in radial stress at interface obtained by FEM and analytical approaches at different temperatures are presented in Table 4.5. Table 4.6 shows the difference in inner hoop stress at interface obtained by FEM and analytical approaches at different temperatures. The deviation arises from the numerical method used and the slight difference between estimated values of elastic modulus and thermal expansion.

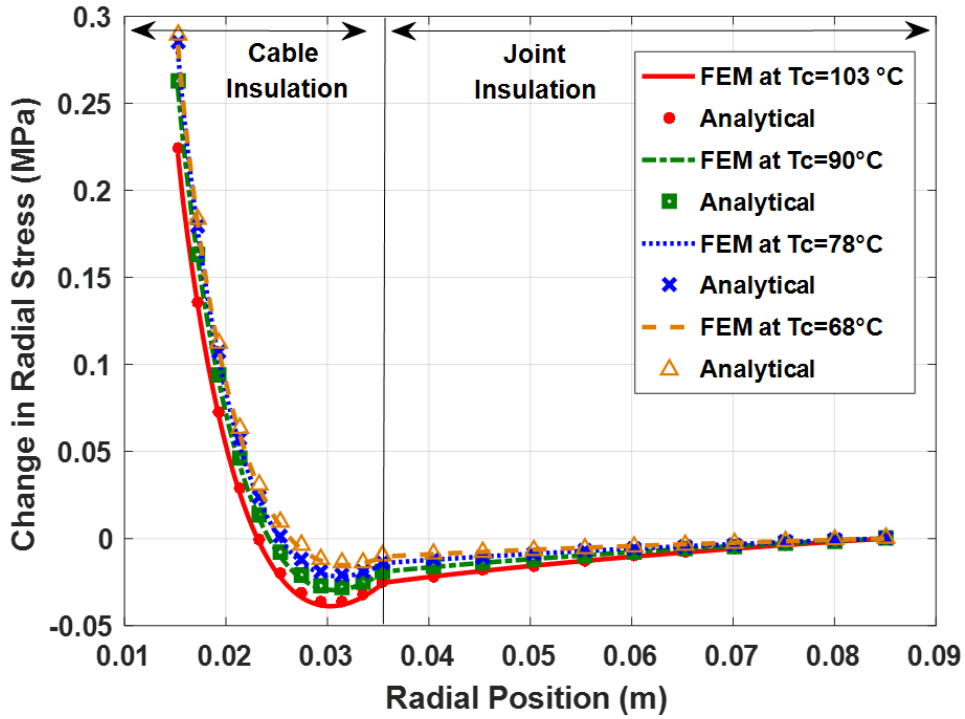

Figure 4.11: The change in radial stress at different conductor temperatures.

Table 4.4: Comparison of radial stress results obtained by FEM & analytical approaches at interface

Approach	FEM	Analytical	Difference
Radial stress at Tc=103℃ (MPa)	0.0256	0.0252	1.35%
Radial stress at Tc=90℃ (MPa)	0.0192	0.0189	1.39%
Radial stress at Tc=78℃ (MPa)	0.0142	0.0140	1.45%
Radial stress at Tc=68℃ (MPa)	0.0104	0.0103	1.53%

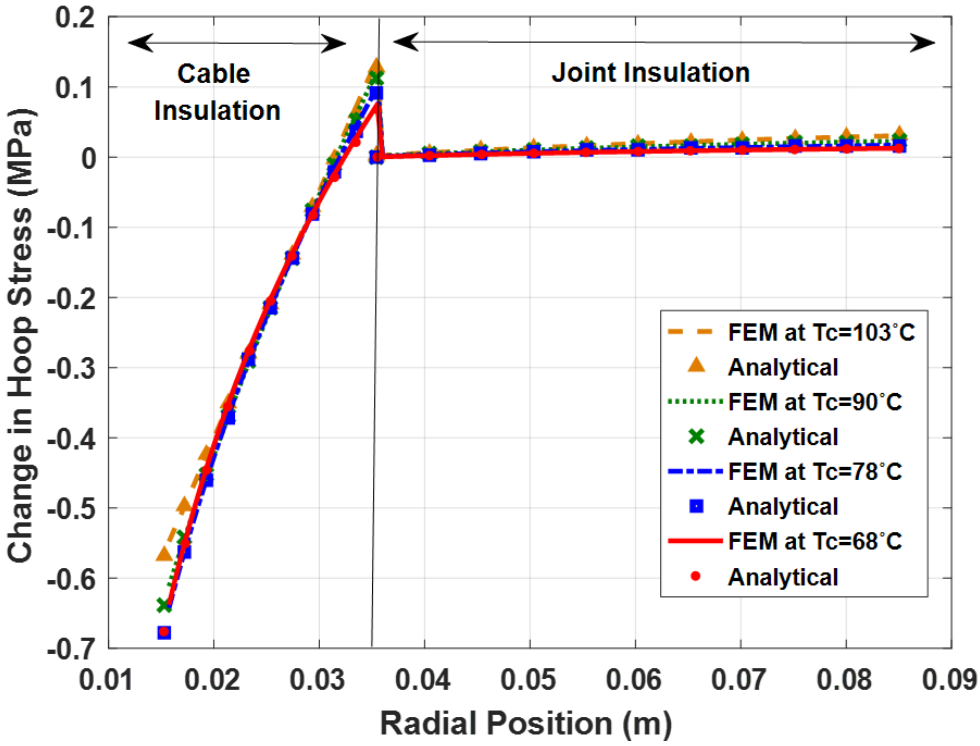

Figure 4.12: change in hoop stress at different conductor temperatures.

Table 4.5: Comparison of inner hoop results obtained by FEM & analytical approaches at interface

Approach	FEM	Analytical	Difference
Inner hoop at Tc=103 ℃ (MPa)	0.1397	0.1289	7.7%
Inner hoop at Tc=90 ℃ (MPa)	0.1221	0.1125	7.8%
Inner hoop at Tc=78 ℃ (MPa)	0.0992	0.0909	8.3%
Inner hoop at Tc=68 ℃ (MPa)	0.0749	0.0677	9.5%

4.5 Sensitivity Analysis

A sensitivity analysis was conducted on the model to investigate the effect of the mechanical properties (e.g. Elastic modulus and thermal expansion) on the change of the radial and inner hoop stress. In this analysis, the limits used for high and low parameters are listed in Table 4.6. The high and low values are chosen when the interface is at 70 ℃. The elastic modulus and thermal expansion of cable and joint insulation E_c, α_c, E_j and α_j respectively with their interactions have been examined. The change in the elastic modulus of the joint insulation and thermal expansion of the cable insulation have the highest effects on the interface pressure as shown in Figure 4.13. The elastic modulus E_c has the lowest impact of 0.044.

The main parameters that affect the change of the inner hoop stress are presented in Figure 4.14.

Table 4.6: High and Low values used in the sensitivity analysis.

Property	High Value	Low Value
α_{Cable} at 70 ˚C	5.044×10^{-4} (˚C^{-1})	2.344×10^{-4} (˚C^{-1})
E_{Cable} at 70 ˚C	51×10^{6} (Pa)	26×10^{6} (Pa)
α_{Joint} at 70 ˚C	4.636×10^{-4} (˚C^{-1})	2.836×10^{-4} (˚C^{-1})
E_{Joint} at 70 ˚C	2.28×10^{6} (Pa)	1×10^{6} (Pa)

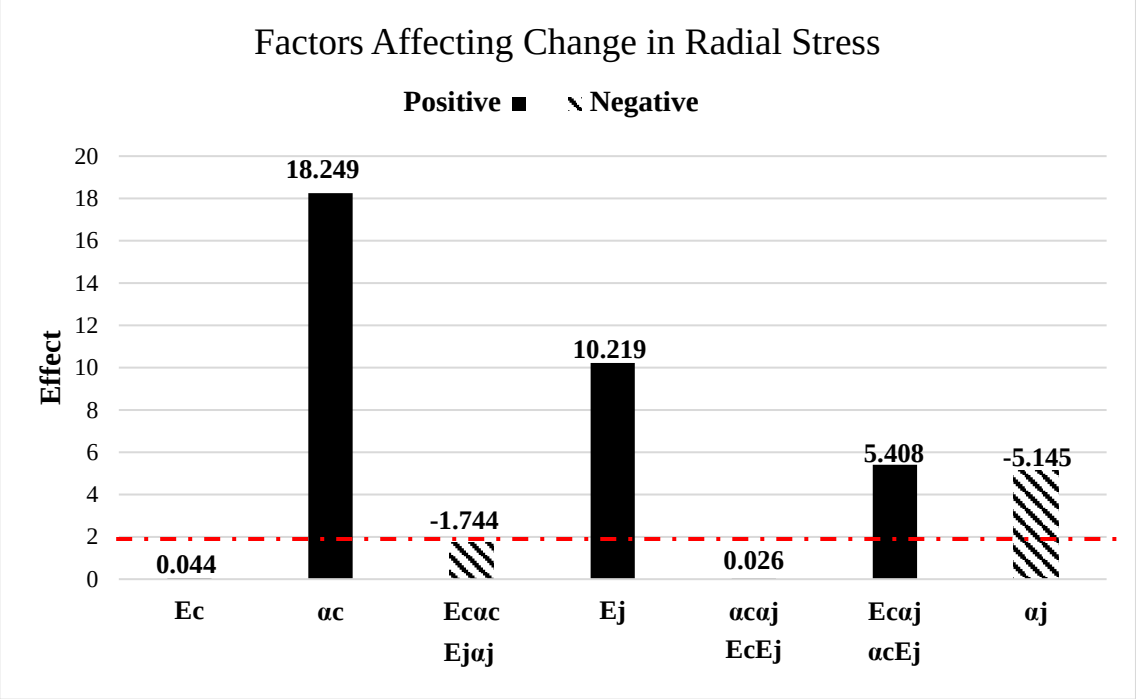

Figure 4.13: Main and interaction effects of thermal expansion and elastic modulus of insulation materials at conductor temperature of 90 °C.

The influence of cable insulation properties is higher than in the radial pressure especially the effect of E_c which has increased from 0.044 to 111.29. Unlike radial pressure, the joint insulation elastic modulus and cable insulation thermal expansion have negative impact on change of inner hoop stress. Based on this study, the thermal expansion of cable and elastic modulus of joint insulation have the highest effect on thermally induced stresses. In addition, ignoring the effect of cable insulation properties on the stresses could affect the accuracy of the results. A numerical significance of 10% of the largest effect is chosen and represented by the red line. Any effect below this line is considered not significant.

Positive effect means that increasing the value of this property will increase the response. The negative effect implies that when the low level changes to high, the response decreases. Increasing cable insulation's thermal expansion and joint insulation's elastic modulus will increase the radial pressure at the interface. However, increasing these two properties will reduce the inner hoop stress at the interface. This explains the reduction in the inner hoop values at the interface of the cable insulation and the semiconducting rubber.

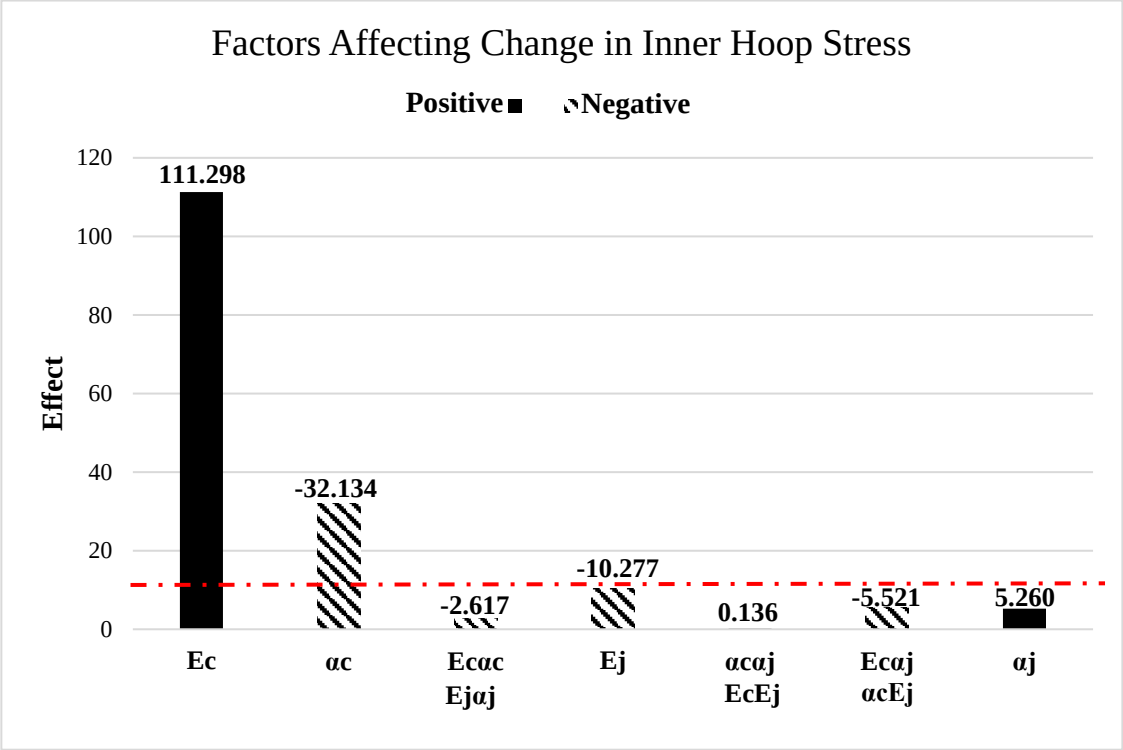

Figure 4.14: Main and interaction effects of thermal expansion and elastic modulus of insulation materials at conductor temperature of 90 °C.

In chapter 3, it is found that the main factors that affect the initial radial pressure are elastic modulus of joint tube, thickness of joint tube and expansion ratio as shown in Figure 3.6. On the other hand, the change in radial pressure is affected by cable insulations' thermal expansion, joint insulations' elastic modulus and thermal expansion as illustrated in Figure 4.13. This indicates the importance of joint insulations' elastic modulus on the initial radial pressure and its change.

In the same manner, the initial hoop pressure in the joint tube is mainly affected by expansion ratio and elastic modulus of the joint tube as illustrated in Figure 3.7. The change in hoop stress is mainly influenced by cable insulations' elastic modulus, thermal expansion and joint insulations' elastic modulus. The common factor that affects both the initial hoop stress and

its change is the elastic modulus of the joint insulation. Cable insulations' elastic modulus and thermal expansion have a significant effect only on the change of hoop stress.

4.6 Temperature Dependency impact

The change in compressive radial stress due to different currents and interface temperature is illustrated in Figure 4.15. The ambient temperature is changed between 55 to -40 ℃. The input current is varied between 897 A and 1297 A. No reduction in the initial radial compressive stress is observed since all values are compressive. At input current of 1297 A for this 132 kV cable joint, this enhancement in the initial compressive stress increases from -0.019 to -0.025 MPa as interface temperature goes up from 24 to 86.5°C. A slight decrease in this stress is observed when the interface temperature is near the critical temperature for cable insulation at 109 ˚C where the elastic modulus drops. Nevertheless, in normal operation interface temperature does not exceed 70 ˚C so no drop in interface pressure is expected. At input current of 897 A the change in radial stress is decreased as temperature decreases until it reaches -20˚C. The increase in the elastic modulus of the joint insulation at low temperature justifies the increase from - 0.0047 to -0.0054 MPa when the interface temperature goes from -10 to - 20˚C.

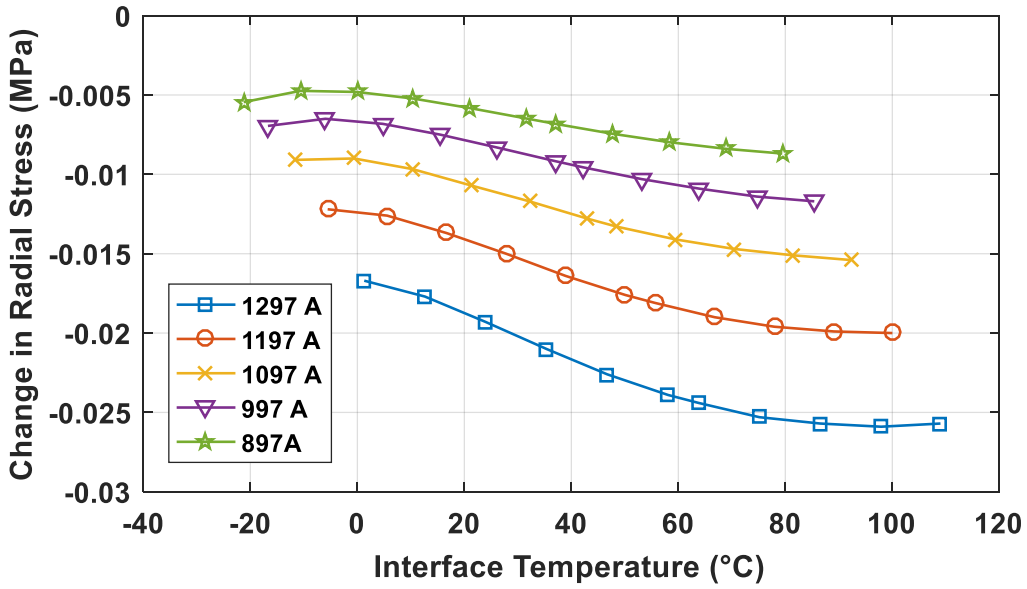

Figure 4.15: Change in radial stress with changing current and interface temperature.

In Figure 4.16 the change in the inner hoop stress caused by different input current and interface temperatures is presented. At high interface temperature the amount of change in

the inner hoop stress is low. At 1297 A the change in inner hoop drops from 0.481 to 0.035 MPa as temperature increases from 23 to 109 ˚C. The change in the elastic modulus of the joint insulation in the same temperature range is not significant at 17%. The inner hoop stress is more affected by properties of the cable insulation. The change in elastic modulus of the cable insulation in the same temperature range is more than 90%. When temperature starts to decrease the inner hoop stress enhances the initial tensile inner hoop up to a certain limit. This enhancement is driven by the increase in the elastic modulus of the cable insulation. The sudden increase in the elastic modulus of the joint insulation is considered as a turning point for the change in inner hoop stress since it starts decreasing as seen in Figure 4.16.

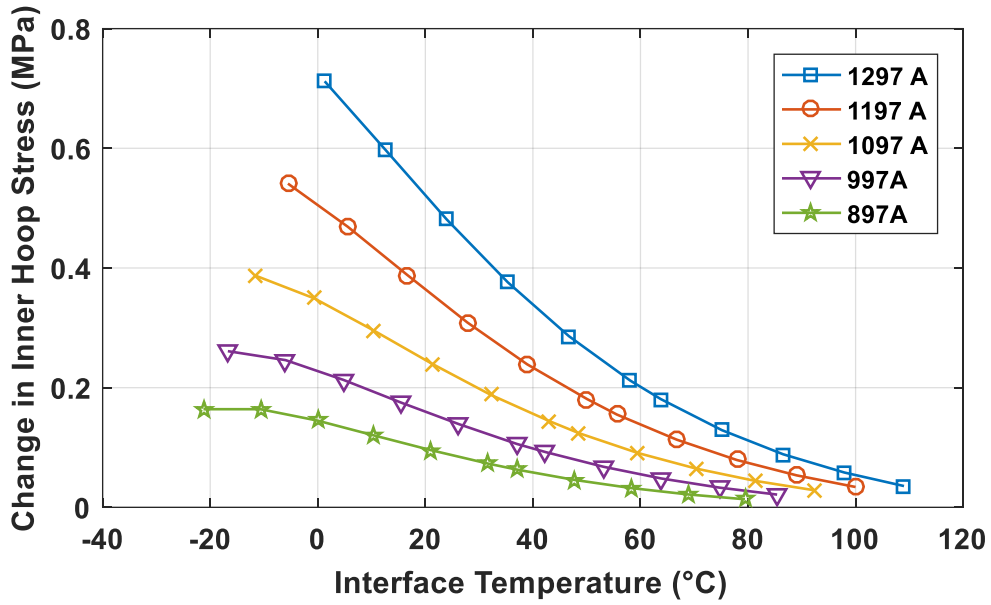

Figure 4.16: Change in inner hoop stress with changing current and interface temperature.

Based on this, the initial radial compressive stress is expected to increase but the extent of this increase will depend on temperature and material properties (e.g. elastic modulus and thermal expansion). The initial inner hoop stress is expected to increase as interface temperature drops, which could be more critical if the initial value is already high close to the tensile strength limit. Tensile stress promotes yielding and compressive stress delays yielding so if any defect is present at the interface, thermally induced stresses could make the condition worse. The thermal expansion of cable insulation and elastic modulus of the joint insulation have the largest effect on thermally induced stresses. Therefore, the effect of cable insulation properties should not be ignored when dealing with thermally induced stresses.

As presented in this chapter, the method helps the designer to determine the change in radial and hoop pressure during operation. Using this method, it is possible to include the effect of

material properties and temperature to calculate the variation in pressure. Calculating the change in pressure is important to make sure that the initial values do exceed any critical limits of the design. Although this method managed to include different parameters, there are ways to improve it. Possible improvements on this approach will be discussed in chapter seven in the future work.

4.7 Summary

This chapter has presented a method for the calculation of thermally induced stresses. This framework presents an improvement in existing algorithms for estimating the change in interface pressure, since it accounts for the variations in temperature dependent properties of the insulating materials. The accuracy of analytical approach has been verified using a model using finite element method. A calculation of change in interface pressure for a 132 kV cable joint has been demonstrated. It has been shown that at a conductor temperature of 90°C, it is noticed that both the initial compressive radial and tensile inner hoop are increased due to temperature increase. In addition, no radial pressure loss is noticed as temperature increases and this is attributed to XLPE's high thermal expansion. The thermal expansion of cable insulation and elastic modulus of joint insulation have the largest effect on thermally induced stresses. The change in cable insulating material properties with temperature is higher which affects the interface pressure. Furthermore, at low temperature the inner hoop stresses could increase the risk of having problems at the interface. The analytical method presented in this chapter managed to link the interface pressure to material properties and temperature.

In the next chapter, thermo-mechanical stresses in a single core cable and a three core cable are investigated. In three-core cable, the core is exposed to higher internal thermo-mechanical stresses than single core cables since it is more constrained and subsequently heated. The effect of temperature on thermo-mechanical properties of insulated cables must is highlighted.

Chapter 5

Analysis of Thermo-Mechanical Stresses in Power Cables

In this chapter, the effect of short circuit current on single core cables is explored. A model that analyses the insulation-sheath interface pressure during short circuit, taking into account the changes of the elastic modulus and thermal expansion of the insulating material as function of temperature is developed. In addition, a 2-D thermo-mechanical coupled model of a three core cable is developed using finite element method in order to examine the mechanical stresses produced inside the cable that would affect the shape of the insulation, and hence the electric field. The proposed model shows an example of the impact of thermomechanical stresses on the electrical field in the deformed areas, which can be useful such that appropriate testing voltages can be determined.

5.1 Effect of Short Circuit Currents on Thermo-mechanical Properties of Insulated Single core Cables

Cables should be able to safely handle the rated short circuit current in abnormal dynamic conditions, such that a through fault does not harm the whole cable. For XLPE insulated cables, the maximum temperature during short circuits should not surpass 250 °C. However, the effect of the thermo-mechanical stresses generated on the speed of degradation of the insulation system is of great importance. Short circuit current is a source of huge heat input to the cable conductor, but more to the sheath. The metallic sheath is expected to carry the full current specified during earth faults. According to [140], the maximum short circuit rating during 1 second for 630mm^2 cable is 90 kA. However, in cables with large conductors, the effect of the fault current on the metallic sheath is a dominant consideration when calculating the short circuit rating. The thermal shock generated by the short circuit causes thermomechanical stress that affects cable insulation especially in the weak zones such as interfaces.

This section analyses the influence of short circuit current on the interface between the cable sheath and insulation. Based on the theory of elasticity, a finite element thermo-mechanical model is proposed of a single core cable, incorporating temperature-dependent properties. The model demonstrates the importance of the mechanical properties of the insulating material, which plays a critical role in understanding the internal thermo-mechanical stresses within a cable.

5.1.1 Multi-Physics of the model

In order to evaluate the internal mechanical stresses generated, the sources of heat inside a cable should be considered. Conductor (W_c), sheath (W_s) and dielectric losses (W_{dielec}) per unit length are calculated according to IEC 60287. R_{ac} is the AC resistance per unit length, I is the conductor current in ampere and λ is the sheath loss multiplier. These losses are set as inputs for the heat transfer physics to find the thermal field distribution. The thermal strain and stress are computed based on the temperature rise from ambient and on the thermal expansion and elastic modulus of the material. Figure 5.1 demonstrates the coupling of the multi-physics model with its inputs.

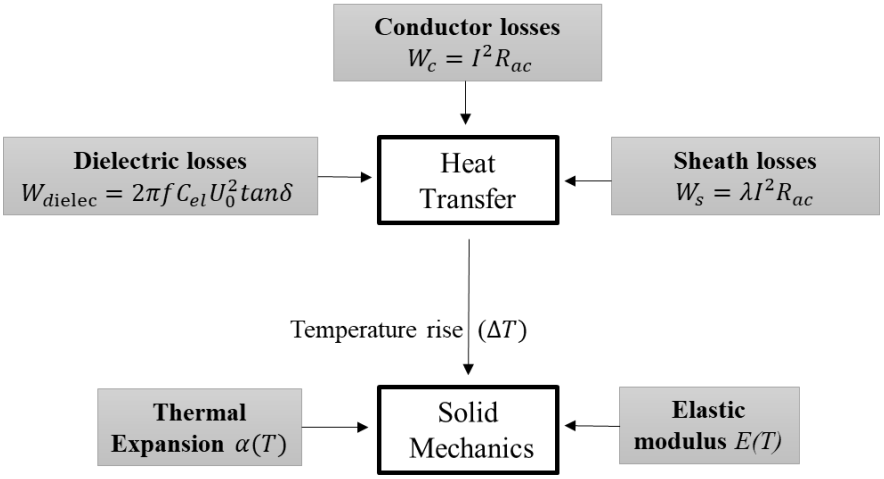

Figure 5.1: Multi-physics coupling with inputs to each physics.

5.1.2 Governing Equations and model parameters

The temperature distribution inside the cable is calculated based on the heat transfer equation of thermal conduction:

$$\rho C_p \frac{\partial T}{\partial t} = \nabla.(k\nabla T) + Q, \tag{5.1}$$

where ρ is the mass density (kg. m^{-3}), C_p the specific heat capacity (J. kg^{-1}. K^{-1}), T the absolute temperature (K), k the thermal conductivity (W. m^{-1}. K^{-1}), and Q is the heat source (W.m^{-3}). The equilibrium equation is used to find the internal forces and it can be written as:

$$\rho \frac{\partial^2 u}{\partial t^2} = \nabla . \sigma + F_v, \tag{5.2}$$

where u and σ are the displacement and the stress (N.m^{-2}), respectively and F_v is the body force per unit volume. In Figure 5.2, the geometry of the model is presented along with the thermal and mechanical boundary conditions. In Table 5.1 and Table 5.2 the cable parameters are listed.

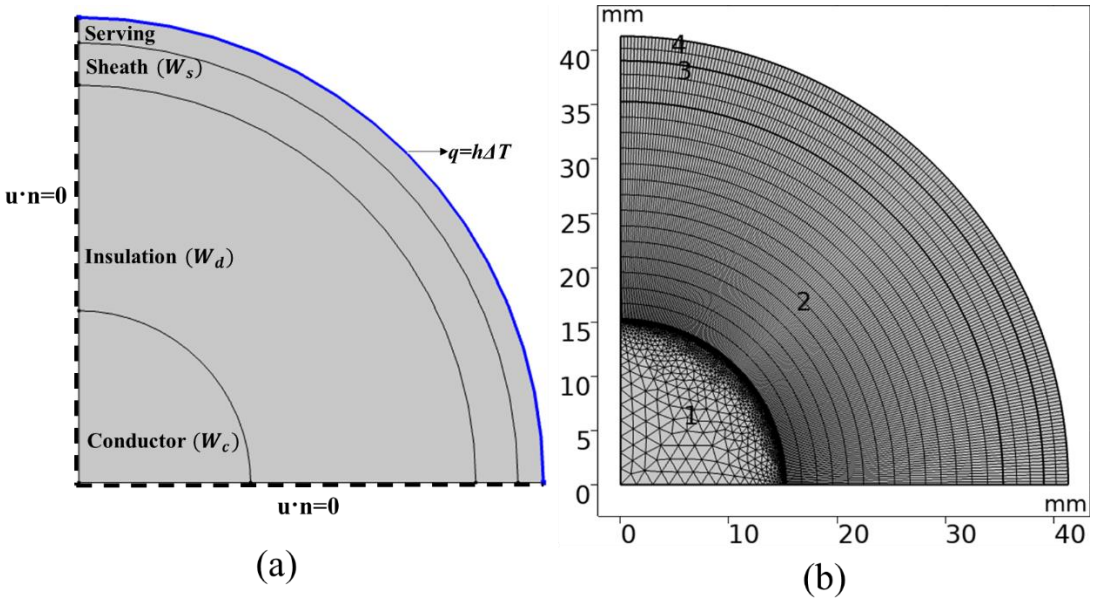

Figure 5.2: (a) Illustration of model geometry and boundary setting (b) Mesh of the Model.

Table 5.1: Specification of Model Cable

Parameter	Value	Unit
Cable Voltage rating	132	kV
Conductor cross section	630	mm^2
Thermal expansion(Cu)	1.9×10^{-5}[26]	$℃^{-1}$
XLPE thermal resistivity	3.5 [8]	Km. W^{-1}
Thermal expansion(Pb)	2.8×10^{-5}[29]	$℃^{-1}$
Serving thermal resistivity	5 [8]	Km. W^{-1}
Ambient temperature	25	℃
Heat transfer coefficient	5.6	$W(m^2. K)^{-1}$

Table 5.2: Geometries of 132 kV Cable [141].

Component	Material	Outer Diameter (mm)
Conductor	Copper	30.5
Insulation	XLPE	70.5
Sheath	Lead	78.1
Outer Sheath	PVC	82.5

The modulus of elasticity and the coefficient of thermal expansion of the insulation as function of temperature were taken from [48], and are defined as:

$$E(T) = 4.488 \times 10^{8} e^{-0.04T(r)} \qquad \alpha(T) = 5.771 \times 10^{-5} e^{0.02T(r)} \tag{5.3}$$

The exponential indices and the constants are found by curve fitting. The change in these properties in terms of temperature areapproximated using an exponential function to avoid anyundefined values of pressure during differential operations. Figure 5.3 shows elastic modulus and the thermal expansion as a function of temperature. Both the data taken from [48] and the approximated functions are provided in the figure. It is worth noting that the approximated function captures the turning point in the elastic modulus. Using the approximated function the elastic modulus drops after 105℃ although the transition is not sharp as the real data to avoid any simulation errors. Moreover, all materials are assumed to be perfectly elastic in this simulation.

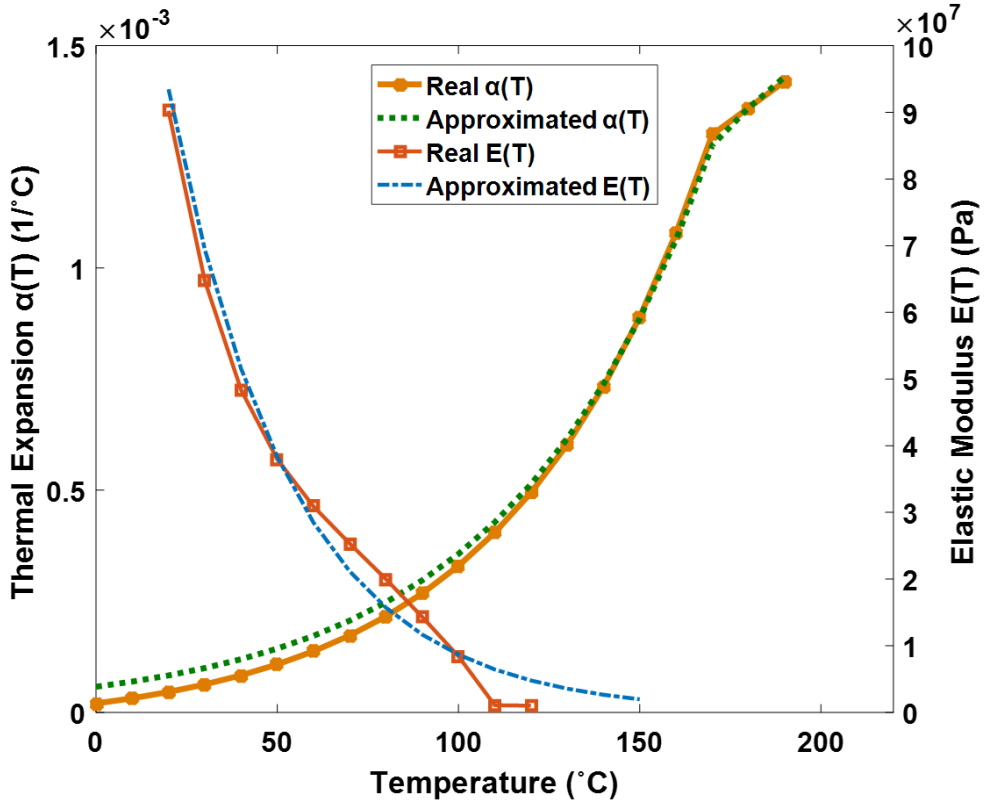

Figure 5.3: Real and approximated data of Elastic modulus and thermal expansion of insulating material [48].

5.1.3 Results

To reduce the computation time, a steady state study was conducted first. Then the output of this study was set as an initial condition for the transient study. Figure 5.4 shows the temperature output from the transient study for cable's conductor and sheath.

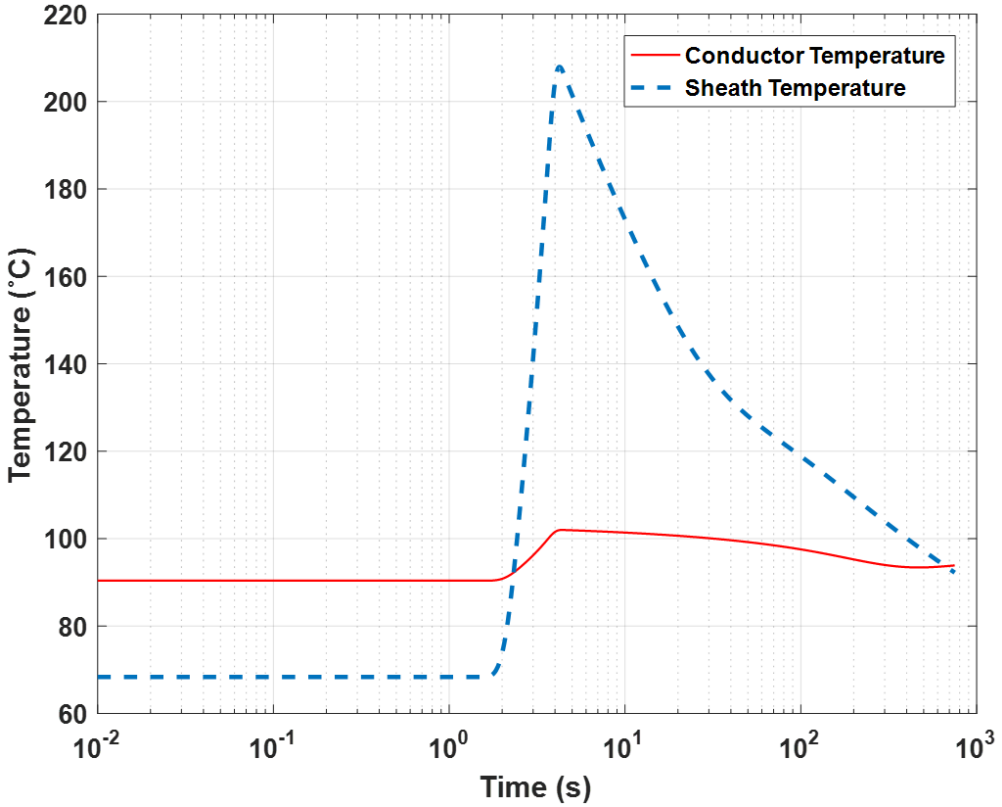

Figure 5.4: Conductor and sheath temperature during 21 kA short circuit for two seconds

The conductor and sheath temperatures in steady state are 90˚C and 68˚C respectively, which are the initial conditions for the transient study. A fault current of 21 kA is injected at the first second and lasts for 2 seconds then goes to zero. This value represents the maximum permissible value for lead sheath with thermal restriction of 210 ℃ [10,142,143]. During the short circuit, the high heat injection into the sheath will heat up the cable sheath which reaches a temperature of almost 210˚C. In Figure 5.5, the change in elastic modulus and thermal expansion during the short circuit at the insulation-sheath interface is illustrated. The elastic modulus dropped from 29 MPa to 1.2 MPa due to the temperature increase. Unlike the thermal expansion which is directly proportional to temperature the elastic modulus is inversely proportional to temperature. The pressure at insulation/sheath interface along with the temperature change is shown in Figure 5.6. It should be noted that the pressure is assumed zero at the time the cable is first energised.

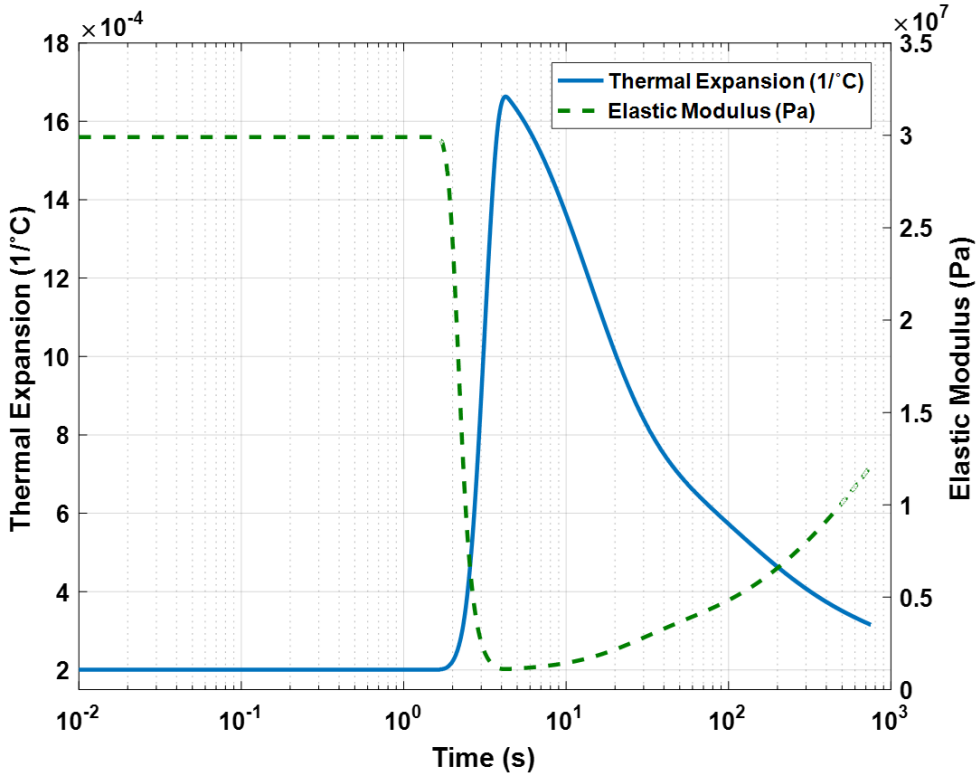

Figure 5.5: Elastic modulus and thermal expansion of the insulation at sheath to insulation interface during 21kA short circuit.

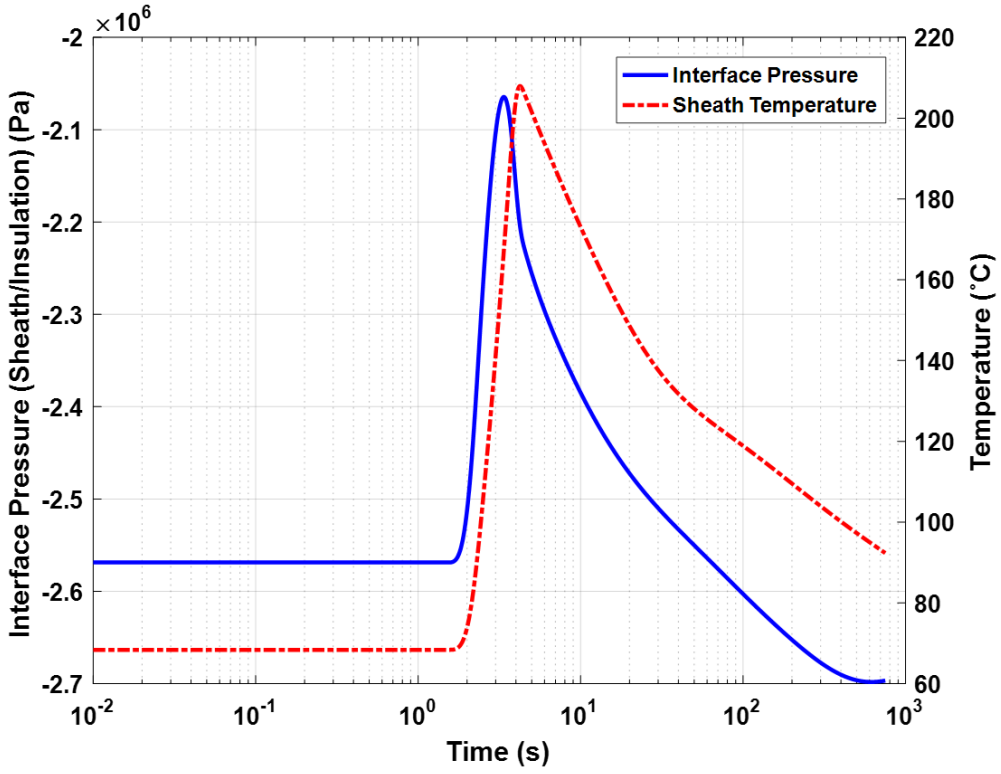

Figure 5.6:Interface Pressure and Temperature at insulation/sheath interface during 21kA short circuit.

The pressure value is negative indicating a compressive pressure. The pressure has fallen from 2.569 MPa to 2.066 MPa meaning that the pressure has lost 20% of its initial value (i.e. the value immediately before the fault) because of the short circuit. The initial interface pressure value was restored within the first 50 seconds of the simulation. The ability to restore the initial interface pressure in less than 50 seconds can be explained by the high thermal expansion of the insulation. It is noted that even after passing 50 seconds, the pressure is higher than the initial value since the temperature at the interface is still higher (95 ℃) than the initial value (68 ℃). To show the influence of the thermal expansion on the interface pressure, different insulation thermal expansion values were tested. With lower thermal expansion coefficients the drop in the interface pressure increases and it takes longer time for the interface to restore its initial value as shown in Figure 5.7.

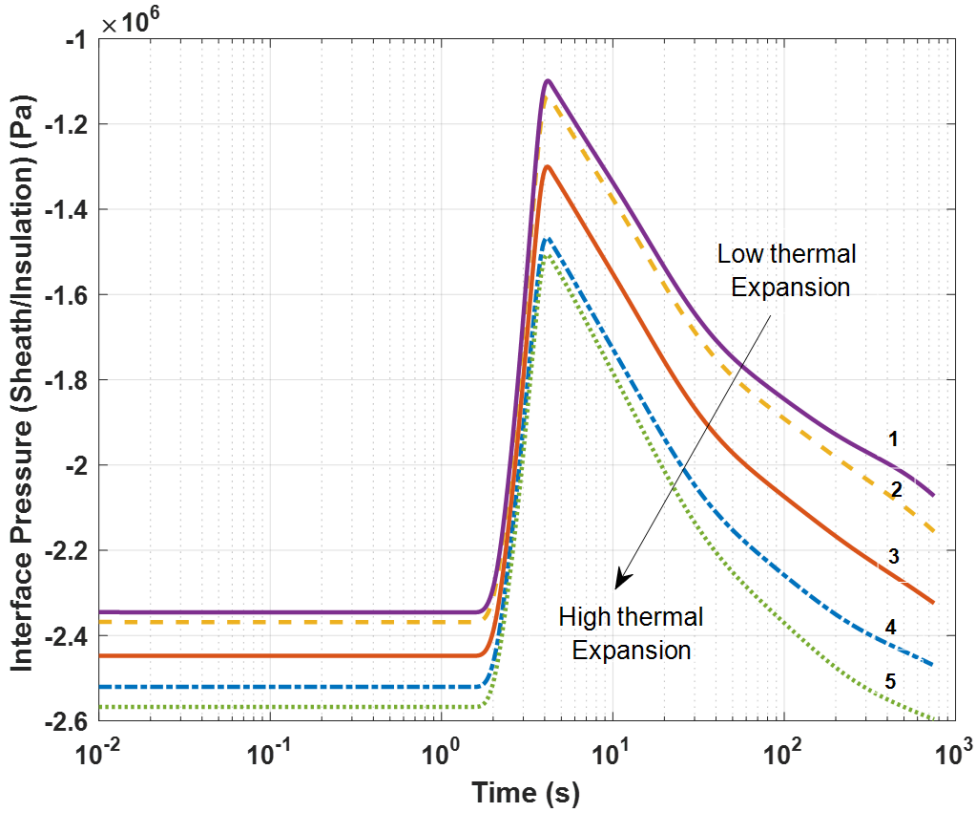

Figure 5.7: Interface Pressure with different insulation thermal expansion coefficient (Low thermal Expansion: 4×10^{-4}- High thermal Expansion: 7×10^{-4} ℃$^{-1}$).

Table 5.3 summarizes the initial values of interface pressure for each value of thermal expansion at 90˚C with relative change in the interface pressure during the short circuit. The five curves that represents the five thermal expansion values used during the short circuit is illustrated in Figure 5.8. As the thermal expansion increases, the initial value of the interface

pressure at 90˚C increases. During the short circuit, increasing the thermal expansion has minimized the drop from 53% to 40% and managed to restore the initial value of the pressure during the simulation time. It can be seen the thermal expansion 1 has the lowest thermal expansion values and thermal expansion 5 has the highest.

Table 5.3: Interface Pressure with different thermal expansion values

Interface Pressure curve	Interface Pressure at 90℃ (MPa)	Pressure drop during short circuit (%)	Initial value restored at t=750s
1	-2.34	53%	No
2	-2.36	52%	No
3	-2.44	46%	No
4	-2.47	42%	No
5	-2.56	40%	Yes

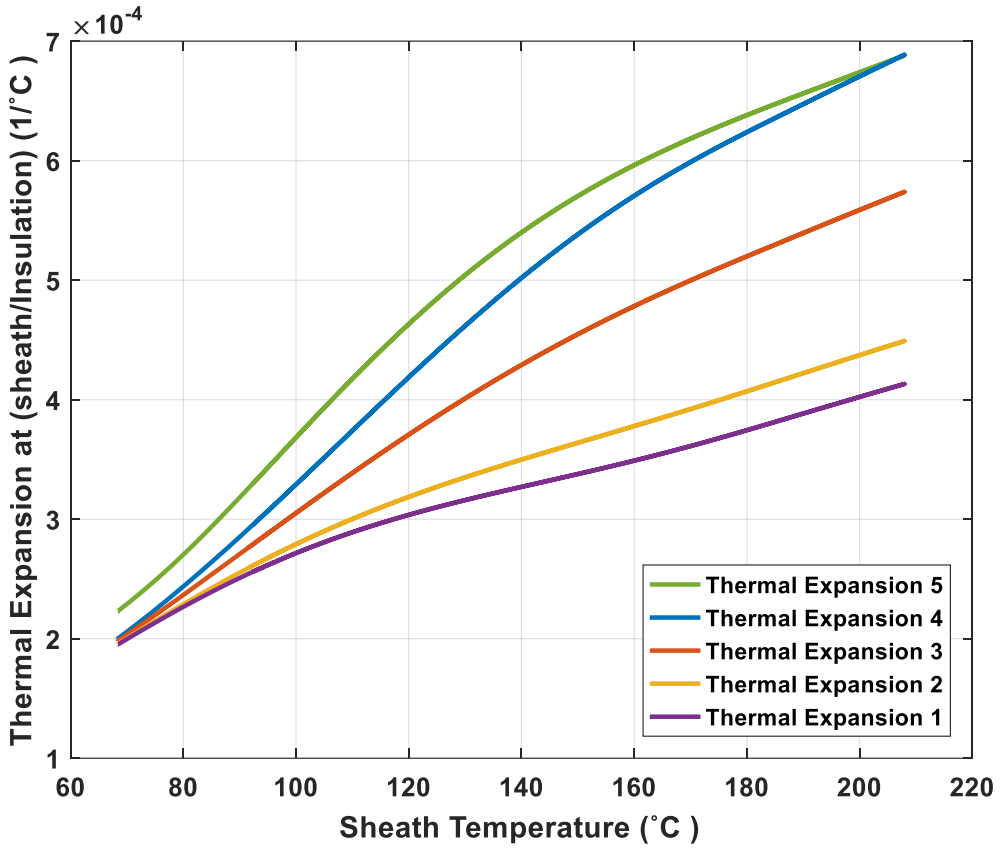

Figure 5.8: Different Thermal Expansion during 21kA short circuit for 2s.

To investigate the difference in pressure response when considering the material properties as a function of temperature or as constant values, the simulation is solved with different assumptions as shown in Table 5.4. The functions used to express the change in the

mechanical properties are the same as equation 5.7. The relative change of pressure at the interface from its initial value (at 90˚C**)** is calculated.

Table 5.4: Pressure change during short circuit for different scenarios.

Factor		Interface Pressure at 90℃ (MPa)	Interface Pressure change during short circuit (%)	Pressure initial value restored
Elastic Modulus	Thermal Expansion			
E*(T)*	$\alpha(T)$	-2.56	-24%	Yes
30×10^{6}	$\alpha(T)$	-3.45	-7%	Yes
E*(T)*	2.2×10^{-4}	-2.36	-60%	No
30×10^{6}	2.2×10^{-4}	-3.16	-37%	Yes

The behaviour of the interface pressure at insulation-sheath for different scenarios is presented in Figure 5.9. The same short circuit current value and duration 21 kA for 2s is applied for all the cases in Figure 5.9. In all cases, a pressure drop is observed during the short circuit even when the elastic modulus and thermal expansion is constant. The huge heat input in the sheath will make the sheath expand faster than the insulation causing pressure drop at the interface at the first second. Polymers have smaller thermal diffusivity (10^{-7}m^2/s) than metals for example it takes 1s for heat to diffuse around 0.3 mm which explains the delay [112]. When both properties are considered constant as shown in Figure 5.9, the pressure is restored because of the huge increase in temperature. Comparing the results of constant and variable thermal expansion in Figure 5.9, it shows that assuming constant thermal expansion instead of assuming it as a function of temperature, can increase the pressure drop and restore it slower depending on the elastic modulus assumption. Moreover, it is acknowledged that with increasing temperature, the volumetric thermal expansion of cable insulations such as XLPE is about 10 times higher than that of copper or aluminum and because the XLPE is more elastic than the conductor is and becomes softer at higher temperatures, the insulation will then be detained by the resultant pressure. The decrease in the elastic modulus lowers the interface pressure but the large thermal expansion and increase in temperature helps in restoring the interfacial pressure.

To explore the effect of different short circuit durations, a short circuit value of 21 kA is applied for 0.5 second, 1 second and 2 seconds as shown in Figure 5.10. It can be observed that as the duration of short circuit current increases the drop in interface pressure increases. This behaviour is justified by the higher temperature reached as the short circuit duration is

increased. In addition, as the duration of short circuit current increases the pressure does not restore its initial value since the insulation temperature did not reach its initial value.

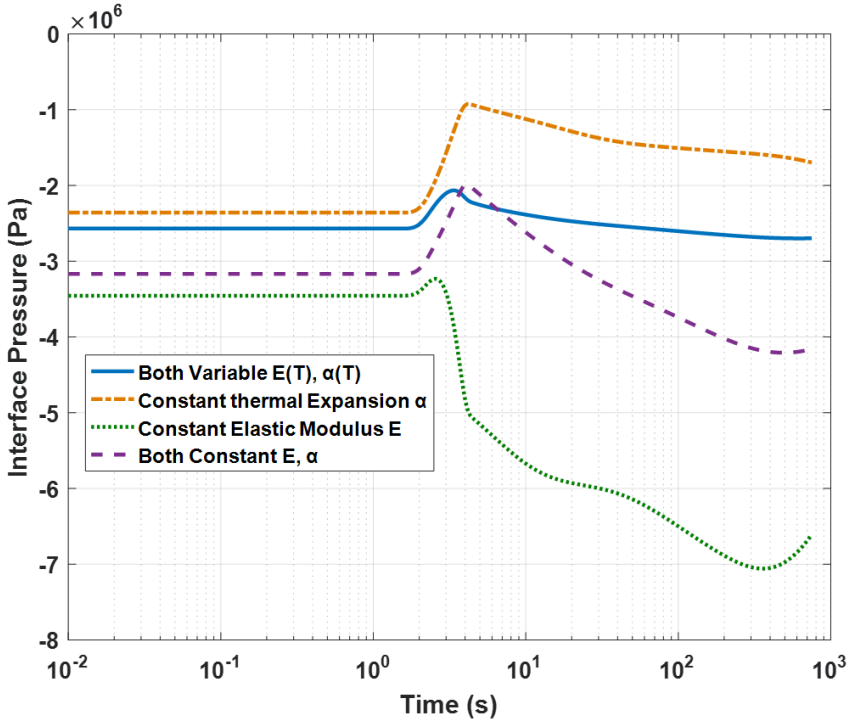

Figure 5.9: Interface Pressure at Insulation/Sheath interface for 21 kA 2s with different assumptions.

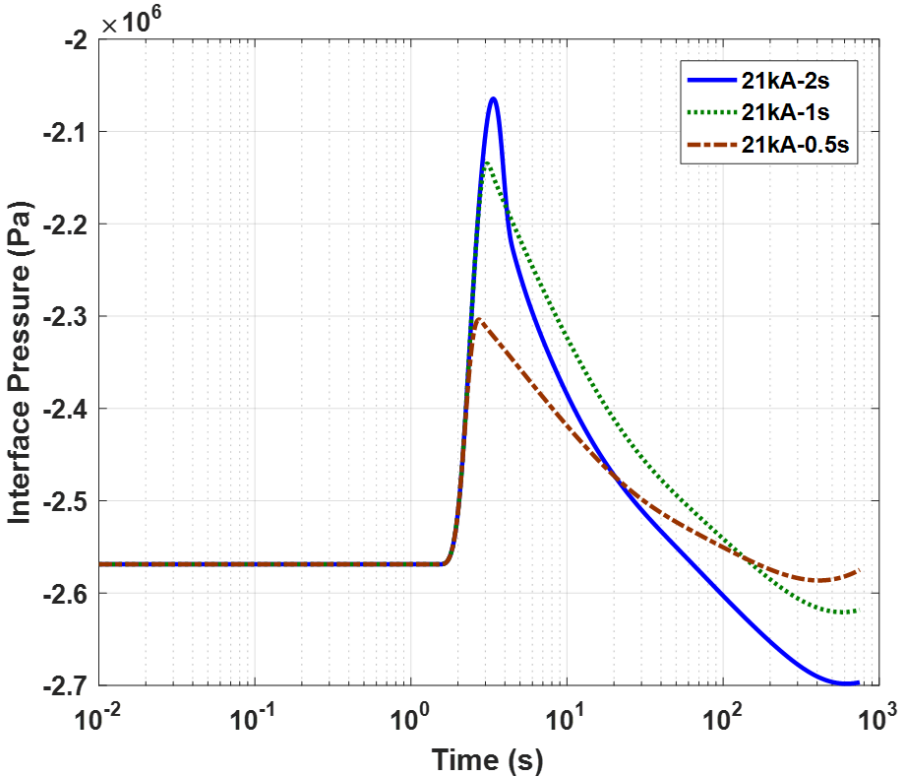

Figure 5.10: Different Short Circuit Duration for 21kA.

Figure 5.11 shows two different short circuit values and durations, 21 kA for two seconds and 30 kA for 1 second. The interface pressure profile in the two cases in not that different since in both cases sheath temperature reaches almost the same temperature. The sheath temperature in the 30 kA case is a little bit higher than 21 kA case which 215 °C.

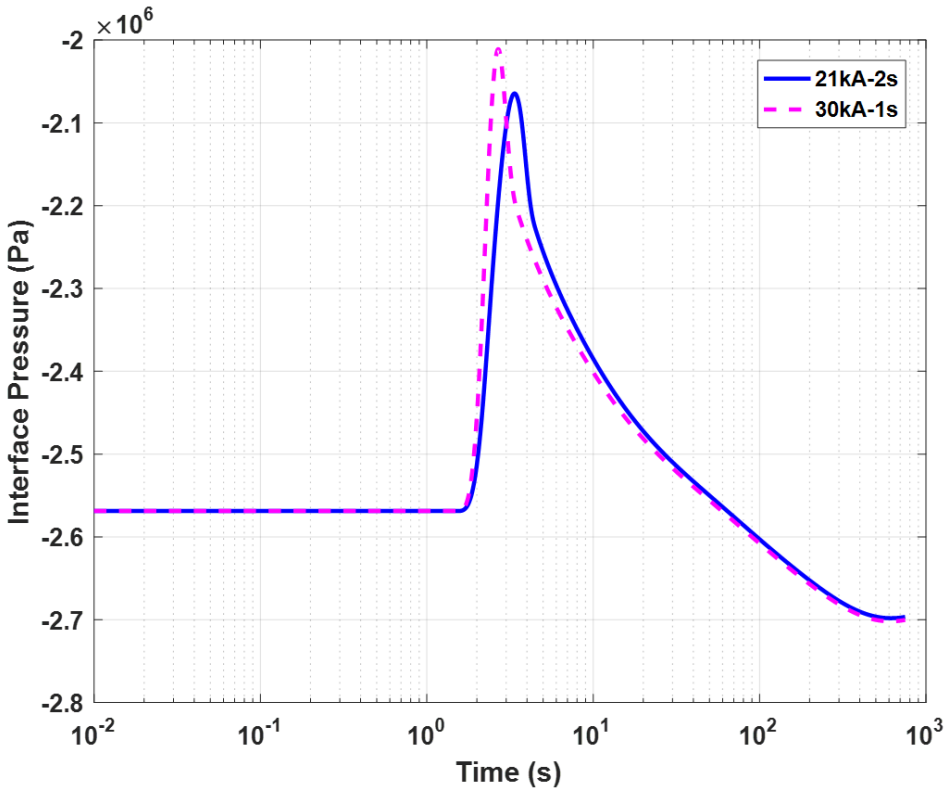

Figure 5.11: Different values and Durations of Short Circuit.

This part presents a model that analyses the insulation-sheath interface pressure during short circuit, taking into account the changes of the elastic modulus and thermal expansion of the insulating material as function of temperature. The model shows the significance of the mechanical properties as a function of temperature. It was found that, the change of elastic modulus with temperature lowers the interface pressure during short circuits. This could be an issue if partial discharge is initiated in any gap or void created. Moreover, the high thermal expansion of insulation with high temperature can restore that drop in pressure. Insulating material with high thermal expansion coefficient is useful in maintaining the dielectric integrity, but will also lead to a greater force being exerted on the sheath in normal directions. The thermomechanical stresses inside is expected to be higher than stresses in single core cables. In the following section thermo-mechanical stresses in three core cables are explored.

5.2 Thermo-Mechanical Stress in Three Core Submarine Power Cable

Power delivery from offshore wind farms is dependent on the performance of power cables. However, the variable and uncontrollable nature of wind resources mean the loading on these circuits is more dynamic. Cables are tested to assure that they will function as expected throughout their entire lifetime. Nevertheless, according to CIGRE TB 490 recommendations, electrical testing of single core is allowed but not required for three core cables. But in case one core is tested instead of the three cores as a whole this could be considered a deviation from the real case. Since the core are highly concentric, not fully laid up cables, which may be more eccentric. Due to sheath deformation arising from thermomechanical forces, the lead (Pb) sheath could deform plastically increasing the chances of forming gaps at the interface.

In the following section, using finite element modelling, a 2D thermal-mechanical coupled model is established. The deformed cable model is then studied through an electrical model.

5.3 Three core Submarine Power cable model

In this part, a description of the model physics, governing equations, material properties and boundary conditions is presented.

5.3.1 Description of the Cable and Parameters

A 132 kV three phase XLPE insulated SL-type (each phase in separate lead sheath) submarine cable with 1000 mm^2 conductors is modelled. The three cores are protected and covered together using layers of polyethylene and single steel armour wires as shown in Figure 5.12.

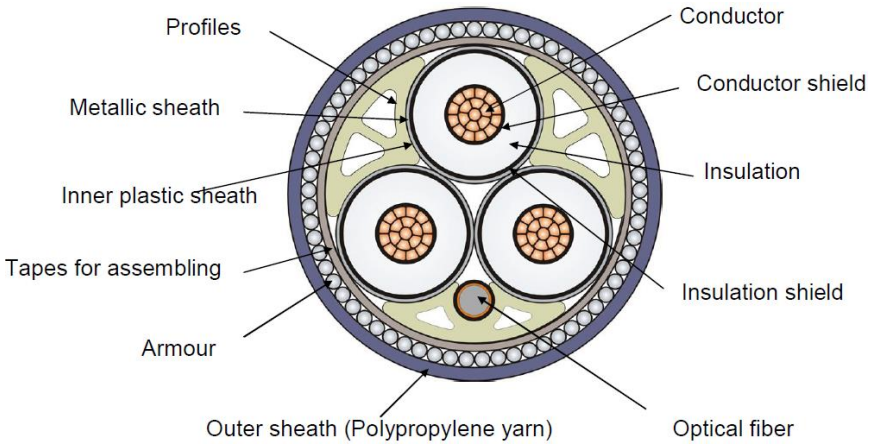

Figure 5.12: Illustration of Typical Three-Core SL Type Cable [126].

The cable dimensions and thermal material properties are presented in Table 5.5 and it is taken from [144].

Table 5.5: Cable Dimensions and Material Properties [144].

Geometry	Material	Thermal Conductivity ($Wm^{-1}K^{-1}$)	Volumetric Heat Capacity ($MJm^{-3}K^{-1}$)	Radius (mm)
Conductor	Copper	320	3.45	20
Conductor Screen	Semicon XLPE	0.5	2.4	21.5
Insulation	XLPE	0.286	2.4	38.5
Insulation Screen	Semicon XLPE	0.5	2.4	40
Water Tape	Undefined Polymer	0.286	2.4	41.5
Sheath	Lead	35.3	1.45	43.8
Inner Sheath	Semicon PE	0.5	2.4	46
Bedding and filler	Polypropylene yarn	0.123	1.9	101
Armour	Steel	18	3.8	106.5
Serving	PE	0.2	1.7	111

The simplified cross section of the three core cable is shown in Figure in 5.13. Materials mechanical properties are listed in Table 5.6.

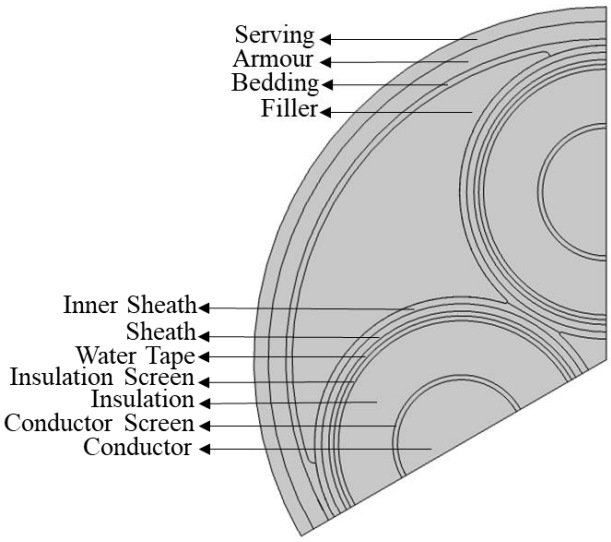

Figure 5.13: Simplified cross section of XLPE Insulated Three-Core HVAC Cable.

Table 5.6: Materials mechanical properties.

Component	Material	Thermal Expansion (K^{-1})	Young's Modulus (Pa)	Poisson's ratio
Conductor	Copper	19×10^{-6} [26]	110×10^{9} [34]	0.35 [43]
Conductor screen	Semicon XLPE	20×10^{-5}	160×10^{6}	0.46
Insulation	XLPE	25×10^{-5}	120×10^{6}	0.46 [95]
Insulation screen	Semicon XLPE	20×10^{-5}	160×10^{6}	0.46
Water blocking tape	Polymer	10×10^{-5} [148]	100×10^{6}	0.46
Sheath	Lead	28.9×10^{-6} [29]	16×10^{9} [29]	0.44 [43]
Inner sheath	PE	15×10^{-5}	1×10^{9}	0.45
Bedding & Filler	Polypropylene	10×10^{-5} [147]	85×10^{6}	0.42 [146]
Armour	Steel	12.3×10^{-6} [34]	200×10^{9}	0.30 [45]
Serving	PE	15×10^{-5} [146]	1×10^{9}	0.45 [146]

5.3.2 Mechanical Physics Boundary Conditions

Under the mechanical physics, the circumference of the cable should be defined as fixed constraint (e.g. **u**=0) to fulfil the requirement for a constrained cable (e.g. buried in the soil). In addition, only one third of the cable is simulated and symmetry is assumed as seen in Figure 5.14 Under the mechanical physics, contact pairs are defined and adhesion with no separation is assumed for the contacts inside each core except for the sheath-water blocking

tape interface, which has a static friction only [148]. Moreover, cable cores are assumed to be in contact to avoid any mesh deformations in the narrow area between the cores.

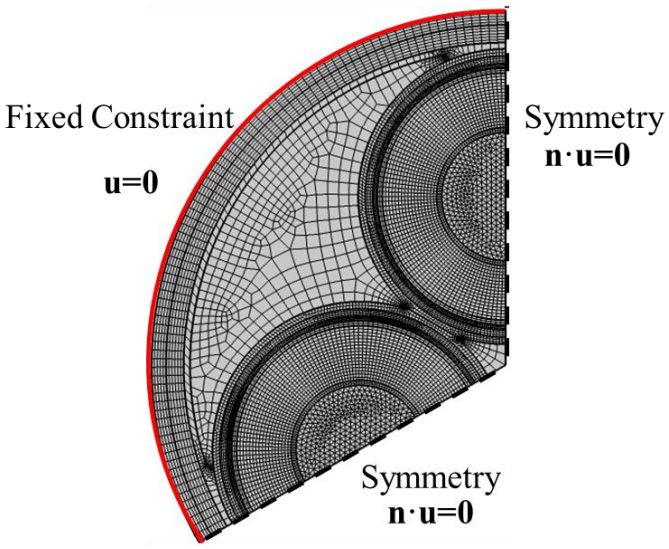

Figure 5.14: Simplified cross section of the three-phase export cable showing the mesh and mechanical Boundary Conditions

5.3.2.1 Contact Modelling

When studying mechanical stresses and deformation, modelling of contact interaction is important. Contact surfaces are the regions of the boundary surface that are in contact. The contact forces deform objects [149]. Due to deformation, detached boundary surfaces can come into contact and boundary surfaces that are initially in contact could be separated. To model contact between boundaries, the penalty method is adopted. The penalty method is based on the assumption that there is a stiff spring between the contacting boundaries. The stiffness of this spring is represented by a value known as the penalty factor. A large penalty parameter satisfies the contact constrains more accurately. However, the resulting system of equations may become ill conditioned and unstable as the penalty factor increases. As a result, the choice of a convenient penalty factor is a matter of compromise between accuracy and stability [149]. The contact pressure T_n in the normal direction is defined as:

$$T_n = \begin{cases} -p_n d_g + p_0 & d_g < \dfrac{p_0}{p_n} \\ 0 & d_g \geq \dfrac{p_0}{p_n} \end{cases} \tag{5.4}$$

where d_g is the effective gap distance, p_n is the penalty parameter, and p_0 is the pressure at zero gap.

5.3.2.2 Plastic Deformation Model

Materials undergo temporary (elastic) deformation when subjected to a stress level below their yield stress (elastic limit). In the elastic region, the material can fully recover its original shape upon unloading. The stress strain relation will be linear and governed by Hooke's law as long as the stress does not exceed the elastic limit. If the stress is further increased beyond the elastic limit, the amount of deformation increases but this extra amount is permanent (not recoverable upon unloading). After passing the yield stress, the material will deform in the plastic region. Different models are used to approximate stress strain behaviour of materials. For ductile materials, there are different ways to describe the increase in stress needed to continue plastic deformation known as strain hardening. If no strain hardening is included, the material is said to be perfectly plastic. In this case, the plastic curve is horizontal and stress in the plastic region does not depend on plastic strain. The introduction of strain hardening can be through linear or power law relations. The Ludwik equation is used [42,45. 150],

$$\sigma = \begin{cases} E\epsilon_{elastic}, & \sigma < \sigma_Y \\ \sigma_Y + k\epsilon_p^n, & \sigma \geq \sigma_Y \end{cases} \tag{5.5}$$

where E is the elastic modulus N.m^{-2}, σ_Y is the yield stress N.m^{-2}, $\epsilon_{elastic}$ and ϵ_p are the elastic and plastic strain respectively. The constants *k* and *n* depend on the nature of the material, temperature and strain. The constant *k* is known as the strength coefficient and *n* is the hardening exponent. If the stress is in the elastic region namely (ϵ_p=0,$\sigma \leq \sigma_Y$) then it has a linear relation with the strain. On the other hand, when the strain develops after exceeding the elastic limit it is prescribed by nonlinear relationship as in equation (5.8). This relation can be easily transformed to perfectly plastic model by setting *n* to equal zero.

5.3.3 Thermal Physics Boundary Conditions

To model thermal stresses inside a power cable, heat sources must be identified and calculated. There are four main heat sources within a power cable: conductor, sheath, armour and dielectric losses. The losses are calculated based on IEC 60287 standard. To calculate the heat source presented by the conductor, sheath and armour losses per unit length equations (2.22-2.30) in chapter two are used. The sheath loss factors can be determined using [8, 50]:

$$\lambda_s = \frac{R_s}{R_{AC}} \cdot \frac{1.5}{1 + \left(\frac{R_s}{x}\right)^2} \tag{5.6}$$

$$x = 2\omega \ln\left(\frac{2s}{d_s}\right) \cdot 10^{-7} \tag{5.7}$$

where R_s is the sheath resistance, s and d_s are the distance between cable axes in mm and the sheath diameter respectively. The armour loss factor for an armour surrounding a three core is determined using [8, 50]:

$$\lambda_a = 1.23 \frac{R_a}{R_{AC}} \left(\frac{2c}{d_a}\right)^2 \frac{1}{\left(\frac{2.77 R_a 10^6}{\omega}\right)^2 + 1} \cdot \left(1 - \frac{R_{AC}}{R_s}\lambda_s\right) \tag{5.8}$$

where R_a is the armour resistance, c is the distance that separates the conductor axis from the cable axis and d_a is the diameter of the armour in mm. In the heat transfer module, the contact interface is modelled as a thin layer with a low thermal resistance using thermal contact boundary condition. In addition, the thermal environment was represented by an environment having an external heat transfer coefficient 5.6 ($W.m^2.K^{-1}$). It is worth noting that changing this value will not change the temperature difference within each layer. It will only shift the temperature profile as shown in Figure 5.15.

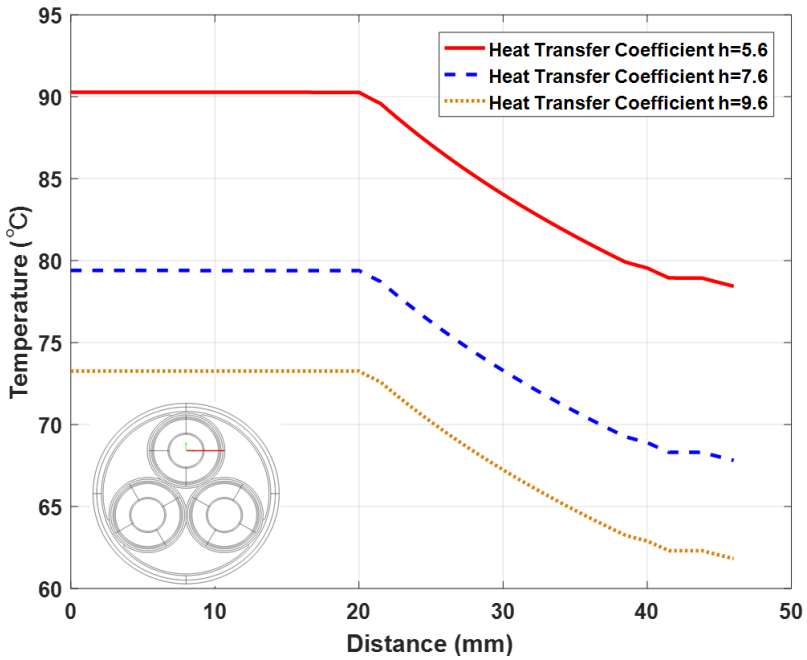

Figure 5.15: Temperature Profile in One Core of a Three Core Cable for Different heat Transfer Coefficients.

The steady state temperature distribution of a 132 kV three core submarine power cable is shown in Figure 5.16a. It is noticed that the highest temperature is inside the cores and it gradually decreases as the outer radius of the cable in reached. However, the temperature distribution inside the cable is not uniform. This can be observed even more clearly in Figure 5.16b where the temperature distribution in the sheath is illustrated. The part of the sheath facing the cores is at higher temperature (82°C) than the part facing the armour which is at 73°C. On the other hand, temperature distribution in a single core is radially and uniformly distributed as shown in Figure 5.17a. This will result in a uniform distribution of temperature in the sheath and temperature difference will equal at any point. This observation could be very important when dealing with thermo-mechanical stresses. More specifically, the non-uniform distribution of temperature around the sheath may cause a non-uniform distribution of mechanical stress that must be taken into account when dealing with thermo-mechanical stresses in cables.

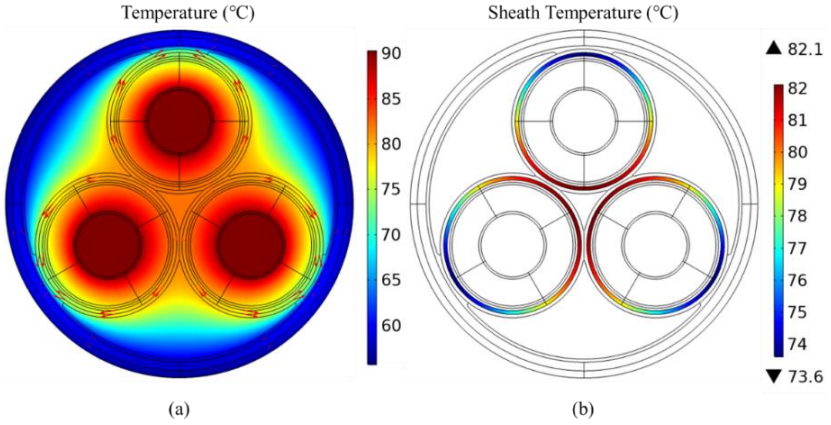

Figure 5.16: (a) Temperature distribution of a three core cable at 90°C with heat flux vectors (b) Sheath Temperature Distribution.

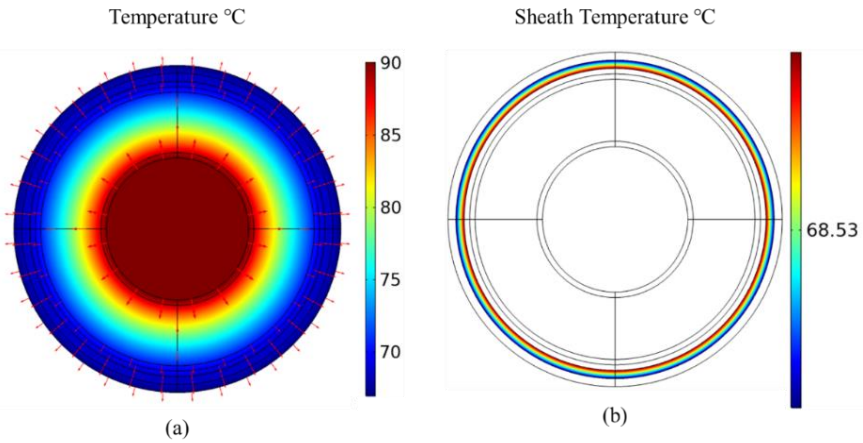

Figure 5.17: (a) Temperature distribution of a single core cable at 90°C with heat flux vectors (b) Sheath Temperature Distribution.

5.3.4 Model Coupling

Once the heat sources have been set with the appropriate boundary conditions, the heat transfer equation of thermal conduction is solved for the temperature distribution as shown in Figure 5.18. More details about this equation is found in chapter two in section 2.5. For the structural analysis, the thermal strain and stress are found by applying the equilibrium equation. The equation is presented in Figure 5.18 as a reminder. The equation is discussed in chapter two in section 2.6.

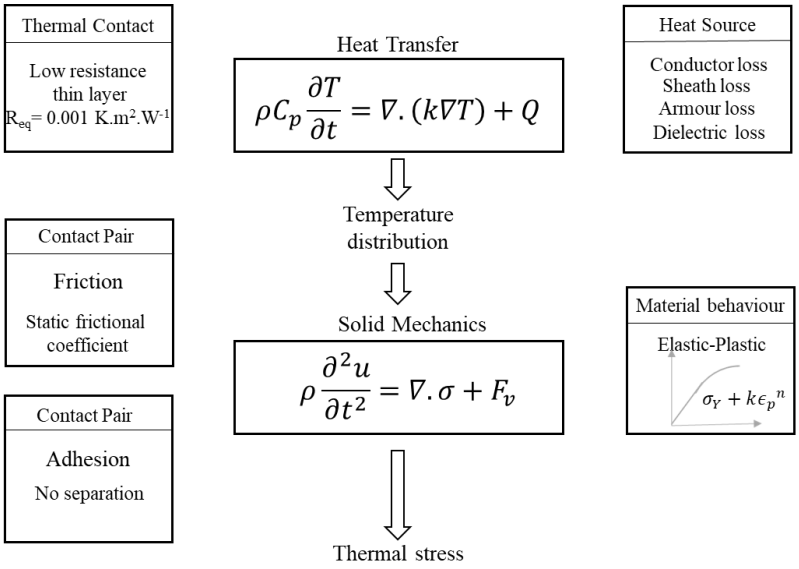

Figure 5.18: Multi-physics interaction

5.4 Model Assumptions

Modelling of submarine power cables is not an easy task because of their complex structure. There are set of assumptions considered in this model and they are presented in Table 5.7. In addition, three sensitivity analyses are conducted to investigate some of these assumptions effect on sheath plastic strain.

Table 5.7: Model Assumptions and Justifications

Number	Assumption	Justification
1	The core are assumed perfectly identical	To improve computational efficiency, and so symmetry can be assumed.
2	The conductor Screen and the insulation screen are bonded with the insulation	This assumption can be justified since the three layers (conductor screen, insulation and insulation screen) are manufactured simultaneously in a triple extrusion system. In this simulation, the outer and inner semi-con are bounded with the insulation since the interest here is in the bulk deformation.
3	The bedding is attached to the filler	The bedding is attached with the filler, to avoid mesh deformation for the bedding layer due to its small thickness and low mechanical strength.
4	Armour is represented by a tube rather than of wires	Considering the armour as a tube could be an over estimation. However, the motivation here is to consider the worst case in terms of radial stresses.
5	Residual stresses within cable cores are not included	It was found by [90] that residual stresses in radial direction has no influence on the electrical performance of the cable since it is aligned with the electric field direction. In addition, residual stresses will decay with time because of stress relaxation.
6	The pressure and expansion of gases which are generated from by-products of crosslinking reaction is not included	The generation of gases is considered to have minimal since it depends on the degassing process. Moreover, in the case presented the sheath thickness is sufficiently thick so the pressure developed from the gases if any is expected to have low impact on the sheath (i.e. less than 0.5 MPa).

5.4.1 Analysis of Model Parameters and Assumptions

In this part a sensitivity analysis is undertaken to quantify the relative importance of some assumptions. Figure 5.19 shows sheath plastic strain inside three-core cable at 90°C. As illustrated in Figure 5.19, it is clear that plastic strain of the sheath in not uniformly distributed. This is because of the non-uniform distribution of temperature generated develops a non-uniform distribution of stresses. Moreover, each core is affected by the stresses from the other cores and the armour, where the largest strains are located.

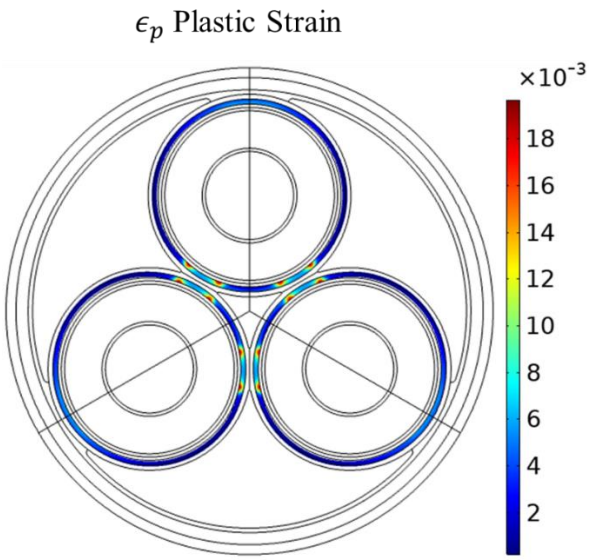

Figure 5.19: Sheath plastic strain at conductor temperature of 90°C

In order to identify the sensitivity of the model to different parameters, a parametric sensitivity analysis was conducted using an L8 orthogonal array. Usually this type of analysis is done to identify the impact of underlying assumptions in a model. The L8 orthogonal method is an attractive technique since it uses the minimal number of runs and at the same time it provides an essential information on main effects of the factors studied. Three studies were conducted. The aim of these studies is to recognize the parameters that affect the plastic strain of the sheath.

5.4.1.1 Cable Material Properties Effect on Sheath Plastic Strain

In the first study, the effect of four factors on sheath plastic strain are examined. These factors are:

1. Elastic modulus (E_{XLPE}).
2. Thermal expansion of XLPE (α),
3. Filler's elastic modulus (E_{filler}).
4. Armour elasticity (E_{Armour}).

The high and low levels used in this analysis of each factor are shown in Table 5.8. In addition, the responses from different runs are presented on Table 5.9. The results of this study are presented in Figure 5.20. The results were obtained at a conductor temperature of 90°C. Cable insulation's thermal expansion and elastic modulus have the highest impact on sheath plastic strain. The elasticity of the filler has a negative effect implying that when

filler's elasticity changes from low level to high, the sheath plastic strain decreases. The elastic modulus of armour has the lowest effect on sheath plastic strain among the four main factors tested since the outer boundary is assumed fixed. These findings show that the high bulk thermal expansion of the insulation has to be accommodated by the cable sheath. A red line is added to represent significance of these factors. A numerical significance of 10% of the largest effect is chosen. This results in considering any effect that exceeds 10% of the largest effect to be significant. Based on this, the thermal expansion has the highest effect on plastic strain then XLPEs' elastic modulus and the elastic modulus of the filler come in the second and third place, respectively.

Table 5.8: Factors with two levels for investigation

Factor	High level (1)	Low Level (0)
Elastic modulus of XLPE	120 (MPa)	50 (MPa)
Thermal Expansion of XLPE	2.5×10^{-4} ($°C^{-1}$)	1×10^{-4} ($°C^{-1}$)
Elasticity of filler	130 (MPa)	85 (MPa)
Elasticity of Armour	2×10^{11} (Pa)	2×10^{9} (Pa)

Table 5.9: Responses from different runs using main and interaction effects.

Run	Elastic modulus XLPE (1)	Thermal expansion XLPE (2)	1&2 4&7	Elastic modulus filler (4)	2&7 1&4	1&7 2&4	Elastic modulus armour (7)	Sheath plastic strain
1	0	0	1	0	1	1	0	0.0002
2	1	0	0	0	0	1	1	0.0023
3	0	1	0	0	1	0	1	0.0055
4	1	1	1	0	0	0	0	0.0189
5	0	0	1	1	0	0	1	0.0006
6	1	0	0	1	1	0	0	0.0004
7	0	1	0	1	0	1	0	0.0014
8	1	1	1	1	1	1	1	0.0128

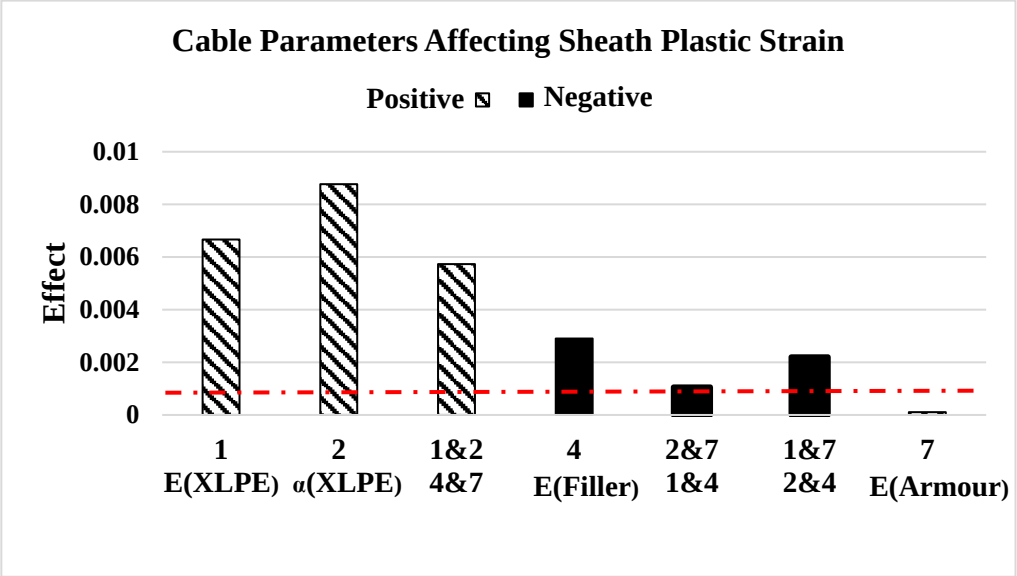

Figure 5.20: Plot of the Effect on Sheath plastic strain with Fixed Armour.

5.4.1.2 Sheath Material Constant Effect on its Plastic Strain

Here the effect of the following parameters on sheath plastic strain are studied:

1. The yield stress (σy).
2. Strength coefficient (*k*)
3. Hardening exponent (*n*)

In Table 5.10, the factors high and low values are presented. Usually *n* is between 0.2 and 0.5, whereas the values of *k* varies between G/100 and G/1000, G being the shear modulus [42, 45]. The outcome of each run is illustrated in Table 5.11. As shown in Figure 5.21, where the effects are presented, the yield stress and strength coefficient have a negative effect on the plastic strain. As yield stress increases, the plastic strain decreases. As mentioned earlier the values of these constants depend mainly on the nature of the material and additives used to strengthen the sheath. Based on the line of significance, the yield stress has the highest effect on plastic strain then strength coefficient and hardening exponent come in the second and third place, respectively.

Table 5.10: Factors with two levels

Factor	High level (1)	Low level (0)
Yield Stress	65 (MPa)	5.5 (MPa)
Strength coefficient	50 (MPa)	4 (MPa)
Hardening exponent	0.2	0.5

Table 5.11: Results from different simulations using main and interaction effects.

Run	Yield Stress (1)	Strength coefficient (2)	1&2	Hardening exponent (4)	1&4	2&4	Sheath Plastic strain
1	0	0	1	0	1	1	0.0304
2	1	0	0	0	0	1	0.0148
3	0	1	0	0	1	0	0.0213
4	1	1	1	0	0	0	0.0080
5	0	0	1	1	0	0	0.0310
6	1	0	0	1	1	0	0.0154
7	0	1	0	1	0	1	0.0251
8	1	1	1	1	1	1	0.0124

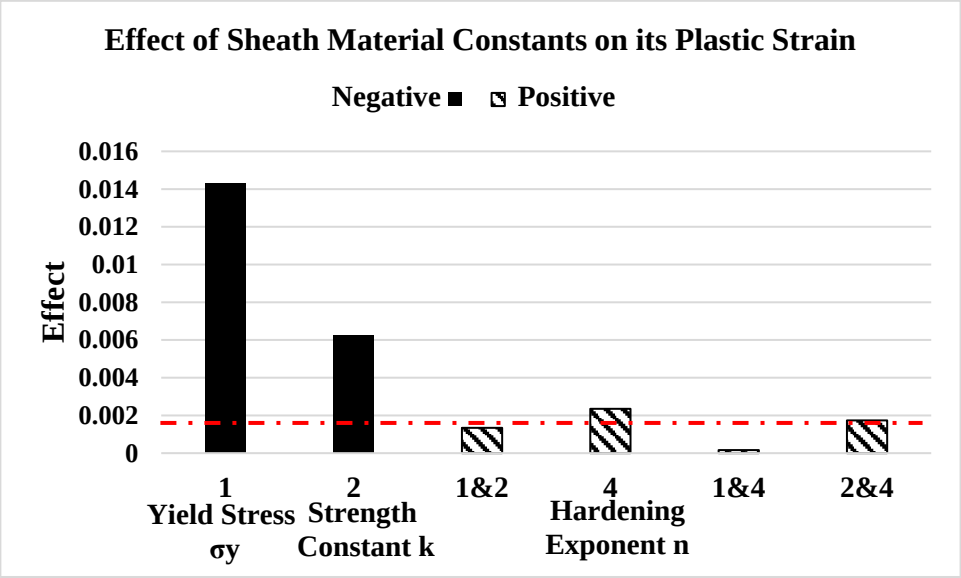

Figure 5.21: Results of sensitivity analysis

5.4.1.3 Effect of XLPE Changing Properties on Sheath Plastic Strain

In the previous two studies, the elastic modulus and thermal expansion of XLPE were assumed constant. XLPE's elastic modulus and thermal expansion are functions of temperature. The influence of temperature on the mechanical properties of XLPE is more pronounced than EPR as an example. At high temperature, the elastic modulus of XLPE decreases while the thermal expansion increases. The impact of assuming constant properties on sheath plastic strain is investigated. Table 5.12 shows that assuming constant mechanical properties leads to higher sheath plastic strain by 13.5% in comparison to temperature dependent properties. It is evident that temperature dependent properties must be taken into account for a relevant prediction of sheath plastic strain.

Table 5.12: Impact of Varying Properties on Sheath Plastic strain (σy=30 MPa, *k*=33.61 MPa, *n*=0.27 [150]).

Factor		Plastic strain at 90 °C
Elastic Modulus	Thermal Expansion	
E(T)	*α*(T)	0.0171
120×10^{6}	*α*(T)	0.0493
E(T)	2.5×10^{-4}	0.0024
120×10^{6}	2.5×10^{-4}	0.0194

Based on the results from these studies, it can be observed that the effect of XLPE's thermal expansion on sheath plastic strain in radial direction is the highest among the other cable parameters. Moreover, selecting designs with high sheath yield stress and high strength constant will reduce the sheath plastic strain. Furthermore, it is important to consider temperature dependent properties when determining the deformations to avoid over estimation.

5.5 The effect of mechanical deformation on electric field

In this part, the deformed geometry from the thermomechanical model was imported into an electrical model. The electrical field distribution inside the deformed cable core is investigated.

5.5.1.1 Heating and Cooling

To calculate thermally induced deformations and stresses both the inertia and thermo-mechanical coupling terms in the governing equations can be neglected. The inertia effects become significant and need to be considered for those cases which face sudden rapid heating or thermal shock. In this work, thermal stresses under steady state temperature field are determined. In non-linear problems, load ramping is used to improve robustness. The input starts from zero and is increased incrementally reaching full value then it goes back to zero as shown in Figure 5.22.

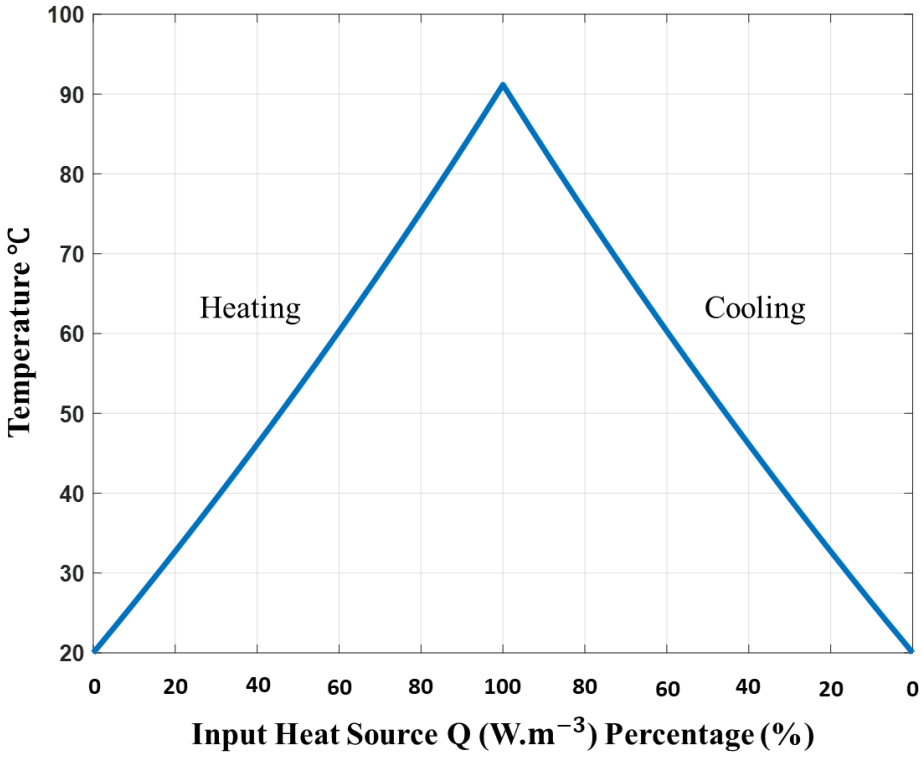

Figure 5.22: Temperature of core during heating and cooling

In Figure 5.23, the change in XLPE's thermal expansion due to temperature change is shown. It can be noticed how the thermal expansion increases as temperature increases and decreases as temperature goes down, which is the expected behaviour.

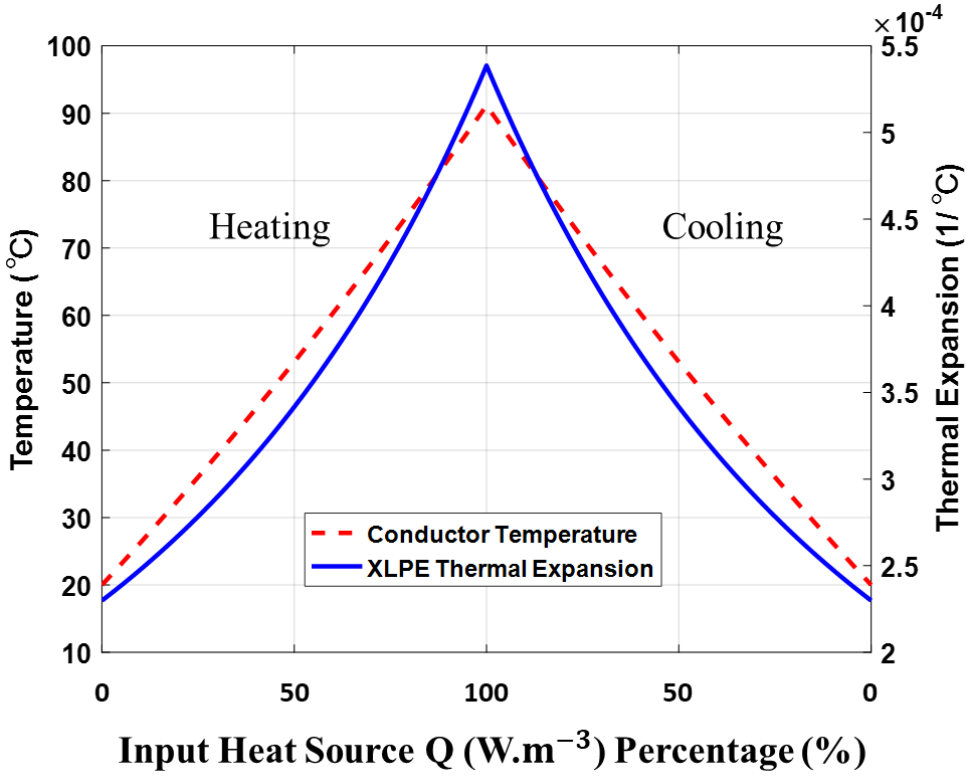

Figure 5.23: Change of Insulation Thermal Expansion with Temperature.

In addition, the change in XLPE's elastic modulus with temperature is illustrated in Figure 5.24. At low temperature, the elastic modulus is at its highest value and as temperature increases the elastic modulus drops down. This outcome shows the model's ability to reflect temperature changes on XLPE's properties. However, Figures 5.23 and 5.24 show these changes only at one point. To explore the effect of the non-uniform distribution of temperature in the insulation on the distribution of XLPE's elastic modulus and thermal expansion, Figure 5.25 is presented. As it can be seen from Figure 5.25a, the non-uniform distribution of temperature in the insulation resulted in a non-uniform distribution of thermal expansion and Young's modulus within the cable insulation presented in Figure 5.25b and Figure 5.25c. At high temperature regions (closer to the conductor) the insulation's elastic modulus is the lowest. While thermal expansion has the highest value at the same regions. Indeed this non-uniform distribution of temperature and properties is generating a non-uniform distribution of thermo-mechanical stresses affecting the cable sheath. In Figure 5.26 the Von Mises stress distribution, plastic strain and temperature distribution in the cable sheath are illustrated.

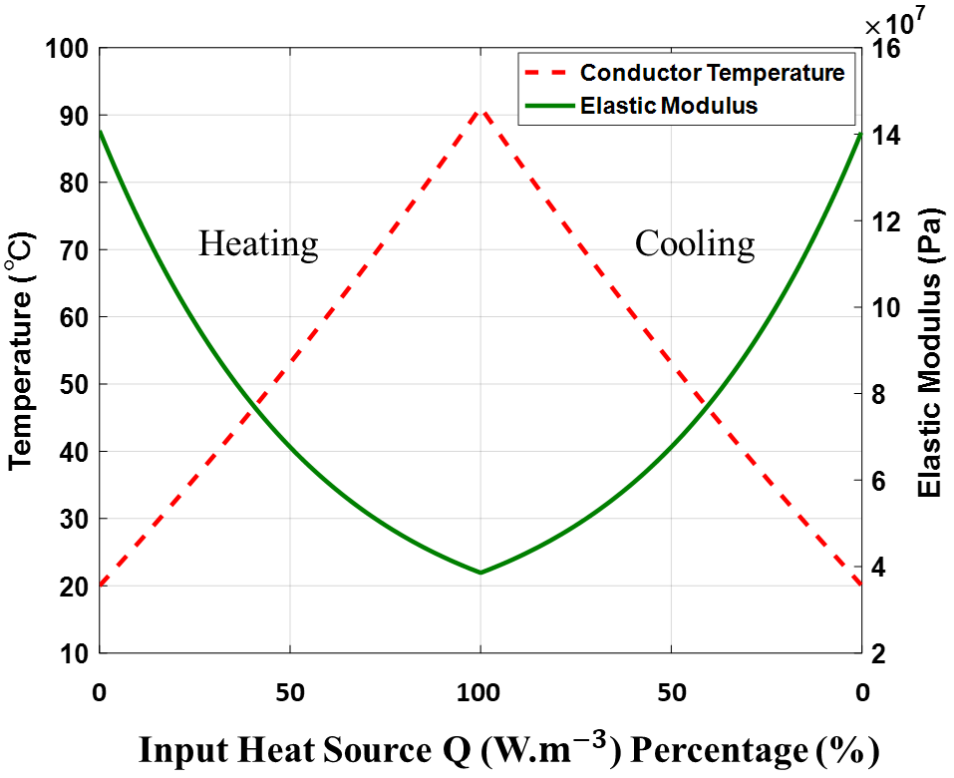

Figure 5.24: Change of Insulation Elastic Modulus with Temperature.

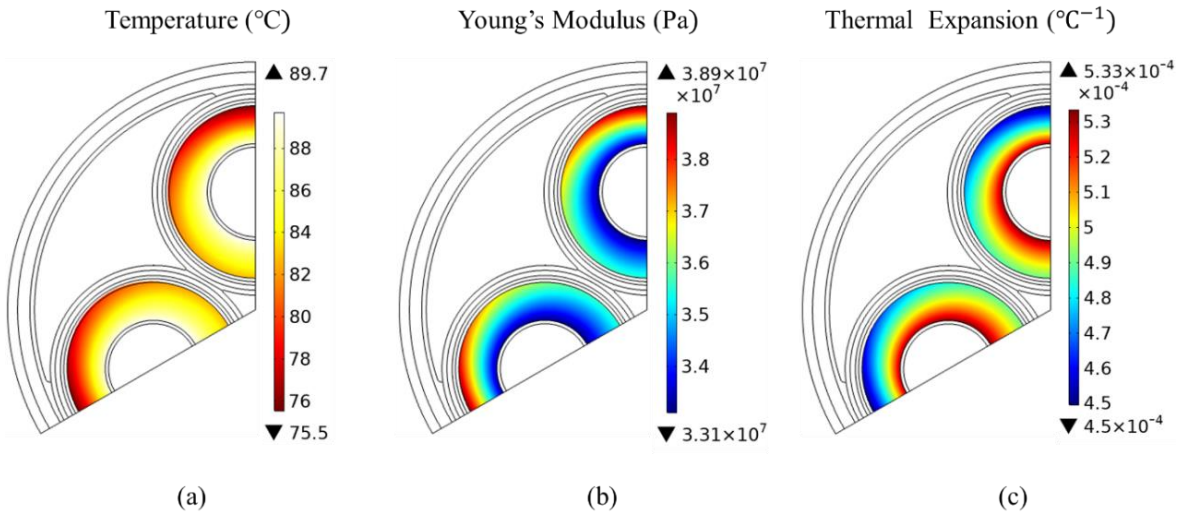

Figure 5.25: (a) Temperature Distribution at Conductor Temperature of 90°C. (b) Insulation Elastic Modulus Distribution at Conductor Temperature of 90°C. (c) Insulation Thermal Expansion Distribution at Conductor Temperature of 90°C.

It worth mentioning that the von Mises stress is defined as the maximum equivalent stress produced by the combination of tensile, compression, bending and shear loading. As seen from Figure 5.26a, the highest stress are located as the parts of sheath facing the other cores and the amrour. In addition, Figure 5.26b shows the plastic strain in the sheath and it can be observed that there is a high plastic strain at locations of high stress. The temperature distribution in the cable sheath is shown in Figure 5.26c, where the non-uniform distribution of temperature can be easily noticed.

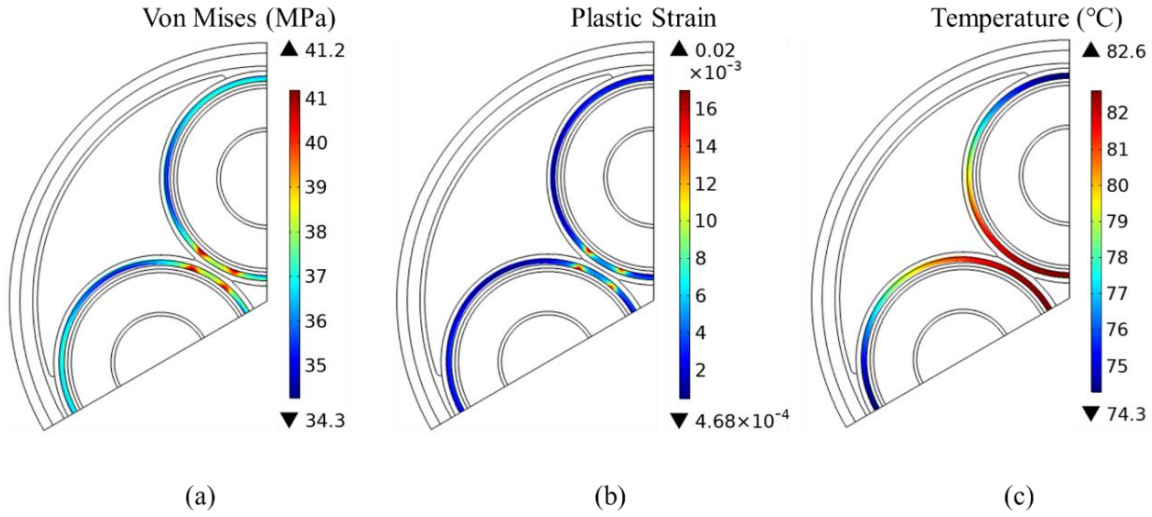

Figure 5.26: (a) Von Mises Stress Distribution in the sheath at Conductor Temperature of 90°C. (b) Plastic Strain Distribution at 90°C. Temperature Distribution in sheath at Conductor Temperature of 90°C.

In Figure 5.27 the deformed mesh at conductor temperature of 90℃ is presented. During heating and at conductor temperature of 90℃ there are no signs of separation or gaps as shown in Figure 5.27. However, after cooling it can be noticed that there is a sign of separation between the water blocking tape and lead sheath. Figure 5.28 illustrates the deformed mesh after the cable has cooled down. It is worth noting that the gap started to appear when the insulation cooled down and went back to initial position since it is considered elastic. The bulk insulation (cable insulation+ water blocking tape + semicon) has a high thermal expansion, causing the deformed regions at the interface to be filled during the heating period. The chances of any gaps being developed are reduced. Nevertheless, in the cooling stage, the insulation shrinks back as the temperature decreases. Due to sheath plastic deformation and the fact that there is no adhesive bond between the water blocking tape and sheath, a gap was created. The sheath expanded during the heating period and did not fully recover to its original dimensions during the cooling period because of sheath plastic deformation.

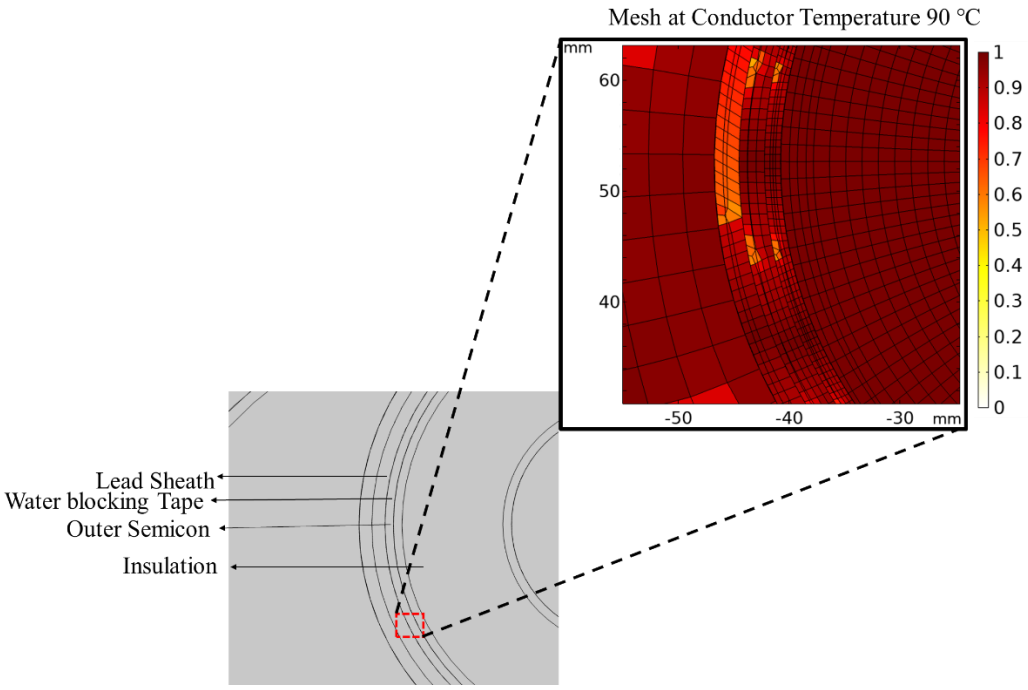

Figure 5.27: Deformed mesh plot at Conductor Temperature 90℃

The adhesive bond between the bulk insulation and sheath should have the ability to absorb the expansion and contraction at the interface without losing its bond to the layers [123, 124]. If there is no bond like the case presented or the bond lost its adhesion or fails by delamination a gap is created during cooling.

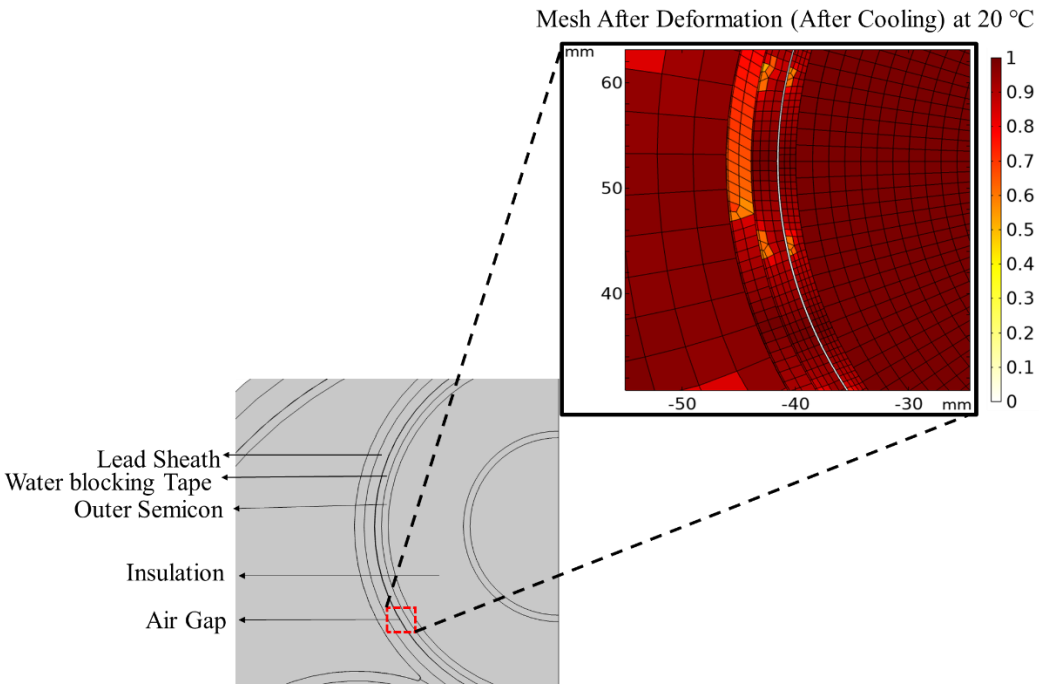

Figure 5.28: Deformed mesh plot after cooling down to 20°C

Figure 5.29 summarizes this observation. The lead is subjected to mechanical stresses higher than its yield stress, which resulted in permanent deformation of the sheath as shown in Figure 5.29a. The sheath lost its circular round shape, which can be easily noticed when temperature goes down and the bulk insulation returns to its initial position as illustrated in Figure 5.29b. In the next section an electric field simulation is presented to explore the electric filed in the gap.

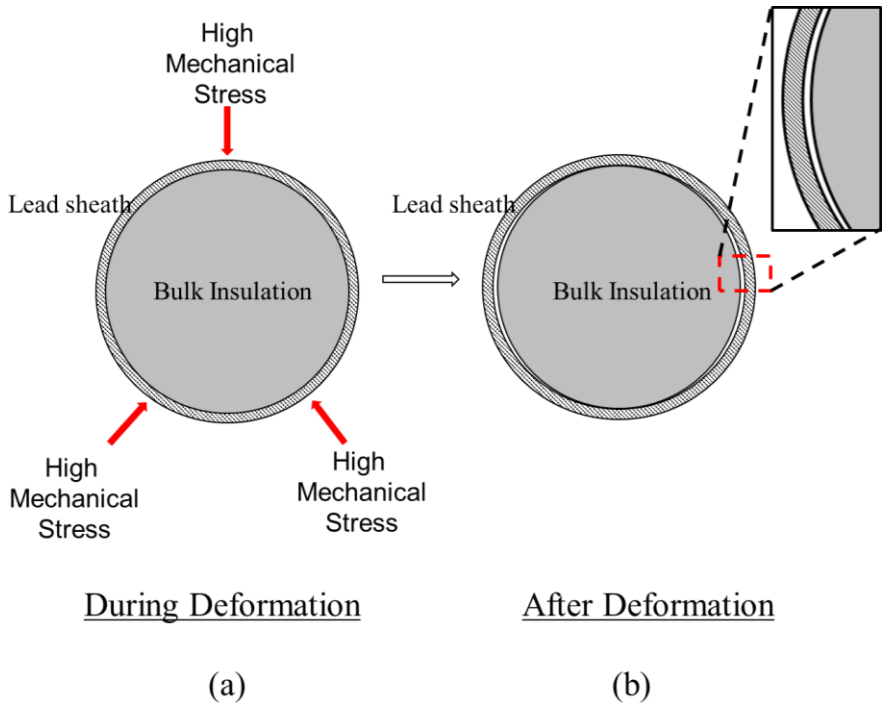

Figure 5.29: Summary Cable Sheath Deformation.

5.5.1.2 Electrical Model of Deformed Geometry

In this section an electric model of the deformed geometry is established. The calculation of the electric field distribution is determined using finite element method. The governing equations used to calculate electric fields are given as:

$$\nabla \cdot \boldsymbol{J} = Q_{jv} \tag{5.9}$$

$$\boldsymbol{J} = \sigma \boldsymbol{E} + j\omega \boldsymbol{D} \tag{5.10}$$

$$\boldsymbol{E} = -\nabla V, \tag{5.11}$$

where $\boldsymbol{J}$ is the current density (A.m^{-2}), σ is the electric conductivity (S.m^{-1}), $\boldsymbol{D}$ denotes the electric displacement density (C.m^{-2}), ω the angular frequency, $\boldsymbol{E}$ is the electric field (V.m^{-1}), V is the electric potential (V) and ρ is the free charge density (C.m^{-2}). Equation (5.9) is the current continuity equation and it can be rewritten in terms of the electric potential using equations (5.10), (5.11) and $\boldsymbol{D}=\varepsilon\boldsymbol{E}$ to be:

$$-\nabla \cdot ((\sigma + j\omega\varepsilon)\nabla V) = 0, \tag{5.12}$$

where ε is the permittivity of the material. The boundary conditions of the electrical model are illustrated in Figure 5.30. Table 5.13 lists materials permittivity and resistivity used in the model. The phase voltage U_0=77 kV at 50 Hz is applied at the high voltage boundary. Zero voltage is set at sheath boundary.

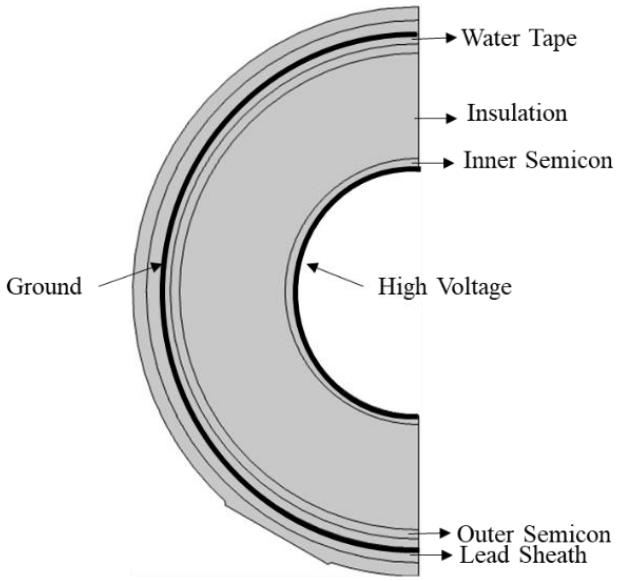

Figure 5.30: The Electrical Model of the deformed core

Table 5.13: Parameters of materials in electrical model

Material	Relative Permittivity	Resistivity [Ω·m]
Semi-con	>1000 [12]	0.1-10 [12]
XLPE	2.3 [154]	1×10^{18} [154]
Water blocking tape	>1000 [12]	1×10^{3} [151]

5.5.1.3 Description of the Air Gap and Simulation Results

The deformed geometry is meshed as illustrated in Figure 5.31. It is noticed that the gap thickness is not uniform along the gap. The gap shape is shown in Figure 5.32a. The area and perimeter of the gap are 9.7 mm^2 and 227.8 mm respectively. In Figure 5.32b part of the mesh in the gap is shown with thicknesses of the gap at different locations. The values of these thicknesses are determined using COMSOL. The voltage across the gap is also shown in Figure 5.32b. In Figure 5.33 the electric field magnitude along the gap is determined. The electric field has the highest values at the locations with lowest thickness. To check the sensitivity of the model to mesh refinements, mesh density is increased. The first full mesh consisted of 218803 triangular elements and this is increased up to 851500 triangular elements. It is observed that areas where the gap is very thin are sensitive to the mesh refinements. Sharp edges and thin areas could lead to local singularities where the electric field appears to depend on the mesh.

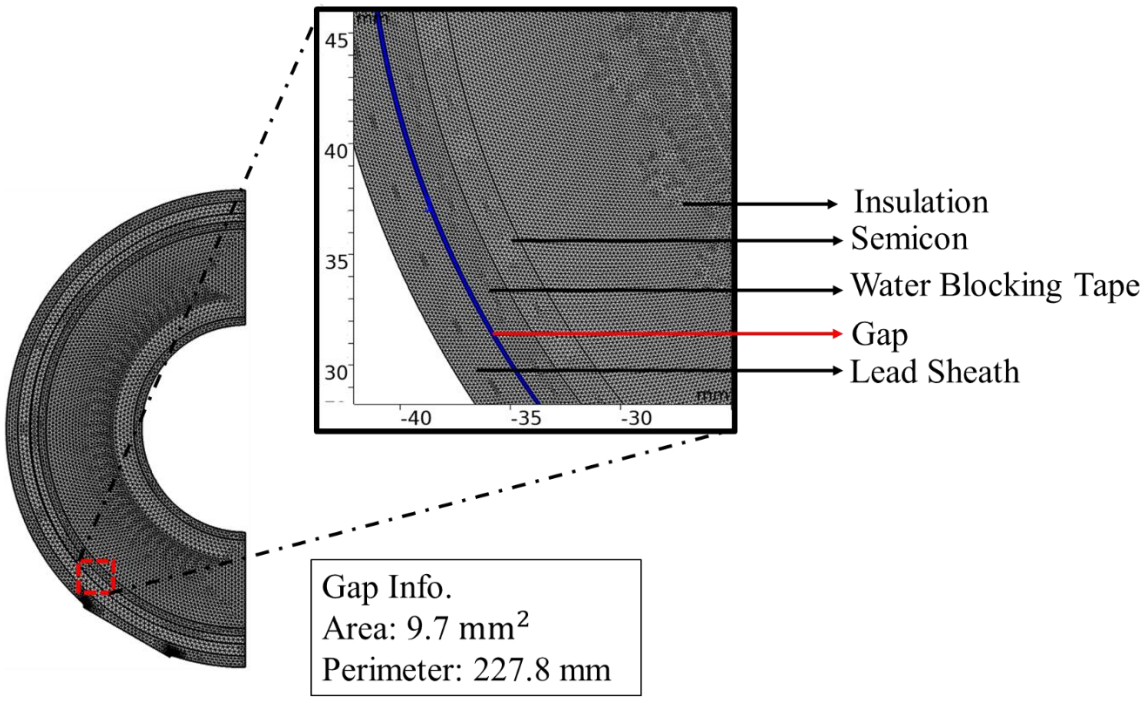

Figure 5.31: Geometry Mesh showing the air Gap created due to deformation.

In other parts of the gap, simulations with increased mesh elements in all regions resulted in a change in the electric field within 6%. Therefore, in case the highest values resulted in this simulation are disregarded since it could be considered as local singularities, the other values of electric field at other locations of the gap are worth considering. Most of the electric field values determined are below 3 kV/mm. This is based on a water blocking tape having a resistivity of 0.1 MΩ.cm. Lower values are resulted if a tape with lower electrical resistivity is utilized. Water tapes must have sufficient mechanical strength to absorb the expansion of the cable core. In addition, the tape must be semi-conductive to allow charge transfer from the outer screen of the insulation to metallic sheath. However, there are no clear limits for the tape resistivity. These parameters could be crucial especially if the sheath is plastically deformed. It is important to use a water blocking tape with a low electrical resistivity as possible.

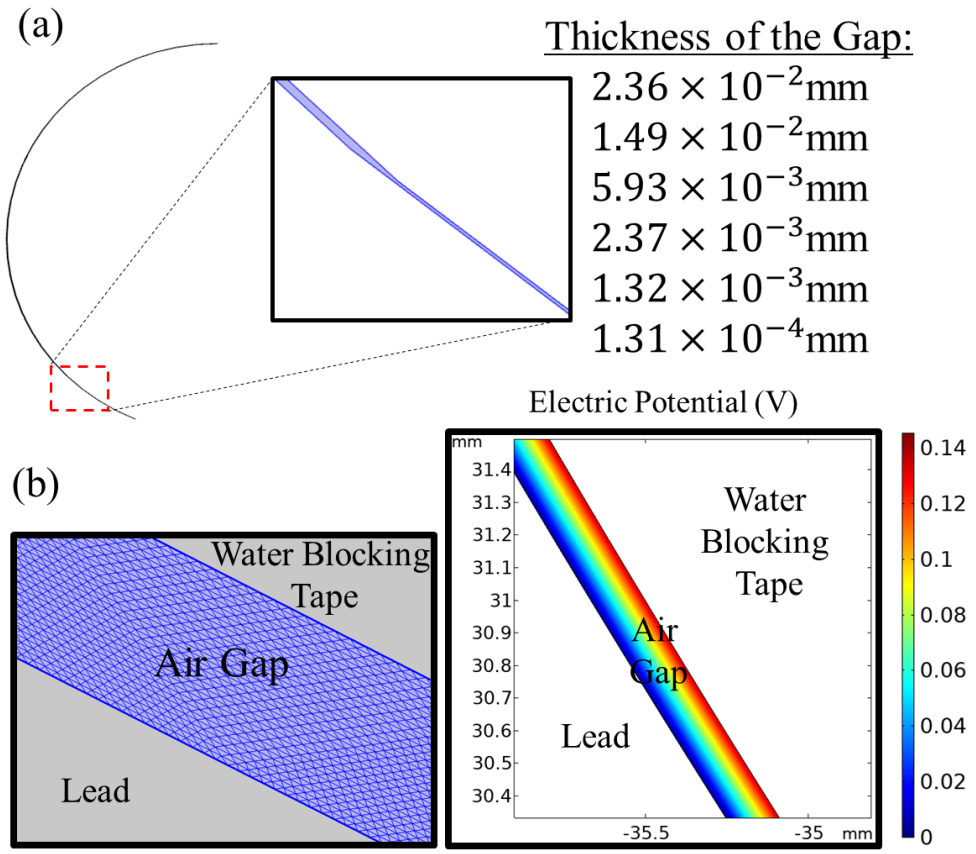

Figure 5.32: (a) Air Gap Shape (b) Mesh in the Air Gap with Voltage across the Gap.

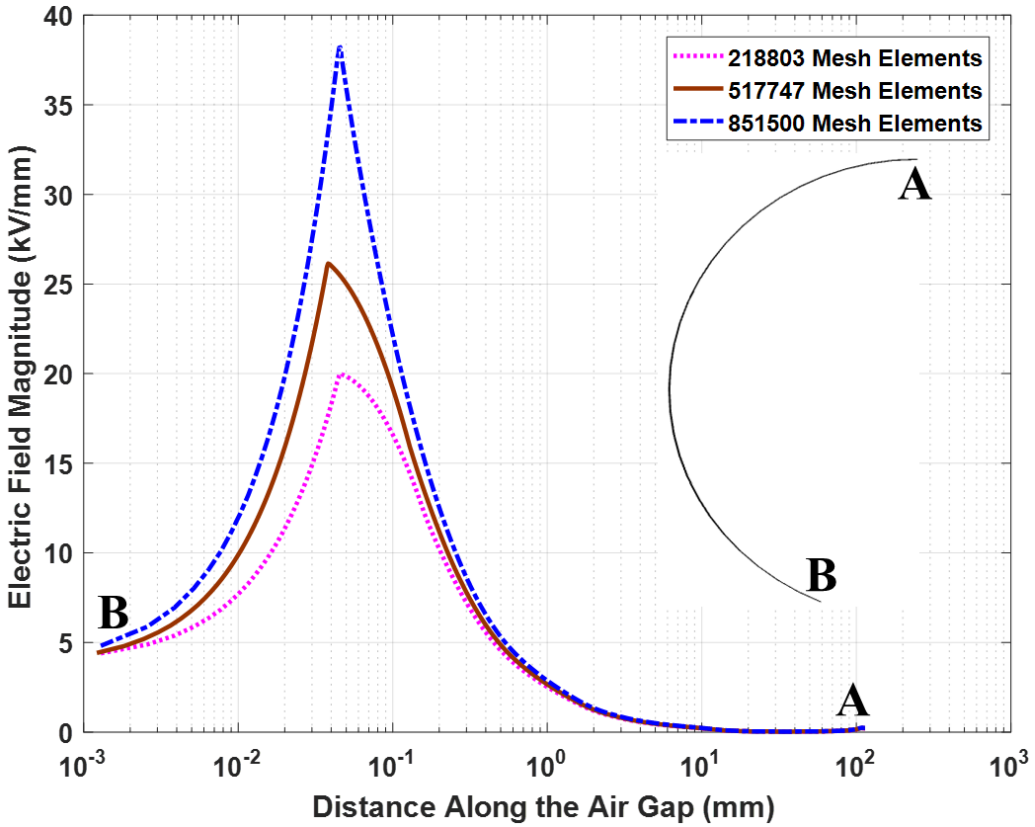

Figure 5.33: Electric Field along the air gap with increasing mesh density.

The area of the air gap for different yield stress is presented in Table 5.14. It is noticed that as the yield stress increases the gap area is decreased. This behaviour is expected since as the yield stress increases the plastic strain decreases and the deformation is decreased.

Table 5.14: Area of the Air Gap for different Sheath's Yield Stress.

Sheath Yield Stress (MPa)	Area of the Gap (mm^2)
20	10.9
30	9.7
40	7.0
50	4.0
60	1.6

To compare the electric field between 30 and 40 MPa yield stresses. The electric field for a deformed geometry of the cable having a sheath yield stress of 30 and 40 MPa are illustrated in Figure 5.34. The cut line for Figure 5.34 is shown as well. It can be noticed that the electric field in the 40 MPa (0.40 $kV.mm^{-1}$) case is higher than the 30 MPa case (0.21 $kV.mm^{-1}$) at the air gap. This is because of gap thickness for 40 MPa is 0.008 mm and for 30 MPa case the thickness is 0.02 mm at the same point.

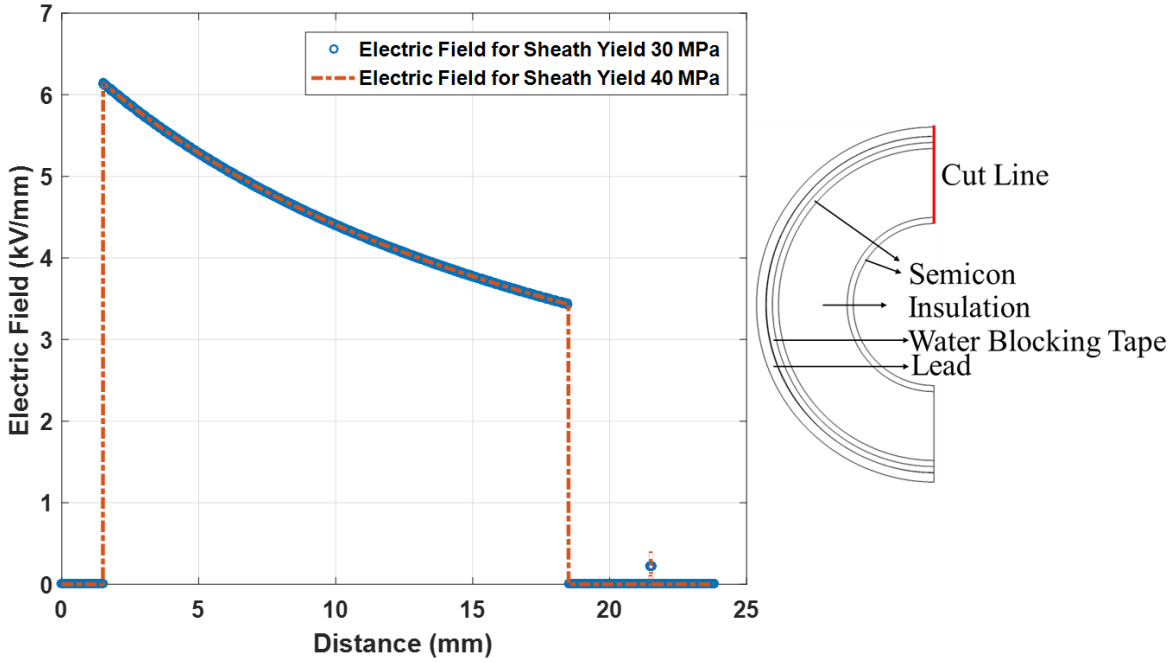

Figure 5.34: Electric in a Deformed Core for 30 and 40 MPa Sheath Yield Stress.

The electric filed values as sheath yield stress increase could increase in the gap since the plastic strain is expected be lower and therefore the gap area is smaller. However, it is difficult to make a solid conclusion since the gap has a non-uniform shape and thickness.

To conclude the results presented in this study are not intended to discuss any reported failures. The electric field values are highly dependent on the deformation level and the quality of the materials used. This work highlights the benefits gained of testing a three core cable as a whole cable with armour rather than a single core. The chances of spotting a defect while testing the whole cable is higher because of the higher thermo-mechanical stresses generated inside a three core. In case a low quality material is used either a sheath with a low yield or water blocking tape with a high electric resistivity or even the insulation itself, testing the whole cable would expose the cores to higher thermo-mechanical stresses that will make it easier to spot a defect if any.

5.6 Summary

This work uses finite element method to model thermomechanical stresses inside AC three core submarine cables. The key parameters that influence sheath plastic strain are investigated. In addition, an electrical model is developed to study the electrical field distribution in the deformed geometry. Sheath plastic deformation in radial direction is

highly influenced by XLPE's thermal expansion and elastic modulus. Sheath yield stress and strength coefficient are inversely proportional to sheath plastic strain. It is recommended to have a sheath with high yield stress and high strength coefficient to decrease sheath plastic strain. When compared with temperature dependent properties, assuming a cable insulation with constant thermal expansion and a constant elastic modulus will result in a change in sheath plastic strain. Thus, temperature dependent properties assumption is required for an accurate prediction of sheath plastic deformation. The chances of developing a gap or layers being separated increases during cooling. XLPE's high thermal expansion reduces this possibility during heating. The gap created between the water blocking tape and sheath could increase the electric field intensity inside the cable. The increase in the electrical field is highly dependent on the deformation level. Electrical resistivity of water blocking tape plays a significant role in reducing the electrical field in the air gap if created. The resistivity must be as low as possible. Electrically testing the three-core cable instead of the single core could be beneficial to ensure that any deformation that could occur in service is seen during testing.

Chapter 6

Conclusion and Future Work

This thesis has demonstrated an analysis of some aspects related to thermo-mechanical stresses in cables and joints. Thermo-mechanical stresses generated inside cables could affect the electrical performance of the cable system. Interfaces in cable joints are the weakest part in a cable joint. The interface should be mechanically robust to guarantee high breakdown strength at the interface, otherwise the electrical performance of the interface would be at risk. In this work, the mechanical and thermo-mechanical stresses of interfaces in cable joints are assessed. In addition, a finite element model analysis has been developed for three core submarine cables where the thermo-mechanical stresses generated inside these cables are examined. This chapter outlines summarizes the main research outcomes and suggests future research projects related to thermo-mechanical stress in the cable system.

6.1 Research Results

The radial and circumferential stresses inside a joint tube are determined based on a hyper-elastic model using finite element model. It is concluded that limiting only the expansion ratio without linking it to material's elasticity could increase the possibility of introducing high circumferential stress. Circumferential stresses could reach 50% of the tensile strength of the material depending on the elastic modulus and expansion ratio. A stiff semiconducting deflector may generate high circumferential at the interface between the deflector and joint insulation. This will increase the risk of creating defects if the material is weak. To achieve the needed pressure with stiff materials low expansion ratio is enough. While with soft materials high expansion ratios are required to reach the needed pressure.

An improved analytical method to determine the change in interface pressure has been proposed. The method takes into account the change in elastic modulus and thermal expansion with temperature. It is found that thermal expansion of cable insulation and elastic modulus of joint insulation have the highest effect on the thermal stresses. Between 25°C to 90°C there is no indication of a pressure drop in the radial direction due to the high thermal expansion of cable insulation. On the other hand, an increase in the tensile circumferential stresses is noticed at low temperatures. This increases the possibility of facing defects at the interface if it is already weak.

The thermo-mechanical behaviour of single core cables at short circuit is explored. It is noticed that the thermal expansion of cable insulation has a significant impact on the thermo-mechanical behaviour of the cable. At the interface between sheath and insulation, the high thermal expansion managed to reduce the effect of huge heat input at the interface in terms of pressure drop. However, it is found that the high thermal expansion could pose a greater force on the sheath in the radial direction.

In three core submarine power cables, it is found that the sheath deformation is affected by cable insulation's thermal expansion the most. Sheath yield stress in inversely proportional to sheath plastic strain. For accurate prediction of sheath plastic strain, temperature dependent properties should be considered. It is concluded that XLPE's high thermal expansion reduces the risk of creating a gap during heating. During cooling the chances of layers being separated are higher. If a gap is created, the electric field intensity will increase in the defected area. The deformation level affects the increase in the electric field. The electrical resistivity of the water blocking tape has a considerable impact on the electric field in the gap between sheath and water blocking tape if created. It is concluded that testing the three core submarine cable as a whole with armour could be more beneficial than testing a single core. Some defects could be easily noticed during the three core testing.

6.2 Recommendations for Future Work

A number of areas have been recognised which deserve more investigation. A key issue worthy of further work is the exploration of the behaviour of silicone rubber and cable insulation under cyclic loading and if this will affect the interface pressure over long term operation taking into account viscoelastic behaviour. Polymers in general have a viscoelastic behaviour where strain steadily increases over time under the applied stress. When the applied stress is removed all or part of strain in a viscoelastic material will recover over a period of time. Different models were developed to describe the behaviour of XLPE under various temperatures and stresses. However, limited attention has been giving to the effect of insulation mechanical behaviour on the electrical field profile in joints.

In the manufacture of such cables there are inherent risks to successful product. The influence of XLPE on the interface pressure and the electrical integrity of the cable could be worse if the desired degree of crosslinking is not fully achieved. In crosslinking, the structure of Polyethylene (PE) is modified and the thermomechanical stability of PE is improved. The upper operation temperature is increased from 70°C to 90°C. Resistance to deformation and cracking, tensile strength and elastic modulus are all mechanical properties which are also

enhanced by crosslinking. However, achieving the desired thermal and mechanical enhancements is highly dependent on crosslinking process. Crosslinking degree of 80% is common for high voltage cable applications. But, if the degree of crosslinking is not reached, the chance of having an insulation with a lower operation temperature (less than 90℃) is increased. Moreover, as the degree of crosslinking decreases the thermal expansion increases which could pose higher radial stress on the interface.

It would be worth extending the 2D thermo-mechanical model by doing a three dimensional model of a three core cable taking different parameters into account. It is known that the cable cores in a three core cable are twisted in a helix shape which could affect the deformation in the axial direction. In addition, the axial stress in pitched armour wires will result in an inward radial stress. Furthermore, modelling the thermo-mechanical stresses during short circuit currents since conditions could be worse in case of a sharp transient, especially when there is a significant heat generated inside the sheath by circulating current.

It is also recommended to expand the work to include HVDC cables. It is known that the electric conductivity in HVDC cables is a function of temperature and electric field. After reaching steady state, the electric field distribution will to be inverted. It would be worth investigating the effect of thermo-mechanical deformations on the electrical behaviour of HVDC cables.

Appendix A

Electric Field Simulation of a 132 kV Cable Joint

To explore the electric stress distribution in a cable joint at interfaces, an electrical model for a 132 kV silicone rubber premolded cable joint is developed. This electric field analysis can be done through an electrostatic field analysis or a complex electric field analysis. In an electrostatic field analysis, the electric field distribution is found by considering the material permittivity only. While in a complex electric field analysis, both permittivity and resistivity (or electrical conductivity) are required to find the electric field. The later approach is conducted when semiconducting materials are used since their resistivity is smaller than common insulators which will make the conductive and capacitive effects comparable. In this section, the permittivity and resistivity of the materials are considered.

Description of the Cable Joint

The joint design used within this section is based on a 132 kV 630 mm^2 XLPE cable joint. The two parts of the conductor are connected using a copper ferrule which is covered with a polymeric insulation. A pre-expanded joint tube made of silicone rubber is used to cover the connected parts. The main part of the joint tube is the joint insulation that is made of silicone rubber with sufficient thickness to withstand electrical stress. The joint tube also includes an inner deflector of semiconducting silicone rubber. The task of the inner deflector is to shield the copper ferrule and the two cut ends of the cable insulation. Moreover, two stress cones made of semiconducting silicone rubber are included in the joint tube. Their main function is to mitigate the magnitude of the longitudinal component of electrical stress at the cable-joint interface. Additionally, the joint insulation is covered with a semiconducting silicone rubber for protection.

Governing Equations

The electrical field distribution can be found by solving for the electrical potential using the following equations [152]:

$$\nabla \cdot \boldsymbol{J} = Q_j \qquad (A.1)$$

$$\boldsymbol{J} = \sigma \boldsymbol{E} + j\omega \boldsymbol{D} \qquad (A.2)$$

$$\boldsymbol{E} = -\nabla \boldsymbol{V}, \qquad (A.3)$$

where $\boldsymbol{J}$ is the current density (A.m^{-2}), σ is the electric conductivity (S.m^{-1}), $\boldsymbol{D}$ denotes the electric flux density (C.m^{-2}), ω the angular frequency, $\boldsymbol{E}$ is the electric field (V.m^{-1}), $\boldsymbol{V}$ is the electric potential (V) and Q_j is the rate of charge generation (C.m^{-2}). Equation (A.1) is the current continuity equation and it can be rewritten in terms of the electric potential using equations (A.2), (A.3) and $\boldsymbol{D}=\varepsilon \boldsymbol{E}$ to be:

$$-\nabla \cdot ((\sigma + j\omega\varepsilon)\nabla V) = 0, \qquad (A.4)$$

where ε is the permittivity of the material. The first term is associated with conductive properties of the material and the second term is linked to the capacitive properties.

Model Geometry and Boundary Conditions

The model geometry and boundary conditions are illustrated in Figure A.1 and Figure A.2, respectively. The phase voltage $U_0 = 132/\sqrt{2}$ =77 kV at 50 Hz is applied at the high voltage boundary. Zero voltage is set at outer boundary. Table A.1 lists materials permittivity and resistivity used in the model.

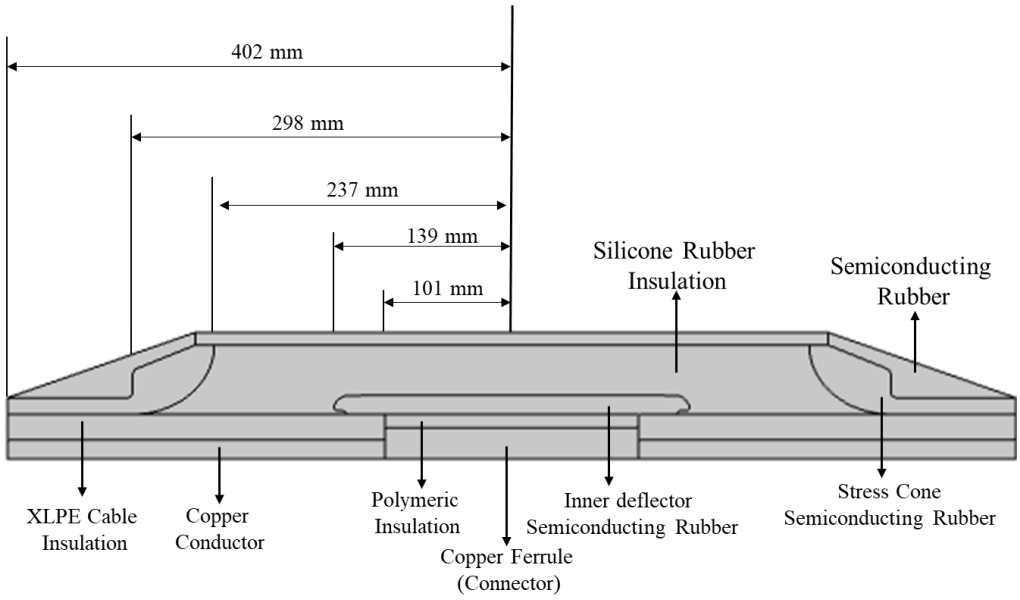

Figure A.1: 2D axial-symmetric 132 kV one piece premolded cable joint model geometry.

Appendix A

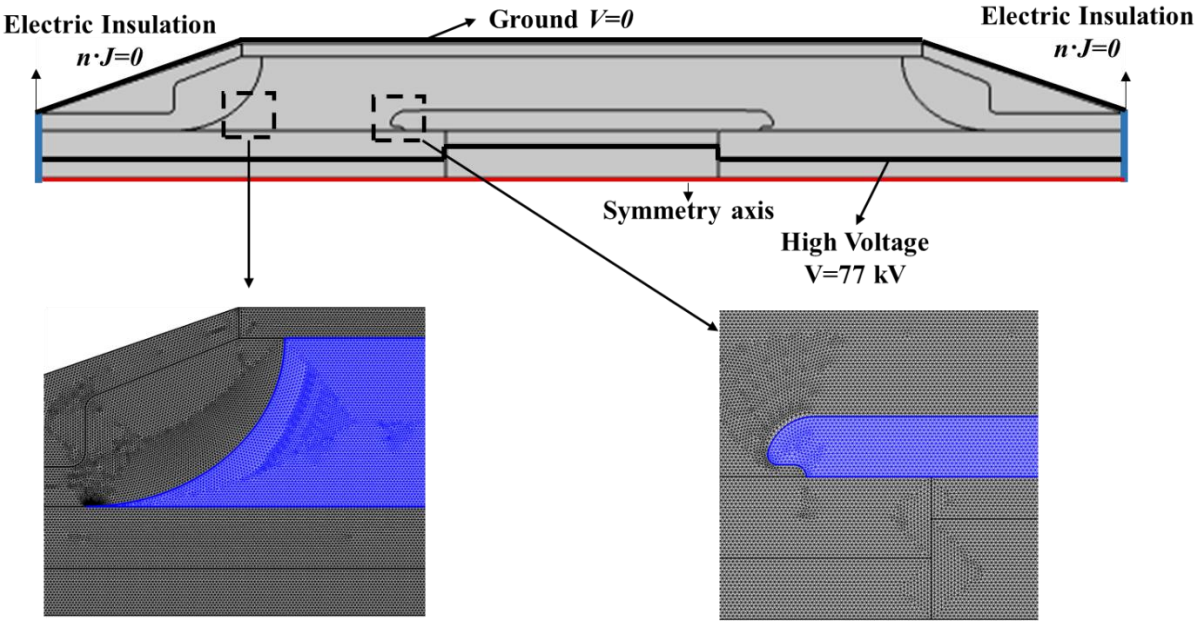

Figure A.2: Model Boundary Conditions and Mesh.

Table A.1. Electrical Properties of Materials in Electrical Simulation [153, 154].

Material	Permittivity	Electrical Conductivity ($S \cdot m^{-1}$)
XLPE Cable Insulation	2.3	1×10^{-18}
Copper Conductor	1	6×10^{7}
Semiconducting Silicone Rubber	20	1×10^{-2}
Silicone Rubber	3.2	3×10^{-14} [84]
Connector Insulation	50	1×10^{-18}

The electric field distribution in the cable joint is shown in Figure A.3. It can be noticed that high electric field at the critical locations namely, tip of the inner deflector, interface between inner deflector and joint insulation, starting point of the stress cone and interface between cable and joint insulation. The electrical field at the interface between central deflector and silicone rubber insulation is illustrated in Figure A.4. The electrical field norm presents the magnitude of the electric field and it is shown in Figure A.4a.

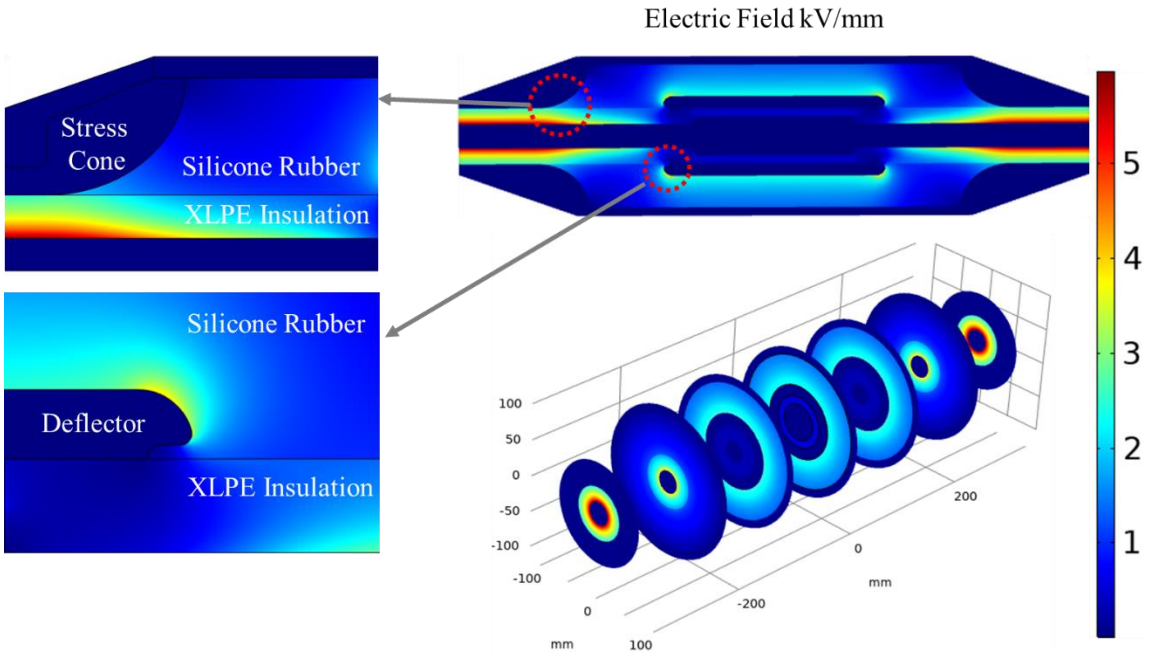

Figure A.3: Distribution of Electric field Norm in the simulated joint.

In addition, the normal and tangential components of the electric field are illustrated in Figure A.4c and Figure A.4d, respectively. It can be seen that at the interface of inner deflector and joint insulation, the high electric stress is mainly because of the normal component of the electric field. The electric conductivity of the inner deflector is responsible for limiting the tangential component of the electric field at the interface. Moreover, the highest value of electric field norm is located at the tip of the central deflector reaching 3.6 $kV.mm^{-1}$. It is worth noting that at the middle of the deflector symmetry could be assumed at this point. Figure A.5 shows the electric field at the interface of cable and joint insulation. The tangential component near the stress cone reached a value of 0.5 $kV.mm^{-1}$, which is lower than tangential component near the tip of the deflector 1.2 $kV.mm^{-1}$. Although, the values of the tangential electric field is lower than the breakdown strength at the interface, any defect could lead to partial discharge and promote the initiation of an electrical tree. Moreover, the conductivity of semiconducting rubber is not the only factor that controls the tangential component. A smoother and lower tangential component could be obtained by optimizing the shape of tip as in [155] and length of the deflector [156]. These results have shown that electric field distribution in the cable joint is not uniformly distributed. It also pointed out the critical points of electrical filed inside the cable joint. This demonstrates the importance of providing special attention to interfaces when designing per-moulded cable joints.

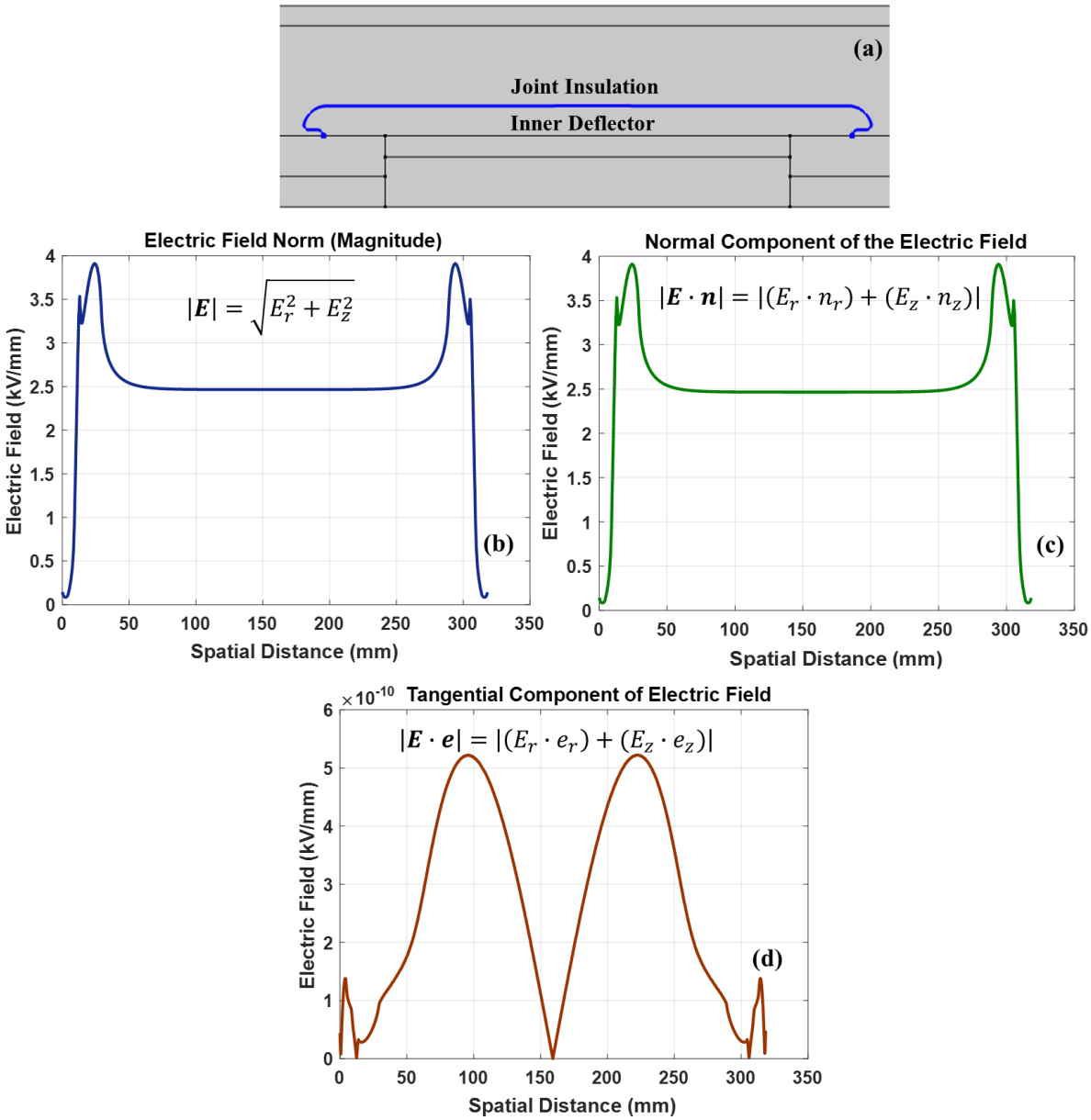

Figure A.4: (a) The cutline along the interface between silicone rubber and semiconducting rubber. (b) Electric field norm (magnitude) at the interface. (c) Normal component of electric field at the interface. (d) Tangential component of electric field at the interface.

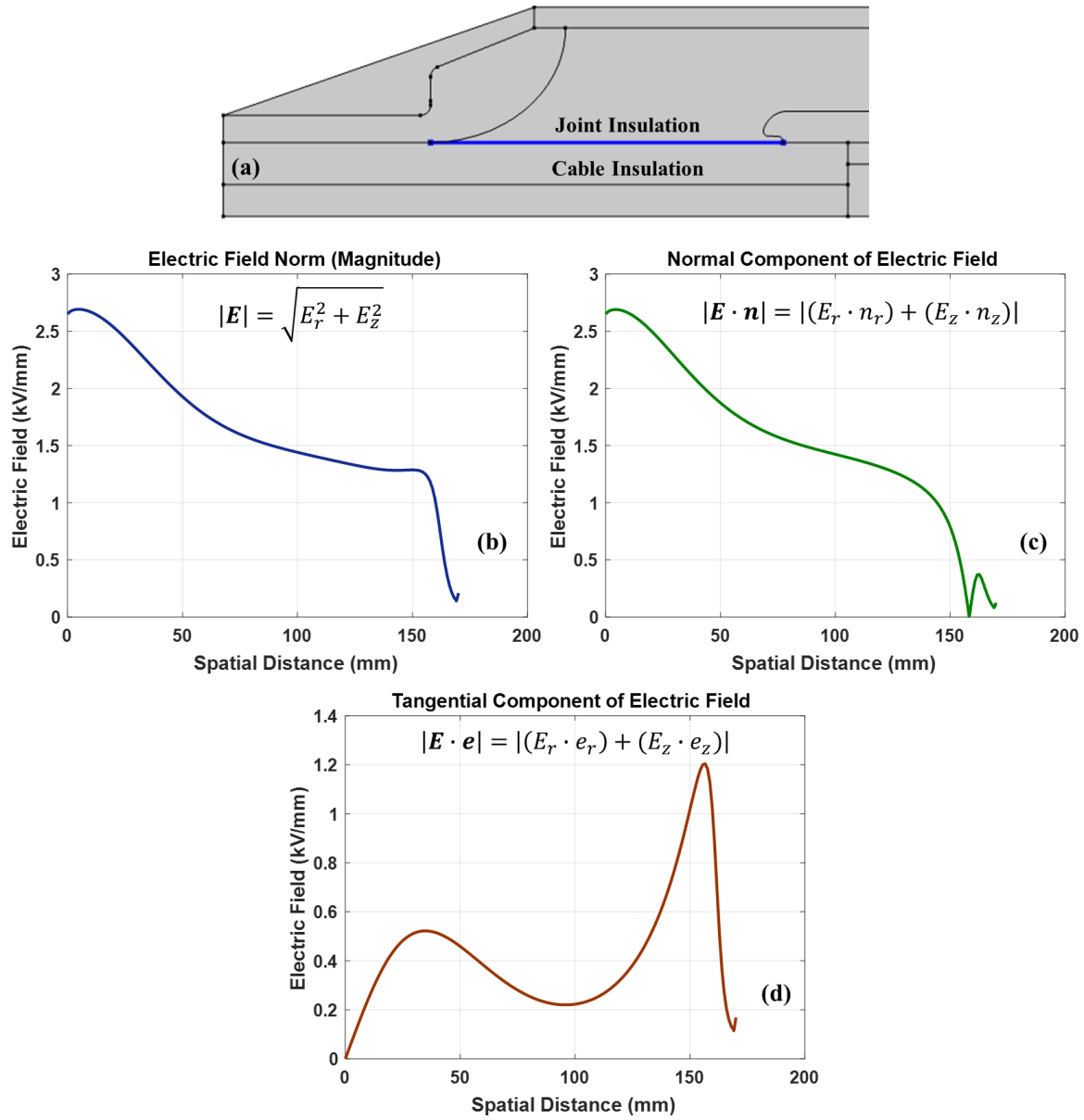

Figure A.5: (a) The cutline along the interface between silicone rubber and cable insulation. (b) Electric field norm (magnitude) at the interface. (c) Normal component of electric field at the interface. (d) Tangential component of electric field at the interface.

Appendix B

Interface between Cable Insulation and Semiconducting Rubber

Another cross section of the cable joint is investigated at conductor temperature of 90℃. This cross section contains the semiconducting rubber layer as shown in Figure B.1a. The change in radial and hoop stresses within the cable joint assembly in air, when the conductor temperature is at 90˚C are shown in Figure B.1b and Figure B.1c respectively. The difference in the interfacial pressure results obtained by FEM and analytical approaches are presented in Table B.1.

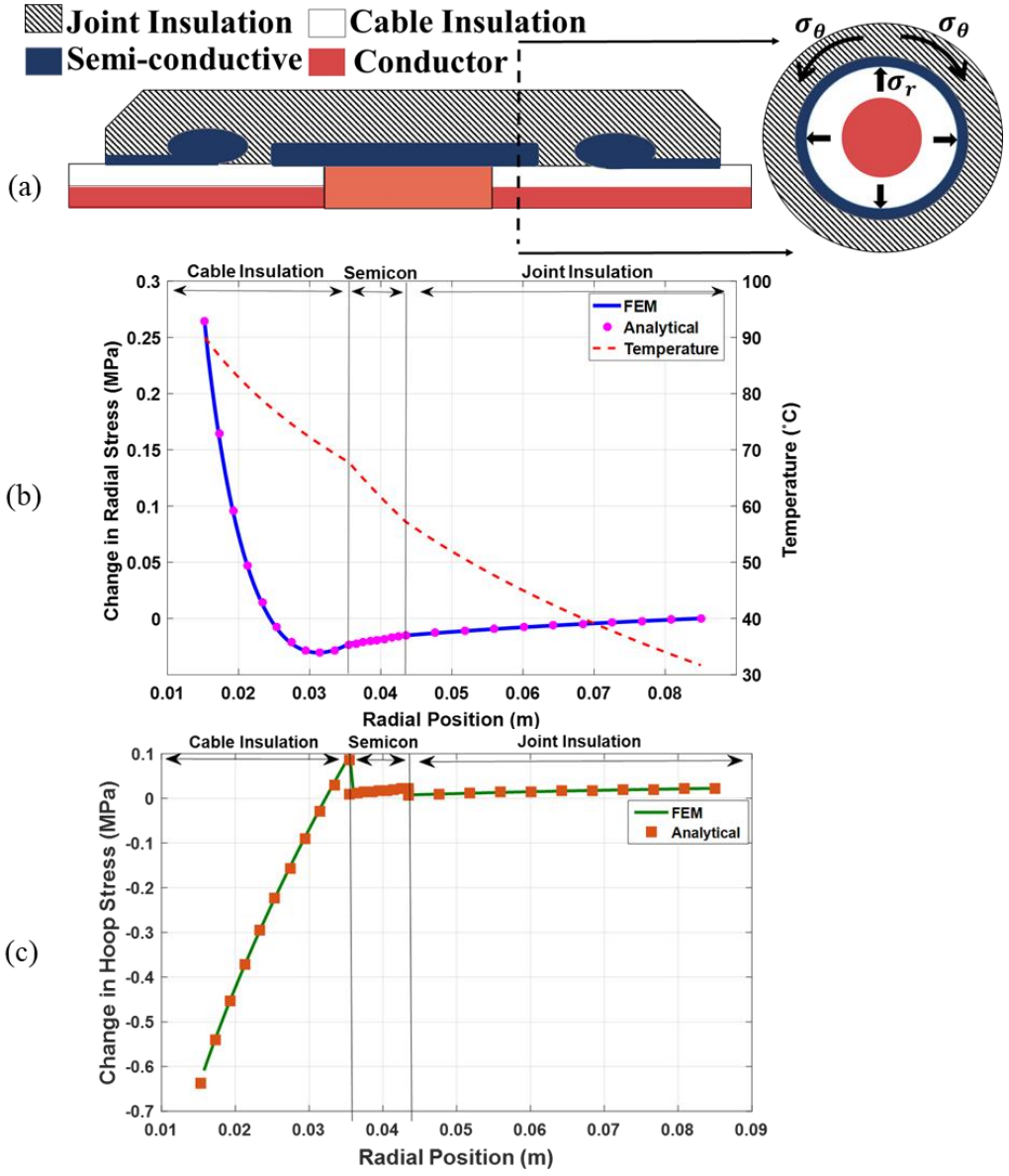

Figure B.1: (a) Cross section of a cable joint. (b) Change in radial stress within the cable joint at 90˚C (c) Change in inner hoop stress within the cable joint at 90 ˚C.

Table B.1. Comparison of results obtained by FEM & analytical approaches.

Approach	FEM	Analytical	Difference
Radial Stress	-2.259×10^4 Pa	-2.348×10^4 Pa	4%
Inner Hoop Stress1	9.65×10^4 Pa	8.641×10^4 Pa	10%
Inner Hoop Stress2	2.235×10^4 Pa	2.278×10^4 Pa	2%

The radial pressure at the interface between the cable insulation and semiconducting rubber is higher than the radial stress at the interface between the cable insulation and joint insulation. This is expected since the semiconducting rubber has a higher elastic modulus than the joint insulation. The negative sign in the radial pressure indicates that it's compressive which means that the initial radial compressive pressure will increase.

The inner hoop at two points is listed as seen in Table B.1. Inner hoop stress1 is the inner hoop between the cable insulation and semiconducting rubber. Inner hoop stress2 is the inner hoop at the interface between semiconducting rubber and joint insulation. It is noticed that the inner hoop at these two points at 90 ℃ conductor temperature are both tensile. Both values are lower than the inner hoop stress at the interface between cable insulation and joint insulation (1.22×10^5 Pa). In addition, the inner hoop stress1 (9.65×10^4 Pa) is higher than inner hoop stress2 (2.23×10^4 Pa).

List of References

[1] H. Orton, “Power cable Technology Review,” State Grid, *High Voltage Engineering*, 2015, vol.41, pp. 1057-1067, no. 4.

[2] Wind EUROPE, “Wind Energy in Europe in 2018 Trends and Statistics,” 2019.

[3] J. Z. Hansen, “Failures in MV Joints (XLPE Cables) in Heavily Loaded Cable Systems Connecting Large Wind Turbines to the Distribution System,” *NORDAC 2012*, Espoo, Finland, 2012.

[4] A. Ametani, T. Ohno and N. Nagaoka, Cable System Transients Theory, Modeling and Simulation, IEEE Press John Wiley, 2015.

[5] W. A. Thue, “Electric Power Cable Engineering,” 2nd edition, New York: Marcel Dekker, 2005

[6] M. A. Laughton and D. J. Warne, Electrical Engineer’s Reference Book, 16th edition, Newnes, 2003.

[7] T. Worzyk, *Submarine Power Cables: Design, Installation, Repair Environmental Aspects*, Springer, 2009.

[8] G. J. Anders, *Rating Of Electric Power Cables*, IEEE Press, 1997.

[9] F. Da Silva, C. Bak, “Electromagnetic Transients in Power Cables,” Springer Science & Business Media, 2013.

[10] ABB. XLPE Land Cable Systems - User’s guide, rev 5 edition, 2010.

[11] Canadian Copper CCBDA (156), “Wolfe Island Wind Farm,” 2008.

[12] B. Gustavsen, J. A. Martinez and D. Durbak, “Paramter Determination for Modeling System Transients-Part II: Insulated Cables, *IEEE Transactions on Power Delivery*, vol. 20, no. 3, 2005.

[13] G. Mazzanti, J. Castellon, G. Chen, J. C. Fothergill, M. Fu, N. Hozumi, J. H. Lee, J. Li, M. Marzinotto, F. Mauseth, P. Morshuis, C. Reed, I. Troia, A. Tzimas and K. Wu, “ The Insulation of HVDC Extruded Cable System Joints. Part 1: Review of Materials, Design and

Testing Procedures," IEEE Transactions on Dielectrics and Electrical Insulation, vol.26, no.3, 2019.

[14] Accessories for HV Cables with Extruded Insulation, CIGRÉ Technical Brochure 177, 2001-02-01.

[15] J. Di, W. Mei, Z. Qian and G. Tang, "Technical Trends of Intermediate Joints for HV XLPE Cable in China," IEEE International Conference on Engineering Technologies and Applied Sciences (ICETAS), 2017.

[16] A. Toya, M. Shimazu, S. Umeda and Satoshi, "Recent Technologies of Joints for HV and EHV Cables in Japan," Transactions on Electrical and Electronic Engineering IEEJ Trans., vol. 2, pp.523-530, 2007.

[17] Cigre, "Interfaces In Accessories for Extruded HV and EHV Cables," Joint Task Force 21/15, 2002.

[18] O. Kuusisto, "The Effects of Installation-Based Defects in Medium Voltage Cable Joints," Bachelor Thesis, Helsinki Metropolia University of Applied Sciences, 2016.

[19] IEC Standard 60505-1999, "Evaluation and Qualification of Electrical Insulation Systems."

[20] J. Densley, "Aging Mechanisms and diagnostics for power cables-an Overview," IEEE Electrical Insulation Magazine, vol. 17, no. 1, 2001, pp. 14-22.

[21] T. Tanaka, "Aging of Polymeric and Composite Insulating Materials. Aspects of interfacial performance in aging," IEEE Transactions on Dielectrics and Electrical Insulation, vol. 9, no. 5, 2002, pp. 704-716.

[22] F. Mauseth, H. L. Halvorson and S. Hvidsten, "Diagnostic Testing of Thermally Aged Medium Voltage XLPE Cable Joints," Electrical Insulation and Dielectric Phenomena (CEIDP), Annual Report Conference on, 2012, pp.823-826.

[23] R. Ross, "Dealing with interface problems in polymer cable terminations," IEEE Electrical Insulation Magazine, vol. 15, no. 4, 1999, pp.5-9.

[24] J. Becker, J-L. Parpal, M-H. Luton, R. Schroth, B. Parmigiani, S. Katakai, H. Geene, J. Svahn and J. Head, “Thermal Ratings of HV Cable Accessories,” IEC TC 20 a Task Force TF 21(B1)-10, 2004.

[25] J. Kaumanns, M. Bacchini, G. Gehlin, B. Gregory, D. Johnson, T. Kurata, H. May, C. Pye, R. Reinoso, J. Samuel, J. Tarnowski, R. Thillart, M. Vilhelmsen and D. Wald, “CIGRE WG B1.34: Mechanical Forces in Large Conductor Cross-Section XLPE Cables,” *9th International Conference on Insulated Power Cables, Jicable*, 2015, D3.2.

[26] F. Steennis, P. Soepboer, J. Mosterd, P. Buys, P. Oosterlee, L. Bokma and R. Meier, “The Effect of High Current Loads on Joints in MV Cable Systems,” *21th International Conference on Electricity Distribution, CIRED*, 2011.

[27] B. Hennuy, F. Steennis, B. Aerns, P. Oosterlee, P. Leemans, P. Soepboer, T. Van Rijn, R. Meier, E. De Ridder, H. Granjean, M. Van Den Berg, P. Buys and L. Bokma, “Measurement of the Force Induced by Thermal Expansion of Conductor of MV Impact on MV Joints,” *22th International Conference on Electricity Distribution, CIRED*, 2013.

[28] J. Pilgrim, J. Hunter, N. Palmer, B. Gregory and D. Mooehouse, “Measurement of Thermomechanical Properties of 400 kV 2500 mm^2Cable, *9th International Conference on Insulated Power Cables, Jicable*, 2015, D3.5.

[29] B. Gregory and S. Galloway, “Mechanical Effects on Extruded Dielectric Cables and Joints Installed in Underground Transmission Systems in North America,” EPRI, Palo Alto, CA, Technical Report, 2004.

[30] K. D. Haim and K. U. Bentkowski, “Reliability of Mechanical Connectors for Medium Voltage Cables,” *21th International Conference on Electricity Distribution, CIRED*, 2011.

[31] V. Buchhloz, M. Colwell, H. E. Orton and J. Y. Wong, “Elevated Temperature Operation of XLPE Distribution Cable Systems,” IEEE Transactions on Power Delivery, 1993.

[32] C. Katz, A. Dima, A. Zidon, M. Ezrin, W. Zengel and B. Bernstein, “Emergency Overload Characteristics of Extruded Dielectric Cables Operating at 130 ℃ and above,” IEEE Transaction on Power Apparatus and Systems, vol. PAS-103, no. 12, 1984.

[33] D. R. Askeland, P. P. Fulay and W. J. Wright, “The Science and Engineering of Materials”, Sixth Edition, Cengage Learning, 2011.

[34] M. P. Groover, Fundamentals of Modern Manufacturing Materials, Processes and Systems, 4th edition, John Wiley, 2010.

[35] E. Elgstrom, “Practical Implementation of Hyperelastic Materials Methods in FEA Models,” Master thesis, Department of Mechanical Engineering, Blekinge Institute of Technology, Karlskrona, Sweden, 2014.

[36] A. N. Gent, *Engineering with Rubber*, 3rd edition, Hanser, Munich, 2012.

[37] J. Bergstrom, Mechanics of Solid Polymers Theory and Computational Modeling, William Andrew Elsevier, 2015.

[38] M. Shahzada, A. Kamranb, M. Z. Siddiquia and M. Farhana, "Mechanical Characterization and FE Modelling of a Hyperelastic Material," Materials Research, 2015.

[39] J. Seng, “Inverse Modelling of Material Parameters for Rubber like Materials: Create a New Methodology of Predicting the Material Parameters Using Indentation Bending Test,” PhD dissertation, Liverpool John Moore’s University, 2015.

[40] O.H.Yeoh, "Some Forms of the Strain Energy Function for Rubber," Rubber Chemistry and Technology, 1993.

[41] R. W. Ogden, “Large deformation isotropic elasticity-on the correlation of theory and experiment for incompressible rubberlike solids,” Royal Society of London. Series A, Mathematical and Physical Sciences, 1972.

[42] N.E. Dowling, Mechanical Behaviour of Materials: Engineering Methods for Deformation, Facture and Fatigue, 4th Edition, PEARSON, 2013.

[43] W. F. Hosford, Mechanical Behaviour of Materials, 2nd edition, Cambridge University Press, 2010.

[44] W. F. Hosford and R. M. Caddell, Metal Forming-mechanics and metallurgy, Cambridge University Press, 2007.

[45] M. A. Meyers and K. K. Chawla, Mechanical Behaviour of Materials, 2nd edition, Cambridge University Press, 2009.

[46] R. Ebewele, Polymer Science and Technology, CRC Press, 2000.

[47] N. Bowler and S. Liu, “Aging Mechanisms and Monitoring of Cable Polymers,” International Journal of Prognostics and Health Management, 2015.

[48] R. M. Eichhorn, “A Critical Comparsion of XLPE and EPR for Use as Electrical Insulation on Underground Power Cables,” IEEE Transactions on Electrical Insulation, 1981, vol.6.

[49] P. A. Tipler and G. Mosca, Physics for Scientists and Engineers: Volume1, New York: Worth Publishers, 2008.

[50] IEC Electric Cables - Calculation of the Current Rating - Current Rating Equations (100 % Load Factor) and Calculation of Losses - General. International Electrotechnical Commission Standard 60287-11, edition 2.0, December, 2006.

[51] D. Chatziperros and J. A. Pilgrim, “Review of the Accuracy of Single Core Equivalent Thermal Model (SCETM) for Offshore Wind Farm (OWF) Cables,” IEEE Transactions of Power Delivery, vol. 33, no. 4, 2018.

[52] G. J. Anders and George Georgallis, “Transient analysis of 3-core SL-type submarine cables with jacket around its core,” Jicable ’15, Versailles, France, 2015

[53] L. D. Ramirez, W. Kamara and G. J. Anders, “Thermal analysis of 3-core SL-type cables with jacket each core using the IEC Standard,” Jicable 19, Versailles, France, 2019.

[54] A. Shedaghat and F. de Leon, “Thermal Analysis of Power Cables in Free Air: Evaluation and Improvement of the IEC Standard Ampacity Calculations,” IEEE Transactions of Power Delivery, vol. 29, no. 5, 2014.

[55] M. H. Sadd, Elasticity: Theory, Applications, and Numerics, 3rd edition, Academic Press, 2014.

[56] W. S. Slaughter, “The Linearized Theory of Elasticity,” Springer Science & Business Media, 2002.

[57] A. C. Ugural and S. K. Fenster, “Advanced Mechanics of Materials and Applied Elasticity,” Pearson Education, 2012.

[58] V. Vullo, *Circular Cylinders and Pressure vessels Stress: Analysis and design*, Springer, 2014.

[59] D. Kunze, B. Parmigiani, R. Schroth and E. Gockenbach, "Macroscopic internal interfaces in high voltage cable accessories," *CIGRE*, 2000, 15-203.

[60] S. M. Hasheminezhad, "Tangential electric breakdown strength and PD inception voltage of solid-solid interfaces," Ph.D. thesis, Norwegian University of Science and Technology, 2016.

[61] E. Kantar, S. Hvidsten, F. Mauseth and E. Ildstad, "A Stochastic Model for Contact Surfaces at Polymer Interfaces Subjected to an Electrical Field," Tribology International, vol. 127, pp.361-371, 2018

[62] D. Fournier, C. Dang and L. Paquin, "Interfacial Breakdown in Cable Joints," *IEEE International Symposium on Electrical Insulation*, pp. 450-452, 1994.

[63] D. Fournier and L. Lamarre, "Interfacial breakdown phenomena between two EPDM surfaces," *6th International Conference on Dielectric Materials, Measurements and Applications,* 1992.

[64] C. Dang and D. Fournier, "Dielectric performance of interfaces in premolded cable joints," IEEE Transaction on Power Delivery, vol. 12, no. 1, pp. 29-32, 1997.

[65] B. Du, L. Gu, X. Zhang and X. Zhu, "Fundamental research on dielectric breakdown between XLPE and silicone rubber in HV cable joint," IEEE (ICPADM), 2009.

[66]B. Du and L. Gu, "Effects of interfacial pressure on tracking failure between XLPE and silicone rubber," IEEE Transaction on Dielectrics and Electrical Insulation, vol. 17, no. 6, pp. 1922-1930, 2010.

[67] J. C. Fothergill, "Filamentary electromechanical breakdown," IEEE Transactions on Electrical Insulation, vol. 26, no. 6, pp. 1124-1129, 1991.

[68] E. Kantar, D. Panagiotopoulos and E. Ildstad, "Factors Influencing The Tangential AC Breakdown Strength of Solid-Solid Interfaces," IEEE Transactions on Dielectrics and Electrical Insulation, vol.23, no.3, 2016.

[69] E. Kantar, E. Ildstad and S. Hvidsten, "Effect of Material Elasticity on the Longitudinal AC Breakdown Strength of solid-Solid Interface," IEEE Transactions on Dielectrics and Electrical Insulation, vol. 26, no. 2, 2019.

[70] G. Chen and C. H. Tham, “Electrical Treeing Characteristics in XLPE Power Cable Insulation in Frequency Range between 20 and 500Hz,” IEEE Transactions on Dielectrics and Electrical Insulation, vol. 16, no. 1, 2009.

[71] H. Z. Ding and B. R. Varlow, “Thermodynamics Model for Electrical Tree Propagation Kinetics in Combined Electrical and Mechanical Stresses,” IEEE Transactions on Dielectrics and Electrical Insulation, vol. 12, no. 1, 2005.

[72] B. R. Varlow, “Electrical treeing as a mechanically driven phenonmenon,” Proceedings of 1998 International Symposium on Electrical Insulating Materials. 1998 Asian International Conference on Dielectrics and Electrical Insulation and 30th Symposium on Electrical Insulating Materials, 1998.

[73] B. X. Du, J. G. Su, Jin Li and Tao Han, “Effect of Mechanical Stress on Treeing growth Characteristics in HTV Silicon Rubber,” IEEE Transactions on Dielectrics and Electrical Insulation, vol.24, no.3, 2017.

[74] B. X. Du, J. G. Su and Tao Han, “Compressive Stress Dependence of Electrical Tree Growth Characteristics in EPDM,” IEEE Transactions on Dielectrics and Electrical Insulation, vol.25, no.1, 2018.

[75] M. N. Arbab and D. W. Auckland, “Growth of Electrical trees in Solid Insulation,” IEE Proceedings A - Physical Science, Measurement and Instrumentation, Management and Education, vol. 136, no. 2, pp. 73-78, 1989.

[76] D. W. Auckland and B. R. Varlow, “Dependence of Electrical Tree Inception and Growth on Mechanical Properties,” IEE Proceedings A - Science, Measurement and Technology, vol. 138, no. 1, pp. 51-54, 1991.

[77] X. Chen, Y. Xu, X. Cao and S. M. Gubanski, “Electrical Treeing Behaviour at High Temperature in XLPE Cable Insulation Samples,” IEEE Transactions on Dielectrics and Electrical Insulation, vol. 22, no. 5, 2015.

[78] S. Kobayashi, D. Muto, S. Tanaka, H. Lizuka, H. Niinobe and M. Suetsugu, “Development of Factory Expanded Cold Shrinkable Joint for EHV XLPE Cables,” JICABLE 03 International Conference on Insulated Power Cables, 2003.

[79] H. Suzuki, S. Kobayashi, T. Ono, H. Nomura, H. Kurihara, H. Lizuka, D. Muto and S. Tanaka, “Development of Cold-Shrinkable Joint for 110 kV XLPE Cables,” Furukawa Review, no.19, 2000.

[80] L. Song, J. Chen, H. Qin and T. Li, “Lifetime Prediction of Silicone Rubber Cold Shrinkable Joint Based on Accelerated thermal aging,” IEEE International Conference on High Voltage Engineering and Application (ICHVE), 2016.

[81] Z. Tian, L. Sun, J. Wang and X. Bai, “A Study Simulation on Relationship Between Young’s Modulus of Cable Joints and Interface Pressure Based on Finite element Method,” *J. Phys.: Conf. Ser.,* 2019.

[82] A. Samual, “Improvement of Silicone Rubber for High Voltage applications by addition of fillers,” PhD. Thesis, ETH Zurich, 2015.

[83] S. Ansorge and B. Arnold, “Jointing of High Voltage Cable Systems,” PFISTERER IXOSIL AG, 2005

[84] P.Gaedicke and R. Krabs, “Prefabricated Cold-shrink Splice System for MV Power Cables,” Power Engineering Journal, 1996.

[85] H. Takei, K. Mochizuki, K. Yokosuka, K. Takahashi, I. Takaoka, T. Tashiro, H. Kawahara and Y. Hane,” Development of Cold-shrinkable Straight-Through Joints for 22 kV XLPE Cables,” Furukawa Review, 2000.

[86] T. Liu, B. Hui, M. Fu, S. Hou, B. Luo and G. Wang, “Experimental and Simulation Analysis of Electrical Breakdown for 220 kV Silicone Rubber Pre-moulded Cable Joints,” *IEEE Int. Electr. Insul. Conf. (INSUCON),* 2017.

[87] S. Zierhut, T. Klein, E. Wendt and L. Zuhlke, “Influence of expansion on electric field distribution of stress cones for high voltage cable accessories,” *Jicable 9th International Conference on Insulated Power Cables,* E7.2, 2015.

[88]J. Cardinaels, P. Heuillet and P. Meyer, “Study of the Viscoelastic Behaviour of Cold-shrinkable Joints for MV Cables, *IEEE Transmission and Distribution Conf.* 1999.

[89] S. Lee, Y. Kim, I. Lee and N. Amyot, “Influence of Internal Residual Mechanical Stresses on Local Dielectric Strength of EHV Extruded XLPE Cables,” *IEEE Electr. Insul. Conf. Electr. Manu. Coil. Winding Conf.,* 2001.

[90] N. Amyot, E. David, S. Y. Lee and I. H. Lee, “Influence of Post Manufacturing Residual Mechanical Stress and Crosslinking By-products on Dielectric Strength of HV Extruded Cables,” IEEE Trans. on Dielectr. Electr. Insul., vol.9, pp. 458-466, 2002.

[91] H. Niinobe, S. Yokoyama, Y. Torai and S. Kaneko, “Compact Transition Joints For Up to 154kV Power Cable,”Jicable, 2007.

[92] Y. Nakanishi, A. Fujimori, S. Fukunaga, T. Tanabe, M. Kobayashi, N. Shiseki and K. Ando, “Development of Prefabricated Joint for 275-kV XLPE Cable,” IEEE Transactions on Power Delivery, Vol.10, no. 3, 1995.

[93] T. Akiyama, T. Inoue, H. Inoue, K. Fudamoto, Z. Iwata and S. Gotoh, “Development of Prefabricated Joint for 154 kV XLPE Cable,” IEEE Transactions on Power Delivery, Vol.6, no. 2, 1991.

[94] T. Tanaka, Y. Sekii, H. Satoh and M. Yamaguchi, “Development of Prefabricated Type Straight through Joint for 275 kV XLPE Cable,” IEEE Transactions on Power Delivery, vol.7, 1992.

[95] N. Amyot and E. David, “A Study of Interfacial Pressure Behavior for Two Types of Thermally Cycled Coldshrikable Joints,” *Electrical Insulation, Conference Record of the 2002 IEEE International Symposium on*, 2002.

[96] J. Cui, W. Qiu, S. Huang, T. Sun, Z. Lu, S. Wang, F. Chen, D. Yu, X. Wang and K. Wu, “Mechanical Property Analysis, Simulation and Theoretical Calculation of Silicon Rubber Joint Assembled in HV Cable under Certain Circumstances,” *2nd International Conference on Electrical Materials and Power Equipment*, 2019.

[97] CIGRE WG B1.34 Mechanical forces in large cross section cables systems, Dec. 2016.

[98] B. Keane, G. Schwarz and P. Thernherr, "Electrical equipment in cold weather applications," *Industry Applications Society 60th Annual Petroleum and Chemical Industry Conference*, 2013.

[99] H. St-onge, C. H. de Tourreil, M. Braunovic, M. Duval and R. Bartnikas, “Thermal Capability of Solid Dielectric Cable Materials,” *IEEE/PES Transmission and Distribution Conference and Exposition*, 1979.

[100] R. G. Fletcher, J. F. Bradley and H. E. Orton, “Elevated Temperature Operation of XLPE Distribution Cable System,” *2nd International Conference on Properties and Applications of Dielectric Materials*, 1988.

[101] M. M. Jensen, “Overload Capacity of Polymer Insulated Medium Voltage Cables,” Master thesis, Department of Electrical Engineering Technical Institution of Denmark (DTU), Lyngby, Denmark, 2011.

[102] S. Yoshida, M. Tan, S. Yagi, S. Seo and M. Isaka, “Development of Prefabricated Type Joint for 275kV XLPE Cable,” *IEEE International Symposium on Electrical Insulation*, 1990.

[103] D. Zhang, Y. Han, H. Liu and W. Shen, “Determination of the Pressure Distribution at the XLPE Cable-Rubber Interface in a Self –Pressurized Joint,” High Voltage Engineering, 2007.

[104] F. Claeys, “Premoulded Joints for Voltages from 72 to 245 kV,” Third International Conference on Power Cables and Accessories 10kV - 500kV, 1993.

[105] M. Song and Z. Jia, “Calculation and Simulation of Mechanical Pressure of XLPE-SR Surface in Cable Joints,” *12th International Conference on the Properties and Applications of Dielectric Materials (ICPADM),* 2018.

[106] J. Zhidong, Z. Yujin, F. Weinan, Z. Bin, Y. Jiao and L. Guojun, “Analysis of the Interface Pressure of Cold Shrinkable Joint of 10kV XLPE Cable,” High Voltage Engineering, vol. 43, no. 2, pp. 661-665, 2017.

[107] Y. Luo, Z. Han, X. Lei, M. Zhou, H. Ye and H. Wang, “Techniques for Designing Prefabricated Cable Accessories Based on Hyperelastic Materials Models,” *12th International Conference on the Properties and Applications of Dielectric Materials (ICPADM),* 2018.

[108] C. Li and H. Qin, “A Study of the interfacial Pressure in Cable Joint Based on Finite Element Method,” Advanced Materials Research. 2014.

[109] X. Wang, C. C. Wang, K. Wu, D. M. Tu, S. Liu and J. K. Peng, “An Improved Optimal Design Scheme for High Voltage Cable Accessories,” IEEE Transactions on Dielectrics and Electrical Insulation, 2014, vol.21,no.1.

[110] A. A. Aldhuwaian, “Failure Experience on 380 kV Joints and Terminations in Saudi Arabia Transmission Netwrok,” Jicable’19, A4-3, France, 2019.

[111] T. Andritsch, A. Vaughan and G. Stevens, "Novel Insulation Materials for High Voltage Cable Systems," IEEE Electrical Insulation Magazine, vol.33, pp. 27-33, 2017.

[112] X. Qi and S. Boggs, "Thermal and Mechanical Properties of EPR and XLPE Cable Compounds," IEEE Electr. Insul. Mag., vol. 22, pp.19-24, 2006.

[113] C. D. Hooper and G. Marshall, "Low Temperature Elastic Behavior of Fourteen Computed Elastomers," Materials Division Propulsion and Vehicle Engineering Laboratory, NASA Technical Memorandum, 1964.

[114] N. Amyot and D. Fournier, "Influence of Thermal Cycling on the Cable Joint Interfacial Pressure," *IEEE International Conference on Solid Dielectrics*, 2001.

[115] D. Fournier and L. Lamarre, "Effect of Pressure and Temperature on Interfacial Breakdown between Two Dielectric Surfaces," *Conference on Electrical Insulation and Dielectric Phenomena*, 1992.

[116] IEEE Standard for Extruded and Laminated Dielectric shielded cable joints rated 2.5kV to 500kV, IEEE Std 404, 2012.

[117] V. Buchhloz, M. Colwell, H. E. Orton and J. Y. Wong, "Elevated Temperature Operation of XLPE Distribution Cable Systems," IEEE Transactions on Power Delivery, vol.8, no.3, 1993.

[118] M. Kellow and H. St-Onge, "Thermo-Mechanical Failure of Distribution Cables Subjected to Emergency Loading," IEEE Transaction on Power Apparatus and Systems, Vol. PAS-101, no. 7, 1982.

[119] C. Katz, A. Dima, A. Zidon, M. Ezrin, W. Zengel and B. Bernstein, "Emergency Overload Characteristics of Extruded Dielectric Cables Operating at 130℃ and above," IEEE Transaction on Power Apparatus and Systems, Vol. PAS-103, no. 12, 1984.

[120] P. L. Cinquemani, F. L. Kuchta, M. M. Rahan, F. Ruffinazzi and A. Zaopo, "105℃/140℃ Rated EPR Insulated Power Cables," IEEE Transaction on Power Delivery, vol. 11, no. 1, 1996.

[121] C. Dang, J. Cote and J. Tranowski, "Emergency-Temperature Testing on MV Jacketed Reduced-Wall TRXLPE Aluminum Cable Systems in Duct Back," IEEE Transactions on Power Delivery, vol. 33, no.6, 2018.

[122] S. Pelissou, J. Cote, S. St-Antoine and J. Dallaire, “Emergency conditions applied to triplex medium voltage XLPE cables having flat strap neutrals,” Jicable, 2007.

[123] R. Butterbach and R. Heucher, “Advantages of Hot Melt Adhesives for Overlap Bonding and Sealing in Power Cables,” *Jicable 95*, B5.5, 1995.

[124] IEEE Guide for the Selection, Testing, Application and Installation of Cables having Radial-Moisture Barriers and/or Longitudinal Water Blocking, IEEE Std 1142, 2009.

[125] CIGRE WG B1.43-TB 623 Recommendations for Mechanical Testing of Submarine Cables, June, 2015.

[126] CIGRE WG B1.27-TB 490 Recommendations for testing of long AC submarine cables with extruded insulation for system voltage above 30 (36) to 500 (550) kV, 2012.

[127] DNV-RP-F401, Electrical power cables in subsea applications. Recommended practice, 2012.

[128] R. B. Hetnarski, “Thermal Stresses IV-mechanics and mathematical methods-series of handbooks”, Elsevier, 1996.

[129] K. Bathe, Finite Element Procedures, 2ed edition, Prentice Hall, 2014.

[130] S. T. Mau, “Introduction to Structural Analysis: Displacement and Force Methods,” CRC Press, 2012.

[131] R. B. Hetnarski and M. R. Eslami, “Thermal Stresses: Advanced Theory and Applications,” Springer, 2019.

[132] Z. Y. Huang, J. A. Pilgrim, P. L. Lewin and S. G. Swingler “Dielectric Thermal-mechanical Analysis and Constrained High Voltage DC Cable Rating,” IEEE Transactions on Dielectrics and Electrical Insulation, vol.22, 2015.

[133] L. Bernardi,R. Hopf, A. Ferrari, A.E. Ehret and E. Mazza, “On the large strain deformation behavior of silicone-based elastomers for biomedical applications,” Polymer Testing, vol. 58, pp. 189-198, 2017.

[134] L. Meunier, G. Chagnon, D. Favier, L. Orgeas and P. Vacher, “Mechanical experimental characterisation and numerical modelling of an unfilled silicone rubber,” Polymer Testing, vol. 27, pp. 765-777, 2008.

[135] M.H.R. Ghoreishy, M. Firouzbakht and G. Naderi, “Parameter determination and experimental verification of Bergström–Boyce hysteresis model for rubber compounds reinforced by carbon black blends,” Materials and Design, vol. 53, pp. 457-465, 2014.

[136] L.A.Gracia, E.Liarte, J.L.Pelegay and B.Calvo, “Finite element simulation of the hysteretic behaviour of an industrial rubber. Application to design of rubber components,” Finite Elements in Analysis and Design, vol. 46, pp. 357-368, 2010.

[137] J. R. Davis, *Tensile Testing*, Second edition, ASM International, Ohio, 2004.

[138] D.M. Grove and T.P. Davis, *Engineering Quality and Design*, Longman, 1992.

[139] *NIST/SEMATECH e-Handbook of Statistical Methods*, http://www.itl.nist.gov/div898/handbook/, 2019.

[140] C. Bayliss and B. Hardy, Transmission and Distribution Electrical Engineering, 3rd ed. Newnes, 2006.

[141] R. Huang, “Dynamic Rating for Improved Operational Performance,” PhD thesis, University of Southampton, Southampton, UK, 2015.

[142] J. M. Domingo Capella, “Study of the Behaviour of a n-metal Cable Screen Subject to an adiabatic short circuit,” Jicable15, E5.3, 2015.

[143] IEC 60949, “Method for Calculation of Thermally permissible Short-Circuit Currents, taking into account non-adiabatic heating effects,” 2008.

[144] S. Catmull, R. D. Chippendale, J. A. Pilgrim, G. Hutton and P. Cangy, “Cyclic Load Profiles for Offshore Wind Farm Cable Rating,” vol. 31, no.3, 2016.

[145] D. R. Askeland, P. P. Fulay and W. J. Wright, “The Science and Engineering of Materials”, Sixth Edition, Cengage Learning, 2011.

[146] “Typical Engineering Properties of High Density Polythylene,” INEOS Olefins & Polymers USA, 2009. [Online]. Available:http://www.ineos.com/Global/Olefins%20and%20Polymers%20USA/Products/Technical%20information/Typical%20Engineering%20Properties%20of%20HDPE.pdf [Accessed 2019].

[147] D. Tripathi, “Practical Guide to Polypropylene,” Rapra Technology, 2002.

[148] IEEE Guide for Selection and Design of Aluminum Sheaths for Power Cables IEEE Power Engineering Society IEEE Std 635™-2003.

[149] G. Hirota, S. Fisher and A. State, “An Improved Finite Element Contact Model for Anatomical Simulations,” The Visual Computer, vol. 19, pp. 291-309, 2003.

[150] P. Christiansen, J. H. Hattel, N. Bay and P. AF Martins, “Physical Modeling and Numerical Simulation of V-die Forging Ingot with Central Void,” Journal of Mechanical Engineering Science, vol. 228, no. 13, 2014.

[151] GECA Tapes [Online], https://geca-tapes.com/products/, [Accessed 2019].

[152] U. A. Bakshi and A. V. Bakshi, Electromagnetic Theory, 1st ed. Pune-India: Technical Publications, 2009.

[153] H. A. Illias, Z. H. Lee, A. H. A. Bakar, H. Mokhlis, G. Chen and P. L. Lewin, “Electric Field Distribution in 132 kV One Piece Premolded Cable Joint Structure,” IEEE International Conference on Condition Monitoring and Diagnosis, 2012.

[154] H. A. Illias, G. Chen and P. L. Lewin, “Comparison between three-capacitance, analytical-based and finite element analysis partial discharge models in condition monitoring,” IEEE Transactions on Dielectrics and Electrical Insulation, vol. 24, no. 1, 2017.

[155] D. Yonetsh, T. Hara, S. Shimada and M. Kaji, “Electric Field Optimization of the Power Cable Joint by Using Evolutionary Calculation Method,” Electrical Engineering in Japan, vol. 150, no. 4, 2005.

[156] G. Greshnyakov, S. Dubitskiy and N. Korovkin, “Optimization of Capacitive and Resistive Field Grading Devices for Cable Joint and Termination,” International Journal of Energy, vol. 9, 2015.